CRYSTAL DYNAMICS AND RELATED SOLID STATE PROPERTIES OF POLYMERS

A Thesis

Submitted to

Osaka University

in Fulfillment of the Requirements

for the Degree

of

Doctor of Science

by

Teizo Kitagawa

November, 1968

CONTENTS

PREFACE

Spectroscopic, thermodynamic, elastic, and crystallographic measurements have been carried out on polymer crystals. The basic theory for each measurement has been established, although often the theory is written for the simplest model such as monoatomic cubic crystal and is not quite applicable to polymer crystals. Accordingly, interpretations of individual data have been made but no consistent analyses have been carried out systematically with realistic structure models.

All these data, however, are related directly or indirectly with the force field of the crystal. Accordingly, in the present series of studies, available experimental data on the crystalline region of polyethylene were systematically analysed on the basis of the force field of the polyethylene crystal.

Before proceeding to numerical calculation, correlations of individual experimental data with the intrachain and interchain force field and/or normal vibrations were theoretically treated with the real structure of polyethylene crystal. For most data, theories for polymer crystals were written out so as to be readily programmed for numerical calculations with electronic computers. It was also necessary to develop approximate method of calculations without affecting numerical values of interest.

In the present thesis studies, practical methods were finally worked out for systematically treating several

physical properties of polymer crystals, namely

Intrachain and interchain force field,

Infrared absorption and Raman scattering due to lattice vibrations or interchain vibrations,

Splitting of infrared bands and Raman lines due to intrachain vibrations,

Frequency distribution of crystal vibrations,

Specific heat below 150°K and especially specific heat below 10°K,

Elastic and inelastic neutron-scattering cross sections and their anisotropy,

Sound velocity and macroscopic elastic constants and Young's moduli,

Temperature factor tensor for x-ray diffraction intensity,

Symmetry of crystal vibrations and frequency dispersion curves,

Infrared bands due to combinations of crystal vibrations.

The physical properties calculated, in the present studies, on the polyethylene crystal are in good agreement with corresponding experimental data. Various experimental data are now interpreted consistently on the basis of the intrachain and interchain potential functions. The present force field may also be used for estimating some new physical properties, for example, the frequency distribution curves of perdeuterated polyethylene crystal or elastic constants of polyethylene crystal.

In the present treatments, various physical properties were treated with harmonic force field. However, as forthcoming projects, thermal expansion or temperature dependency

of vibrational frequencies and elastic constants are still left for theoretical treatments on the basis of anharmonic force fields. Physical properties of disordered part or amorphous region of polymer material are left for next higher stage of theoretical treatments.

Teizo Kitagawa

ACKNOWLEDGMENTS

The author wishes to express his sincere gratitude to Professor Tatsuo Miyazawa for his guidance and kind encouragement. The author is also grateful to Professor Masao Kakudo of Osaka University, Dr. Kunio Fukushima of Shizuoka University, and Dr. Tsuneo Takano of Osaka University for their help and encouragement. Thanks are also due to Mrs. Yoshiko Tanigawa, Mr. Hiromu Sugeta and all other members of the Professor Miyazawa's laboratory and Mr. Nobuo Tanaka of Tottori University for their help and discussions.

The author is indebted to Dr. Mitsuo Tasumi of the University of Tokyo for his stimulating discussions.

The author is grateful to Professor Akiyoshi Mitsuishi of Osaka University for the measurement of far infrared spectrum of polyethylene and to Professor Akira Odajima of Hokkaido University for his discussions.

LIST OF PAPERS

A) PAPERS CONTAINED IN THIS THESIS

1) Crystal Vibrations, Specific Heat, and Elastic Moduli of the Polyethylene Crystal.

T. Miyazawa and T. Kitagawa
J. Polymer Sci., B2, 395 (1964).

2) Frequency Distribution of Crystal Vibrations and Specific Heat of Polyethylene.

T. Kitagawa and T. Miyazawa
Rept. Progr. Polymer Phys., Japan, 8, 53 (1965).

3) Inelastic Scattering Cross Section of Neutron by Crystal Vibrations of Polyethylene.

T. Kitagawa and T. Miyazawa
Rept. Progr. Polymer Phys., Japan, 10, 185 (1967).

4) Inelastic Scattering Cross Section of Neutron by Crystal Vibrations of Polyethylene.

T. Kitagawa and T. Miyazawa
J. Chem. Phys., 47, 337 (1967).

5) Interchain Potential, Frequency Spectrum, Specific Heat, and Root Mean Squared Displacement in Polyethylene Crystal.

T. Kitagawa and T. Miyazawa
Rept. Progr. Polymer Phys., Japan, 11, 219 (1968).

6) Cross-section for Multi-phonon Scattering of Neutrons by Crystalline Polyethylene.

T. Kitagawa and T. Miyazawa
J. Polymer Sci., B6, 83 (1968).

B) REFERENCE PAPERS

1) Interchain Potential, Frequency Distribution and Specific Heat of Polyoxymethylene Crystal.

T. Kitagawa and T. Miyazawa
Inter. Symp. Macromol. Chem., Tokyo (paper 2.5.04)(1966).

2) Interchain Potential, Frequency Distribution and Specific Heat of Polyoxymethylene Crystal.

T. Kitagawa and T. Miyazawa
Rept. Progr. Polymer Phys., Japan, 9, 175 (1966).

3) Thermal Expansion of Polyethylene Crystal in the Quasi Harmonic Approximation.

A. Odajima, T. Maeda, M. Sato, T. Kitagawa and T.Miyazawa
Rept. Progr. Polymer Phys. Japan, 11, 209 (1968).

4) Energy Difference between Rotational Isomers of Methyl Ethyl Ether.

T. Kitagawa and T. Miyazawa
Bull. Chem. Soc. Japan, 41, 1976 (1968).

ABSTRACT

Chapter I NORMAL VIBRATIONS AND RELATED PHYSICAL PROPERTIES OF ORTHORHOMBIC CRYSTALS.

The crystal vibrations are specified with phase-difference vectors of vibrational displacements, and accordingly Cartesian symmetry coordinates of orthorhombic crystals were derived in a general form. A practical method was derived for calculating the frequency distribution, specific heat and Young's moduli along the direction perpendicular to the chain axis.

As a preliminary study, polyethylene crystal was treated where methylene groups were regarded as single dynamic units. Since the experimental specific heat of polyethylene obeys the T^3 law below 10°K, the coefficient of T^3 was derived analytically and is found to be nearly proportional to $P^{-3/2}$, where P is proportional to the interchain force constants.

Chapter II NORMAL VIBRATIONS, INTERCHAIN FORCE FIELD, FREQUENCY DISTRIBUTION AND SPECIFIC HEAT OF POLYETHYLENE CRYSTAL.

In the refined treatment, vibrational displacements of hydrogen atoms as well as of carbon atoms were taken into account. The force field of Schachtschneider and Snyder was used as the intrachain potential function. Four hydrogen-hydrogen interaction terms as introduced by Tasumi and Shimanouchi were incorporated as the interchain potential function. The force constants were adjusted with reference to experimental data on the specific heat below 10°K, the infrared-active lattice vibrations and band splitting of intrachain vibrations.

There are thirty-six branches of crystal vibrations, but only eight of them lie in the region below 700 cm^{-1}. Therefore, a practical method was worked out for treating

low-frequency crystal vibrations only. The computer-time was drastically shortened, although calculated frequencies were accurate within 3 cm^{-1}.

The frequency distribution below 700 cm^{-1} was numerically calculated with the root-sampling method, for treating the specific heat of the crystalline region.

The calculated results of the optically-active lattice-vibration frequencies, band splitting of intrachain vibrations, Young's moduli, frequency distribution and specific heat agree closely with corresponding experimental data.

Chapter III ACOUSTIC PHONONS AND LOW-TEMPERATURE SPECIFIC HEAT OF POLYETHYLENE CRYSTAL.

The specific heat below $10^{o}K$ depends primarily upon three acoustic branches of crystal vibrations. Accordingly, the dynamical matrix for three acoustic phonons were derived by the second order perturbation method. Interactions among acoustic modes were thus incorporated, and the constant-frequency surfaces were, in fact, distorted from ellipsoidal surfaces. From the volume surrounded by those surfaces, the frequency distribution was obtained analytically and was found to agree well with the frequency distribution calculated from the root-sampling method. The specific heat calculated from the frequency distribution of the acoustic phonons agrees closely with the experimental data by Tucker and Reese.

Chapter IV SYMMETRY OF CRYSTAL VIBRATIONS, DISPERSION CURVES AND INFRARED BANDS DUE TO COMBINATION VIBRATIONS.

Frequency dispersion curves of the polyethylene crystal were calculated on the surfaces of the first Brillouin zone. The symmetry properties of those branches and the compatibility of the dispersion curves were derived on the basis of k group of the space group. The irreducible multiplier corepresentation developed by Maradudin was also applied to polyethylene crystal, and the degeneracy due to time reversal

symmetry was deduced. The theoretical degeneracy derived from the group-theoretical analyses coincides exactly with the results of numerical calculation of vibrational frequencies.

Combinations of crystal vibrations with $+\delta$ and of those with $-\delta$ may become infrared-active. The symmetry of combination levels is derived from direct product of the irreducible representation of the k group. From the frequency distribution of combination vibrations, infrared bands are expected near 240, 280 and 380 cm^{-1}, in good correspondence with the bands observed near 240, 280 and 340 cm^{-1}.

Chapter V ELASTIC CONSTANTS OF POLYETHYLENE CRYSTAL.

Born's formulation of elastic constants is not necessarily convenient for treating molecular crystals. The matrix formulation by Shiro is much more useful for treating molecular crystals. Also symmetry consideration is readily applicable to matrix formulations.

For the orthorhombic crystal of polyethylene, the elastic constants of c_{11}, c_{22}, c_{33}, c_{23}, c_{31}, and c_{12} belongs to A_g species while c_{44}, c_{55}, and c_{66} belong to B_{1g}, B_{2g}, and B_{3g} species, respectively. These elastic constants of polyethylene were calculated from the force field of the polyethylene crystal.

Correlations of elastic constants with dispersion curves of acoustic phonons are discussed. The dynamical matrix for the elastic waves of three-dimensional continuum is equivalent to the dynamical matrix for the three acoustic phonons.

The Young's moduli along the a, b, and c axes of polyethylene were also calculated, in good agreement with the experimental results of the X-ray diffraction measurement by Sakurada et al.

Chapter VI A REFINED METHOD FOR TREATING ONE- AND MULTI-PHONON NEUTRON-SCATTERING CROSS SECTIONS.

In crystals containing hydrogen atoms, thermal neutrons are scattered primarily from hydrogen nuclei (incoherent scattering). For inelastic scattering, there is no selection rule related with symmetry properties of crystal vibrations, and accordingly the energy spectrum of inelastically scattered neutrons provides important informations on normal vibrations of crystals and polymer chains.

The basic theory of neutron scattering has already been established, although the model used is too simple to be applicable to vibrational analyses on polyethylene crystal.

In the present study, therefore, the differential cross sections for one-phonon and multi-phonon scattering processes were derived from Fermi's pseudo potential and Born's first approximation. The concept of transition probabilities was used and the equations for cross sections were written so as to be readily programmed for electronic computers.

Multi-phonon scattering cross sections derived here are essentially identical with those derived from time dependent correlation function, although the present formulation is much more convenient for numerical calculations.

Chapter VII NEUTRON SCATTERING BY CRYSTAL VIBRATIONS OF POLYETHYLENE.

As for polyethylene crystal, the differential cross sections of neutron-scattering have been measured at various temperatures with both of the up- and down-scattering techniques. The anisotropy of the scattering cross sections has also been observed for uniaxially oriented target of polyethylene crystal.

For theoretical analyses of these experimental data, the differential cross sections for one-, two- and three-phonon processes were calculated from the vibrational frequencies and vibrational displacements of hydrogen nuclei involved in crystal vibrations of polyethylene.

The anisotropic cross sections and phonon density curves calculated for the up- and down-scattering experimental conditions are in accord with the experimental results on the scattering peak-intensities and anisotropy.

Chapter VIII TEMPERATURE FACTOR FOR X-RAY DIFFRACTION OF POLYETHYLENE CRYSTAL.

From the polyethylene crystal, x-ray is primarily scattered by electron clouds of carbon atoms. As the scattering angle is increased, intensities of diffraction peaks are lowered because of thermal vibrations of scattering atoms.

In the present study, the mean squared displacements of carbon atoms were calculated from the vibrational frequencies and vibrational displacements of carbon atoms involved in crystal vibrations of polyethylene.

The temperature factor tensor was calculated, in good agreement with the experimental data on the magnitude and anisotropy. From the numerical calculation, three principal axes of the temperature factor tensor were obtained; the first one is parallel to the chain axis, and the second and third ones are normal and parallel, respectively, to the skeletal plane.

CHAPTER I

NORMAL VIBRATIONS AND RELATED PHYSICAL PROPERTIES OF ORTHORHOMBIC CRYSTALS

I-1 INTRODUCTION

Physicochemical properties of polyethylene crystal have been investigated in various ways and it is significant, at present stage, to relate them with one another self-consistently. Some of them are concerned with frequencies or atomic displacements of thermal vibrations and therefore may be treated systematically on the basis of the potential function of the crystal.

Wunderlich has measured the specific heat of polyethylene[1] and, referring to all the observed values[2], has obtained the specific heat of the crystal part of polyethylene with the use of extrapolation method.[3] It obeys T^3 law at the lowest temperature and is almost proportional to T in the temperature region below 70°K. Stockmeyer and Hecht[4] have studied the specific heat of an anisotropic crystal and have derived it as function of atomic force constants where the anisotropy has been taken into account through force constants assumed in a tetragonal lattice. Tarasov[5] has regarded chain polymers as elastic rods which have weak interactions between the nearest neighbors. He represented the specific heat of polymer crystals with two Debye temperatures, namely, θ_1 and θ_3, which are one-dimensional and three-dimensional characteristic temperatures, respectively. By adjusting θ_1 and θ_3 suitably, the experimental values of the specific

heat of polyethylene crystal may be represented in fairly wide region of temperature.[3] However, the model used does not match the polyethylene crystal and the physical meaning of θ_1 and θ_3 is not always clear, because low-frequency optical modes of interchain vibrations lie velow the cut-off frequencies of acoustic branches and the frequency distribution might not be simple like Debye approximation.

On the other hand, the intramolecular force field of hydrocarbon molecules have been refined systematically.[6-9] Also the general theory of molecular vibrations of chain polymers have been already established.[10-11] Accordingly, it is now practical to treat the crystal vibrations of polyethylene on the basis of the intrachain and interchain potential functions.

Previously Wilson's GF matrix method[12] was applied to optical active vibrations of three dimensional crystal,[13] but Cartesian coordinate system is convenient for treating all vibrations including acoustic branches and optically inactive modes. Accordingly, in the present study, basic formulation of normal coordinate treatment and a practical method of calculating the frequency distribution and specific heat were provided. Since the frequency of the internal modes of methylene group lie above 700 cm^{-1} and they contribute little to the specific heat below 150°K, methylene groups were regarded as single dynamic unit on the preliminary calculation about polyethylene crystal.

I-2 NORMAL COORDINATE TREATMENT

Normal modes of the orthorhombic crystals are specified

with a set of three phase differences, δ_a, δ_b, and δ_c which are phase differences of vibrational displacement between two adjacent unit cells along the a, b, and c axes, respectively. The travelling direction of a phonon is parallel to k vector (k_a, k_b, k_c) of the phonon, which is related with the phase difference vector as $\delta_a = a_o k_a$, $\delta_b = b_o k_b$, and $\delta_c = c_o k_c$ where a_o, b_o and c_o are lattice constants. For a given phase difference vector, there are 3n modes of crystal vibrations where n is the number of atoms per unit cell. Accordingly 3n Cartesian symmetry coordinates for a given phase difference vector were derived as

$$S(\delta) = U(\rho,\delta)X(\rho) \tag{1.1}$$

where $S(\delta)$ is a Cartesian symmetry coordinate vector with 3n components, $U(\rho,\delta)$ is a unitary matrix for symmetry transformation and $X(\rho)$ is a Cartesian displacement coordinate vector of ρ-th unit cell. The kinetic energy (T) and potential energy (V) of crystal are represented in a matrix form as

$$2T = \tilde{\dot{S}}(\delta)M_S\dot{S}(\delta) \tag{1.2}$$

$$2V = \tilde{S}(\delta)F_S(\delta)S(\delta) \tag{1.3}$$

where

$$M_S = U(\rho,\delta)M_X\tilde{U}(\rho,\delta)$$

$$F_S(\delta) = U(\rho,\delta)\tilde{B}(\rho)F_R B(\rho)\tilde{U}(\rho,\delta)$$

M_S is 3n dimensional diagonal matrix whose elements are mass of atoms, F_R is the potential energy matrix of crystal based on the internal coordinate system and $B(\rho)$ is a usual B matrix[12], that is, $R = \sum_\rho B(\rho)X(\rho)$. $F_S(\delta)$ is the potential energy matrix based on the Cartesian symmetry coordinate system, dimension of which is 3n.

The Cartesian symmetry coordinates can be written as linear combination of the normal coordinates, $Q(\delta)$, of the crystal.

$$S(\delta) = L^{0}(\delta)Q(\delta) \tag{1.4}$$

With the use of normal coordinates, the kinetic energy and potential energy are represented as

$$2T = \tilde{\dot{Q}}(\delta)E\dot{Q}(\delta) \tag{1.5}$$

$$2V = \tilde{Q}(\delta)\Lambda(\delta)Q(\delta) \tag{1.6}$$

where E is unit matrix and $\Lambda(\delta)$ is a diagonal matrix whose elements are eigenvalues ($\lambda_{ii}=4\pi^2c^2\nu_i^2$). The equivalence of two types of representations, that is (1.2), (1.3) and (1.5) (1.6), leads us to the secular determinant,

$$\left| M_S^{-1}F_S(\delta) - \Lambda(\delta) \right| = 0 \tag{1.7}$$

The eigenvector matrix of $M_S^{-1}F_S(\delta)$ is proved to be $L^{0}(\delta)$. Since a symmetric matrix is more convenient to treat, the dynamical matrix defined by (1.8) is used instead of $M_S^{-1}F_S(\delta)$,

$$D_S(\delta) = M_S^{-\frac{1}{2}}F_S(\delta)M_S^{-\frac{1}{2}} \tag{1.8}$$

where $M_S^{-\frac{1}{2}}$ is a diagonal matrix, the elements of which are inverse of square root of atomic mass. Then the eigenvector matrix of the dynamical matrix becomes unitary and is represented as $L_S(\delta)$.

$$L_S(\delta) = M_S^{\frac{1}{2}}L^{0}(\delta) \tag{1.9}$$

The use of $S(\delta)$ reduces the secular determinant of the crystal vibrations into the corresponding blocks of phase difference vector, each of which is 3n-dimensional symmetric matrix, called Fourier transformed dynamical matrix. The incorporation of the space symmetry of the crystal may reduce the dynamical matrix into smaller blocks.

I-3 SYMMETRY COORDINATES

n atoms in the unit cell can be classified into several sets ($\beta=1,2,\cdots\cdots,n_s$) of equivalent atoms on the basis of the space symmetry. For the β-th set with m_β equivalent atoms, $3m_\beta$ symmetry coordinates may be constructed for $\delta=0$ and the same type of symmetry coordinates can be applied to other sets of atoms on the equivalent sites. On the other hand, under thermal vibrations, full symmetry of the space group is not always kept. The symmetry of crystal vibrations is generally characterized by k group[14], which is a subgroup of the point group of the space group. The dynamical matrix $D_S(\delta)$ of the crystal vibrations may possibly be factorized into symmetry species of the k group. Usually, on the surface of the first Brillouin zone, some operations beside identity operation make the k vector invariant while, at the inner points of the zone, only the identity operation constitutes the k group. Accordingly, at the general points of the first Brillouin zone, symmetry transformations factorize the dynamical matrix no more and only numerical diagonalization yields the eigen-frequency of the crystal vibrations. Then the coordinates which take the shortest time for numerical diagonalization on general value of phase difference vector is the most suitable for the present treatment. Since the highest symmetry is satisfied at $\delta=0$, the dynamical matrix may be factorized into the smallest blocks with the symmetry transformation, each of which belongs to the irreducible representation of the point group of the space group. The compatibility relation shows that symmetry coordinates at $\delta=0$ also belong yet to one of symmetry species of k group

on the adjacent surface of the Brillouin zone. Besides, so-called time reversal degeneracy need not be considered for $\delta=0$.[15] Accordingly, the symmetry coordinate at $\delta=0$ is used through whole the δ space, which are derived below.

A symmetry operation, R_i of the space group consists of rotation, α_i and nonprimitive translation τ_i. α_i is three dimensional orthogonal matrix and τ_i is index vector. Both of ρ and τ are represented as the set of a coefficient with regard to the lattice constants. Supposing $\rho_j^\beta(L)$ and $\eta_j^\beta(L)$ ($j=1,2,\cdots m_\beta$) are the index vector of j-th atom of βth set of atoms in L-th unit cell and its atomic displacement vector, respectively, then

$$\eta_j^\beta(L) = (1/N)^{\frac{1}{2}}\Sigma_\delta\, \xi_j^\beta(\delta)\exp\left[-i\rho_j^\beta(L)\delta\right] \qquad (1.10)$$

where N is the total number of unit cells, $\xi_j^\beta(\delta)$ is the amplitude factor of j-th atom of βth set and summation runs over N points in the region of $0\leq|\delta_a|, |\delta_b|, |\delta_c|\leq\pi$. The inverse transformation of (1.10) provides

$$\xi_j^\beta(\delta) = (1/N)^{\frac{1}{2}}\Sigma_L\, \eta_j^\beta(L)\cdot\exp\left[i\rho_j^\beta(L)\delta\right] \qquad (1.11)$$

The irreducible representation of the point group (the k group at $\delta=(0,0,0)$) associated with orthorhombic system is always one dimensional. Supposing the operation R_j transforms ρ_1^β into ρ_j^β, the symmetry coordinate corresponding to μ-th irreducible representation is given by

$$S^\mu(\delta)^\beta=(m_\beta N)^{-\frac{1}{2}}\sum_{R_j}^{m_\beta}\sum_L \Gamma^\mu(\alpha_j)\alpha_j\eta_j^\beta(L)\exp\left\{i\left[\alpha_j\rho_1^\beta(L)+\tau_j\right]\delta\right\} \qquad (1.12)$$

where $\Gamma^\mu(\alpha_j)$ is the character of μ-th irreducible representation of the point group of the space group for operation R_j. Thus derived $S^\mu(\delta)^\beta$ is complex-number coordinate while real-number coordinate is more convenient for computation. The

corresponding real number coordinate may be derived with standing wave as,[16-17]

$$S^{\mu c}(\delta)^{\beta}=(2/m_{\beta}N)^{\frac{1}{2}}\sum_{R_j}\sum_{L}\Gamma^{\mu}(\alpha_j)\cdot\alpha_j\eta_j^{\beta}(L)\cos\{[\alpha_j\rho_1^{\beta}(L)+\tau_j]\delta\}$$
$$S^{\mu s}(\delta)^{\beta}=(2/m_{\beta}N)^{\frac{1}{2}}\sum_{R_j}\sum_{L}\Gamma^{\mu}(\alpha_j)\cdot\alpha_j\eta_j^{\beta}(L)\sin\{[\alpha_j\rho_1^{\beta}(L)+\tau_j]\delta\} \quad (1.13)$$

and then the atomic displacement vector becomes

$$\eta_j^{\beta}(L)=(2/N)^{\frac{1}{2}}\sum_{\delta>0}\xi_j^{c\beta}(\delta)\cos[\rho_j^{\beta}(L)\delta]+\xi_j^{s\beta}(\delta)\sin[\rho_j^{\beta}(L)\delta] \quad (1.14)$$

where the summation runs over N/2 points in half of the first Brillouin zone. By this transformation, the order of the dynamical matrix is generally doubled as

$$\begin{bmatrix} D_1(\delta) & \widetilde{D_2}(\delta) \\ D_2(\delta) & D_1(\delta) \end{bmatrix}$$

where $D_1(\delta)$ is symmetric matrix and $D_2(\delta)$ is skew symmetric matrix.[16] The method of diagonalizing the doubled dynamical matrix has been established.[16]

When center of inversion exists in the crystal(D_{2h}), the operation changes η_j^{β} and δ into $-\eta_j^{\beta}$, and $-\delta$ without nonprimitive translation and therefore, both of $S^{\mu c}(\delta)^{\beta}$ and $S^{\mu s}(\delta)^{\beta}$ become either symmetric or antisymmetric to inversion on any value of δ. Accordingly, the existence of the center of inversion removes the cross terms $D_2(\delta)$ of two types of coordinates of $S^{\mu c}(\delta)$ and $S^{\mu s}(\delta)$. Then the dynamical matrix of doubled order is reduced to two identical real symmetric matrices of 3n dimension.

I-4 SYMMETRY COORDINATES FOR POLYETHYLENE CRYSTAL

The crystal structure of orthorhombic polyethylene has been analysed by Bunn[18] with X-ray diffraction method. Two molecular chains pass along the c axis and there are four methylene groups per unit cell. Since methylene group

is regarded as single dynamic unit, all atoms are equivalent, that is, $n=4$, $n_s=1$, $m_1=4$. On the incorporation of freedom of hydrogen atoms, n_s would become 3. The symmetry of the unit cell is P_{nam}, isomorphous to point group D_{2h}. Lattice constants at room temperature are $a_o=7.40$, $b_o=4.93$ and $c_o=2.54$ Å and valence angle of C-C-C is 112°. The setting angle of the skeletal zigzag plane is reported to be 48.7° to the a axis.

As shown in Fig. 1, unit cells are specified with three integers, h, k, and l instead of vector **L** of preceding section. h denotes the index of the unit cell along the a axis, k along the b axis and l along the c axis, respectively. On the primitive translation, one of the indexes varies by whole number. Two molecular chains in a unit cell are specified with the set of two indexes as (h,k) and $(h+\frac{1}{2},k+\frac{1}{2})$. Two methylene groups in the same chain may be distinguished by the last index as $(l+1/4)$ and $(l-1/4)$. The index vectors of four methylene groups are as follows;

$$\rho_1(h,k,l)=(h,k,l+1/4) \qquad \rho_3(h,k,l)=(h+\tfrac{1}{2},k+\tfrac{1}{2},l+1/4)$$
$$\rho_2(h,k,l)=(h,k,l-1/4) \qquad \rho_4(h,k,l)=(h+\tfrac{1}{2}.k+\tfrac{1}{2},l-1/4)$$

α_i and $\boldsymbol{\tau}_i$ for eight operations of polyethylene crystal are given in Table A1. The real symmetry coordinates derived in (1.13) are represented in Table 1, where summation about h, k and l and factor $(2N)^{-\frac{1}{2}}$ are omitted. Because of the summation, apparent difference of sign of h, k, and l has no physical meaning. For instance, $(+h,+k,+l-1/4)$ is equivalent to $(-h,-k,-l-1/4)$ and $(h+\frac{1}{2},k+\frac{1}{2},l-1/4)$ is equivalent to $(h-\frac{1}{2},k-\frac{1}{2},l-1/4)$. The components of $\boldsymbol{\xi}_j$ are written as x_j, y_j and z_j in Table 1. Thus derived twenty-four symmetry

coordinates (twelve for $S^{\mu c}(\delta)$, and twelve for $S^{\mu s}(\delta)$) are divided into two groups by center of inversion. After the operation of inversion, the following twelve coordinates are invariant; $S_x^c(A_g)$, $S_y^c(A_g)$, $S_z^s(A_u)$, $S_x^c(B_{3g})$, $S_y^c(B_{3g})$, $S_z^s(B_{3u})$, $S_x^s(B_{1u})$, $S_y^s(B_{1u})$, $S_z^c(B_{1g})$, $S_x^s(B_{2u})$, $S_y^s(B_{2u})$, $S_z^c(B_{2g})$, where the symbol in bracket denotes the symmetry at $\delta=0$. These are symmetric and the others are antisymmetric to inversion. In D_{2h} system, the irreducible volume of the first Brillouin zone is 1/8 of the first Brillouin zone and therefore $0 \leq \delta_a, \delta_b, \delta_c \leq \pi$ is sufficient. $U(\rho,\delta)$ of (1.1) for the polyethylene crystal is given in Table 2.

I-5 POTENTIAL FUNCTION

Infrared spectrum and intrachain potential function of polyethylene have been studied in detail.[19-23] Normal frequencies of polyethylene single chain[8] and of the crystal[24], have been calculated rigorously as function of δ_c by Tasumi. It deduces that the maximum frequency of the skeletal bending branch and the internal rotation branch lie near 500 cm^{-1} and 200 cm^{-1}, respectively.

In the present study, three types of intermethylene potential terms, p_1, p_2 and p_3 in Fig. 2, which are relatively in close contacts, are incorporated as well as the intrachain potential function. The equilibrium distances and the number of potential terms per unit cell are shown in Table 3. The potential energy of the crystal is written in a quadratic form of displacement,

$$2V=\sum[K(\Delta r)^2+H(\Delta\phi)^2+F(\Delta q)^2+Y(\Delta t)^2+P_1(\Delta p_1)^2+P_2(\Delta p_2)^2+P_3(\Delta p_3)^2]$$

where Δr is bond stretching, $\Delta\phi$ is skeletal bending, Δt is

internal rotation, and Δq is repulsion terms of nonbonded carbons in a chain. Δp_1, Δp_2 and Δp_3 are change of intermethylene distance. K, H, Y, F, P_1, P_2, and P_3 are their force constants. Summation runs over the crystal. The values of K, H, Y, and F were chosen so as to reproduce the ν-δ_c curve closely which had been obtained in the complete treatment of polyethylene single chain.[8] The interchain force constants were adjusted on the basis of the specific heat below 10°K, where in order to decrease the number of parameters, P_1 is assumed to be equal to P_2 because of nearly same distances.

I-6 LATTICE VIBRATIONS AND THE FREQUENCY DISTRIBUTION

Dispersion curves of low frequency crystal vibrations are drawn against δ_c in Fig. 3, where δ_a and δ_b are set to be 0. If there is no interaction between adjacent molecules, all of these eight branches would approach to 0 cm^{-1} as δ_c approaches to 0, and there would appear four doubly degenerate curves. At the limit of δ_c=0, three of these curves would correspond to translations along three orthogonal axes and one of them would correspond to rotation around the chain axis. However, on account of interchain interactions the degeneracy is actually removed and the dispersion curves do not cross one another. Here, three of eight curves still approach to 0 cm^{-1} as δ_c approaches to 0. They are acoustic branches of the crystal. The remaining five modes are optical lattice vibrations whose frequencies and symmetry species are shown in Fig. 4. B_{1u} and B_{2u} vibrations are antiparallel translatory vibrations along the b and a axes, respectively. They are infrared active modes.

There are two lattice vibrations of rotation around the chain axis. The mode, in which two chains rotate in the same direction, belongs to B_{3g} while the other belongs to A_g. They are expected to be Raman active. The last mode, anti-parallel translatory vibration along the c axis belongs to A_u which is inactive both in Raman and infrared spectrum. The experimental value of this frequency is expected to be observed only in neutron inelastic scattering.

For representative combinations of δ_a, δ_b and δ_c, $D_S(\delta)$ was derived and diagonalized. All these calculations have been carried out with NEAC-2201 electronic computer. As the representative values of δ_a and δ_b, nine values (10°, 30°, 50°, 70°, 90°, 110°, 130°, 150°, 170°) were adopted. For every set of δ_a and δ_b, ten values of δ_c (0°, 5°, 10°, 20°, 40°, 60°, 90°, 120°, 150°, 180°) were taken up. Variation of δ_a or δ_b provides small change of frequency whereas that of δ_c shows great change. It comes from the fact that the contribution of intrachain force field does not vary with δ_a or δ_b but varies with δ_c. For larger δ_c, all modes behave as the intrachain vibrations. When ν varies sensitively with δ, δ space should be divided more finely in order to obtain correct frequency distribution. For this reason the dispersion curves against δ_c were picked up for every set of δ_a and δ_b, and the frequencies were interpolated for intermediate values of δ_c with the use of cubic curve,

$$\nu = a + b\delta + c\delta^2 + d\delta^3 \qquad (1.15)$$

The coefficients a, b, c and d are determined so as the curve passes through four successive standard points. On the

real computation of interpolation, frequencies were obtained at 20' intervals of δ_c with the use of (1.16), which is a practical expression of (1.15),

$$\nu=(\nu_1\ \nu_2\ \nu_3\ \nu_4)\begin{bmatrix}1 & 1 & 1 & 1\\ \delta_1 & \delta_2 & \delta_3 & \delta_4\\ \delta_1^2 & \delta_2^2 & \delta_3^2 & \delta_4^2\\ \delta_1^3 & \delta_2^3 & \delta_3^3 & \delta_4^3\end{bmatrix}^{-1}\begin{bmatrix}1\\ \delta\\ \delta^2\\ \delta^3\end{bmatrix} \qquad (1.16)$$

where ν_1, ν_2, ν_3 and ν_4 are the frequencies obtained from the diagonalization of the dynamical matrix corresponding to δ_1, δ_2, δ_3, and δ_4, respectively. As for the small values of δ_c ($0^\circ<\delta_c<5^\circ$), ν is assumed to be subject to even function of δ_c as

$$\nu = a' + b'\delta^2 + c'\delta^4 \qquad (1.17)$$

where the coefficients were determined in the same way with (1.16). As shown in Fig. 3, dispersion curves are fairly complicated for small values of δ_c ($\delta_c< 60^\circ$) whereas they are relatively monotonous on large δ_c. In order to reproduce delicate behavior of dispersion curves by interpolation, more points were taken as standard points for $\delta_c< 60^\circ$. It was confirmed for arbitrary set of δ_a and δ_b that the interpolated frequencies are coincident with those obtained by diagonalization of the dynamical matrix within ±1 cm^{-1} and therefore the method is justified.

Thus about 350,000 frequencies were calculated and collected. The frequency distribution below 600 cm^{-1} is shown in Fig. 5, where the fraction of the number of vibrations for frequency interval 5 cm^{-1} is plotted against the frequency. Two peaks appear about 500 and 190 cm^{-1}. These two peaks

had been expected from the dispersion curves of polyethylene single chain. They correspond to cut-off frequency of skeletal bending and internal rotation branch, respectively. The existence of these two peaks has been confirmed by the experiment of neutron inelastic scattering.[25-26)]

I-7 SPECIFIC HEAT

There are four methylene groups per unit cell and eight branches lie below 600 cm^{-1}. Therefore, in the frequency distribution below 600 cm^{-1}, two degrees of freedom are contained per methylene group. On the calculation of the specific heat per methylene group, the frequency distribution function is normalized to 2, that is,

$$\sum_{\nu} g(\nu) = 2 \tag{1.18}$$

Since the specific heat due to the crystal vibrations is sum of the contribution of each oscillator, it is derived as

$$C_v/R = \sum_{\nu} g(\nu)x^2\exp(-x)\left[1-\exp(-x)\right]^{-2} \tag{1.19}$$

where $x=hc\nu/kT$ and ν is regarded as the average frequency of the division of the frequency distribution. On the numerical calculation, the frequency distribution was derived at the frequency interval of 1 cm^{-1}. The specific heat of the polyethylene crystal is shown in Fig. 6, where solid line is the calculated value and the open circles are experimental ones which had been extrapolated to 100% crystallinity by Wunderlich[3)]. The contribution of the internal modes of methylene group is estimated as large as 0.002 at 100°K and 0.038 at 150°K.

The specific heat below 10°K depends upon three acoustic branches which are concerned primarily with interchain force

constants. In order to adjust the interchain force constants from the observed value of the specific heat, the specific heat was derived as function of interchain force constants. Each element of the dynamical matrix is expanded into power series of δ_a, δ_b and δ_c where higher terms more than second power were neglected. Then the expanded dynamical matrix was subjected to similarity transformation with $\mathbf{L}_S(\delta_0)$ which is the eigenvector matrix of $\mathbf{D}_S(\delta_0)$ for very small value of phase difference, δ_0. Since $\mathbf{D}_S(0)$ is completely reduced to small blocks of each irreducible representation, the cross terms of $\mathbf{D}_S(\delta)$ between different species are very small for small δ. Thereby, $\mathbf{D}_S(\delta)$ is almost diagonalized with the similarity transformation of $\mathbf{L}_S(\delta_0)$ near $\delta=0$. A few terms which remain as off-diagonal terms after the transformation, are proportional to first power of phase differences and correspond to the interaction of acoustic branches and the overall rotational modes. They have effects of lowering the frequency of acoustic branches. Accordingly, the cross terms were incorporated to diagonal terms with the use of second order perturbation method. The resultant diagonal terms corresponding to three acoustic branches are represented as

$$\begin{aligned} 4\pi^2c^2\nu_1^2 &= A_1\delta_a^2 + B_1\delta_b^2 + C_1\delta_c^2 \\ 4\pi^2c^2\nu_2^2 &= A_2\delta_a^2 + B_2\delta_b^2 + C_2\delta_c^2 \\ 4\pi^2c^2\nu_3^2 &= A_3\delta_a^2 + B_3\delta_b^2 + C_3\delta_c^2 \end{aligned} \qquad (1.20)$$

The coefficients, A_i, B_i and C_i are given in Table 4 in the function of interchain force constants. ν_3 is associated with the translation along the c axis to which the skeletal bending force constants contribute and C_3 becomes large. But to the

eigenvalues of ν_1 and ν_2 modes, the contribution of the intra-chain force field starts from δ_c^4, which is proved by expanding G matrix of the chain vibrations. For this reason, ν_3 gets large sensitively in proportion to δ_c but ν_1 and ν_2 do not. In Table 4, the frequency of ν_3 mode does not depend upon the force constant of P_1. Also P_1 contributes to none of C_1, C_2 and C_3, while P_3 contributes to none of A_1, A_2 and A_3. These results are reasonable from the following consideration. Since p_1 is situated in the ab plane as shown in Fig. 2, the stretching of the spring p_1 is altered with neither the translation of the plane as a whole along the c axis nor the change of phase difference along the c axis, in the first order. As p_3 is essentially on the bc plane, it is not concerned with the phase difference along the a axis.

On the other hand (1.20) states that the constant frequency surfaces of the acoustic branches are three dimensional ellipsoid in δ space. Since the allowed values of phase differences distribute uniformly in the unit cell of reciprocal lattice under the cyclic boundary condition,[27] the volume surrounded by the constant frequency surface is proportional to the number of acoustic phonons lying below the frequency. Supposing $V(\nu)$ is the volume surrounded by the surface corresponding to the frequency ν and the first Brillouin zone then it is derived as

$$V(\nu) = (4\pi/3) \sum_{i=1}^{3} (4\pi^2 c^2 \nu^2)^{3/2} (A_i B_i C_i)^{-\frac{1}{2}} \qquad (1.21)$$

Since the total volume of the first Brillouin zone is $8\pi^3$ where four methylene groups are contained, the volume normalized to one methylene group is $V(\nu)/32\pi^3$. Then the fraction of number

of acoustic phonons between ν and $\nu+d\nu$ per methylene group is $g(\nu)d\nu$, where $g(\nu)$ is represented as

$$g(\nu) = \pi c^3 \sum_i (A_i B_i C_i)^{-\frac{1}{2}} \nu^2 = \rho\nu^2 \qquad (1.22)$$

Then the T^3 law of the specific heat is derived as

$$C_v/R = \rho(k/hc)^3 T^3 \int_0^\infty x^4 \exp(-x)\left[1-\exp(-x)\right]^{-2} dx \qquad (1.23)$$

where $x=hc\nu/kT$. The dependency of the specific heat upon the interchain force constants is obtained by the substitution A_i, B_i and C_i from Table 4 into (1.22). It leads us to the result that C_v is nearly proportional to $P^{-3/2}$, where P is the interchain force constant.

On the other hand, the experimental values of the specific heat can be expressed approximately as follows.

$$C_v/R^{1)} = 1.90\cdot10^{-5}T^3$$

$$C_v/R^{28)} = 1.68\cdot10^{-5}T^3$$

Since Reese's value includes about 10% error[28], the force constants were adjusted to give rise to the intermediate value of two observed specific heat. Thus the analysis yields $P_1=P_2=0.025$ and $P_3=0.003$ md/Å and the specific heat calculated from the set is

$$C_v/R = 1.86\cdot10^{-5}T^3$$

The contribution of each acoustic branch is estimated as

$$C_v(a)=1.52, \quad C_v(b)=0.31, \quad C_v(c)=0.027 \quad (\times10^{-5}RT^3)$$

where a, b and c mean that the vibrational displacement is parallel to the a, b and c axes, respectively. The acoustic phonons associated with the translation along the c axis contribute little to the specific heat. It comes from the fact that the constant frequency surface of that branch is very oblate ellipsoid and the volume is much smaller than two

remaining ones. Above 10°K the experimental value of the specific heat deviates gradually from T^3 law and then becomes nearly proportional to T. It means that the force field which controls the atomic motion is nearly three dimensional for lower frequency whereas it is really one dimensional for higher frequency modes. The excitation of intrachain vibrational modes makes C_v proportional to T.

I-8 YOUNG'S MODULI

Young's moduli perpendicular to the chain axis depends upon the interchain potential. Then comparison of the calculated values of Young's moduli with the observed values is one of ways of examining the correctness of the interchain force constants.

The potential energy of the crystal is represented with three coordinates, which are totally symmetric displacement along the a and b axes (Δa, Δb) and overall rotation around the chain axis (θ). The former two coordinates correspond to the external deformation and the latter corresponds to the internal deformation of the crystal under the condition of rigid molecules.

$$2V = \tilde{\beta}\, \mathbf{C}\, \beta \qquad \tilde{\beta} = (\Delta a\ \Delta b\ \Delta\theta) \tag{1.24}$$

When the unit cell is lengthened by Δa with the external force f_a, then at equilibrium state, f_a is balanced with $-(\partial V/\partial \Delta a)$. Accordingly the deformation of unit cell under arbitrary external force can be derived from (1.24) with the inverse matrix of $\mathbf{C}$ as

$$\begin{bmatrix} \Delta a \\ \Delta b \\ \Delta\theta \end{bmatrix} = \begin{bmatrix} s_{11} & s_{12} & s_{13} \\ s_{21} & s_{22} & s_{23} \\ s_{31} & s_{32} & s_{33} \end{bmatrix} \begin{bmatrix} \partial V/\partial \Delta a \\ \partial V/\partial \Delta b \\ \partial V/\partial \Delta\theta \end{bmatrix} \tag{1.25}$$

where s_{ij} is inverse matrix of **C** and may be called as elastic compliance matrix. Since there is no external force corresponding to overall rotation of molecules, $\partial V/\partial\Delta\theta$ is always zero. From (1.25), Young's moduli along the a and b axes are derived in accordance with the usual definition.

$$E_a = a_o/(b_o c_o s_{11})$$
$$E_b = b_o/(a_o c_o s_{22}) \qquad (1.26)$$

where a_o, b_o and c_o are lattice constants. From the present potential they are calculated as E_a=0.9, E_b=0.3 ($\times 10^{11}$ d/cm^2), in good agreement with the observed value of E_a=0.4 and E_b=0.3[29]. Poisson's ratio is a ratio of relative deformation. Under the tension along the a axis, it is represented as

$$(\Delta a/a_o):(\Delta b/b_o):\Delta\theta = (s_{11}/a_o):(s_{21}/b_o):s_{31} \qquad (1.27)$$

and under the tension along the b axis, it is

$$(\Delta a/a_o):(\Delta b/b_o):\Delta\theta = (s_{12}/a_o):(s_{22}/b_o):s_{32} \qquad (1.28)$$

Usually the sign of s_{11} and s_{21} or s_{22} and s_{12} are different from each other, because shortening appears in the perpendicular direction on pulling the crystal along one direction.

I-9 DISCUSSIONS

On the estimation of intermethylene force constants, Lennard-Jones potential of methane gas[30] was tried. The second derivative of the potential function is written as

$$d^2V/dr^2 = 2.008\cdot10^9 r^{-14} - 1.630\cdot10^5 r^{-8} \quad (\text{kcal/Å}^2) \qquad (1.29)$$

where r is distance of two methane molecules (in Å). Since the values at the equilibrium distances may be regarded as harmonic force constants, putting r of the corresponding intermethylene distances, 4.12, 4.18 and 4.51 Å into (1.29) yields P_1=0.018, P_2=0.015 and P_3=0.002 md/Å, respectively.

The specific heat below 10°K calculated from these force constants is slightly larger compared with the observed value. It suggests that the estimation of intermethylene distances might not always be appropriate.

On the other hand, Tasumi[24] has incorporated four types of interhydrogen potential in the normal coordinate treatment of polyethylene crystal and determined the force constants from the observed values of the band splitting of methylene rocking, twisting and scissoring vibrations. The force constants seem to lie nearly on the Buckingam's potential function for hydrogen atoms. Odajima[31] has treated the elasticity of polyethylene crystal theoretically and found that de Boer's potential of H····H repulsion provides proper set of interchain force constants. The second derivative of de Boer potential[33] is written as

$$d^2V/dx^2 = 150\exp(-3.53x) \qquad (\text{mdyne/Å}) \qquad (1.30)$$

where x is H····H distance. When we apply these function to the present case, the intermethylene distances might be converted into the corresponding H····H distances of the same van der Waals' contacts. Supposing the real intermethylene distance is r then a tentative H····H distance, r*, which gives the equivalent contact to those two methylene groups, might be given by

$$r^* = (r_H/r_{CH_2})r \qquad (1.31)$$

where r_H and r_{CH_2} are van der Waals' radii of hydrogen and methylene group, respectively. Pauling[32] has estimated r_H=1.2 and r_{CH_2}=2.0 Å. Assuming x=r* gives rise to P_1=0.024, P_2=0.022 and P_3=0.003 md/Å for the corresponding intermethylene

distances of 4.12, 4.18 and 4.51 Å, respectively. They agree closely with those of Table 2 which have been adjusted on the basis of the observed value of the specific heat below 10°K. The agreement suggests that this kind of assumption may be applicable to calculating configulational energy of complex molecules.

Though the present calculation is preliminary, general feature of the frequency distribution became explicit. Two prominent peaks corresponding to the cut-off of the skeletal vibrations and a few weak peaks due to optical branches of lattice vibrations such as anti-parallel translational or overall rotational modes, are recognized. The cut-off of the skeletal bending branch is concerned mainly with the intra-chain force field and ν-δ_c curve, which depends little upon δ_a and δ_b, is almost straight line below 450 cm^{-1}. It leads us to the result that frequency distribution is nearly constant near 300 cm^{-1} and the specific heat behaves as if Debye's one-dimensional elastic continuum[34] at proper temperature region. Therefore Tarasov's characteristic frequency ν_1 might physically correspond to the cut-off of the skeletal bending mode, whereas no peak is expected at ν_1 from Tarasov's theory. The other characteristic frequency ν_3, below which the frequency distribution is proportional to ν^2, is not determined uniquely from Fig. 5, where several peaks due to optical lattice vibrations are found below 200 cm^{-1}. Accordingly, the frequency distribution predicted by Tarasov is unlike that of polyethylene crystal.

Generally the specific heat is not always sensitive to fine structure of the frequency distribution, however, the

specific heat below 10°K is sensitive to the interchain potential function. Because it depends mainly upon three acoustic branches and little upon optical branches. Then low temperature specific heat may be used for the adjustment of intermolecular force constants.

Montroll et al.[35] have studied the frequency distribution of crystals analytically. In the case of one-dimensional crystal, the frequency distribution is proportional to $(\nu_m^2-\nu^2)^{-\frac{1}{2}}$ near ν_m where ν_m is the cut-off frequency. While for two-dimensional crystal, the shape of peak is logarithmic, that is, proportional to $\nu^{-1}\log 4(3\nu_m^2-\nu^2)^{-1}$. In three-dimensional crystal, no peak appears but several discontinuities exist in the derivative of the distribution function. Therefore edges might be expected in the frequency distribution.[35] The present calculation may be considered as an experiment from the view of theoretical frequency distribution. Since the peaks at 500 and 200 cm^{-1} had been expected from normal coordinate treatment of isolated polyethylene chain, they correspond to one-dimensional case, in good agreement with the theoretical prediction. However, the theoretical prediction is not always reproduced below 180 cm^{-1} where the frequency distribution is expected to be associated with three-dimensional property of the force field.

The approximation of regarding methylene group as single dynamic unit might induce some errors on the estimation of vibrational frequencies. In the incorporation of the freedom of hydrogen atoms, the frequency of rotational mode would increase whereas that of translational mode would decrease.

The difference of the two models in which the interchain potential works between two methylene groups or between two hydrogen atoms, appears in the effective force constants. On the rotation of molecules around the chain axis, change of inter-hydrogen distance is much larger than the change of inter-methylene distance. Then the energy increment due to the identical rotation is larger in the former under the same force constant. In other words, the effective force constants would become larger in the former. This effect overcomes the effect of increase of moment of inertia and in consequence the frequency of the vibrational mode would get higher, whereas for the translational modes, change of inter-hydrogen distance is smaller or, at most, equal to change of inter-methylene distance.

On the other hand, if the electron clouds of hydrogen atoms were in van der Waals' contacts in equilibrium configuration, the potential energy of the two atoms might constitute the effective interchain potential function and acting point of the interchain forces really on hydrogen atom. Then the direction and magnitude of the interchain potential would vary from the present approximation. For instance, P_3 is the smallest term in the present treatment whereas the corresponding term of H····H potential would become the largest term because of the smallest distance. For these reasons, comparisons of the calculated values with observed values were not carried out in detail in the present treatment. The calculated values which are not influenced by the present approximation were discussed, while for detailed discussion about numerical values, the improvement of model is indispensable.

However, from the present treatment, the way of treating the crystal vibrations and the related quantities systematically may be established.

SUMMARY

The symmetry coordinates of the crystal vibrations for arbitrary phase difference vector were derived in general form and were really confirmed by the application of them to polyethylene crystal. The lattice vibrations, dispersion curves, frequency distribution, the specific heat and Young's moduli of polyethylene crystal were treated in regarding methylene group as single dynamical unit. The specific heat below $10^{\circ}K$ were derived as function of interchain force constants and it was shown that the specific heat is nearly proportional to $P^{-3/2}$ where P is proportional to interchain force constant. The interchain force constants adjusted from the specific heat below $10^{\circ}K$ are $P_1=0.025$, $P_2=0.025$ and $P_3=0.003$ md/Å, which are in good agreement with the values obtained from modified de Boer potential.

In the present study, the practical method of treating crystal vibrations and the related properties were established but the improvement is necessary in crystal model; the incorporation of freedom of hydrogen atom.

REFERENCES

1) B.Wunderlich, J. Chem. Phys., 37, 1207 (1962).

2) F.S.Dainton, D.M.Evans, F.E.Hoare, and T.P.Melia, Polymer, 3, 277 (1962).

3) B.Wunderlich, J. Chem. Phys., 37, 1221 (1962); J. Polymer Sci., C-1, 41 (1963).

4) W.H.Stockmeyer and C.E.Hecht, J. Chem. Phys., 21, 1954 (1953).

5) V.V.Tarasov, J. Chem. Phys., (U.S.S.R), 24, 111 (1950); J. Am. Chem. Soc., 80, 5052 (1958).

6) T.Shimanouchi, Pure. Appl. Chem. 7, 261 (1962).

7) H.Takahashi, T.Shimanouchi, K.Fukushima and T.Miyazawa, J. Mol. Spectry, 13, 43 (1964).

8) M.Tasumi, T.Shimanouchi and T.Miyazawa, J. Mol. Spectry., 9, 261 (1962); 11, 422 (1963).

9) J.H.Schachtschneider and R.G.Snyder, Spectrochim. Acta, 19, 117 (1963).

10) P.Higgs, Proc. Roy. Soc. (London) A220, 472 (1953).

11) T.Miyazawa, J. Chem. Phys., 35, 693 (1961); J. Polymer Sci., 55, 215 (1961).

12) E.B.Wilson, J. Chem. Phys., 7, 1047 (1939); 9, 76 (1942).

13) T.Shimanouchi, M.Tsuboi and T.Miyazawa, J. Chem. Phys., 35, 1597 (1961).

14) J.C.Slater," Quantum Theory of Molecules and Solids" vol-2, McGRAW-HILL company, New York (1965).

15) A.A.Maradudin and S.H.Vosko, Rev. Mod. Phys., 40, 1 (1968).

16) T.Miyazawa, K.Fukushima and Y.Ideguchi, J. Chem. Phys., 38, 2709 (1963).

17) C.Kittel, "Quantum Theory of Solids" p.16, John Wiley Sons, New York (1963).

18) C.W.Bunn, Trans. Faraday Soc., 35, 482 (1939).

19) J.R.Nielsen and R.F.Holland, J. Mol. Spectry., 4, 488 (1960); 6, 394 (1961).
J.R.Nielsen and A.H.Woollett, J. Chem. Phys., 26, 1391 (1957).

20) R.G.Snyder, J. Mol. Spectry., 4, 411 (1960); 7, 116 (1961).

21) S.Krimm, C.Y.Liang, and G.B.B.M.Sutherland, J. Chem. Phys., 25, 543; 549 (1956).

22) R.G.Brown, J. Chem. Phys., 38, 221 (1963).

23) T.P.Lin and J.L.Koenig, J. Mol. Spectry, 9, 228 (1962).

24) M.Tasumi and T.Shimanouchi, J. Chem. Phys., 43, 1245 (1965).

25) H.R.Danner, G.J.Safford, H.Boutin, and M.Berger, J. Chem. Phys., 40, 1417 (1964).

26) J.L.Donovan, G.C.Summerfield and J.S.King, Bull. Am. Chem. Soc., II-9, 533 (1964).

27) M.Born and K.Huang, "Dynamical Theory of Crystal Lattices" Clarendon Press, Oxford (1954).

28) W.Reese and J.E.Tucker, J. Chem. Phys., 43, 105 (1965).

29) I.Sakurada, T.Ito and K.Nakamae, J. Polymer Sci., C-15, 75 (1966).

30) I.Miyagawa. Nippon Kagaku Zasshi, 75, 1169, 1173, 1177 (1954).

31) A.Odajima and T.Maeda, J. Polymer Sci., C-15, 55 (1966).

32) L.Pauling, "The Nature of Chemical Bonds" Cornell University Press, Ithaca, New York (1960).

33) J. de Boer, Physica, 1, 363 (1942).

34) P.Debye, Ann. d Phys., 39, 789 (1912).

35) A.A.Maradudin, E.W.Montroll and G.H.Weiss, Solid State Phys. suppl. 3 (1963).

Table-1 Symmetry coordinates in real number space

$$\begin{pmatrix} S_x^c(A_g) & S_x^s(A_g) \\ S_y^c(A_g) & S_y^s(A_g) \\ S_z^c(A_u) & S_z^s(A_u) \\ S_x^c(B_{3g}) & S_x^s(B_{3g}) \\ S_y^c(B_{3g}) & S_y^s(B_{3g}) \\ S_z^c(B_{3u}) & S_z^s(B_{3u}) \\ S_x^c(B_{1u}) & S_x^s(B_{1u}) \\ S_y^c(B_{1u}) & S_y^s(B_{1u}) \\ S_z^c(B_{1g}) & S_z^s(B_{1g}) \\ S_x^c(B_{2u}) & S_x^s(B_{2u}) \\ S_y^c(B_{2u}) & S_y^s(B_{2u}) \\ S_z^c(B_{2g}) & S_z^s(B_{2g}) \end{pmatrix} = \begin{pmatrix} +x_1 & -x_2 & +x_3 & -x_4 \\ +y_1 & -y_2 & -y_3 & +y_4 \\ +z_1 & +z_2 & -z_3 & -z_4 \\ +x_1 & -x_2 & -x_3 & +x_4 \\ +y_1 & -y_2 & +y_3 & -y_4 \\ +z_1 & +z_2 & +z_3 & +z_4 \\ +x_1 & +x_2 & +x_3 & +x_4 \\ +y_1 & +y_2 & -y_3 & -y_4 \\ +z_1 & -z_2 & -z_3 & +z_4 \\ +x_1 & +x_2 & -x_3 & -x_4 \\ +y_1 & +y_2 & +y_3 & +y_4 \\ +z_1 & -z_2 & +z_3 & -z_4 \end{pmatrix} \cdot \begin{pmatrix} \cos(\rho_1\delta) & \sin(\rho_1\delta) \\ \cos(\rho_2\delta) & \sin(\rho_2\delta) \\ \cos(\rho_3\delta) & \sin(\rho_3\delta) \\ \cos(\rho_4\delta) & \sin(\rho_4\delta) \end{pmatrix}$$

$\rho_1(h,k,l) = (h,k,l+1/4)$ $\qquad$ $\rho_3(h,k,l) = (h+\frac{1}{2},k+\frac{1}{2},l+1/4)$

$\rho_2(h,k,l) = (h,k,l-1/4)$ $\qquad$ $\rho_4(h,k,l) = (h+\frac{1}{2},k+\frac{1}{2},l-1/4)$

In this representation, the factor $(2N)^{-\frac{1}{2}}$ and summation about h, k, and l are omitted.

Table-2 Transformation matrix for symmetry coordinates, $U(\rho\delta)$

	$X_1(h,k,l)$	$X_2(h,k,l)$	$X_3(h,k,l)$	$X_4(h,k,l)$
$S^{(1)}(\delta)$	u_1^c	u_2^c	u_3^c	u_4^c
$S^{(2)}(\delta)$	u_1^c	u_2^c	$-u_3^c$	$-u_4^c$
$S^{(3)}(\delta)$	$-u_1^s$	u_2^s	$-u_3^s$	u_4^s
$S^{(4)}(\delta)$	$-u_1^s$	u_2^s	u_3^s	$-u_4^s$

$$u_1^c=\begin{bmatrix}\cos(\rho_1\delta) & 0 & 0\\ 0 & \cos(\rho_1\delta) & 0\\ 0 & 0 & -\sin(\rho_1\delta)\end{bmatrix} \quad u_1^s=\begin{bmatrix}\sin(\rho_1\delta) & 0 & 0\\ 0 & \sin(\rho_1\delta) & 0\\ 0 & 0 & -\cos(\rho_1\delta)\end{bmatrix}$$

$$u_2^c=\begin{bmatrix}-\cos(\rho_2\delta) & 0 & 0\\ 0 & -\cos(\rho_2\delta) & 0\\ 0 & 0 & -\sin(\rho_2\delta)\end{bmatrix} \quad u_2^s=\begin{bmatrix}-\sin(\rho_2\delta) & 0 & 0\\ 0 & -\sin(\rho_2\delta) & 0\\ 0 & 0 & -\cos(\rho_2\delta)\end{bmatrix}$$

$$u_3^c=\begin{bmatrix}\cos(\rho_3\delta) & 0 & 0\\ 0 & -\cos(\rho_3\delta) & 0\\ 0 & 0 & -\sin(\rho_3\delta)\end{bmatrix} \quad u_3^s=\begin{bmatrix}\sin(\rho_3\delta) & 0 & 0\\ 0 & -\sin(\rho_3\delta) & 0\\ 0 & 0 & -\cos(\rho_3\delta)\end{bmatrix}$$

$$u_4^c=\begin{bmatrix}-\cos(\rho_4\delta) & 0 & 0\\ 0 & \cos(\rho_4\delta) & 0\\ 0 & 0 & -\sin(\rho_4\delta)\end{bmatrix} \quad u_4^s=\begin{bmatrix}-\sin(\rho_4\delta) & 0 & 0\\ 0 & \sin(\rho_4\delta) & 0\\ 0 & 0 & -\cos(\rho_4\delta)\end{bmatrix}$$

$\rho_1=(h,k,l+1/4)$, $\rho_3=(h+\frac{1}{2},k+\frac{1}{2},l+1/4)$

$\rho_2=(h,k,l-1/4)$, $\rho_4=(h+\frac{1}{2},k+\frac{1}{2},l-1/4)$

X_1, X_2, X_3 and X_4 are Cartesian displacement coordinate vector of four atoms in the unit cell(h,k,l).

$(2N)^{-\frac{1}{2}}\Sigma_{(h,k,l)}$ is omitted in each term.

Table-3 Force constants and the equilibrium distance

	num. per unit cell	force constant		distance
K	4	4.0	md/Å	1.53 Å
H	4	0.59	md·Å	
Y	4	0.047	md·Å	
F	4	0.35	md/Å	2.5 Å
P_1	4	0.025		4.12
P_2	8	0.025		4.18
P_3	4	0.003		4.51

Table-4 The coefficient of phase differences in the dynamical matrix for acoustic branches.

ν_1	A_1=0.0143P_1	+0.0201P_2		
	B_1=0.0143P_1	+0.0201P_2	+0.0110P_3	
	C_1=	+0.0201P_2	+0.0003P_3	
ν_2	A_2=0.0035P_1	+0.0124P_2		
	B_2=0.0035P_1	+0.0124P_2	+0.0646P_3	
	C_2=	+0.0124P_2	+0.0161P_3	
ν_3	A_3=	+0.0033P_2		
	B_3=	+0.0033P_2	+0.0056P_3	
	C_3=	+0.0033P_2	+0.0014P_3	+0.0620

ν_1, ν_2 and ν_3 are acoustic branches along the a, b and c axes, respectively.

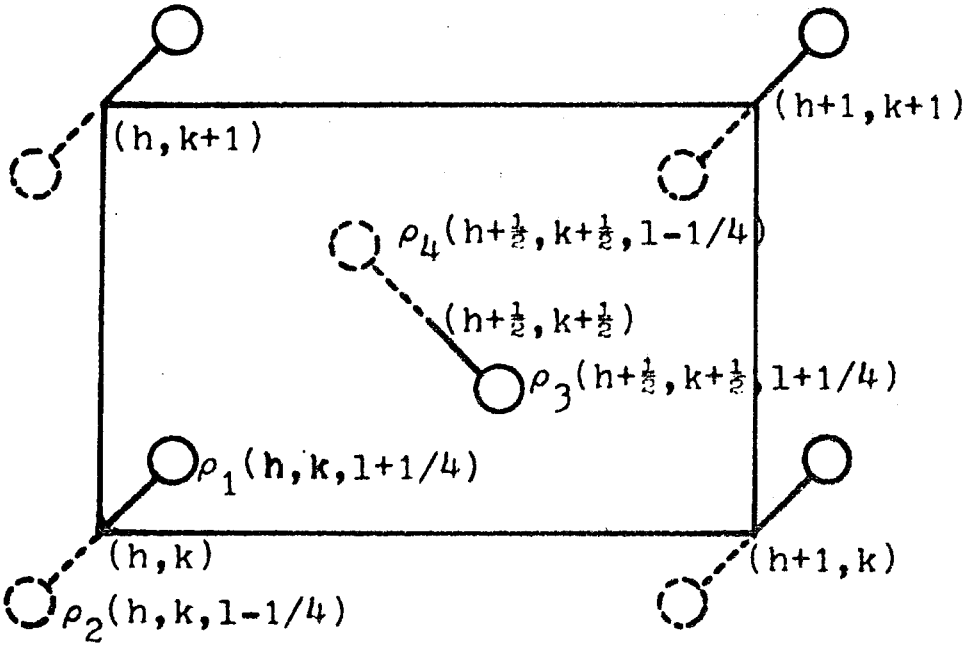

Fig. 1 Representative atoms and their index vectors in the unit cell (h,k,l)

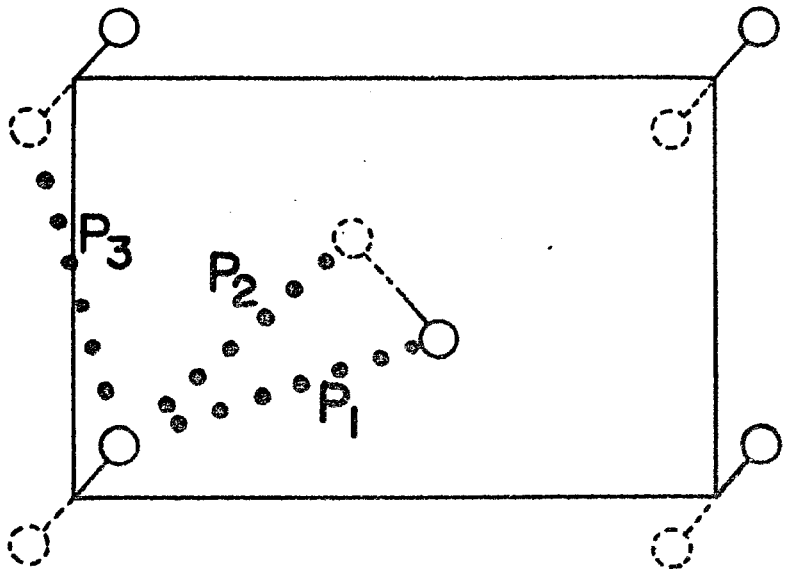

Fig. 2 The interchain potential in polyethylene crystal.

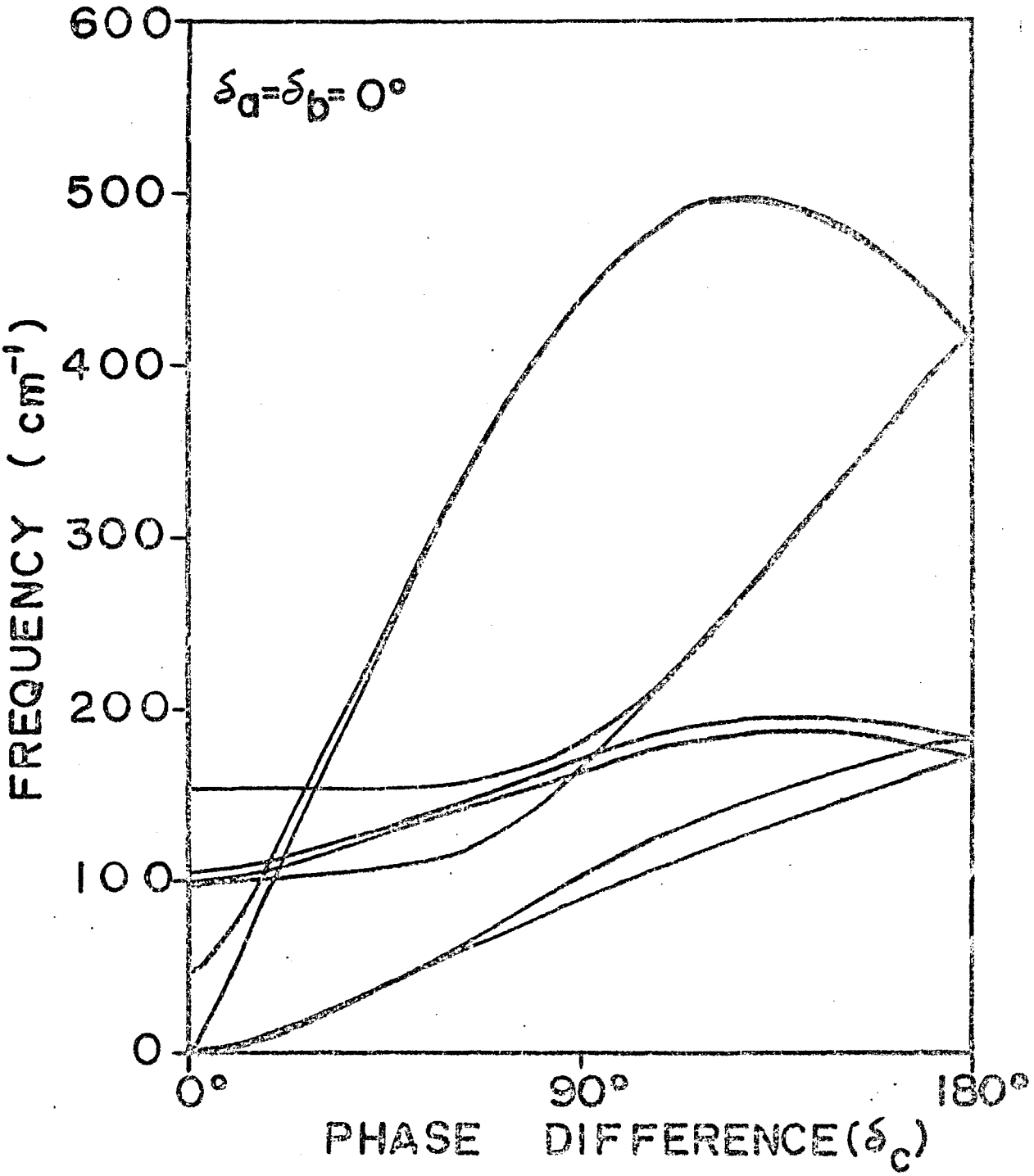

Fig. 3 Dispersion curves of vibrational frequency against the phase difference along the c axis.

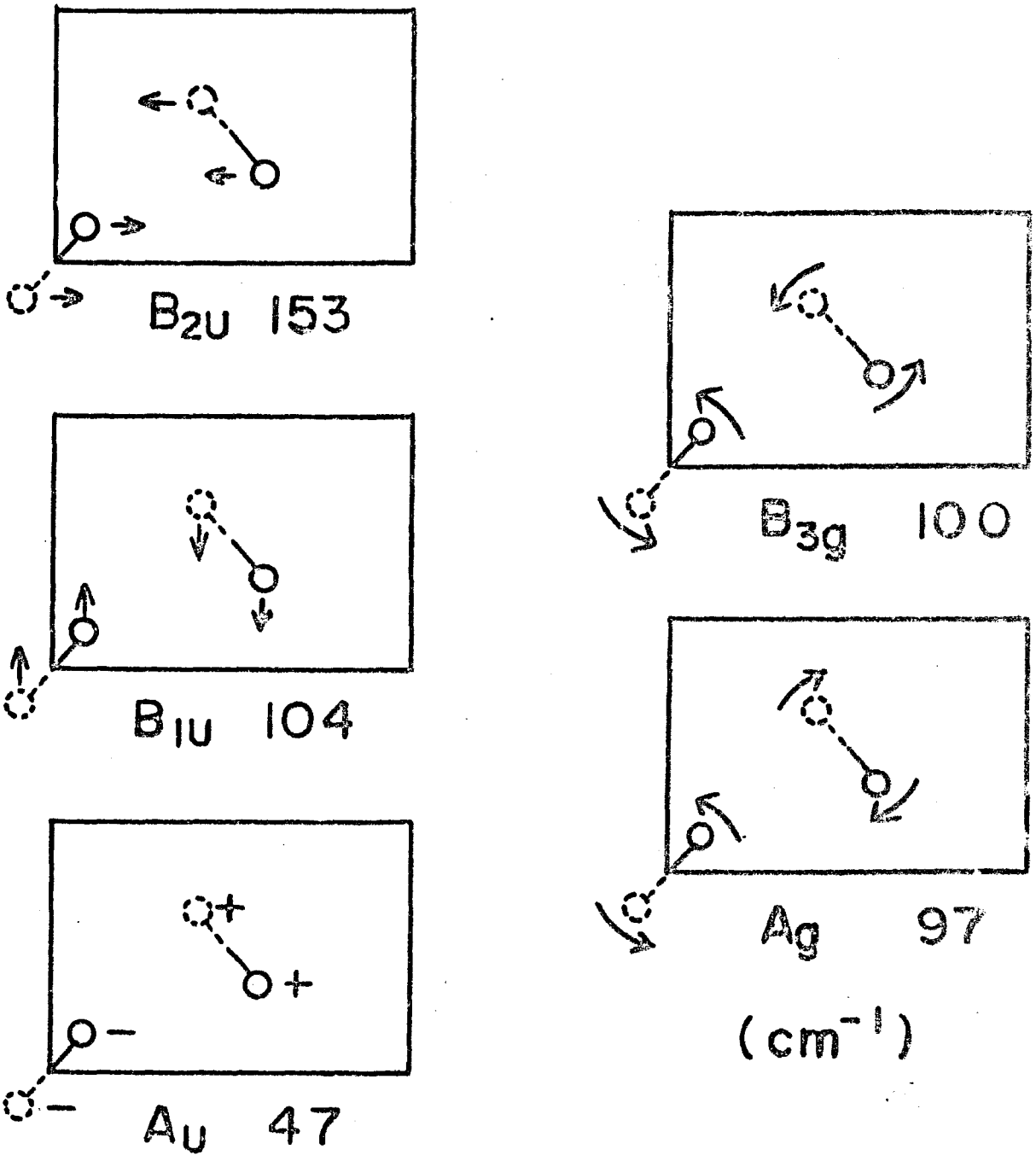

Fig. 4 Optical lattice vibrations of polyethylene crystal.

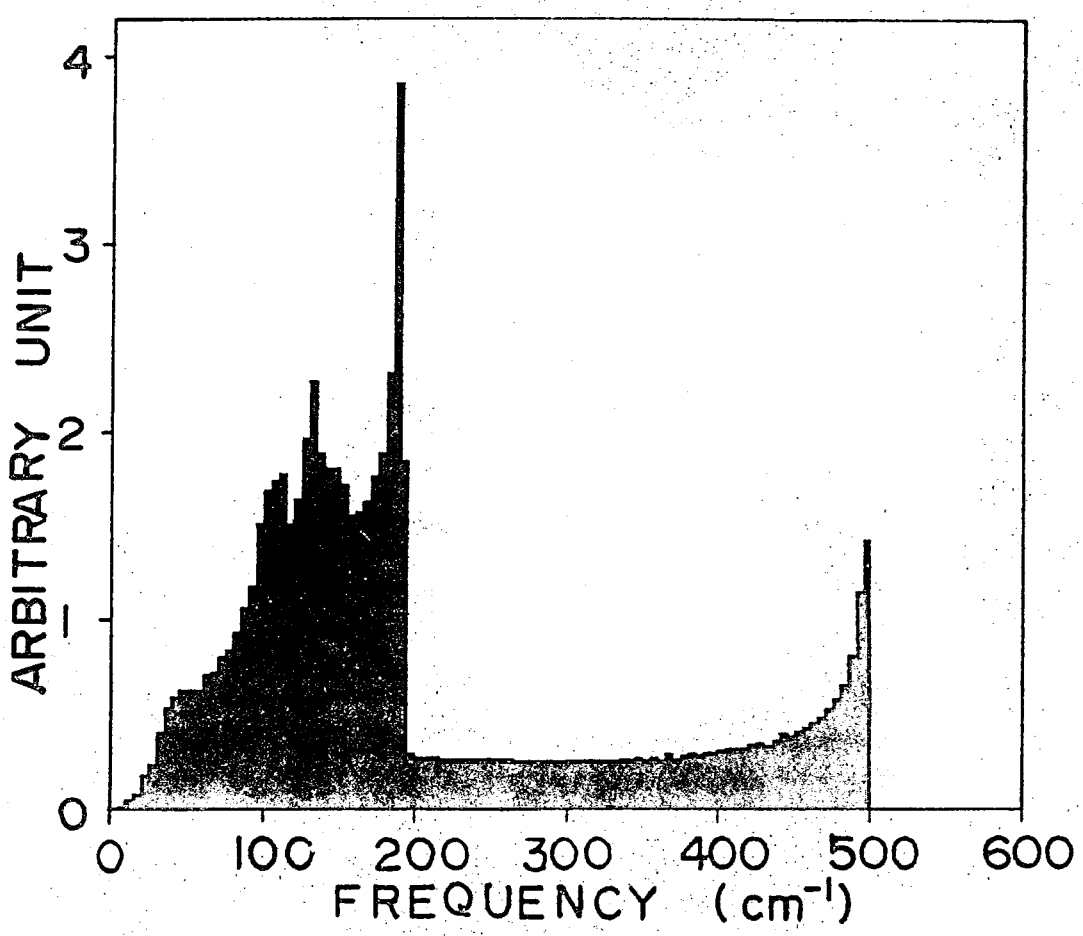

Fig. 5 The frequency distribution of polyethylene crystal. The number of vibrational modes per frequency interval of 5 cm^{-1} is plotted against the vibrational frequency.

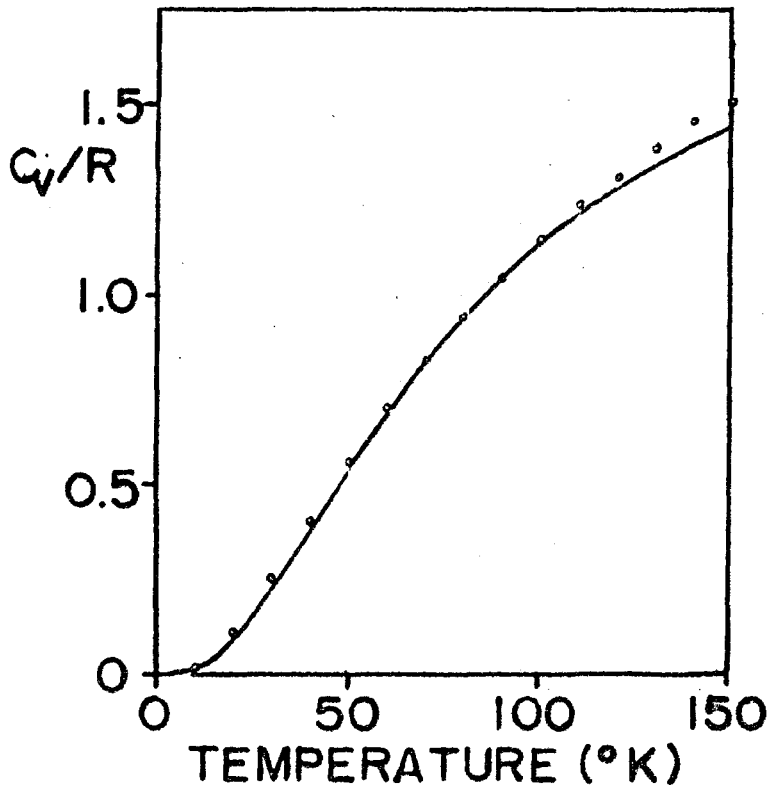

Fig. 6 The specific heat of polyethylene crystal. Open circles are experimental values[1] and solid line shows the calculated values.

CHAPTER II

NORMAL VIBRATIONS, INTERCHAIN FORCE FIELD, FREQUENCY DISTRIBUTION AND SPECIFIC HEAT OF POLYETHYLENE CRYSTAL

II-1 INTRODUCTION

Polyethylene crystal is the simplest polymer crystal and the systematic treatment about the dynamical properties is of great interest since various kinds of the experimental results have been obtained. Wunderlich has deduced the specific heat of crystal part of polyethylene by the use of extrapolation method about the crystallinity referring to all the observed values measured by others.[2] Tucker and Reese have found that the specific heat of the polyethylene crystal is proportional to T^3 below $9^\circ K$ whereas that of amorphous part has excess heat capacity corresponding to $\theta_E=23^\circ K$ even at the lowest temperature.[3] Afterwards Wunderlich has confirmed his presumptive value by measuring the specific heat of single crystal of polyethylene. These values seem to lie nearly on the theoretical curve derived by Tarasov[5] who regarded polymer chains as elastic rods with weak interactions between the nearest neighbors. However, Tarasov's model cannot be used for analyzing other physical properties particularly spectroscopic properties of polymer crystals.

On the other hand, infrared bands of methylene rocking and scissoring vibrations in normal hydrocarbon crystals show band splitting due to intermolecular interactions.[6-7] These band splitting have also been observed in high density

polyethylene and their polarizations have been investigated.[8-9] Now the intrachain potential functions about molecular vibrations have been systematically studied and reliable force constants are available.[10] Especially for n-paraffin molecules, detailed analysis of spectroscopic data have been carried out.[11-13] The general theory of molecular vibrations of chain molecules has already been established.[14-16] Accordingly, it is practical to treat dynamical properties of polyethylene crystal self-consistently on the basis of the interchain potential as well as the intrachain potential functions.

General method of treating crystal vibrations and related solid state properties has been studied[17] and the method was confirmed in the preliminary calculation about polyethylene crystal, in the preceding chapter, where methylene groups were regarded as single dynamic unit. In the present treatment the Cartesian symmetry coordinates are applied to more realistic model and the frequency distribution, the specific heat, the lattice vibrations, the splitting of the intrachain vibrations and Young's moduli are calculated with the intrachain and interchain potential functions.

II-2 CRYSTAL STRUCTURE

The crystal structure of orthorhombic polyethylene crystal has been analysed by Bunn with X-ray diffraction method.[18] There are four methylene groups per unit cell and two molecular chains pass through a unit cell along the c axis. Symmetry of the unit cell is isomorphous to point group D_{2h}. The setting angle of the skeletal zigzag plane

with respect to the a axis (θ in Fig. 1) has been reported as 48.7° by Bunn[18] but the value seems uncertain. Teare[19] has obtained 47.7° for orthorhombic single crystal of $C_{36}H_{74}$. Salem[20] has assumed 44° on the calculation of the cohesive energy about normal paraffin molecules. Shearer and Vand[21] has obtained $41^{\circ}23'$ for monoclinic $C_{36}H_{74}$, while Smith[22] got 42° analysing the structure of several single crystals of normal hydrocarbon molecules. Snyder has measured the intensity ratio of polarized infrared bands which are B_{1u} and B_{2u} components of the band splitting and concluded that θ should be smaller than 45°.[6] This setting angle might depend upon temperature. Since, in the present study, the dynamical properties at low temperature are treated, the lattice constants at $-196^{\circ}C$ obtained by Swan[23] were used and was assumed to be 45°. The structural parameters used are $a_o=7.155$, $b_o=4.899$, $c_o=2.547$, d(C-C)=1.54, and d(C-H)=1.09 Å. The skeletal bond angle ($\angle$C-C-C) is usually larger than the tetrahedral angle in normal hydrocarbon crystals and $\angle C-C-C=111^{\circ}47'$, calculated from the lattice constants, was used while $\angle$H-C-H is assumed to be tetrahedral angle.

II-3 POTENTIAL FUNCTION

Schachtschneider and Snyder[13] has carried out the force field calculation of normal hydrocarbon molecules from C_2H_6 to $C_{14}H_{30}$ and $-(CH_2)_n-$. They obtained the force constants for valence force field which can reproduce 270 frequencies of fundamentals within 0.25% of the standard deviation. Since five coordinates of six valence angles around carbon atom are

independent, local symmetry coordinates were used. The definition is same with those used by Tasumi[12] whereas the transformation matrix is slightly modified as shown in Table 1 on account of the departure of the skeletal valence angle from the tetrahedral angle. The coordinates are shown in Fig. 2. Δr^{Hs} is CH_2 symmetric stretching, $\Delta\delta$ is CH_2 scissoring, $\Delta\gamma$ is skeletal bending, $\Delta\alpha^{W}$ is CH_2 wagging, and Δr^{C} is skeletal stretching coordinates which are in-plane vibrations. Δr^{Ha} is CH_2 antisymmetric stretching, $\Delta\alpha^{r}$ is CH_2 rocking, $\Delta\alpha^{t}$ is CH_2 twisting and Δt is internal rotation coordinates which are out-of-plane vibrations. The potential energy matrix for intrachain coordinates are shown in Table 2 which was transformed from the force constants of valence force field except for that of internal rotation. Since internal rotation vibration in normal paraffin molecules is so difficult to observe in spectroscopic measurements that the force constant is not definite. Accordingly the diagonal term of Δt was adjusted as 0.075 mdÅ with reference to the observed values of the specific heat near 60°K[1].

Previously Tasumi and Shimanouchi[24] have treated the lattice vibrations of k=0 modes of polyethylene crystal incorporating four types of H···H interaction terms. The set of force constants, determined from the band splitting, can reproduce the frequency of the infrared active lattice vibration. They correspond to the force constants at room temperature. The specific heat below 10°K calculated from the potential is slightly small. On the other hand, the thermal expansion has been found appreciable along the a axis, therefore the interatomic distances at low temperature

are different from those at room temperature. Then the effective force constants will vary with temperature.

In the present study, the same interchain interaction terms were incorporated and the force constants were determined with reference to the observed values of the specific heat below $10^{\circ}K$[3], infrared active lattice vibration[25] and band splitting at $-196^{\circ}C$[6]. Thus adjusted force constants and equilibrium atomic distance at $-196^{\circ}C$ are shown in Table 3.

II-4 LOW FREQUENCY CRYSTAL VIBRATIONS

Derivation of basic equations for the crystal vibrations is provided in Chapter I and the same notation is used here without notice. A practical method of treating low frequency modes of crystal vibrations are derived here.

Crystal vibrations are specified with the set of δ_a, δ_b and δ_c, which are the phase difference of vibrational displacement between adjacent unit cells along the a, b, and c axes, respectively. Since there are twelve atoms per unit cell, there are thirty-six vibrations for a given set of phase differences. Accordingly, thirty-six Cartesian symmetry coordinates were derived from

$$S(\delta) = \sum_{\rho} U(\rho,\delta)X(\rho) \qquad (2.1)$$

$U(\rho,\delta)$ is an unitary matrix for symmetry transformation, which is given in Table 4 and explained later. The symmetry coordinates are represented as linear combination of real normal coordinates of crystal

$$S(\delta) = M_S^{-\frac{1}{2}} L_S(\delta) Q(\delta) \qquad (2.2)$$

$L_S(\delta)$ is an eigenvector matrix of the dynamical matrix and is normalized to unity. The dynamical matrix and its eigenvalue matrix are given by (2.3) and (2.4), respectively.

$$\mathbf{D}_S(\delta) = \mathbf{M}_S^{-\frac{1}{2}}\mathbf{F}_S(\delta)\mathbf{M}_S^{-\frac{1}{2}} \tag{2.3}$$

$$\mathbf{\Lambda}(\delta) = \tilde{\mathbf{L}}_S(\delta)\mathbf{D}_S(\delta)\mathbf{L}_S(\delta) \tag{2.4}$$

$$\tilde{\mathbf{L}}_S(\delta)\mathbf{L}_S(\delta) = \mathbf{E} \tag{2.5}$$

Since the dimension of $\mathbf{D}_S(\delta)$ is 36, diagonalization of $\mathbf{D}_S(\delta)$ for many values of δ requires excessively long computation hours. On the other hand, the preliminary calculation shows the vibrational frequencies change sensitively with δ_c whereas they vary little with δ_a or δ_b. It comes from the fact that the intrachain force constants are much larger than the interchain force constants, that is, from the large anisotropy of the force field of the crystal. Accordingly, the actual computation was carried out in two steps described below. At the first step, the dynamical matrix corresponding to the intrachain potential was diagonalized. Then, at the second step, the interchain potential was incorporated and the corresponding dynamical matrix was diagonalized.

Supposing $\mathbf{F}_S^M$ and $\mathbf{F}_S^C$ are the potential energy matrices of the intrachain and interchain potential, respectively, then $\mathbf{F}_S^M$ depends only upon δ_c while $\mathbf{F}_S^C$ depends upon δ_a, δ_b and δ_c. The dynamical matrices $\mathbf{D}_S^M(\delta_c)$ and $\mathbf{D}_S^C(\delta_a,\delta_b,\delta_c)$, corresponding to $\mathbf{F}_S^M(\delta_c)$ and $\mathbf{F}_S^C(\delta_a,\delta_b,\delta_c)$, are derived in accordance with (2.3) as

$$\mathbf{D}_S(\delta) = \mathbf{D}_S^M(\delta_c) + \mathbf{D}_S^C(\delta_a,\delta_b,\delta_c) \tag{2.6}$$

where

$$\mathbf{D}_S^M(\delta_c) = \mathbf{M}_S^{-\frac{1}{2}}\mathbf{F}_S^M(\delta_c)\mathbf{M}_S^{-\frac{1}{2}} \tag{2.7}$$

$$\mathbf{D}_S^C(\delta_a,\delta_b,\delta_c) = \mathbf{M}_S^{-\frac{1}{2}}\mathbf{F}_S^C(\delta_a,\delta_b,\delta_c)\mathbf{M}_S^{-\frac{1}{2}} \tag{2.8}$$

$\mathbf{D}_S^M(\delta_c)$ is factorized at least into four diagonal blocks $\mathbf{d}_{\kappa\kappa}^M(\delta_c)$ ($\kappa=1\cdots4$) each of which is a nine dimensional matrix

and is associated with the symmetry coordinate vector characterized by $S^{\kappa}(\delta)$ of Table 4. Since the following relations are satisfied about $\mathbf{d}^{M}_{\kappa\kappa}(\delta_c)$,

$$\mathbf{d}^{M}_{11}(\delta_c) = \mathbf{d}^{M}_{22}(\delta_c) = \mathbf{d}^{M}_{33}(2\pi-\delta_c) = \mathbf{d}^{M}_{44}(2\pi-\delta_c)$$

$$\mathbf{d}^{M}_{\alpha\beta}(\delta_c) = 0 \text{ for } \alpha\neq\beta,$$

the calculation of $\mathbf{L}^{M}_{S}(\delta_c)$, the eigenvector matrix of $\mathbf{D}^{M}_{S}(\delta_c)$, is reduced quite simple. The matrix elements of $\mathbf{D}^{C}_{S}(\delta_a,\delta_b,\delta_c)$ is relatively small and the eigenvectors of intrachain optical vibrations are little influenced by the interchain interactions, and therefore $\mathbf{L}^{M}_{S}(\delta_c)$ is almost identical with $\mathbf{L}_{S}(\delta_a,\delta_b,\delta_c)$ for twenty-four modes above 700 cm^{-1}. However, the remaining eight modes (acoustic branches of single chain) are strongly influenced by $\mathbf{D}^{C}_{S}(\delta_a,\delta_b,\delta_c)$. Accordingly, the eight columns corresponding to low frequency modes are picked up and brought into $\mathbf{L}^{M}_{1}(\delta_c)$, a new matrix of 36 rows and 8 columns. The similarity transformation of $\mathbf{D}_{S}(\delta)$ with $\mathbf{L}^{M}_{1}(\delta_c)$ yields

$$\begin{aligned}\mathbf{H}_{S}(\delta_a,\delta_b,\delta_c) &= \widetilde{\mathbf{L}}^{M}_{1}(\delta_c)\left[\mathbf{D}^{M}_{S}(\delta_c) + \mathbf{D}^{C}_{S}(\delta_a,\delta_b,\delta_c)\right]\mathbf{L}^{M}_{1}(\delta_c)\\ &= \mathbf{\Lambda}^{M}_{1}(\delta_c) + \widetilde{\mathbf{L}}^{M}_{1}(\delta_c)\mathbf{D}^{C}_{S}(\delta_a,\delta_b,\delta_c)\mathbf{L}^{M}_{1}(\delta_c) \qquad (2.9)\end{aligned}$$

where $\mathbf{\Lambda}^{M}_{1}(\delta_c)$ is an eigenvalue matrix of low frequency intrachain vibrations. Thus dirived $\mathbf{H}_{S}(\delta_a,\delta_b,\delta_c)$ is a dynamical matrix for low frequency crystal vibrations. Supposing $\mathbf{L}_{H}(\delta_a,\delta_b,\delta_c)$ is the eigenvector matrix of $\mathbf{H}_{S}(\delta_a,\delta_b,\delta_c)$, then the corresponding eight columns of $\mathbf{L}_{S}(\delta_a,\delta_b,\delta_c)$ are calculated from

$$\mathbf{L}^{1}_{S}(\delta_a,\delta_b,\delta_c) = \mathbf{L}^{M}_{1}(\delta_c)\cdot\mathbf{L}_{H}(\delta_a,\delta_b,\delta_c) \qquad (2.10)$$

where $\mathbf{L}^{1}_{S}(\delta_a,\delta_b,\delta_c)$ is (36×8) submatrix of $\mathbf{L}_{S}(\delta_a,\delta_b,\delta_c)$ and

$$\mathbf{\Lambda}_{H}(\delta) = \widetilde{\mathbf{L}}_{H}(\delta)\mathbf{H}_{S}(\delta)\mathbf{L}_{H}(\delta) \qquad (2.11)$$

$$\widetilde{\mathbf{L}}_{H}(\delta)\mathbf{L}_{H}(\delta) = \mathbf{E} \qquad (2.12)$$

The coordinates, which are shifted by $\pi/2$ in phase angle from the present symmetry coordinates, form degenerate pair with the present coordinates while the existence of center of inversion removes $D_2(\delta)$, the cross term between two types of coordinates in the doubled dynamical matrix (section I-3). Therefore, in this case, the Hermitian matrix (complex dynamical matrix) is transformed into two identical real-number symmetric matrices. The other symmetry coordinate vector of the degenerate pair may be given by the symmetry transformation $\bar{U}(\rho,\delta)$. Then the atomic displacement vector of atoms in ρth unit cell is derived as

$$X(\rho) = \sum_{\delta} \tilde{U}(\rho,\delta)M_S^{-\frac{1}{2}}L_S(\delta)Q(\delta) + \tilde{\bar{U}}(\rho,\delta)M_S^{-\frac{1}{2}}L_S(\delta)\bar{Q}(\delta) \quad (2.13)$$

where $Q(\delta)$ and $\bar{Q}(\delta)$ are degenerate pair of real normal coordinate vectors. In the present approximation, the atomic displacement due to low frequency crystal vibrations is represented as

$$X(\rho) = \sum_{\delta} \tilde{U}(\rho,\delta)M_S^{-\frac{1}{2}}L_1^M(\delta_c)L_H(\delta)Q(\delta)_H + \tilde{\bar{U}}(\rho,\delta)M_S^{-\frac{1}{2}}L_1^M(\delta_c)L_H(\delta)\bar{Q}(\delta)_H \quad (2.14)$$

where $Q(\delta)_H$ and $\bar{Q}(\delta)_H$ are degenerate pair of vectors of eight normal coordinates corresponding to low frequency modes. The equation (2.14) is of great importance in treating the neutron scattering cross sections and temperature factor of X-ray diffraction.

II-5 SYMMETRY COORDINATES

Symmetry coordinates are constructed in accordance with the consideration of the preceding chapter (I-4). As n=12, $n_s=3$, $m_\beta=4$ ($\beta=H_1,H_2,C$) in this case, there are three set of twelve symmetry coordinates. Both of $S(\delta)$ and $X(\rho)$ in (2.1) are vectors of order 36 and they are represented with subvectors $S^\kappa(\delta)$ and $X_j(\rho)$ of ninth order, respectively

$$\widetilde{S(\delta)} = \left[\widetilde{S^1}(\delta)\ \widetilde{S^2}(\delta)\ \widetilde{S^3}(\delta)\ \widetilde{S^4}(\delta)\right] \tag{2.16}$$

$$\widetilde{X(\rho)} = \left[\widetilde{X}_1(\rho)\ \widetilde{X}_2(\rho)\ \widetilde{X}_3(\rho)\ \widetilde{X}_4(\rho)\right] \tag{2.17}$$

$S^\kappa(\delta)_\alpha$ which is α component (α=x,y,z) of $S^\kappa(\delta)$, is defined as three component subvector by

$$\widetilde{S^\kappa(\delta)} = \left[\widetilde{S^\kappa(\delta)}_x\ \widetilde{S^\kappa(\delta)}_y\ \widetilde{S^\kappa(\delta)}_z\right] \tag{2.18}$$

$$\widetilde{S^\kappa(\delta)}_\alpha = \left[S^\kappa(\delta)^{H_1}_\alpha\ S^\kappa(\delta)^{H_2}_\alpha\ S^\kappa(\delta)^{C}_\alpha\right]$$

where β in $S^\kappa(\delta)^\beta_\alpha$ characterizes the type of atoms in the unit cell as indicated in Fig. 1 and κ denotes the type of symmetry coordinates and α represents the Cartesian component. The index j in $X_j(\rho)$ is given to each methylene group and therefore $X_j(\rho)$ is nine component vector of Cartesian displacement coordinates of j-th methylene group in ρ-th unit cell. The index vector of atoms in the ρ-th unit cell is written simply as ρ_j.

$$\rho_1 = (h,k,1+1/4) \qquad \rho_3 = (h+\tfrac{1}{2},k+\tfrac{1}{2},1+1/4)$$

$$\rho_2 = (h,k,1-1/4) \qquad \rho_4 = (h+\tfrac{1}{2},k+\tfrac{1}{2},1-1/4)$$

$X_j(\rho)$ is represented with three subvectors as

$$X_j(\rho) = \left[\Delta x_j(\rho)\ \Delta y_j(\rho)\ \Delta z_j(\rho)\right] \tag{2.21}$$

and the constituent subvectors are given by

$$\Delta\alpha_j(\rho) = \left[\Delta\alpha_j^{H_1}\ \Delta\alpha_j^{H_2}\ \Delta\alpha_j^{C}\right]$$

where $\Delta\alpha_j^\mu$ (α=x,y,z) is the α component of atomic displacement vector of μ-th atom in the j-th methylene group. Each element of $\mathbf{U}(\rho,\delta)$ of Table 4 relates subvector $\mathbf{S}^\kappa(\delta)_\alpha$ with subvector $\Delta\alpha_j$, therefore each element denotes three dimensional constant matrix.

II-6 RESULTS

For the set of $\delta_a=\delta_b=\delta_c=0$, the symmetry coordinates belong to one of the irreducible representations of point group D_{2h}. The symmetry property of $\mathbf{S}^\kappa(0)_\alpha$ and its species are shown in Table 5. Frequencies of k=0 vibrational modes were obtained from $\mathbf{D}_S(0)$ and the calculated band splittings are compared with the observed results[6] in Table 6, where branch number follows Tasumi's notation[12]. The calculated band splitting of CH_2 scissoring, $\nu_2(\pi)$, and CH_2 rocking, $\nu_8(\pi)$, are slightly smaller than the observed values at -196°C, since the observed value of the specific heat below 10°K has also been referred in the adjustment of the inter-chain force constants. ν_5 is skeletal bending branch and ν_9 is internal rotation branch, both of which would be acoustic branches of an isolated chain. In the crystal, three of them, that is, $\nu_5(\pi)$, $\nu_9(\pi)$ and $\nu_5(0)$ are the limit of acoustic branches associated with three translations along the a, b and c axes, respectively. The remaining five modes are optical modes of lattice vibrations, whose calculated frequencies and modes are shown in Fig. 3. B_{1u} and B_{2u} are infrared active while A_g and B_{3g} are Raman active. A_u is optically inactive mode.

The dispersion curves of vibrational frequency against phase difference show drastic change along δ_c whereas they change little along δ_a or δ_b. As an example, the dispersion curves along δ_c for $\delta_a=\delta_b=0$ is shown in Fig. 4. Since, on the variation of δ_c, the eight modes change from pure lattice vibrations to the intrachain vibrations such as skeletal bending and internal rotation vibration, the dispersion curves along δ_c becomes similar to those of isolated chain. On the other hand, when $\delta_c=0$, the interchain potential does not contribute to lattice vibrations but the contribution of the interchain potential to lattice vibrations varies with δ_a or δ_b. Therefore, the dispersion curves along δ_a and δ_b are similar to those of molecular crystals[26]. All of the dispersion curves along the special direction in the first Brillouin zone are calculated and described in Chapter IV.

Frequency distribution was made with the method described in section I-6. As the representative values of δ_a and δ_b, nine points (10°, 30°, 50°, 70°, 90°, 110°, 130°, 150°, 170°) and as those of δ_c, ten points (0°, 5°, 10°, 20°, 40°, 60°, 90°, 120°, 150°, 180°) were adopted. For each of these 810 points, $H_S(\delta)$ was derived and diagonalized. The vibrational frequencies at the intermediate points between the representative points, were interpolated at 20' intervals of δ_c with (1.16) and thus about 350,000 frequencies below 700 cm^{-1} were collected in the frequency distribution. In a histogram of Fig. 5, the fraction of number of vibrational modes is drawn against the frequency division of 4 cm^{-1}. Two prominent peaks at 560 and 190 cm^{-1} correspond to the

cut-off of the skeletal bending and the internal rotation vibrations, respectively. These peaks had been anticipated from the normal coordinates treatment of isolated chain.[12] From the present study, several new peaks are expected. The broad peak near 150cm^{-1} arises from in overall rotatory vibrations around the chain axis. The peak at 90 cm^{-1} is due to the antiparallel translatory vibrations perpendicular to the chain axis. The broad peak near 60cm^{-1} is associated with the antiparallel translatory vibration along the chain axis which is really invariant on the change of δ_a and δ_b but varies rapidly with δ_c. The existence of these peaks have been, in fact, confirmed by the energy spectrum of neutron inelastic scattering.[27] However, the cross section of neutron inelastic scattering depends upon the atomic displacement besides frequency distribution, it is treated in detail in Chapter VI.

The specific heat below 150°K was calculated from (1.19) and the frequency distribution where the distribution function used is for every wave number and is normalized to 2 per CH_2 group In Fig. 6, the calculated specific heat is compared with the observed values. Solid line denotes the calculated value and open circles represent the experimental values extrapolated to 100% crystallinity by Wunderlich[1]. Good agreement is obtained below 100°K. Near 100°K the intrachain optical modes begin to contribute to the specific heat and it is shown in Table 7.

Young's moduli perpendicular to the chain axis depends

primarily upon the interchain potential, because the force constants of the intrachain coordinates are much larger than those of the interchain coordinates. Young's moduli were derived in the preceding chapter (I-8) under the assumption of rigid molecule. From the present potential function, Young's moduli perpendicular to the chain axis at -196°C were calculated as

$$E_a = 7.0 \qquad E_b = 9.7 \qquad (\times 10^{10} \text{dyne/cm}^2)$$

and Poison's ratio were calculated as follows;

$$(\Delta a/a_0):(\Delta b/b_0):\theta = 1.0 : -0.4 : -0.7$$

(under tension along the a axis)

$$(\Delta a/a_0):(\Delta b/b_0):\theta = -0.5 : 1.0 : 0.3$$

(under tension along the b axis)

From the Poison's ratio, the length of b axis becomes shorter and the molecular chain rotates to the a axis when crystal is drawn along the a axis. Sakurada et al.[28a] have measured the Young's moduli perpendicular to the chain axis with the use of X-ray diffraction technique. The observed values were E_a=3.1 and E_b=3.8. Recently the measurement has been carried out again on less branched polyethylene sample and thus improved value is E_a=5.0 while the diffraction spot was too weak for E_b to be observed.[28b] Müller[29] has measured the linear compressibility and obtained E_a=10 and E_b=9.0 for $C_{23}H_{48}$. As for the interchain potential, normal paraffin is almost identical with polyethylene and Müller's values are also applicable to polyethylene crystal. Young's moduli calculated from the present potential is intermediate of

two observed values.

II-7 DISCUSSIONS

Remarkable development in the present study lies on making use of $H_S(\delta)$, the dynamical matrix of low frequency crystal vibrations. Great care was given to get correct $L_S^M(\delta_c)$ and to know the limitation of the exactness of the calculated results. As one of the examinations of the present treatment, the eigenfrequency of crystal vibrations for arbitrary phase difference was obtained from the diagonalization of $D_S(\delta)$. The eigenfrequencies of $H_S(\delta)$ are compared with those from $D_S(\delta)$ in Table 8. As δ_c gets larger, $\lambda_1^M(\delta_c)$ becomes larger and then the perturbation by $D_S^C(\delta)$ has less effect upon $\lambda_H(\delta)$. The deviation of the eigenfrequency of $H_S(\delta)$ from that of $D_S(\delta)$ was confirmed to be at most 3 cm^{-1}. Since the frequency of lattice vibrations of k=0 modes is calculated directly from $D_S(0)$, it is exact though the peak position in the frequency distribution is justified within 3 cm^{-1}.

The intrachain potential function obtained by Tasumi[12] is very similar to Schachtschneider's potential except for the skeletal bending force constant. The former gives the cut-off of the skeletal bending branch near 500cm^{-1} while the latter gives rise to the cut-off at 560cm^{-1}. Schaufele[30] has measured the frequency of accordion vibrations of various normal hydrocarbon crystals with laser Raman spectrum and found the Raman lines at 536 and 556 cm^{-1} for $C_{94}H_{190}$. Therefore the cut-off of the skeletal bending branch might

be above 500 cm^{-1}. Young's moduli along the chain axis calculated from Tasumi's potential is comparable with the observed value[28a] and that from Schachtschneider's is a little larger. Since the complete single crystal is not used on the measurement of Young's moduli of polyethylene, the observed value might be the least limit. At the present stage, the observed frequency of laser Raman spectrum seems more reliable than the Young's moduli, the intrachain potential function obtained by Schachtschneider[13] was adopted. The diagonal term of At is commonly set to be 0.108 mdÅ for many hydrocarbon molecules. The vibration is optically inactive for planar zigzag structure and the presumptive value from C_2H_6 is not always appropriate to polyethylene crystal. On the other hand, the specific heat from 30°K to 70°K is fairly sensitive to peak position of internal rotation branch. Accordingly, the force constant was adjusted as 0.075 mdÅ so as to reproduce well the specific heat near 60°K with trial and error method.

The calculated specific heat deviates from the observed values above 120°K. Though seven freedoms are left per one methylene group, the contribution of methylene symmetric and anti-symmetric stretching vibrations are negligible below 150°K. Appropriate representative frequencies were picked up from the dispersion curves of isolated chain and their contribution to the specific heat was calculated. Thus estimated value is as large as 0.002 at 100°K and 0.038 at

150°K which are mainly due to methylene rocking vibrations. Even if the contribution of optical branch is added to that of lattice vibrations, the calculated value is slightly smaller than the observed one. Anharmonicity of the potential function would induce the mutual interaction of normal coordinates and also make the separation of vibrational energy levels smaller. The additional heat capacity due to these two effects is proportional to T at relatively high temperature. Accordingly the incorporation of the anharmonicity might improve the calculated value of the specific heat.

The lattice vibrations for $\delta_a=\delta_b=\delta_c=0$ depends upon the interchain force constants. The eigenvalues of five optical modes are given by

$$\begin{aligned}
A_u \quad & \lambda_z = 0.1117P_1 + 0.1260P_2 \\
B_{1u} \quad & \lambda_y = 0.4127P_1 + 0.1100P_2 + 0.0408P_3 \\
B_{2u} \quad & \lambda_x = 0.0460P_1 + 0.3343P_2 + 0.2443P_3 \\
B_{3g} \quad & \lambda_{rot} = 1.8032P_1 + 0.0303P_2 + 0.1365P_3 \\
A_g \quad & \lambda_{rot} = 0.0016P_1 + 0.9480P_2 + 0.4914P_3
\end{aligned} \tag{2.23}$$

where λ is $(4\pi^2c^2\nu^2\times10^5/N_0)$($N_0$; Avogadro's number) and P_i is the interchain force constant represented in (mdyne/Å). When the setting angle (θ in Fig. 1) is altered, the coefficients in (2.23) change a little. Schaufele[31] has measured Raman effect of polyethylene with laser source and found two Raman lines at 167 and 122 cm^{-1}. They are not confirmed to be due to lattice vibrations of the crystal. The frequency of B_{3g}, calculated from the present potential is in close agreement with one of the observed values ($122cm^{-1}$), whereas the other is not in so good agreement. Infrared active

lattice vibrations are calculated at 73cm^{-1}(B_{1u}) and 93cm^{-1} (B_{2u}). One of them has been really observed at 73cm^{-1} (298°K)[32] and at 79cm^{-1}(100°K)[25]. It has been confirmed that the band comes from the crystal part of polyethylene[25] and that the band shows reasonable shift by deutration[33]. The polarization of the band was measured to be parallel to the a axis[34]. Since B_{1u} includes dipole moment along the a axis, the assignment became confident. Dean and Martin[35] has found the other band at 109cm^{-1} at 2°K. However, the band is so weak that it is not definite, at present stage, for the band to be due to B_{2u} lattice vibration. Though we have measured the far infrared spectrum of high density polyethylene at 70°K with thick sample, we could not find sharp absorption peak. Further investigation is necessary, especially on the dependency of the band intensity upon the crystallinity.

Tasumi and Krimm[36] has studied the reason of the weakness of the infrared band of B_{2u} lattice vibration. The possibility that only B_{1u} band borrows the band intensity from B_{1u} component of methylene rocking vibration was concluded to be unlike. The assumption that two bands overlap at 79cm^{-1}(at 77°K) lead us to unreasonable set of force constants.

The dipole moment of methylene group is so small that dipole-dipole interaction or -multipole interaction might not be significant. Tasumi and Krimm[36] has examined it theoretically and shown that the frequency of lattice

vibrations is little influenced with dipole interactions, though there was some ambiguity about the position of dipole-moment of methylene group. Accordingly van der Waals' potential seems sufficient as for interchain H···H interaction. On the other hand, Harada and Shimanouchi[37] have treated the lattice vibrations of benzene crystal, assuming several types of intermolecular potential between carbon-hydrogen and hydrogen-hydrogen. The force constants adjusted with reference to the observed values of band splitting and lattice vibration lie on the reasonable curve with regard to the atomic distances. From the curve, the force constant for C···H coordinate in polyethylene is presumed to be at most 0.0028 md/Å for the shortest distance of 3.21 Å. As shown in Fig. 7, the atomic distances for C···H is relatively large. Accordingly the C···H potential might contribute little to the frequency of lattice vibrations.

In the present study, any analytical function is not used on the determination of the interchain force constants. In this sence, the force constants obtained here are experimental. On the other hand, theoretical potential function of nonbonded hydrogens have been studied in various way.[38] Since the force constant is the second derivative of the potential function, the values at the corresponding atomic distances in polyethylene crystal were estimated from these theoretical potential functions and are shown in Table 9. The band splitting for methylene rocking and scissoring vibrations and the frequency of B_{1u} lattice vibration,

calculated from the force constants, are also shown in Table 9. The sets of theoretical force constants provide commonly large band splitting for methylene rocking whereas small value for methylene scissoring vibration. Tasumi's set of force constants gives rise to good fit to the observed values of band splittings and B_{1u} lattice vibration but the specific heat below $10^{\circ}K$ calculated from it is slightly small. The result suggests that the unique set of interchain force constants is difficult to obtain and the least square method with reference to the reliable observed values might be practical.

In our treatment, the band splittings of methylene rocking vibrations for several values of δ_c[6] were incorporated into least square calculation by the use of first order perturbation method. Taking many points of δ_c for methylene rocking leads to put high weight on the vibration. Therefore the least square method involves some ambiguity about weighting. Regardless of the weight, the analysis yields $P_2 < P_3$ whereas the interatomic distance is contrary. Several reasons may be pointed out. First, the uncertainty of the experimental value of setting angle (θ) makes the H····H distances obscure. For reference, the inter-hydrogen distances at $-196^{\circ}C$ for three setting angles and those at room temperature for $\theta=42^{\circ}$(Smith's model[22]) are shown in Table 10. It is obvious that the order of atomic distance depends upon temperature and the setting angle. Secondly, the electron cloud of composite atoms in molecular crystal is not always spherical, and the potential curve of nonbonded atoms might

depend upon the direction[39]. For instance, P_3 term which is in outer side of methylene group might be more similar to usual spherical H····H potential than P_2 term which passes inner side of methylene group. Thirdly, extremely anisotropic thermal expansion is observed[23),40-41)] along the a axis and the order of the atomic distances might change even below 77°K.

On the other hand the thermal expansion and temperature dependency of infrared band of B_{1u} lattice vibration suggest that anharmonicity of the potential function is not disregarded at higher temperature. Theoretical development about the treatment of anharmonicity in crystal vibrations would be the urgent problem for the future improvement.

SUMMARY

The low frequency modes of lattice vibrations of polyethylene crystal were treated with the use of $H_S(\delta)$ matrix. The approximation makes computation time much shorter than the straightforward method and the result is correct within the limitation of 3 cm^{-1}.

As the intrachain potential, the force constants obtained by Schachtschneider and Snyder were used where the force constants of internal rotation was adjusted as 0.075 mdÅ with reference to the observed specific heat near 60°K. As for the interchain potential, four types of H····H interaction terms were incorporated. The force constants were

adjusted from the observed values of the specific heat below $10^{\circ}K$, the frequency of B_{1u} lattice vibration and the band splitting of methylene rocking and scissoring vibrations. Thus the frequency distribution below $700cm^{-1}$, the specific heat below $150^{\circ}K$, Young's moduli perpendicular to the chain axis, the frequency of lattice vibrations for $k=0$ modes, and the band splittings of the intrachain vibrations were calculated, in good agreement with the corresponding observed values.

REFERENCES

1) B.Wunderlich, J. Chem. Phys., 37, 1203 (1962); 37, 1207 (1962). J. Polymer Sci., C-1, 41 (1963).

2) I.V.Sochara, Dokl. Akad. Nauk. (U.S.S.R.), 130, 126 (1960), (data for $T > 17^{\circ}K$).

F.S.Dainton, D.M.Evans, F.E.Hoare, and T.P.Melia, Polymer, 3, 277 (1962), (data for $T > 22^{\circ}K$).

L.L.Isaacs and C.W.Garland, J. Phys. Chem. Solid, 23, 311 (1962)(data for $1.85 < T < 5.3^{\circ}K$).

W.Reese and J.E.Tucker, J. Chem. Phys., 43, 105 (1965). (data for $1.0 < T < 4.5^{\circ}K$ which are not included in ref.1).

3) J.E.Tucker and W.Reese, J. Chem. Phys., 46, 1388 (1967).

4) B.Wunderlich, J. Phys. Chem., 69, 2078 (1965).

5) V.V.Tarasov, J. Am. Chem. Soc., 80, 5052 (1958).

6) R.G.Snyder, J. Mol. Spectry., 4, 411 (1960); 7, 116 (1961).

7) R.F.Holland and J.R.Nielsen, J. Mol. Spectry., 8, 383 (1962).

8) J.R.Nielsen and R.F.Holland, J. Mol. Spectry., 4, 488 (1960); 6, 394 (1961).

9) S.Krimm, C.Y.Liang and G.B.B.M.Sutherland, J. Chem. Phys., 25, 549 (1956).

10) T.Shimanouchi, Pure Appl. Chem., 7, 261 (1962).

11) H.Takahashi, T.Shimanouchi, K.Fukushima and T.Miyazawa J. Mol. Spectry., 13, 43 (1964).

12) M.Tasumi, T.Shimanouchi and T.Miyazawa, J. Mol. Spectry., 9, 261 (1962); 11, 422 (1963).

13) J.H.Schachtschneider and R.G.Snyder, Spectrochim. Acta, 19, 117 (1963).

14) P.Higgs, Proc. Roy. Soc., (London) A220, 472 (1953).

15) T.Miyazawa, J. Chem. Phys., 35, 693 (1961).

16) T.Miyazawa, K.Fukushima and Y.Ideguchi, J. Chem. Phys., 38, 2709 (1963).

17) T.Miyazawa and T.Kitagawa, J. Polymer Sci., B-2, 395 (1964).

18) C.W.Bunn, Trans. Faraday Soc., 35, 482 (1939).

19) P.W.Teare, Acta Cryst., 12, 294 (1959).

20) L.Salem, J. Chem. Phys., 37, 2100 (1962).

21) H.M.Sheare and V.Vand, Acta Cryst., 9, 379 (1956).

22) A.E.Smith, J. Chem. Phys., 21, 2229 (1953).

23) P.R.Swan, J. Polymer Sci., 56, 403 (1962).

24) M.Tasumi and T.Shimanouchi, J. Chem. Phys., 43, 1245 (1965).

25) J.E.Bertie and G.E.Whalley, J. Chem. Phys., 41, 575 (1964).

26) T.Miyazawa and M.Nakamura, Annual Meeting of Chem. Soc. Japan, Osaka (1968).

27) H.R.Danner, G.J.Safford, H.Boutin, and M.Berger. J. Chem. Phys., 40, 1417 (1964).

W.R.Myers, J.L.Donovan, and J.S.King, J. Chem. Phys., 42, 4299 (1965).

(There are many reports and these two are representative measurements with up-scattering and down-scattering techniques, respectively.)

28a) I.Sakurada, T.Ito and K.Nakamae, J. Polymer Sci., C-15, 75 (1966).

28b) I.Sakurada, K.Kaji, K.Nakamae and E.Shikata, Symposium on Macro Molecules, 2F09, Matsuyama (1968).

29) A.Müller, Proc. Roy. Soc., A-154, 624 (1936); A-178, 227 (1941).

30 R.F.Schaufele and T.Shimanouchi, J. Chem. Phys., 47, 3605 (1967).

31) R.F.Schaufele, private communication.

32) R.V.McKnight and K.D.Möller, J. Opt. Soc. Am., 54, 132 (1964)

33) S.Krimm and M.I.Bank, J. Chem. Phys., 42, 4059 (1965).

34) S.Krimm and M.I.Bank, private communication.

35) G.D.Dean and D.H.Martin, J. Chem. Phys. Letters, 1, 415 (1967).

36) M.Tasumi and S.Krimm, J. Chem. Phys., 46, 755 (1967).

37) I.Harada and T.Shimanouchi, J. Chem. Phys., 44, 2016 (1966).

38) C.A.Coulson and C.W.Haigh, Tetrahedron 19, 527 (1963).

39) A.Odajima and T.Maeda, J. Polymer Sci., C-15, 55 (1966).

40) E.A.Cole and D.R.Holmes, J. Polymer Sci., 46, 147 (1960).

41) M.Kakudo and R.Ullman, J. Polymer Sci., 45, 91 (1960).

Table-1 Matrix Element of Symmetry Transformation

	$\Delta\theta_{l+1/4}$	$\Delta\theta_{l+1/4}$	$\Delta\alpha^{1}_{l+1/4}$	$\Delta\alpha^{2}_{l+1/4}$	$\Delta\alpha^{3}_{l+1/4}$	$\Delta\alpha^{4}_{l+1/4}$
$\Delta\gamma_{l+1/4}$	0.915317	-0.175597	-0.181218	-0.181218	-0.181218	-0.181218
$\Delta\delta_{l+1/4}$	0	0.888666	-0.229278	-0.229278	-0.229278	-0.229278
$\Delta\alpha^{w}_{l+1/4}$	0	0	0.5	0.5	-0.5	-0.5
$\Delta\alpha^{r}_{l+1/4}$	0	0	0.5	-0.5	0.5	-0.5
$\Delta\alpha^{t}_{l+1/4}$	0	0	0.5	-0.5	-0.5	0.5

	$\Delta r^{H1}_{l+1/4}$	$\Delta r^{H2}_{l+1/4}$
$\Delta r^{Ha}_{l+1/4}$	$(1/2)^{\frac{1}{2}}$	$(1/2)^{\frac{1}{2}}$
$\Delta r^{Ha}_{l+1/4}$	$(1/2)^{\frac{1}{2}}$	$-(1/2)^{\frac{1}{2}}$

Table-2 The Intrachain Potential Energy Matrix of Polyethylene

	$\Delta r^{Hs}_{l+3/4}$	$\Delta\delta_{l+3/4}$	$\Delta\gamma_{l+3/4}$	$\Delta\alpha^{w}_{l+3/4}$	$\Delta r^{C}_{l+\frac{1}{2}}$
$\Delta r^{Hs}_{l+3/4}$	4.562				
$\Delta\delta_{l+3/4}$	0	0.575			
$\Delta\gamma_{l+3/4}$	0	0.121	1.024		
$\Delta\alpha^{w}_{l+3/4}$	0	0	0	0.627	
$\Delta r^{C}_{l+\frac{1}{2}}$	0	-0.117	0.225	-0.261	4.427
$\Delta r^{Hs}_{l+1/4}$	0	0	0	0	0
$\Delta\delta_{l+1/4}$	0	0.008	0.030	-0.029	0
$\Delta\gamma_{l+1/4}$	0	0.030	0.122	-0.068	0
$\Delta\alpha^{w}_{l+1/4}$	0	0.029	0.068	-0.041	0
Δr^{C}_{l}	0	-0.117	0.225	0.261	0.064

	$\Delta r^{Ha}_{l+3/4}$	$\Delta\alpha^{r}_{l+3/4}$	$\Delta\alpha^{t}_{l+3/4}$	$\Delta t_{l+\frac{1}{2}}$
$\Delta r^{Ha}_{l+3/4}$	4.530			
$\Delta\alpha^{r}_{l+3/4}$	0	0.705		
$\Delta\alpha^{t}_{l+3/4}$	0	0	0.659	
$\Delta t_{l+\frac{1}{2}}$	0	0	0	0.075
$\Delta r^{Ha}_{l+1/4}$	0	0	0	0
$\Delta\alpha^{r}_{l+1/4}$	0	0.065	0.065	0
$\Delta\alpha^{t}_{l+1/4}$	0	-0.065	-0.065	0
Δt_{l}	0	0	0	0

Table-3 The Interchain Potential of Polyethylene Crystal

	d(Å)	P(md/Å)	n
P_1	2.879	0.004_2	8
P_2	2.712	0.010_1	8
P_3	2.505	0.006_4	4
P_4	2.502	0.011_2	4

d; inter-atomic distance at -196°C.

P; the force constant of the inter-molecular potential.

n; the number of the potential terms per unit cell.

Table-4 Unitary matrix for symmetry transformation $U(\rho\delta)$.

	Δx_1	Δy_1	Δz_1	Δx_2	Δy_2	Δz_2	Δx_3	Δy_3	Δz_3	Δx_4	Δy_4	Δz_4
$S^1(\delta)_x$	$+c_1$	0	0	$-c_2$	0	0	$+c_3$	0	0	$-c_4$	0	0
$S^1(\delta)_y$	0	$+c_1$	0	0	$-c_2$	0	0	$-c_3$	0	0	$+c_4$	0
$S^1(\delta)_z$	0	0	$-s_1$	0	0	$-s_2$	0	0	$-s_3$	0	0	$-s_4$
$S^2(\delta)_x$	$+c_1$	0	0	$-c_2$	0	0	$-c_3$	0	0	$+c_4$	0	0
$S^2(\delta)_y$	0	$+c_1$	0	0	$-c_2$	0	0	$+c_3$	0	0	$-c_4$	0
$S^2(\delta)_z$	0	0	$-s_1$	0	0	$-s_2$	0	0	$+s_3$	0	0	$+s_4$
$S^3(\delta)_x$	$-s_1$	0	0	$-s_2$	0	0	$-s_3$	0	0	$-s_4$	0	0
$S^3(\delta)_y$	0	$-s_1$	0	0	$-s_2$	0	0	$+s_3$	0	0	$+s_4$	0
$S^3(\delta)_z$	0	0	$+c_1$	0	0	$-c_2$	0	0	$+c_3$	0	0	$-c_4$
$S^4(\delta)_x$	$-s_1$	0	0	$-s_2$	0	0	$+s_3$	0	0	$+s_4$	0	0
$S^4(\delta)_y$	0	$-s_1$	0	0	$-s_2$	0	0	$-s_3$	0	0	$-s_4$	0
$S^4(\delta)_z$	0	0	$+c_1$	0	0	$-c_2$	0	0	$-c_3$	0	0	$+c_4$

c_j denotes three dimansional constant matrix of $\cos(\rho_j\delta)$.

s_j denotes three dimensional constant matrix of $\sin(\rho_j\delta)$.

Table-5 Symmetry properties of Cartesian symmetry coordinates at $\delta=0$.

	E	C_2^a	C_2^b	C_2^c	1	$\sigma_g(bc)$	$\sigma_g(ac)$	$\sigma_g(ab)$	species
$S^1(\delta)_{x,y}$	1	1	1	1	1	1	1	1	A_g
$S^1(\delta)_z$	1	-1	-1	1	-1	1	1	-1	B_{3u}
$S^2(\delta)_{x,y}$	1	-1	-1	1	1	-1	-1	1	B_{3g}
$S^2(\delta)_z$	1	1	1	1	-1	-1	-1	-1	A_u
$S^3(\delta)_{x,y}$	1	1	-1	-1	-1	-1	1	1	B_{1u}
$S^3(\delta)_z$	1	-1	1	-1	1	-1	1	-1	B_{2g}
$S^4(\delta)_{x,y}$	1	-1	1	-1	-1	1	-1	1	B_{2u}
$S^4(\delta)_z$	1	1	-1	-1	1	1	-1	-1	B_{1g}

Table-6 The Splitting of Intrachain Vibrations

branch	symmetry	and wave number			$\Delta\nu_{cal}$	$\Delta\nu_{obs}$
$\nu_1(0)$	A_g	2873	B_{3g}	2869	4	—
$\nu_2(0)$	A_g	1441	B_{3g}	1457	-16	(-24)
$\nu_3(0)$	B_{3u}	1175	A_u	1183	-8	—
$\nu_4(0)$	A_g	1130	B_{3g}	1129	1	—
$\nu_5(0)$	B_{3u}	0	A_u	54	—	—
$\nu_6(0)$	A_g	2936	B_{3g}	2940	-4	—
$\nu_7(0)$	A_g	1167	B_{3g}	1168	-1	—
$\nu_8(0)$	B_{3u}	1090	A_u	1086	4	(6)
$\nu_9(0)$	A_g	146	B_{3g}	121	—	—
$\nu_1(\pi)$	B_{1u}	2854	B_{2u}	2856	-2	0
$\nu_2(\pi)$	B_{1u}	1482	B_{2u}	1472	10	13
$\nu_3(\pi)$	B_{1g}	1431	B_{2g}	1428	3	—
$\nu_4(\pi)$	B_{1g}	1079	B_{2g}	1073	6	—
$\nu_5(\pi)$	B_{1u}	0	B_{2u}	92	—	—
$\nu_6(\pi)$	B_{1u}	2917	B_{2u}	2916	1	—
$\nu_7(\pi)$	B_{1g}	1314	B_{2g}	1318	-4	—
$\nu_8(\pi)$	B_{1u}	722	B_{2u}	712	10	13
$\nu_9(\pi)$	B_{1u}	72	B_{2u}	0	—	—

Table-7 The specific heat of polyethylene crystal

Temp.(^{o}K)	C_v/R(obs.)	C_v/R (calc.) lattice	intrachain
10	0.0162		
20	0.1129	0.0953	
30	0.2548	0.2322	
40	0.4045	0.3895	
50	0.564	0.547	
60	0.703	0.692	
70	0.828	0.819	
80	0.939	0.929	
90	1.042	1.025	
100	1.136	1.108	0.002
110	1.228	1.181	0.004
120	1.298	1.246	0.008
130	1.376	1.305	0.014
140	1.454	1.357	0.023
150	1.525	1.404	0.038

Table-8 The eigen-frequency for $\delta_a=\delta_b=\delta_c=0.1$ (cm^{-1})

symmetry at $\delta=0$	ν from $D_S(\delta)$	ν from $H_S(\delta)$
A_g	146	147
B_{3g}	122	122
B_{1u}	72	73
B_{2u}	6.0	6.1
B_{3u}	36.3	36.3
A_u	65	65
B_{1u}	4.6	4.6
B_{2u}	92	93

$D_S(\delta)$ is the original dynamical matrix whose dimension is 36.
$H_S(\delta)$ is the dynamical matrix for low frequency lattice vibrations whose dimension is 8.

Table-9 The Intermolecular Force Constants from the Theoretical Potential Functions.

	P_1	P_2	P_3	P_4	$\Delta\nu_{rock}$	$\Delta\nu_{bend}$	$\nu(B_{1u})$
Barton	0.0021	0.0046	0.0120	0.0120	16	1	56
Hill	0.0006	0.0016	0.0053	0.0054	6	4	33
Eyring	0.0039	0.0080	0.0195	0.0197	26	3	75
Winstein	0.0018	0.0042	0.0118	0.0120	15	1	54
Hendrickson	0.0026	0.0055	0.0144	0.0145	19	2	62
Hendrickson Bartell	0.0026	0.0057	0.0152	0.0153	20	1	63
Barton	0.0030	0.0066	0.0171	0.0173	22	2	81
Bartell	0.0059	0.0117	0.0272	0.0277	37	5	91
Müller	0.0061	0.0140	0.0397	0.0400	50	2	98
de Boer	0.0057	0.0104	0.0210	0.0220	31	7	86
Tasumi I	0.0045	0.0133	0.0080	0.02	10	12	79
Shimanouchi II	0.0038	0.0153	0.0120	0.02	11	11	80
Present Study	0.0042	0.0101	0.0064	0.0112	10	10	73

Table-10 The Interatomic Distances (Å)

model	Temp.	P_1	P_2	P_3	P_4
$\theta=42^\circ$	298°K	2.956	2.765	2.769	2.595
$\theta=42^\circ$	77°K	2.877	2.625	2.599	2.534
$\theta=45^\circ$	77°K	2.879	2.712	2.505	2.502
$\theta=48^\circ$	77°K	2.884	2.804	2.417	2.484

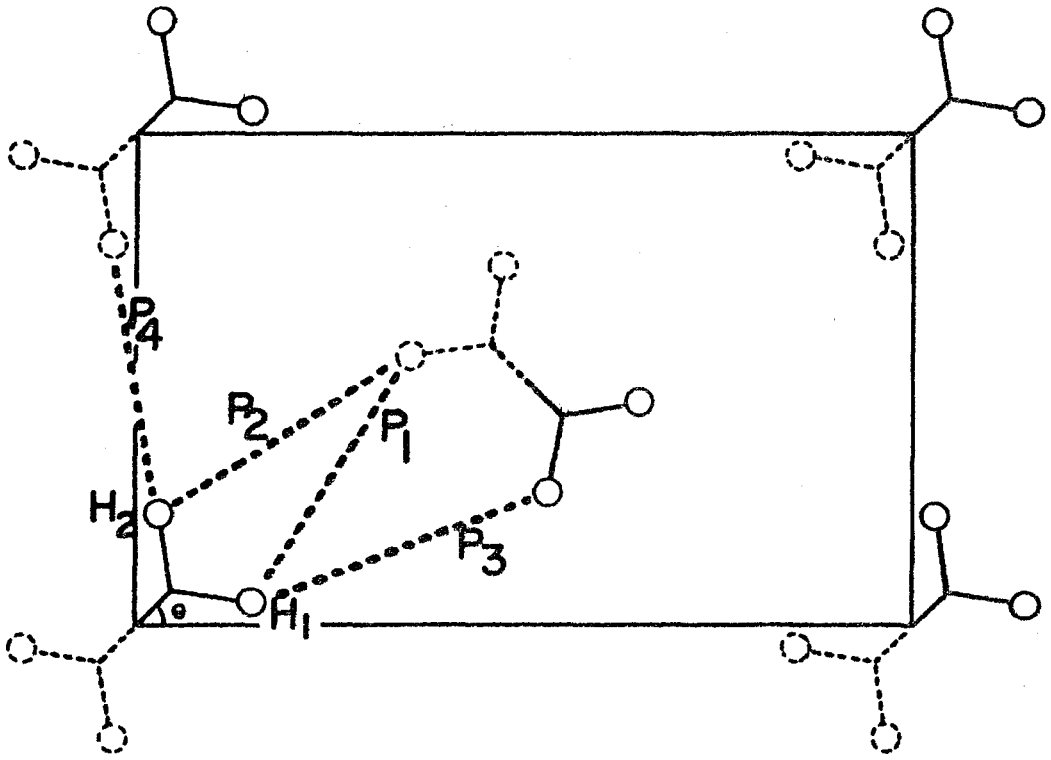

Fig. 1 Interchain potential in polyethylene crystal.

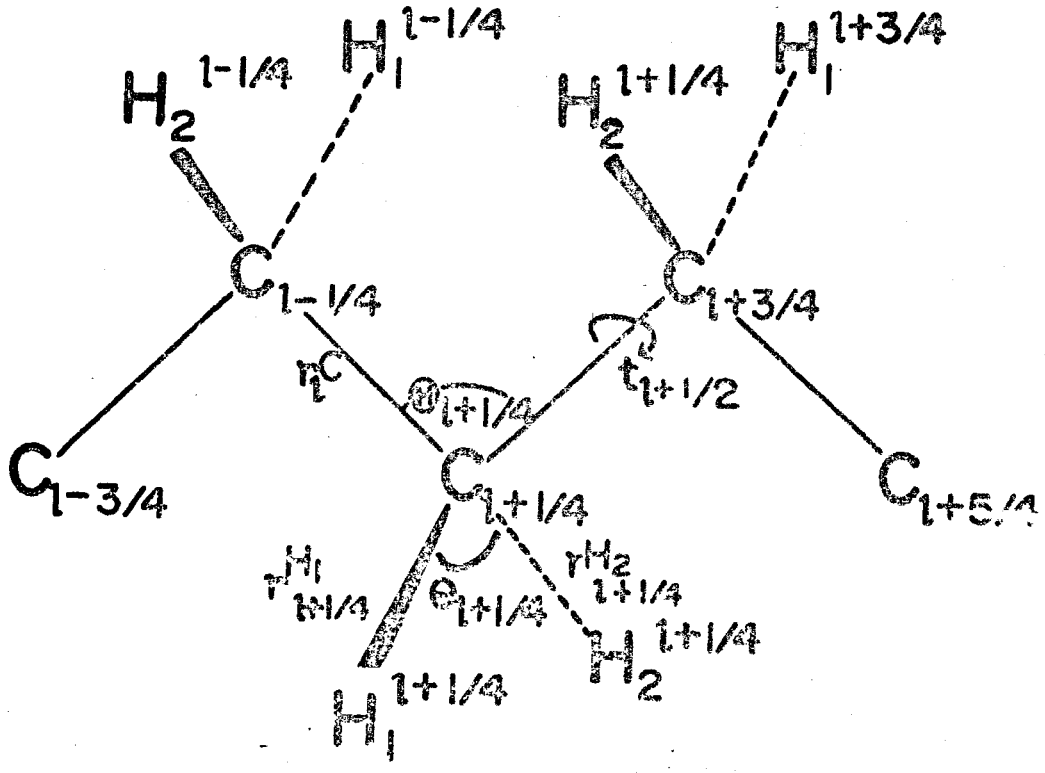

$$\alpha^1_{l+1/4} = \angle C_{l-1/4} C_{l+1/4} H_1^{l+1/4}$$

$$\alpha^2_{l+1/4} = \angle C_{l-1/4} C_{l+1/4} H_2^{l+1/4}$$

$$\alpha^3_{l+1/4} = \angle C_{l+3/4} C_{l+1/4} H_1^{l+1/4}$$

$$\alpha^4_{l+1/4} = \angle C_{l+3/4} C_{l+1/4} H_2^{l+1/4}$$

Fig. 2 The internal coordinates for intrachain vibrations of polyethylene molecules

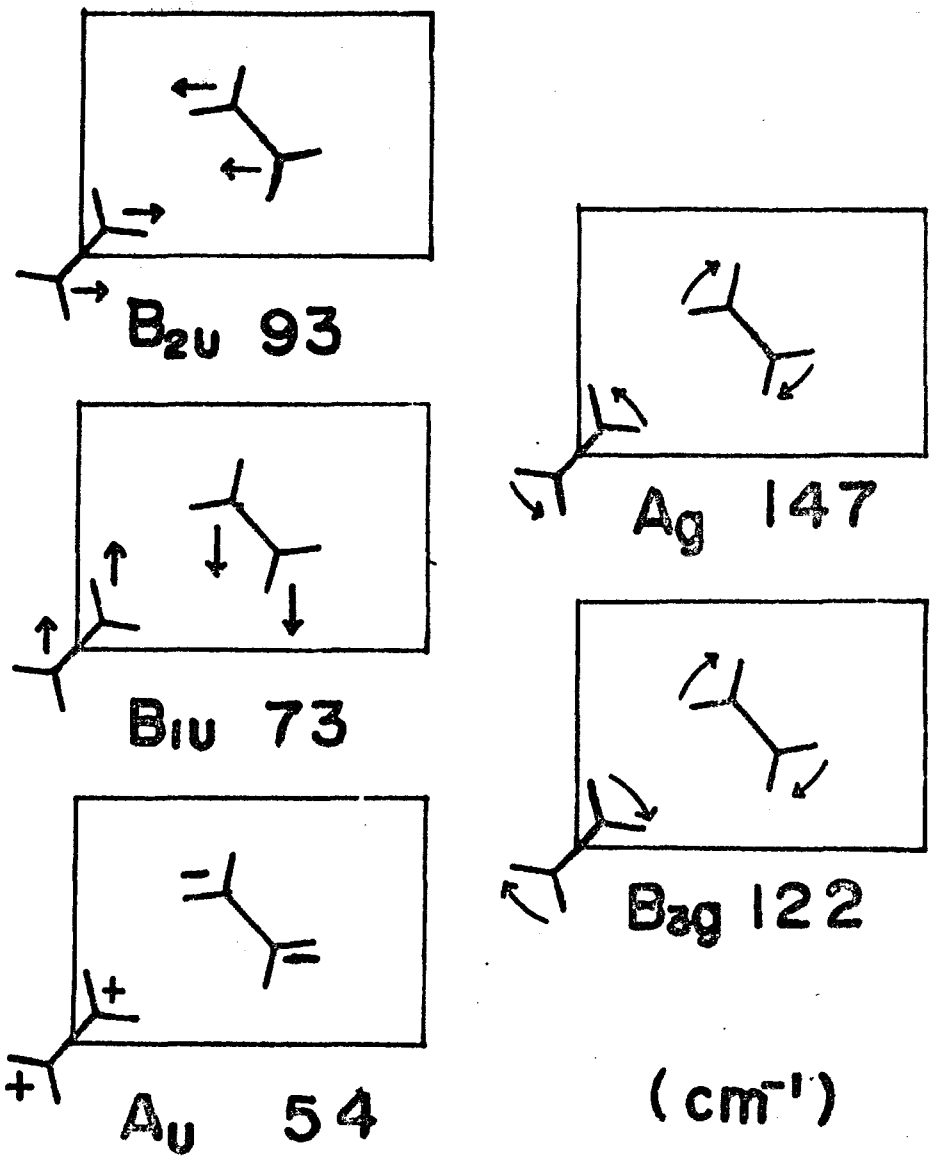

Fig. 3 Frequency and symmetry of optical modes of lattice vibrations ($\delta_a=\delta_b=\delta_c=0$).

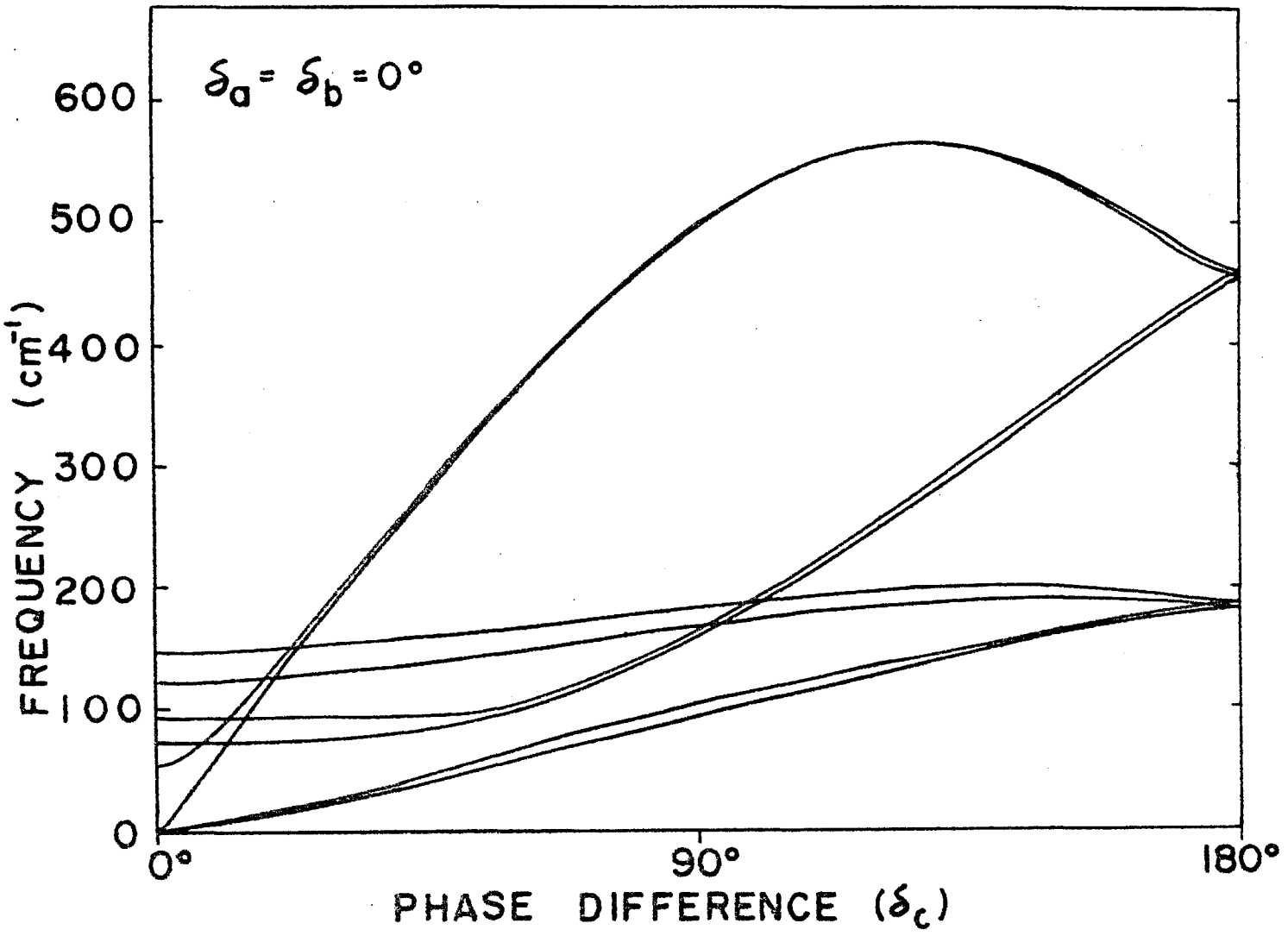

Fig. 4 Dispersion curves of vibrational frequencies of lattice vibrations along $(0,0,\delta_c)$

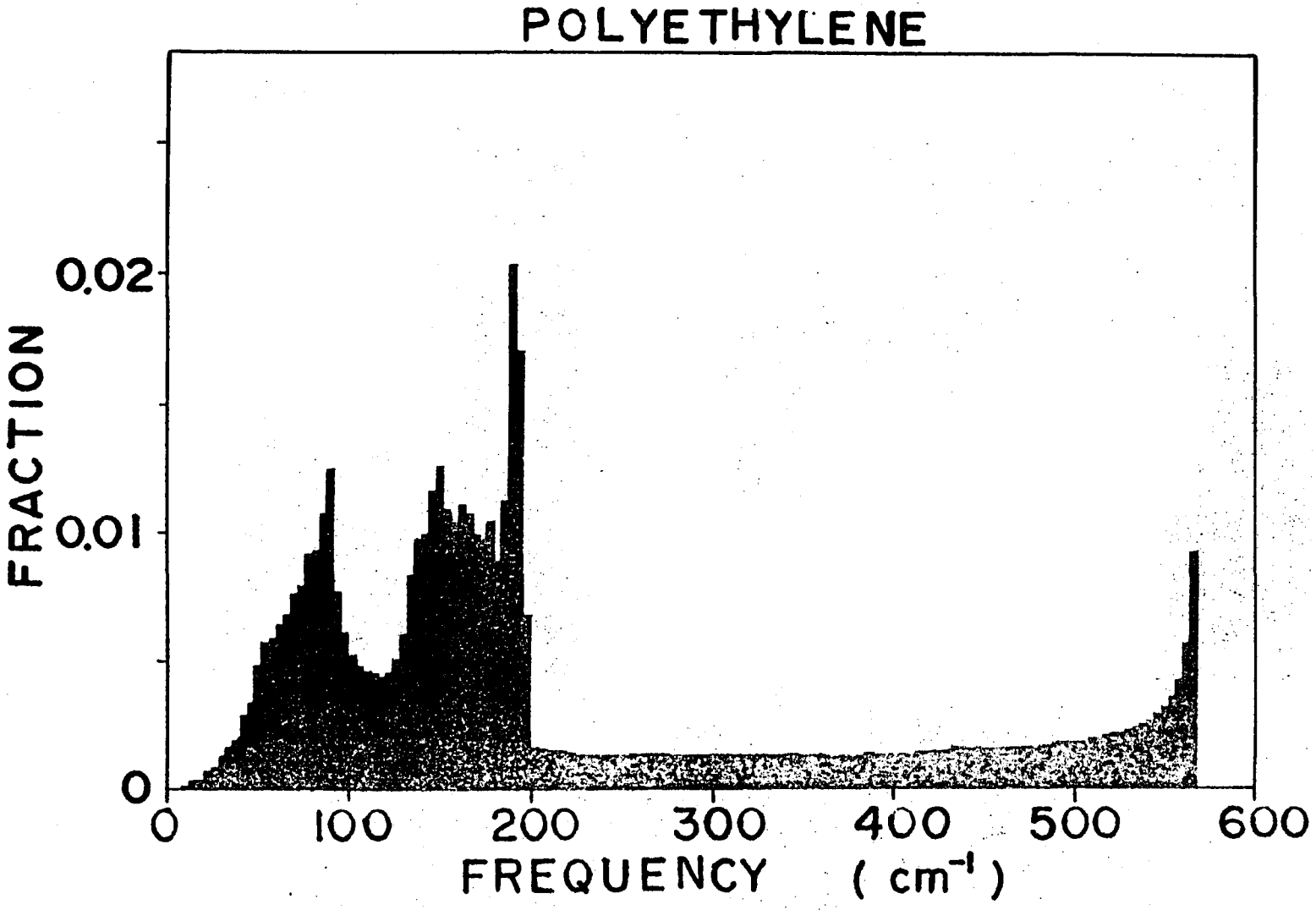

Fig. 5 Frequency distribution of crystal vibrations. The fraction of number of vibrational modes per 4 cm^{-1} is plotted against the frequency.

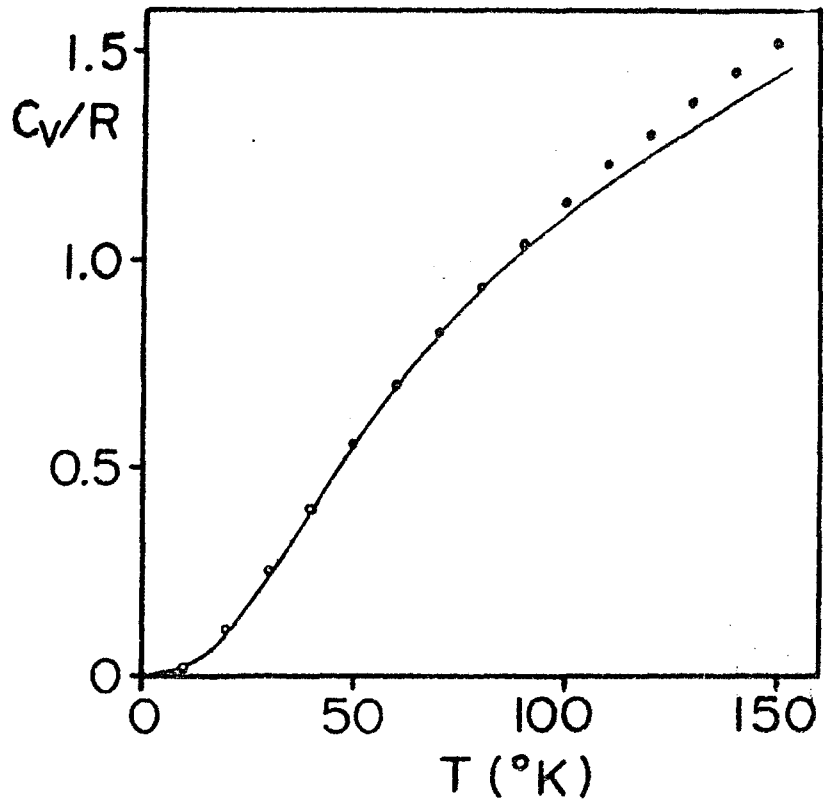

Fig. 6 The specific heat of polyethylene crystal. open circles are observed values[1)] and solid line shows the calculated specific heat per methylene group.

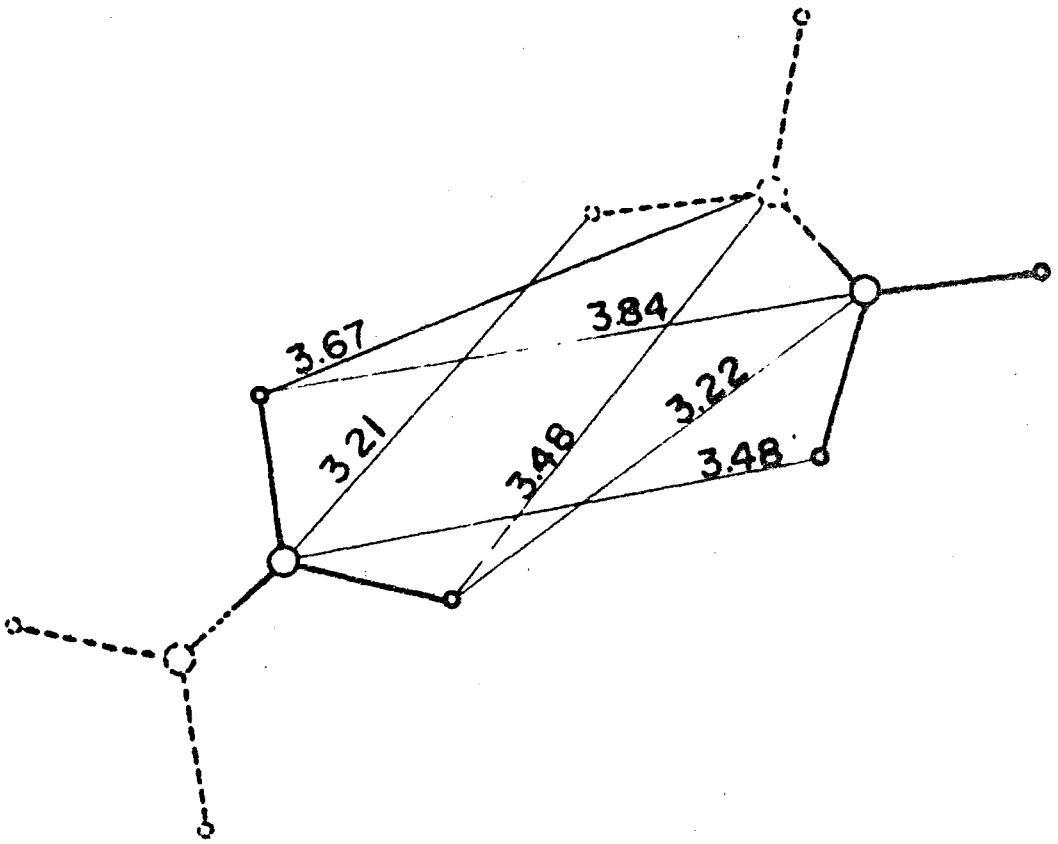

Fig. 7. The atomic distances of the interchain C·····H contacts at -196°C.

CHAPTER III

ACOUSTIC PHONONS AND LOW-TEMPERATURE SPECIFIC HEAT OF POLYETHYLENE CRYSTAL

III-1 INTRODUCTION

There are three acoustic branches of crystal vibrations, the frequencies of which approach to 0 cm^{-1} as $|\delta|$ approaches to 0. At the limit of $|\delta| = 0$, the acoustic branches become overall-translations of the crystal along three orthogonal directions. In molecular crystals, the frequencies of acoustic vibrations depend primarily upon inter-molecular potential function.

On the other hand, for extremely small value of $|\delta|$, the period of atomic displacement becomes infinitely large and then the deformation due to acoustic vibrations would be regarded as homogeneous deformation. For instance, the longitudinal acoustic vibrations along the a, b and c axes correspond to σ_1, σ_2 and σ_3 of the elastic deformations, respectively. The atomic displacements in transverse acoustic vibrations are similar to those of σ_4, σ_5 and σ_6. Accordingly, the frequencies of acoustic vibrations are represented with the macroscopic elastic constants.

The specific heat at the lowest temperature depends primarily upon the acoustic vibrations. Since, in the polyethylene crystal, there is no free electron, the specific heat is proportional to T^3 below $9^{\circ}K$.[1] The coefficient is determined largely from the interchain force constants. As

the experimental data are obtained from careful observations[1], the data of the heat capacity are possibly used to adjusting the interchain force constants.

Debye's theory[2] on the specific heat assumes that the velocity of acoustic phonon does not depend upon the direction of travelling but depends on the type of modes, that is, transverse or longitudinal. This approximation is not valid for highly anisotropic crystal such as polyethylene. The velocity of the longitudinal mode travelling to the chain axis much higher than the velocity of longitudinal modes travelling perpendicularly to the chain axis. Previously Odajima has treated the elastic constants and low temperature specific heat, assuming de Boer type interchain potential, where the specific heat is calculated from Eq.(1.23) of Chapter I, and deviation of constant frequency surfaces of acoustic phonons from ellipsoid had been disregarded.

In the present study, the velocity of acoustic phonons is calculated for various directions of travelling, from which the frequency distribution for acoustic phonons and the specific heat below $9^{\circ}K$ were calculated. The several sets of interchain force constants, deduced from the observed frequency of the B_{1u} lattice vibration[4] and the band splitting of methylene rocking and scissoring vibrations[5], were examined and adjusted so as to reproduce the observed value of the specific heat below $9^{\circ}K$. Thus obtained force constants are $P_1=0.0042$, $P_2=0.0101$, $P_3=0.0064$ and $P_4=0.0112$ md/Å. The constant frequency surfaces of

three acoustic branches are calculated under the incorporation of mutual interactions of the branches.

III-2 DYNAMICAL MATRIX FOR ACOUSTIC PHONONS

The dynamical matrix for three acoustic vibrations can be derived in two alternative ways; the perturbation method about the dynamical matrix of whole lattice vibrations and the equation for elastic waves of three dimensional elastic continuum.[6] The former has first been worked out in the present study and explained below in detail.

The matrix elements of $\mathbf{D}_S^M(\delta_c)$ and $\mathbf{D}_S^C(\delta_a,\delta_b,\delta_c)$ of (2.6) are expanded into power series of δ_a, δ_b and δ_c as

$$\mathbf{D}_S^M(\delta_c) = \mathbf{D}_m^0 + \sum_i \mathbf{D}_m^i(\delta_c) \tag{3.1}$$

$$\mathbf{D}_S^C(\delta_a,\delta_b,\delta_c) = \mathbf{D}_c^0 + \sum_i \mathbf{D}_c^i(\delta_a,\delta_b,\delta_c) \tag{3.2}$$

where $\mathbf{D}_m^0$ and $\mathbf{D}_c^0$ include constant terms and $\mathbf{D}_m^i$ and $\mathbf{D}_c^i$ include i-th power of phase differences. Supposing the eigenvector matrix of $\mathbf{D}_S^M(\delta_c)$ near $\delta_c=0$ is represented as

$$\mathbf{L}_S^M(\delta_c) = \mathbf{L}_m^0\left[\mathbf{E} - \mathbf{P}(\delta_c)\right] \tag{3.3}$$

where $\mathbf{L}_m^0$ is the eigenvector matrix of $\delta_c=0$ and $\mathbf{E}$ is unit matrix, then (3.4) is derived from the condition for $\mathbf{L}_S^M(\delta_c)$ to be eigenvector matrix of $\mathbf{D}_S^M(\delta_c)$.

$$P(\delta_c)_{ii} = 0$$

$$P(\delta_c)_{jk} = -P(\delta_c)_{kj} = \left[\tilde{\mathbf{L}}_m^0\mathbf{D}_m^1(\delta_c)\mathbf{L}_m^0\right]_{jk}/(\lambda_j^0-\lambda_k^0) \tag{3.4}$$

where λ_j^0 and λ_k^0 are eigenvalues of $\mathbf{D}_S^M(0)$. Thus the dynamical matrix for low frequency lattice vibrations, $\mathbf{H}_S(\delta_a,\delta_b,\delta_c)$ is obtained in explicit form of δ_a, δ_b and δ_c from

$$\mathbf{H}_S(\delta_a,\delta_b,\delta_c)=\left[\tilde{\mathbf{L}}_m^0-\tilde{\mathbf{P}}(\delta_c)\tilde{\mathbf{L}}_m^0\right]\left[\mathbf{D}_S^M(\delta_c)+\mathbf{D}_S^C(\delta_a,\delta_b,\delta_c)\right]\left[\mathbf{L}_m^0-\mathbf{L}_m^0\mathbf{P}(\delta_c)\right] \tag{3.5}$$

The interaction of acoustic branches with intrachain vibrations has already been incorporated through $P(\delta_c)$ and, in next place, the interaction of the acoustic branches with optical branches of low frequency lattice vibrations are introduced with the use of second order perturbation method. The matrix elements concerned with three acoustic branches are represented as

$$H_A(\delta)_{\alpha\alpha} = A_\alpha \delta_a^2 + B_\alpha \delta_b^2 + C_\alpha \delta_c^2 \quad (\alpha=a,b,c) \qquad (3.6)$$

$$H_A(\delta)_{\alpha\beta} = d_{\alpha\beta}\delta_\alpha\delta_\beta$$

where α denotes the direction of the atomic displacement of the acoustic phonon and $d_{\alpha\beta}$ is concerned with the mutual interaction of three acoustic phonons. The coefficients, A_α, B_α, C_α and $d_{\alpha\beta}$ are derived as function of the interchain force constants in Table 1. Since the potential term P_4 is essentially on the bc plane, it does not contribute to the coefficient of δ_a at all. As the potential term of P_3 is assumed in ab plane, it contributes neither to the translational mode along the c axis nor to the coefficients of δ_c. Since the longitudinal mode along the c axis includes the deformation of molecule, force constant of the skeletal bending coordinate contributes to C_c which is shown numerically in Table 1. Thus derived $H_A(\delta)$, the dynamical matrix for acoustic phonons, was confirmed to well reproduce the eigenfrequency of original dynamical matrix of the dimension 36. The left column of Table 2 represents the eigenfrequency obtained from the diagonalization of $D_S(\delta)$ and the right column represents that from $H_A(\delta)$, where phase

difference is set to be $\delta_a=\delta_b=\delta_c=0.1$ radian. The deviation is at most 0.2 cm^{-1} and therefore the present approximation is justified.

On the other hand, macroscopic theory about elastic continuum leads to the identical dynamical matrix with acoustic branches. Supposing u, v and w are the atomic displacement along x, y, and z direction, respectively and X_x, X_y and X_z are external forces per unit volume along x direction on the surface normal to x, y, and z axis, respectively, then the equation of motion along x direction is represented as [7]

$$\rho\ddot{u} = (\partial X_x/\partial x) + (\partial X_y/\partial y) + (\partial X_z/\partial z) \qquad (3.7)$$

where ρ is density. The elastic deformation, defined by

$$\sigma_1 = \partial u/\partial x, \quad \sigma_2 = \partial v/\partial y, \quad \sigma_3 = \partial w/\partial z,$$
$$\sigma_4 = (\partial v/\partial z)+(\partial w/\partial y), \quad \sigma_5 = (\partial u/\partial z)+(\partial w/\partial x)$$
$$\sigma_6 = (\partial u/\partial y)+(\partial v/\partial x)$$

induces the restoring force which is in equilibrium with the external force. The external force, which does not give rise to overall-rotation of the crystal is represented as six component vector

$$\mathbf{F} = \mathbf{C}\cdot\boldsymbol{\sigma} \qquad (3.8)$$

where $\mathbf{C}$ is the elastic constant matrix(c_{ij}). Then the equation of motion is rewritten as

$$\rho\ddot{u}=c_{11}(\partial^2u/\partial x^2)+c_{66}(\partial^2u/\partial y^2)+c_{55}(\partial^2u/\partial z^2)$$
$$+(c_{12}+c_{66})(\partial^2v/\partial x\partial y)+(c_{13}+c_{55})(\partial^2w/\partial x\partial z)$$
$$\rho\ddot{v}=c_{66}(\partial^2v/\partial x^2)+c_{22}(\partial^2v/\partial y^2)+c_{44}(\partial^2v/\partial z^2)$$
$$+(c_{12}+c_{66})(\partial^2u/\partial x\partial y)+(c_{23}+c_{44})(\partial^2w/\partial y\partial z)$$

$$\rho\ddot{w}=c_{55}(\partial^2 w/\partial x^2)+c_{44}(\partial^2 w/\partial y^2)+c_{33}(\partial^2 w/\partial z^2) \qquad (3.9)$$
$$+(c_{13}+c_{55})(\partial^2 u/\partial x\partial z)+(c_{23}+c_{44})(\partial^2 v/\partial y\partial z)$$

Under the cyclic boundary condition, the atomic displacements are represented as plane wave such as

$$\begin{aligned} u &= u_0 \exp(i\omega t - i\boldsymbol{\rho}\boldsymbol{\delta}) \\ v &= v_0 \exp(i\omega t - i\boldsymbol{\rho}\boldsymbol{\delta}) \\ w &= w_0 \exp(i\omega t - i\boldsymbol{\rho}\boldsymbol{\delta}) \end{aligned} \qquad (3.10)$$

where ω is angular frequency, $\boldsymbol{\rho}$ is index vector and $\boldsymbol{\delta}$ is phase difference vector. Substitution of u, v, and w from (3.10) into (3.9) yields the secular determinant for elastic waves.

$$\begin{array}{c} \\ T_a \\ T_b \\ T_c \end{array} \left| \begin{array}{ccc} \dfrac{c_{11}\delta_a^2}{a_0^2}+\dfrac{c_{66}\delta_b^2}{b_0^2}+\dfrac{c_{55}\delta_c^2}{c_0^2} & \dfrac{(c_{12}+c_{66})\delta_a\delta_b}{a_0 b_0} & \dfrac{(c_{13}+c_{55})\delta_a\delta_c}{a_0 c_0} \\ & \dfrac{c_{66}\delta_a^2}{a_0^2}+\dfrac{c_{22}\delta_b^2}{b_0^2}+\dfrac{c_{44}\delta_c^2}{c_0^2} & \dfrac{(c_{23}+c_{44})\delta_b\delta_c}{b_0 c_0} \\ \text{symmetric} & & \dfrac{c_{55}\delta_a^2}{a_0^2}+\dfrac{c_{44}\delta_b^2}{b_0^2}+\dfrac{c_{33}\delta_c^2}{c_0^2} \end{array} \right| \qquad (3.11)$$

The eigenvalue of (3.11) is $\rho\omega^2$ and a_0, b_0 and c_0 are lattice constants. T_a, T_b, and T_c denote that atomic displacement is parallel to the a, b and c axes, respectively.

When reliable values of the elastic constants are available, the equation (3.11) is of great use as it is, but when potential function is reliable and c_{ij} is not available as polyethylene crystal, the equation (3.6) may be applicable.

III-3 SPECIFIC HEAT BELOW 10°K

With the use of spherical polar coordinate in δ space[8], the phase differences are written as

$$\delta_a = |\delta| \sin\theta \cdot \cos\phi, \quad \delta_b = |\delta| \sin\theta \cdot \sin\phi, \quad \delta_c = |\delta| \cos\theta$$

where $|\delta|$ is length of phase difference vector. For very small values of phase difference vectors, the frequencies of acoustic phonons are proportional to the magnitude of phase difference vector, that is, $|\delta|$. Supposing ν_{0i} is the frequency of i-th branch at $\delta = \delta_0$, then the velocity of the phonon is given by $\nu_{0i} c(\delta_{0a}^2/a_0^2 + \delta_{0b}^2/b_{0c}^2 + \delta_{0c}^2/c_0^2)^{-\frac{1}{2}}$ and the phase difference which gives ν_i is represented as

$$|\delta_\nu| = (\nu/\nu_{0i})|\delta_0|$$

Thus the constant frequency surface corresponding to ν cm^{-1} may be obtained from the diagonalization of the dynamical matrix for various direction of δ_0. In Fig. 1, the constant frequency surfaces for ν=1.3 cm^{-1} of three acoustic phonons of polyethylene crystal is drawn in δ space, where the axis of δ_c is perpendicular to the paper and the iso-frequency contours for various values of δ_c are projected to $\delta_a\delta_b$ plane. The solid lines are drawn at 0.5° interval of δ_c and other lines are for intermediate values of δ_c, written beside the contour lines. One-eighth of the volume ($0 \leq \delta_a, \delta_b, \delta_c \leq \pi$) surrounded by the constant frequency surfaces is

$$V(\nu) = \sum_{i=1}^{3} \int_0^{\pi/2} \int_0^{\pi/2} \int_0^{\delta_\nu} |\delta_\nu|^2 \sin\theta \cdot d\delta_\nu d\theta d\phi$$

$$= \sum_{i=1}^{3} \int_0^{\pi/2} \int_0^{\pi/2} \int_0^{\nu} (|\delta_0|/\nu_{0i})^3 \nu^2 d\nu \sin\theta d\theta d\phi \qquad (3.13)$$

Then the number of mode between ν and $\nu+d\nu$ is

$$g(\nu)d\nu = [\partial V(\nu)/\partial\nu]d\nu = a\nu^2 \qquad (3.14)$$

where the coefficient, "a" is calculated by replacing the integral in (3.13) with summation as (3.15)

$$a = (1/4\pi^3) \sum_{i}^{3} \sum_{\theta}^{\frac{1}{2}\pi} \sum_{\phi}^{\frac{1}{2}\pi} (|\delta_0|/\nu_{oi})^3 \sin\theta\Delta\theta\Delta\phi \qquad (3.15)$$

where the factor $(1/4\pi^3)$ is introduced so as for $g(\nu)$ to represent the frequency distribution per methylene group, because the irreducible volume (one-eighth) of the first Brillouin zone is π^3 in which four methylene groups are included. Then the specific heat is derived as

$$(C_v/R) = a(k/hc)^3T^3\int_0^\infty x^4\exp(x)[\exp(x)-1]^{-2}dx \qquad (3.16)$$

where $x=(hc\nu/kT)$. The upper limit of integral is conveniently regarded as infinite because the integrated value is almost constant at low temperature for proper ν_m.

Since the frequency is altered sensitively with δ_c, but little with δ_a or δ_b, $\Delta\theta=\pi/90$ and $\Delta\phi=\pi/36$ were adopted on the calculation of (3.15). Finer division was confirmed to yield almost same value. The computation of the formation of the dynamical matrix from the interchain force constants and of its diagonalization, is short enough to examine several sets of the interchain force constants deduced from the least square analysis with regard to other observed values[4-5]. As described in I-7, the coefficient, "a" of (3.15) is nearly proportional to (-3/2)th power of the interchain force constants. The relation is also of use to adjust the interchain force constants. Thus determined values are

$$P_1=0.0042, \quad P_2=0.0101, \quad P_3=0.0064, \quad P_4=0.0112 \text{ md/Å}$$

The specific heat, calculated from above potential, is

$$(C_v/R)_a = 0.971 \cdot 10^{-5} T^3$$
$$(C_v/R)_b = 0.366 \cdot 10^{-5} T^3$$
$$(C_v/R)_c = 0.049 \cdot 10^{-5} T^3$$
$$C_v/R = 1.386 \cdot 10^{-5} T^3$$

where the suffices indicate approximate direction of atomic displacement in acoustic branches. Because of mixing of modes, the definition is not always precise. The contribution of acoustic branch along the a axis is the largest in accordance with the largest volume of constant frequency surface in Fig. 1.

The most recent value of the observed specific heat[1] is

$$C_v/R = 1.35 \cdot 10^{-5} T^3$$

while Wunderlich's value[9] is $1.90 \times 10^{-5} T^3$ and Reese's previous value[10] is $1.67 \times 10^{-5} T^3$. Since the extrapolation to 100% crystallinity has not been carried out in the latter two experimental values, it is reasonable that the calculated value is in good agreement with the most recent value.

III-4 DISCUSSIONS

Prominent difference of the present treatment from Debye's theory lies on the representation of the frequency distribution. As long as frequency is proportional to phase difference in three dimensional crystal, the frequency distribution is proportional to ν^2 and therefore T^3 law is derived. However, in Debye theory, the coefficient, "a" of (3.14) is determined from normalization about freedom and the specific heat includes adjustable parameter Θ_D,

$$(C_v/R) = (9T^3/\theta_D{}^3)\int_0^{\infty} x^4 \exp(x)\left[\exp(x)-1\right]^{-2}$$

whereas, in the present study, the coefficient is determined uniquely from the interchain force constants and the specific heat includes no adjustable parameter. Dependency of the specific heat upon T^3 law is shown in Fig. 2 where open circles are observed values[1)9)]. Solid line denotes the coefficient of T^3 calculated from (3.16) below $9^{\circ}K$ and from (1.19) with the frequency distribution (Fig. 5) of the preceding chapter above $9^{\circ}K$. As temperature is raised, one dimensional property of the dispersion curves of the crystal vibrations begins to take dominant effect upon the specific heat and deviation from T^3 law becomes remarkable. Then the specific heat gets proportional to T and apparent magnitude of the coefficient of T^3 becomes smaller. This tendency of the calculated results is in good agreement with the observed results.

For the calculation of the specific heat at the lowest temperature, the frequency distribution in the lowest frequency region is necessary. In this region, root sampling method does not provide sufficient frequency distribution unless a great number of points in δ space are incorporated. The frequency distribution from 14,580 points in δ space (about 120,000 modes below 700 cm^{-1}) is shown in right histogram of Fig. 3. As the division of δ space gets finer, the frequency distribution approaches to the analytical one. The frequency distribution from 1,180,980 points in δ space are drawn in left histogram of Fig. 3 where solid line is calculated from (3.15). Accordingly the specific heat calculated

from the frequency distribution of root sampling method is smoothly connected with the value from the analytical expression of (3.16).

Since the intrachain potential contributes to $H_A(\delta)_{cc}$, but not to $H_A(\delta)_{bb}$ and $H_A(\delta)_{aa}$, the latter two diagonal terms are commonly small and therefore the off-diagonal term of $H_A(\delta)_{ab}$ becomes comparable with those diagonal terms. Though $H_A(\delta)_{ac}$ and $H_A(\delta)_{bc}$ are as large as $H_A(\delta)_{ab}$, the effect is small because of the large value of $H_A(\delta)_{cc}$ and the constant frequency surface of the translational mode along the c axis becomes apparently oblate ellipsoid along δ_c, the volume of which becomes small. While remarkable departure of the constant frequency surface from an ellipsoid is found in T_a and T_b modes, which results from the mutual repulsion of two acoustic modes which enters through $H_A(\delta)_{ab}$. As shown in Table 1, the potential term of P_4 does not contribute to $H_A(\delta)_{ab}$ whereas, P_1, P_2 and P_3 contribute to it, thereby the repulsion is outstanding in the intermediate direction of δ_a and δ_b axes. The increment of volume of the lowest branch due to the interaction is larger than the decrease of the volume of other branches and the resultant specific heat becomes larger than the value obtained from the ellipsoid of diagonal terms which is estimated from (1.23) as

$$(C_v/R)_a = 0.587\times10^{-5}T^3$$
$$(C_v/R)_b = 0.387\times10^{-5}T^3$$
$$(C_v/R)_c = 0.097\times10^{-5}T^3$$
$$(C_v/R) = 1.071\times10^{-5}T^3$$

In consequence it became evident that the mixing of acoustic modes has the significant effect upon the low temperature specific heat.

SUMMARY

The dynamical matrix for acoustic vibrations were derived with the use of perturbation method. The resultant matrix is equivalent to that derived from the elastic waves. On the calculation of low temperature specific heat, acoustic phonon-phonon interactions were incorporated, which led to larger specific heat than without the interaction. The frequency distribution derived from the constant frequency surface was in good agreement with that of root sampling method. From the present treatment, the interchain force constants were adjusted as P_1=0.0042, P_2=0.0101, P_3=0.0064 and P_4=0.0112 md/Å.

REFERENCES

1) J.E.Tucker and W.Reese, J. Chem. Phys., 46, 1388 (1967).

2) P.Debye, Ann. d. Phys., 39, 789 (1912)

3) A.Odajima, and T.Maeda, J. Polymer Sci., C-15, 55 (1966).

4) J.E.Bertie and G.E.Whalley, J. Chem. Phys., 41, 575 (1964).

5) R.G.Snyder, J. Mol. Spectry., 4, 411 (1960); 7, 116 (1961).

6) M.Born and K.Huang, " Dynamical Theory of Crystal Lattices" Oxford Univ. Press, Oxford (1954).

7) C.Kittel, " Introduction to Solid State Physics", p.94, John Wiley Sons, New York (1953).

8) W.V.Houston, Rev. Mod. Phys., 20, 161 (1948).

9) B.Wunderlich, J. Chem. Phys., 37, 1207 (1962).

10) W.Reese and J.E.Tucker, J. Chem. Phys., 43, 105 (1965).

Table-1 The coefficients of δ for the acoustic branches

A_a	$0.0029P_1$	$+ 0.0209P_2$	$+ 0.0153P_3$	
B_a	$0.0029P_1$	$+ 0.0209P_2$	$+ 0.0153P_3$	$+ 0.0007P_4$
C_a	$0.0550P_1$	$+ 0.0620P_2$	$+ 0$	$+ 0.0007P_4$
A_b	$0.0258P_1$	$+ 0.0069P_2$	$+ 0.0026P_3$	
B_b	$0.0258P_1$	$+ 0.0069P_2$	$+ 0.0026P_3$	$+ 0.0521P_4$
C_b	$0.0258P_1$	$+ 0.0291P_2$	$+ 0$	$+ 0.0683P_4$
A_c	$0.0070P_1$	$+ 0.0079P_2$	0	
B_c	$0.0070P_1$	$+ 0.0079P_2$	$+ 0$	$+ 0.0185P_4$
C_c	$0.0083P_1$	$+ 0.0102P_2$	$+ 0$	$+ 0.0068P_4 + 0.0775$
d_{ab}	$0.0172P_1$	$+ 0.0240P_2$	$+ 0.0125P_3$	
d_{ac}	$0.0245P_1$	$+ 0.0367P_2$	$+ 0.0020P_3$	
d_{bc}	$0.0280P_1$	$+ 0.0235P_2$	$+ 0.0008P_3$	$+ 0.0544P_4$

Table-2 Comparisons of the calculated frequency. (cm^{-1})

mode	ν from $D_S(\delta)$	ν from $H_A(\delta)$
T_a	4.6	4.6
T_b	6.0	6.2
T_c	36.3	36.4

δ is set to be $\delta_a=\delta_b=\delta_c=0.1$.

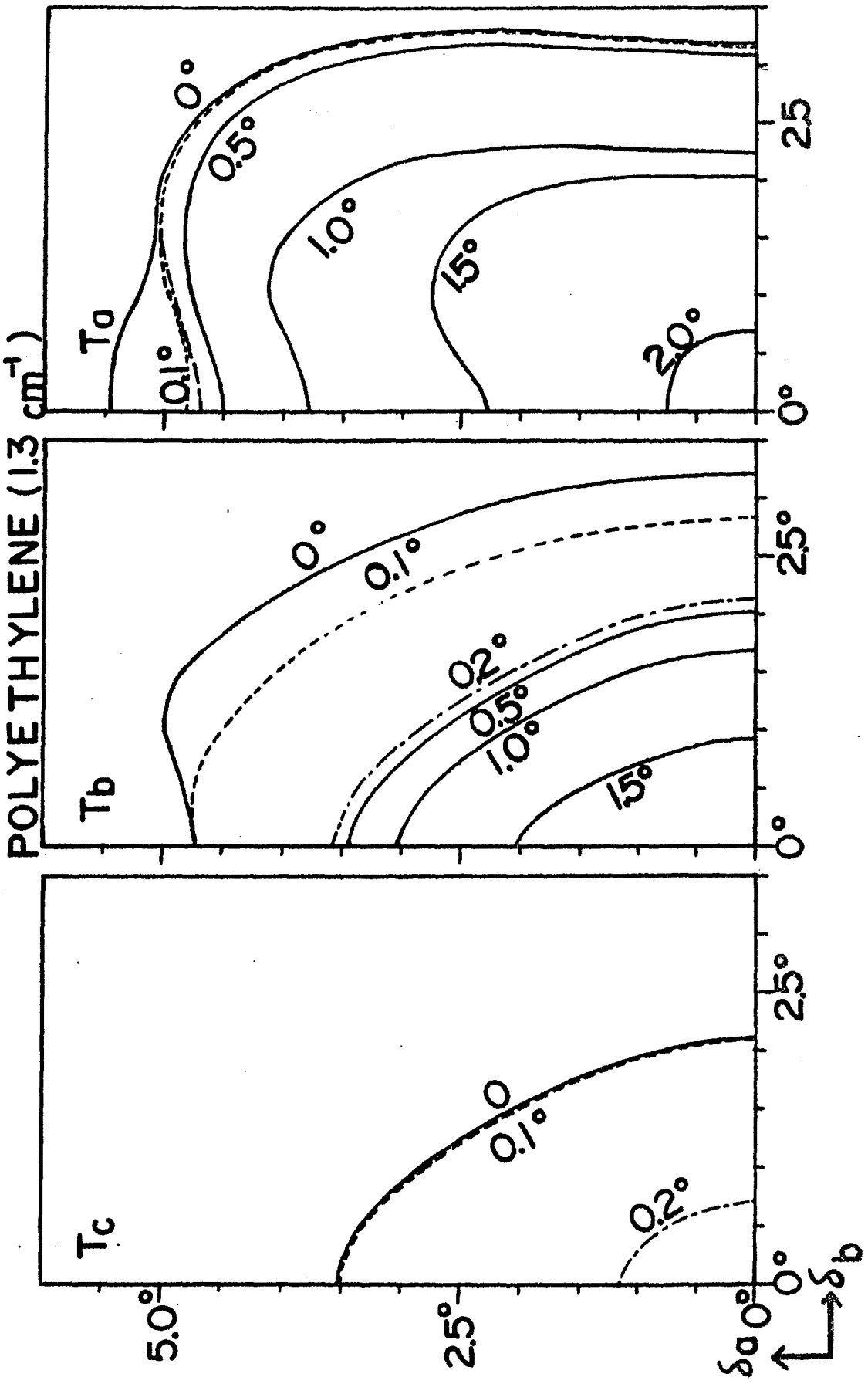

Fig. 1. Constant frequency surfaces of acoustic phonons of polyethylene crystal. The iso-frequency contours are projected on $\delta_a \delta_b$ plane.

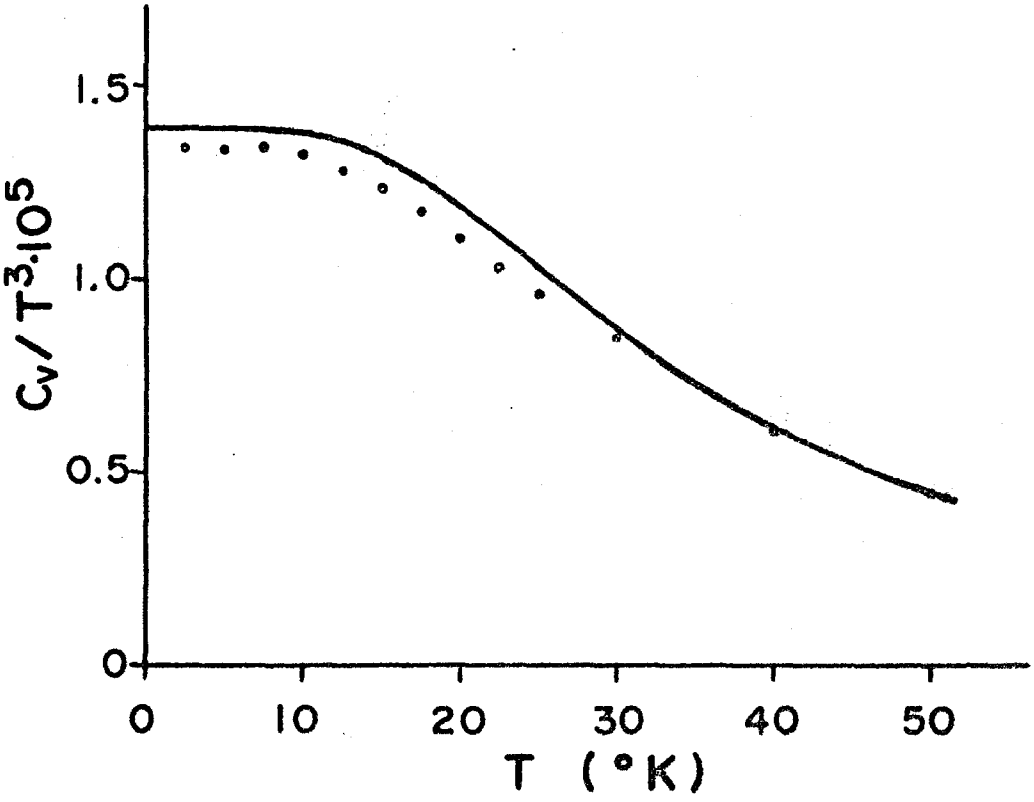

Fig. 2. Dependency of the specific heat upon T^3 law.
o; observed values by Tucker[1] for $T < 30^\circ K$
and by Wunderlich[9] for $T > 30^\circ K$.
—; calculated values.

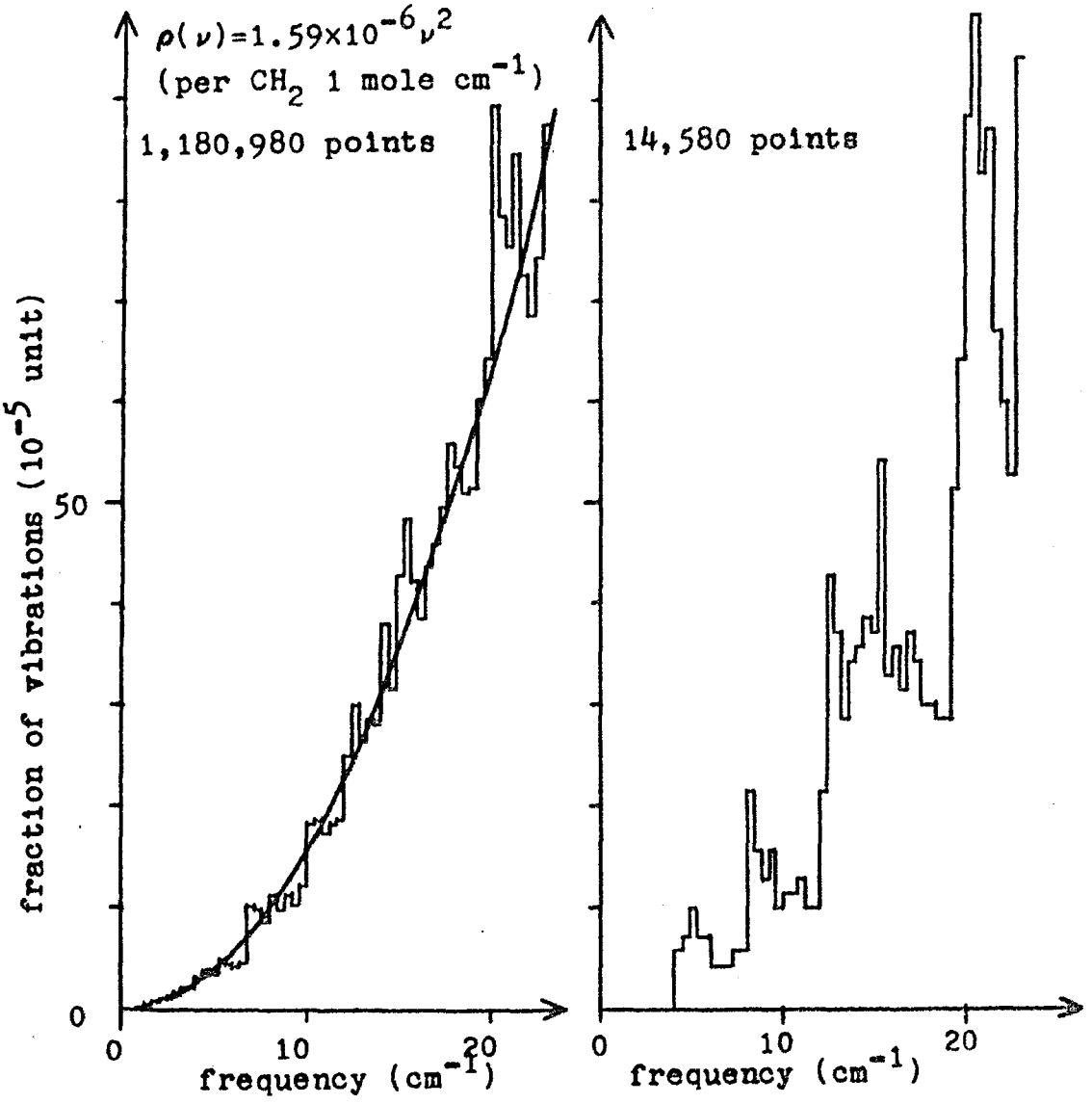

Fig. 3: The frequency distribution of acoustic phonons of polyethylene crystal. Solid line is obtained from (3.15) and histograms are obtained from root sampling method.

CHAPTER IV

SYMMETRY OF CRYSTAL VIBRATIONS, DISPERSION CURVES AND INFRARED BANDS DUE TO COMBINATION VIBRATIONS

IV-1 INTRODUCTION

Because of the translational symmetry of the crystal, the wave functions of the crystal is expanded in Fourier series of reciprocal vectors, where two wave functions corresponding to different k vectors are orthogonal. Then the Hamiltonian of the crystal is specified with k vector. When n atoms are contained per unit cell, there are 3n vibrations for a given k vector, and therefore there are 3n branches of crystal vibrations.

In a simple crystal lattices these branches are approximately classified with respect to atomic displacements. When the atomic displacement is parallel to k vector, the mode is called longitudinal but when the displacement is perpendicular to the k vector, the mode are called transverse. This notation is of great advantage to an isotropic ionic crystals such as NaCl, because photons (electromagnetic field) interact only with transverse modes.[1] However, for highly anisotropic polyethylene crystal, the transverse modes for a given k vector are not always separable from the longitudinal modes and the classification is not valid.

In the present study, the dispersion curves of $-(CH_2)_n-$ and $-(CD_2)_n-$ polyethylene crystals were calculated along the symmetry directions of the Brillouin zone and they are

classified in accordance with their symmetry properties. The dispersion curves of $-(CD_2)_n-$ crystal are expected to be obtained directly from the experiment of the coherent inelastic scattering of neutrons and, in fact, King et al.[2] have recently observed the dispersion curve along δ_c. On the other hand, from the dispersion curves of $-(CH_2)_n-$ crystal, infrared combination bands may be expected in the frequency range of 150-600 cm^{-1}. Since polyethylene crystal is considered to be transparent for infrared radiation in this frequency region with respect to fundamental bands, thick samples were examined and several absorption bands were, in fact, observed.

IV-2 **k** GROUP

An ensemble of the space group operations which make **k** vector invariant is called **k** group which is a subgroup of the point group of the space group.[3] The effect of the space group operation R_h upon exponential function is defined by

$$R_h \exp(i\boldsymbol{\rho}\delta) = \exp(i\alpha_h\boldsymbol{\rho}\delta + i\tau_h\delta) \qquad (4.1)$$

where δ is phase difference vector and $\boldsymbol{\rho}$ is index vector. α_h and τ_h are the rotational operation and the relevant non-primitive translation, respectively. Since α_h is an orthogonal matrix, $(\alpha_h\boldsymbol{\rho})\delta$ is equivalent to $\boldsymbol{\rho}(\alpha_h^{-1}\delta)$.[5] Accordingly, the **k** group is defined as the ensemble of operations which satisfy

$$\alpha_h^{-1}\delta = \delta + 2\pi m \quad (m;\ \text{integer}). \qquad (4.2)$$

The space group of the polyethylene crystal is P_{nam} (D_{2h}^{16})[4] and the corresponding point group is D_{2h}. Symmetry operations of the polyethylene crystal are shown in Table A1 of Appendix I. For $\delta=(0,0,0)$, all of eight operations satisfy Eq.(4.2) and

then the **k** group is D_{2h}. When the value of δ_a varies keeping $\delta_b=\delta_c=0$, Eq.(4.2) is satisfied only with four operations which are R_1=E(identity), $R_2=C_2^a$(screw axis along the a axis), $R_7=\sigma_g$(ac)(glide plane normal to the b axis) and $R_8=\sigma_g$(ab)(glide plane normal to the c axis). Accordingly the **k** group is C_{2v}. While for $\delta=(\pi,0,0)$, the remaining four operations which are $R_3=C_2^b$(screw axis along the b axis), $R_4=C_2^c$(screw axis along the c axis), R_5=i(inversion) and $R_6=\sigma_g$(bc)(glide plane normal to the a axis), again satisfy Eq(4.2). It results from the equivalence of $(\pi,0,0)$ and $(-\pi,0,0)$. The **k** goup again becomes D_{2h} but the irreducible representation is different from that for (0,0,0). All **k** groups of the polyethylene crystal are derived in the present study as shown in Table 1, where the symbol of the special point in the first Brillouin zone follows BSW notation.[6)]

For a given phase difference vector, the **k** group includes only identity operation and the crystal vibrations corresponding to the inner points of the first Brillouin zone are merely factorized into two groups, symmetric and antisymmetric to inversion. The real dynamical matrix of dimension 3n is not endowed with any symmetry property, and is not reducible.

IV-3 IRREDUCIBLE REPRESENTATION OF k GROUP

Dispersion curves along the symmetry directions of phase difference vector belong to one of the irreducible representations of the k group. If the irreducible representation were available, the symmetry coordinates corresponding to each species could be constructed and the modes could be drawn schematically in terms of the atomic displacement. Slater[3] has derived the irreducible representation for 20 space groups but the Table for the space group P_{nam} is not included. Accordingly the irreducible representations and base functions are derived with the use of Slater's method[3].

On successive application of the point group operations to the wave function, the resultant effect is equivalent to one of the point group operations, whereas for the space group operations the situation is different with regard to the effect of nonprimitive translations. Supposing R_j is operated on the exponential function after R_h, then

$$\begin{aligned} R_j R_h \exp(i\rho\delta) &= R_j \exp(i\alpha_h \rho\delta)\cdot\exp(i\tau_h\delta) \\ &= \exp\left[i\alpha_h(\alpha_j\rho+\tau_j)\delta\right]\cdot\exp(i\tau_h\delta) \\ &= \exp(i\alpha_h\alpha_j\rho\delta)\cdot\exp\left[i(\alpha_h\tau_j+\tau_h)\delta\right] \end{aligned} \qquad (4.3)$$

The multiplication table about α is identical with that of the point group operation. However, even though $\alpha_h\alpha_j$ is α_k, $\alpha_h\tau_j+\tau_h$ is not always equal to τ_k. With the use of τ_0 defined by

$$\alpha_h\tau_j + \tau_h = \tau_k + \tau_0 \qquad (4.4)$$

the effect of two successive operations can be represented with one of the space group operations as

$$R_j R_h \phi_0 = \exp(i\mathbf{t}_0\delta) R_k \cdot \phi_0 \qquad (4.5)$$

where $\phi_0 = \exp(i\rho\delta)$. Thus the multiplication table for P_{nam} were derived as shown in Table A2, where the first operations are written in the first row and the second operations in the first column. From the table, the irreducible representations and the base functions were derived. All the irreducible representations of the space group P_{nam} are shown in from Table A3 to Table A20. Some of these are picked up and explained in detail here but the remaining ones are proved in the same way.

For $\delta=(\delta_a,0,0)$ we have four operations, R_1, R_2, R_7 and R_8 which belong to k group. Multiplication table for these are shown in Table 2. Since R_2 and R_7 are accompanied with phase factor, the following type of base functions occur to our minds.

$$\phi_1 = \left[R_1+R_8+\exp(-i\delta_a/2)(R_2+R_7)\right]\phi_0 \qquad (4.6)$$

The application of the operators to ϕ_1 leads us to

$$R_1\phi_1 = \left[R_1R_1+R_1R_8 + \exp(-i\delta_a/2)(R_1R_2+R_1R_7)\right]\phi_0 = \phi_1$$

$$R_2\phi_1 = \left[R_2R_1+R_2R_8 + \exp(-i\delta_a/2)(R_2R_2+R_2R_7)\right]\phi_0$$

$$= \left[R_2+R_7+\exp(-i\delta_a/2)\exp(i\delta_a)(R_1+R_8)\right]\phi_0 = \exp(i\delta_a/2)\phi_1$$

$$R_7\phi_1 = \left[R_7+R_2+\exp(i\delta_a/2)(R_8+R_1)\right]\phi_0 = \exp(i\delta_a/2)\phi_1$$

$$R_8\phi_1 = \left[R_8+R_1+\exp(-i\delta_a/2)(R_7+R_2)\right]\phi_0 = \phi_1$$

Then ϕ_1 is a base function for one dimensional representation. Remaining three functions, derived from the regular representations, are as follows.

$$\phi_2 = \left[R_1+R_8-\exp(-i\delta_a/2)(R_2+R_7)\right]\phi_0$$

$$\phi_3 = \left[R_1-R_8+\exp(-i\delta_a/2)(R_2-R_7)\right]\phi_0$$

$$\phi_4 = \left[R_1-R_8-\exp(-i\delta_a/2)(R_2-R_7)\right]\phi_0$$

and the resultant function after the application of symmetry operations are represented as

$R_1\phi_2=\phi_2$ $R_2\phi_2=-\exp(i\delta_a/2)\phi_2$ $R_7\phi_2=-\exp(i\delta_a/2)\phi_2$ $R_8\phi_2=\phi_2$

$R_1\phi_3=\phi_3$ $R_2\phi_3=+\exp(i\delta_a/2)\phi_3$ $R_7\phi_3=-\exp(i\delta_a/2)\phi_3$ $R_8\phi_3=-\phi_3$

$R_1\phi_4=\phi_4$ $R_2\phi_4=-\exp(i\delta_a/2)\phi_4$ $R_7\phi_4=+\exp(i\delta_a/2)\phi_4$ $R_8\phi_4=-\phi_4$

Thus one dimensional representation of the k group at Σ was derived and is summarized in Table A3, where ϕ_1, ϕ_2, ϕ_3 and ϕ_4 are base functions of Σ_1, Σ_2, Σ_3 and Σ_4, respectively. With the use of the usual point group notation of C_{2v}, Σ_1, Σ_2, Σ_3, and Σ_4 correspond to A_1, B_2, A_2 and B_1, respectively.

The multiplication table for $(\delta_a,\pi,0)$, $(\delta_a,0,\pi)$ and (δ_a,π,π) are proved to be identical with Table 2. Accordingly the irreducible representations for these points are common to that of $(\delta_a,0,0)$. On the other hand, the nonprimitive translations accompanied with C_2^a, C_2^b, and C_2^c are different from each other, therefore the irreducible representations for $(0,\delta_b,0)$ and $(0,0,\delta_c)$ are not simple permutation of δ_a, δ_b and δ_c in the representation for $(\delta_a,0,0)$. For $(0,\delta_b,0)$ and $(\pi,\delta_b,0)$, the multiplication tables are common but different from those for $(0,\delta_b,\pi)$ and (π,δ_b,π). The irreducible representation of the former is one dimensional whereas that of the latter is two dimensional. The irreducible representations for $(0,0,\delta_c)$ and (π,π,δ_c) are one dimensional but those for $(0,\pi,\delta_c)$ and $(\pi,0,\delta_c)$ are two dimensional. As the example, $(0,\pi,\delta_c)$ is picked up. The multiplication table for $(0,\pi,\delta_c)$ is shown in Table 3, where R_1, R_4, R_6 and R_7 belong to the k group. Table 2. is symmetric about diagonal line whereas Table 3.

is not symmetric. In the same way with Eq(4.6), proper linear combinations of regular representations such as

$$\phi_1 = [R_1+R_7 + \exp(-i\delta_c/2)(R_4+R_6)]\,\phi_0 \qquad (4.7)$$

were constructed and subjected to symmetry operations. R_1 and R_4 give rise to the same type of the function, whereas R_6 and R_7 yield different type of function, ϕ_2, as

$$\begin{aligned} R_6\phi_1 &= [R_6(R_1+R_7) + \exp(-i\delta_c/2)R_6(R_4+R_6)]\,\phi_0 \\ &= [R_6+R_4 - \exp(i\delta_c/2)(R_7+R_1)]\,\phi_0 \\ &= \exp(i\delta_c/2).\phi_2 \end{aligned} \qquad (4.8)$$

Accordingly, the irreducible representation becomes two-dimensional.

On the surface of the first Brillouin zone, the **k** group is always C_s and the dynamical matrix is factorized into two blocks with the symmetry transformation. For the example of (π,δ,δ), the symmetry operations of the **k** group are R_1 and R_6. As they are not points of high symmetry, there is no BSW symbol while the irreducible representations for these faces are shown in Tables A11-A13. At the corner of the zone, the symmetry becomes D_{2h} again and there appears degeneracy of the lattice vibrations. The corner of degeneracy does not always coincide with the dimensionality of the irreducible representation. Two typical examples of the irreducible representations for D_{2h} are derived below and the relation of the dimensionality with the degeneracy of energy level is treated later.

The multiplication table of the **k** group at $(\pi,\pi,0)$ is represented as Table 4, where operations are rearranged from Table A2. Supposing that group of operations, A includes R_1,

R_4, R_5 and R_8 while group B includes R_2, R_3, R_6 and R_7, then the multiplication table is simply represented as

	A	B
A	A	B
B	B	-A

where the operations in the first column are applied after those in the first row. If we select the base functions as $\phi_1=(A+B)\phi_0$ and $\phi_2=(A-B)\phi_0$, then the resultant functions after the symmetry operations are as follows;

$$A\phi_1 = \phi_1 \qquad A\phi_2 = \phi_2 \qquad B\phi_1 = -\phi_2 \qquad B\phi_2 = \phi_1$$

Therefore the representation is real and two-dimensional. For the group of order eight, there should be two types of two-dimensional irreducible representations. On the other hand, if we take complex functions such as $\phi_1=(A+iB)\phi_0$ and $\phi_2=(A-iB)\phi_0$, then the symmetry operations yield

$$A\phi_1 = \phi_1 \qquad A\phi_2 = \phi_2 \qquad B\phi_1 = -i\phi_1 \qquad B\phi_2 = i\phi_2$$

and the representation becomes one-dimensional. Since four independent linear combinations are possibly made within the group A or B, eight base functions can be constructed. Thus derived one-dimensional representation is shown in Table A17.

The situation of the k group for (π,π,π) is fairly different from $(\pi,\pi,0)$. As shown in Table 5, multiplication table is neither symmetric nor skew symmetric. If the representation is written with real number, it becomes four dimensional, where the base functions are

$$\phi_1 = (R_1+R_8+R_2+R_7)\phi_0$$
$$\phi_2 = (R_1+R_8-R_2-R_7)\phi_0$$
$$\phi_3 = (R_5+R_4+R_6+R_3)\phi_0$$

$$\phi_4 = (R_5+R_4-R_6-R_3)\phi_0$$

On the other hand, theorem of group theory states that the sum of square of the dimension of the representation is equal to the number of operations[7], therefore four dimensional representation is impossible for the group of order eight. Using complex number in the coefficients of base functions, we can obtain two-dimensional representations which are shown in Table A20.

IV-4 DEGENERACY OF ENERGY LEVEL

Dimensionality of the irreducible representation does not always coincide with the degree of degeneracy of the energy level. A transformation matrix corresponding to symmetry operations of the k group keeps the dynamical matrix invariant and then complex conjugate of the transformation matrix also commutes with the dynamical matrix. Supposing $T(\delta,R_i)$ is the transformation matrix of symmetry operation, R_i, and $T^*(\delta,R_i)$ is its complex conjugate, then

$$\begin{aligned} T(\delta,R_i)D_S(\delta) &= D_S(\delta)T(\delta,R_i) \\ T^*(\delta,R_i)D_S(\delta) &= D_S(\delta)T^*(\delta,R_i) \end{aligned} \qquad (4.9)$$

where $D_S(\delta)$ is dynamical matrix for arbitrary phase difference vector and satisfies the secular equation of

$$D_S(\delta)L_j(\delta) = \lambda_j(\delta)L_j(\delta) \qquad (4.10)$$

where $\lambda_j(\delta)$ and $L_j(\delta)$ are j-th eigenvalue and the corresponding eigenvector, respectively. Multiplying (4.10) from left by $T(\delta,R_i)$ and $T^*(\delta,R_i)$ yields

$$\begin{aligned} D_S(\delta)T(\delta,R_i)L_j(\delta) &= \lambda_j(\delta)T(\delta,R_i)L_j(\delta) \\ D_S(\delta)T^*(\delta,R_i)L_j(\delta) &= \lambda_j(\delta)T^*(\delta,R_i)L_j(\delta) \end{aligned} \qquad (4.11)$$

It shows that both of $T(\delta,R_i)L_j(\delta)$ and $T^*(\delta,R_i)L_j(\delta)$ are eigenvector of $D_S(\delta)$. If $T(\delta,R_i)$ and $T^*(\delta,R_i)$ are inequivalent

two eigenvectors becomes inequivalent and then two linear independent vectors belong to the same eigenvalue. In other words, if $T(\delta,R_1)$ and $T^*(\delta,R_1)$ belong to different species, then extra degeneracy appears.

Maradudin and Vosko[8] have studied the symmetry of crystal vibrations by the use of multiplier co-representation method and derived a simple rule about degeneracy due to time reversal symmetry.

$$\Sigma_R \phi(\delta,A_0R,A_0R)\chi^S(\delta, A_0RA_0R) = g \quad \text{a type} \qquad (4.12a)$$

$$= -g \quad \text{b type} \qquad (4.12b)$$

$$= 0 \quad \text{c type} \qquad (4.12c)$$

$\phi(\delta,A,R)$ is a multiplier representation of the space group operation defined by Eq(4.13).

$$\phi(\delta,A,R) = \exp\left[-i(\delta + A^{-1}\delta)\cdot\tau(R)\right] \qquad (4.13)$$

R is an unitary type operation and A is an antiunitary type operation. For example at point Σ, R_1, R_2, R_7 and R_8 are unitary type operations and R_3, R_4, R_5 and R_6 are antiunitary type operations. A_0 is an arbitrary operator of A type. In the case of the polyethylene crystal, it is convenient to regard A_0 as inversion, because inversion acts always as antiunitary operator for all k groups. $\chi^S(\delta, A_0RA_0R)$ is a character of S-th irreducible representation for the operator A_0RA_0R. When A_0 is inversion, A_0RA_0R is always equal to identity operation for all R in D_{2h} system. Summation runs over all operators in k group where g is order of k group. Supposing the dimension of the irreducible representation is f_S, then energy level is f_S-fold degenerate for a type,

whereas $2f_S$-fold degenerate for b and c type.[8)]

In Table 6, $\phi(\delta, A_0R_1, A_0R_1)$ are derived for all operators of the space group P_{nam}. At each point represented in Table 1, the corresponding value of phase difference is substituted for δ_a, δ_b or δ_c. Thus the type of time reversal symmetry were derived and shown in Table 7. The extra degeneracy due tc time reversal symmetry appears at points of A, C, E, G, Q, F, S, U, and R. At points of Q, S, and R, in particular, the dimension of the irreducible representation is two, therefore the resultant degeneracy of energy level becomes four-fold, which is rarely seen in the molecular vibrations.

IV-5 DISPERSION CURVES AND COMPATIBILITY RELATIONS

Dispersion curves of the frequency of crystal vibrations were calculated and are shown in Fig. 1 - Fig. 8. The corresponding curve of $-(CD_2)_n-$ polyethylene crystal were calculated with the same force constants and are shown in Fig. A1- Fig. A6 of Appendix I. Since eight modes corresponding to low frequency lattice vibrations below 700 cm^{-1} were treated here, four curves appear for doubly degenerate cases and two curves appear for four-fold degenerate cases, in accord with the theoretical prediction of Table 7.

Along $(\delta_a, 0, 0)$ there are eight lattice vibrations which are classified into four groups (Σ_1, Σ_2, Σ_3, and Σ_4) in accordance with the symmetry property about the k group operations. Even for very small values of δ_a, the classification is valid and therefore the symmetry property of the wave function changes continuously on the change of phase difference

from $(\delta_a,0,0)$ to $(0,0,0)$. Then the irreducible representation of the k group changes continuously with the change of phase difference. Substitution of $\delta_a=0$ for the irreducible representation of Table A4 shows how the base functions of Σ point behave at (0,0,0). It is represented in Table 8. When the element of Table 8 is identical with the character of the irreducible representation for (0,0,0), these two species are compatible. For instance A_g and B_{1u} have identical characters with Σ_1, therefore lattice vibrations which belong to A_g or B_{1u} at (0,0,0) are connected with Σ_1 branch on $(\delta_a,0,0)$. This relation is called compatibility relation which is derived from the characters of the irreducible representations, and thus derived compatibility diagram for polyethylene crystal is shown in Table-A21.

IV-6 COMBINATION BANDS OF THE INFRARED ABSORPTION

On the interaction of phonons with photons, total wave vector is always conserved. Since the wave vector of infrared radiation is extremely small compared with the principal vector of the reciprocal space, a photon interacts with a phonon of almost k=0. When a photon interacts with two phonons simultaneously, the conservation law requires that one phonon corresponds to $+\delta$ and the other to $-\delta$.

On the other hand, intensity of infrared absorption band depends upon both the number of infrared active combinations and the squared magnitude of each transition moment. Although a few combinations on the edge of the first Brillouin zone are deduced to be infrared inactive, all combinations on the inner

points of the zone are possibly infrared active and the number of modes is extremely larger inside of the zone than on the edges. Then the infrared spectrum might be qualitatively compared with the number of combination vibrations. Accordingly, the frequency distribution of the binary combination modes were calculated and compared with infrared spectrum, observed at 77°K, in Fig. 9. The infrared band at 79 cm^{-1} is B_{1u} fundamental band which is associated with antiparallel translatory vibration perpendicular to the chain axis.[10-11] Three peaks are expected in the frequency distribution. The calculated peak at 230 cm^{-1} is primarily associated with the combination levels of the overall rotatory vibrations (~150 cm^{-1}) with the antiparallel translatory vibrations perpendicular to the chain axis (~80 cm^{-1}). The peak at 280 cm^{-1} is due to the combination of two rotatory vibrations which really belong to infrared active combinations ($\Sigma_1 \times \Sigma_2$ or $\Lambda_1 \times \Lambda_4$). The calculated peak near 380 cm^{-1} is associated with internal rotation branches. Since the combination of $\Delta_1 \times \Delta_3$ belong to infrared inactive species, these peak might possibly be obscured in infrared spectrum, in good agreement with the observed results. Accordingly the observed bands below 400 cm^{-1} are reasonably explained as combination bands, however the band near 560 cm^{-1} is not assigned reasonably in terms of combination tones.

IV-7 DISCUSSIONS

As discussed in Chapter III, there is no infrared active fundamental band below 700 cm^{-1} except for B_{1u} and B_{2u} lattice vibrations. Dean and Martin[12] have measured the infrared spectrum at $2^{o}K$ and found weak absorption at 109 cm^{-1}. They have assigned it to the B_{2u} lattice vibration. Accordingly the weak absorptions observed in the region of 200-400 cm^{-1} are not due to fundamental lattice vibrations. Since the band intensity becomes stronger as temperature is lowered, the bands cannot be difference combination bands. On assigning these bands to combination tones, transition-moment associated with the transition has to be finite, which is equivalent to state that the product of the initial and final wave functions includes one of the symmetry species of dipole-moment. Supposing the crystal is initially at ground state and two vibrations $\phi_{\alpha}(\delta)$ and $\phi_{\beta}(-\delta)$ are excited by one quantum number on the interaction with photon, then the infrared absorption is possible only when $\phi_{\alpha}(\delta)\phi_{\beta}(-\delta)$ includes one of the symmetry species of dipole moment, where $\phi_{\alpha}(\delta)$ is wave function of α-th crystal vibration for δ. Since the $\phi_{\beta}(-\delta)$ is a complex conjugate of $\phi_{\beta}(\delta)$, the character of symmetry operation for $\phi_{\beta}(-\delta)$ is also complex conjugate of Tables represented in Appendix I. Thus symmetry of $\phi_{\alpha}(\delta)\phi_{\beta}(-\delta)$ is derived from the direct product of the symmetry species. In Table 9, the direct product analysis for $(\delta_a,0,0)$ is shown as an example. This table is common for the point A, C, and E. In point group C_{2v}, dipole moment along the a, b and c axes

belong to A_1, B_2 and B_1 species, respectively. Therefore the combination levels corresponding to $\Sigma_1 \times \Sigma_3$ and $\Sigma_2 \times \Sigma_4$ are infrared inactive. In the same way, the transitions to combination levels corresponding to $\Delta_1 \times \Delta_3$, $\Delta_2 \times \Delta_4$, $\Lambda_1 \times \Lambda_3$, $\Lambda_2 \times \Lambda_4$, and $F_k \times F_k$ are proved to be infrared inactive. For other combinations, direct product includes at least one of the infrared active species.

The frequency distribution for all the infrared inactive combinations was made and is shown in Fig. 10. The combination tones which are infrared inactive on the faces of the Brillouin zone would be weak even though δ is altered. Then combination bands corresponding to peaks in Fig. 10 might be weak even if they correspond to the peak in Fig. 9. In fact infrared absorption near 380 cm^{-1} is weak. However, for the quantitative discussions, band intensity has to be estimated theoretically.

Maradudin[13] has studied the infrared absorption of a defect or disordered crystal. He proved that the peak of frequency distribution is possibly observed as infrared absorption band in such crystals. Since there is a strong peak at 560 cm^{-1} in the frequency distribution of the polyethylene crystal, the infrared absorption band at 560cm^{-1} might be associated with the skeletal bending mode, which appeared in the infrared spectrum because of the disorder. Theoretical development about the disordered crystal is highly desirable.

On the other hand, it is interesting to confirm the existence of four-fold degenerate vibrations in terms of

symmetry coordinates which may be derived for the special value of δ from the base function represented in Appendix I. For convenience sake, σ_i defined by (4.14) was used instead of $R_i\exp(i\rho\delta)$, where x_j, y_j and z_j are atomic displacement of j-th methylene group.

$$\sigma_1=\begin{bmatrix} x_1 \\ y_1 \\ z_1 \end{bmatrix}\cdot\exp(i\rho_1\delta) \qquad \sigma_2=\begin{bmatrix} x_3 \\ -y_3 \\ -z_3 \end{bmatrix}\cdot\exp(i\rho_3\delta) \qquad \sigma_3=\begin{bmatrix} -x_4 \\ y_4 \\ -z_4 \end{bmatrix}\cdot\exp(i\rho_4\delta)$$

$$\sigma_4=\begin{bmatrix} -x_2 \\ -y_2 \\ z_2 \end{bmatrix}\cdot\exp(i\rho_2\delta) \qquad \sigma_5=\begin{bmatrix} -x_2 \\ -y_2 \\ -z_2 \end{bmatrix}\cdot\exp(i\rho_2\delta) \qquad \sigma_6=\begin{bmatrix} -x_4 \\ y_4 \\ z_4 \end{bmatrix}\cdot\exp(i\rho_4\delta)$$

$$\sigma_7=\begin{bmatrix} x_3 \\ -y_3 \\ z_3 \end{bmatrix}\cdot\exp(i\rho_3\delta) \qquad \sigma_8=\begin{bmatrix} x_1 \\ y_1 \\ -z_1 \end{bmatrix}\cdot\exp(i\rho_1\delta) \qquad (4.14)$$

$$\rho_1 = (h,k,l+1/4) \qquad \rho_3 = (h+\tfrac{1}{2},k+\tfrac{1}{2},l+1/4)$$

$$\rho_2 = (h,k,l-1/4) \qquad \rho_4 = (h+\tfrac{1}{2},k+\tfrac{1}{2},l-1/4)$$

According to Table 7, the energy level is doubly degenerate at point U, though the dimension of the representation of k group is one. Substitution of σ_i for R_i in Table A17 provides symmetry coordinates for the k group at point U as

$$\begin{aligned}
U_1 &\quad x_1-x_2+ix_3-ix_4, && y_1-y_2-iy_3+iy_4 \\
U_2 &\quad x_1-x_2-ix_3+ix_4, && y_1-y_2+iy_3-iy_4 \\
U_3 &\quad z_1+z_2-iz_3-iz_4 \\
U_4 &\quad z_1+z_2+iz_3+iz_4 \\
U_5 &\quad z_1-z_2-iz_3+iz_4 \\
U_6 &\quad z_1-z_2+iz_3-iz_4 \\
U_7 &\quad x_1+x_2+ix_3+ix_4, && y_1+y_2-iy_3-iy_4 \\
U_8 &\quad x_1+x_2-ix_3-ix_4, && y_1+y_2+iy_3+iy_4
\end{aligned} \qquad (4.15)$$

Two coordinates included in the pair of U_1 and U_2, U_3 and U_4, U_5 and U_6, and U_7 and U_8, are, in fact, degenerate. U_1 and U_2 correspond to rotational vibration around the chain axis and skeletal stretching modes. The former is connected with G_1, G_4 branch along $(\pi,\delta_b,0)$ as shown Fig. 1 and with A_1, A_2 along $(\delta_a,\pi,0)$ as shown in Fig. 2 while the latter lies above 700 cm^{-1} and is not treated. U_3 and U_4 are translatory vibration along the chain axis. The phase of $(h+\frac{1}{2},k+\frac{1}{2})$ chain is forward or backward by $\pi/2$ from (h,k) chain, and then the vibrational frequency for U_3 and U_4 should be identical. They are connected with G_2, G_3 along $(\pi,\delta_b,0)$ or A_3, A_4 along $(\delta_a,\pi,0)$. U_5 and U_6 are intrachain vibrations while U_7 and U_8 are associated with the translatory vibrations perpendicular to the chain axis.

On the other hand, at point R, the irreducible representations are two-dimensional. Substitution of σ_1 for R_1 in base functions represented in Table A20, yields the symmetry coordinates for (π,π,π).

$$\begin{array}{llll} R_1 & \phi_1 = (z_1+iz_3)\exp(i\pi/4) & R_2 & \phi_1 = (z_1-iz_3)\exp(+i\pi/4) \\ & \phi_2 = (-z_2-iz_4)\exp(-i\pi/4) & & \phi_2 = (-z_2+iz_4)\exp(-i\pi/4) \end{array} \quad (4.16)$$

The energy corresponding to ϕ_1 of R_1 and ϕ_1 of R_2 are equal for the same reason with the case of U_3 and U_4. Then, four functions of (4.16) belong to the same energy level and the existence of four-fold degeneracy may be understood.

The functions, which provide the identical characters with Table A20 but different matrix elements, are also base

function of the k group. For instance, (4.17) and (4.18) are proved to be base functions of the irreducible representation of R_1 and R_2.

$$\begin{aligned}\phi_1(R_1) &= (R_1-iR_2-iR_7+R_8)\exp(i\rho\delta)\\ \phi_2(R_1) &= (R_5-iR_6-iR_3+R_4)\exp(i\rho\delta)\end{aligned} \qquad (4.17)$$

$$\begin{aligned}\phi_1(R_2) &= (R_1+iR_2+iR_7+R_8)\exp(i\rho\delta)\\ \phi_2(R_2) &= (R_5+iR_6+iR_3+R_4)\exp(i\rho\delta)\end{aligned} \qquad (4.18)$$

Substitution of σ_i from (4.14) into R_i from (4.17) and (4.18) leads us to the symmetry coordinates about x and y as

$$\begin{aligned}\phi_1(R_1) &= (x_1+ix_3)\exp(i\pi/4) \quad & \phi_1(R_1) &= (y_1-iy_3)\exp(i\pi/4)\\ \phi_2(R_1) &= (-x_2-ix_4)\exp(-i\pi/4) \quad & \phi_2(R_1) &= (-y_2+iy_4)\exp(-i\pi/4)\\ \phi_1(R_2) &= (x_1-ix_3)\exp(i\pi/4) \quad & \phi_1(R_2) &= (y_1+iy_3)\exp(i\pi/4)\\ \phi_2(R_2) &= (-x_2+ix_4)\exp(-i\pi/4) \quad & \phi_2(R_2) &= (-y_2-iy_4)\exp(-i\pi/4)\end{aligned}$$

Thus the conclusion from time reversal symmetry is really confirmed in terms of symmetry coordinates.

The dispersion curves of $-(CD_2)_n-$ crystal were calculated from the same force field with $-(CH_2)_n-$ crystal and are shown in Appendix.

SUMMARY

Irreducible representation and base function of the k group of the space group, P_{nam} were derived with Slater's method. Dispersion curves of crystal vibrations of normal and deuterated polyethylene crystals were calculated along the symmetry directions. The symmetry of combination tone was analysed on the basis of the symmetry of dispersion curves, and infrared absorption bands recognized at 240 and 280 cm^{-1}

were assigned to combination bands. Simple rule about degeneracy of energy level due to time reversal symmetry, derived by Maradudin and Vosko, was applied to polyethylene crystal and the theoretical prediction was confirmed by the numerical calculations. Symmetry coordinates for point U and R were derived, and two-fold and four-fold degeneracy were really examined in terms of symmetry coordinates, respectively.

REFERENCES

1) M.Born and K.Huang, " Dynamical Theory of Crystal Lattices" Clarendon Press, Oxford (1954).

2) L.A.Feldkamp, G.Venkataraman and J.S.King, private communication.

3) J.C.Slater, " Quantum Theory of Molecules and Solid" vol.2, McGraw-Hill Comp. New York (1965).

5) L.Mariot, " Group Theory and Solid State Physics" (translated by A.Nussbaum).

6) L.P.Bouckaert, R.Smoluchowski and E.Wigner, Phys. Rev., 50, 58 (1936).

7) H.Eyring, J.Walter and G.E.Kimball, " Quantum Chemistry" John Wiley Sons, New York (1944).

8) A.A.Maradudin and S.H.Vosko, Rev. Mod. Phys., 40, 1 (1968).

9) R.V.McKnight and K.D.Möller, J. Opt. Soc. Am. 54, 132 (1964).

10) J.E.Bertie and E.Whalley, J. Chem. Phys., 41,575 (1964).

11) S.Krimm and M.I.Bank, J. Chem. Phys., 42, 4059 (1965).

12) G.D.Dean and D.H.Martin, Chem. Phys. Letters, 1, 415 (1967).

13) A.A.Maradudin, Solid State Physics, 19, 1 (1967).

Table-1 k group of the polyethylene crystal

point	$(\delta_a,\delta_b,\delta_c)$	k group	operations
Γ	(0,0,0)	D_{2h}	E, C_2^a, C_2^b, C_2^c, i, $\sigma_g(bc)$, $\sigma_g(ac)$, $\sigma_g(ab)$
Σ	$(\delta_a,0,0)$	C_{2v}	E, C_2^a, $\sigma_g(ac)$, $\sigma_g(ab)$
A	$(\delta_a,\pi,0)$	C_{2v}	E, C_2^a, $\sigma_g(ac)$, $\sigma_g(ab)$
C	$(\delta_a,0,\pi)$	C_{2v}	E, C_2^a, $\sigma_g(ac)$, $\sigma_g(ab)$
E	(δ_a,π,π)	C_{2v}	E, C_2^a, $\sigma_g(ac)$, $\sigma_g(ab)$
λ	$(0,\delta_b,0)$	C_{2v}	E, C_2^b, $\sigma_g(bc)$, $\sigma_g(ab)$
G	$(\pi,\delta_b,0)$	C_{2v}	E, C_2^b, $\sigma_g(bc)$, $\sigma_g(ab)$
H	$(0,\delta_b,\pi)$	C_{2v}	E, C_2^b, $\sigma_g(bc)$, $\sigma_g(ab)$
Q	(π,δ_b,π)	C_{2v}	E, C_2^b, $\sigma_g(bc)$, $\sigma_g(ab)$
Δ	$(0,0,\delta_c)$	C_{2v}	E, C_2^c, $\sigma_g(bc)$, $\sigma_g(ac)$
D	$(\pi,0,\delta_c)$	C_{2v}	E, C_2^c, $\sigma_g(bc)$, $\sigma_g(ac)$
B	$(0,\pi,\delta_c)$	C_{2v}	E, C_2^c, $\sigma_g(bc)$, $\sigma_g(ac)$
F	(π,π,δ_c)	C_{2v}	E, C_2^c, $\sigma_g(bc)$, $\sigma_g(ac)$
	(δ_a,δ_b,π)	C_s	E, $\sigma_g(ab)$
	(δ_a,π,δ_c)	C_s	E, $\sigma_g(ac)$
	(π,δ_b,δ_c)	C_s	E, $\sigma_g(bc)$
	$(\delta_a,\delta_b,0)$	C_s	E, $\sigma_g(ab)$
	$(\delta_a,0,\delta_c)$	C_s	E, $\sigma_g(ac)$
	$(0,\delta_b,\delta_c)$	C_s	E, $\sigma_g(bc)$
X	(π,0,0)	D_{2h}	E, C_2^a, C_2^b, C_2^c, i, $\sigma_g(bc)$, $\sigma_g(ac)$, $\sigma_g(ab)$
Z	(0,π,0)	D_{2h}	E, C_2^a, C_2^b, C_2^c, i, $\sigma_g(bc)$, $\sigma_g(ac)$, $\sigma_g(ab)$
Y	(0,0,π)	D_{2h}	E, C_2^a, C_2^b, C_2^c, i, $\sigma_g(bc)$, $\sigma_g(ac)$, $\sigma_g(ab)$
U	(π,π,0)	D_{2h}	E, C_2^a, C_2^b, C_2^c, i, $\sigma_g(bc)$, $\sigma_g(ac)$, $\sigma_g(ab)$
T	(0,π,π)	D_{2h}	E, C_2^a, C_2^b, C_2^c, i, $\sigma_g(bc)$, $\sigma_g(ac)$, $\sigma_g(ab)$
S	(π,0,π)	D_{2h}	E, C_2^a, C_2^b, C_2^c, i, $\sigma_g(bc)$, $\sigma_g(ac)$, $\sigma_g(ab)$
R	(π,π,π)	D_{2h}	E, C_2^a, C_2^b, C_2^c, i, $\sigma_g(bc)$, $\sigma_g(ac)$, $\sigma_g(ab)$

Table-2 Multiplication table of k group operations for $(\delta_a, 0, 0)$

	R_1	R_2	R_7	R_8
R_1	R_1	R_2	R_7	R_8
R_2	R_2	$e^a R_1$	$e^a R_8$	R_7
R_7	R_7	$e^a R_8$	$e^a R_1$	R_2
R_8	R_8	R_7	R_2	R_1

$e^a = \exp(i\delta_a)$

Table-3 Multiplication table of k group operations for $(0, \pi, \delta_c)$

	R_1	R_4	R_6	R_7
R_1	R_1	R_4	R_6	R_7
R_4	R_4	$e^c R_1$	$e^c R_7$	R_6
R_6	R_6	$-e^c R_7$	$-e^c R_1$	R_4
R_7	R_7	$-R_6$	$-R_4$	R_1

Table-4 Multiplication table of k group operations for $(\pi, \pi, 0)$

	R_1	R_4	R_5	R_8	R_2	R_3	R_6	R_7
R_1	R_1	R_4	R_5	R_8	R_2	R_3	R_6	R_7
R_4	R_4	R_1	R_8	R_5	R_3	R_2	R_7	R_6
R_5	R_5	R_8	R_1	R_4	R_6	R_7	R_2	R_3
R_8	R_8	R_5	R_4	R_1	R_7	R_6	R_3	R_2
R_2	R_2	R_3	R_6	R_7	$-R_1$	$-R_4$	$-R_5$	$-R_8$
R_3	R_3	R_2	R_7	R_6	$-R_4$	$-R_1$	$-R_8$	$-R_5$
R_6	R_6	R_7	R_2	R_3	$-R_5$	$-R_8$	$-R_1$	$-R_4$
R_7	R_7	R_6	R_3	R_2	$-R_8$	$-R_5$	$-R_4$	$-R_1$

Table-5 Multiplication table of k group operations for (π,π,π)

	R_1	R_8	R_2	R_7	R_5	R_4	R_6	R_3
R_1	R_1	R_8	R_2	R_7	R_5	R_4	R_6	R_3
R_8	R_8	R_1	R_7	R_2	$-R_4$	$-R_5$	$-R_3$	$-R_6$
R_2	R_2	R_7	$-R_1$	$-R_8$	$-R_6$	$-R_3$	R_5	R_4
R_7	R_7	R_2	$-R_8$	$-R_1$	R_3	R_6	$-R_4$	$-R_5$
R_5	R_5	R_4	R_6	R_3	R_1	R_8	R_2	R_7
R_4	R_4	R_5	R_3	R_6	$-R_8$	$-R_1$	$-R_7$	$-R_2$
R_6	R_6	R_3	$-R_5$	$-R_4$	$-R_2$	$-R_7$	R_1	R_8
R_3	R_3	R_6	$-R_4$	$-R_5$	R_7	R_2	$-R_8$	$-R_1$

Table-6 Multiplier corepresentation for space group P_{nam}

R_1	A_0R_1	$\tau(A_0R_1)$	$\delta+(A_0R_1)^{-1}\delta$	$\bar{\delta}\cdot\tau(A_0R_1)$	$\phi(k,A_0R_1,A_0R_1)$
R_1	R_5	$(0,0,0)$	$(0,0,0)$	0	1
R_2	R_6	$(\frac{1}{2},\frac{1}{2},\frac{1}{2})$	$(0,2\delta_b,2\delta_c)$	$\delta_a+\delta_c$	$\exp(-i\delta_b-i\delta_c)$
R_3	R_7	$(\frac{1}{2},\frac{1}{2},0)$	$(2\delta_a,0,2\delta_c)$	δ_a	$\exp(-i\delta_a)$
R_4	R_8	$(0,0,\frac{1}{2})$	$(2\delta_a,2\delta_b,0)$	0	1
R_5	R_1	$(0,0,0)$	$(2\delta_a,2\delta_b,2\delta_c)$	0	1
R_6	R_2	$(\frac{1}{2},\frac{1}{2},\frac{1}{2})$	$(2\delta_a,0,0)$	δ_a	$\exp(-i\delta_a)$
R_7	R_3	$(\frac{1}{2},\frac{1}{2},0)$	$(0,2\delta_b,0)$	δ_b	$\exp(-i\delta_b)$
R_8	R_4	$(0,0,\frac{1}{2})$	$(0,0,2\delta_c)$	δ_c	$\exp(-i\delta_c)$

$\tau(A_0R_1)$ is represented as coefficient vector of (a_0,b_0,c_0) which is a primitive translation.

$\bar{\delta} = [\delta+(A_0R_1)^{-1}\delta]$

$\phi(k,A_0R_1,A_0R_1) = \exp[-i\delta\cdot\tau(A_0R_1)]$

Table-7 The degeneracy of dispersion curves due to time reversal symmetry.

point	g	$\chi^{R}(k,E)$	$\sum_{R_1} \phi(k, A_0R_1, A_0R_1)$	type	t_s	f_s	total
Γ (0,0,0)	8	1	8	a	1	1	1
Σ (δ_a,0,0)	4	1	4	a	1	1	1
A (δ_a,π,0)	4	1	0	c	2	1	2
C (δ_a,0,π)	4	1	0	c	2	1	2
E (δ_a,π,π)	4	1	0	c	2	1	2
λ (0,δ_b,0)	4	1	4	a	1	1	1
G (π,δ_b,0)	4	1	0	c	2	1	2
H (0,δ_b,π)	4	2	2	a	1	2	2
Q (π,δ_b,π)	4	2	-2	b	2	2	4
Δ (0,0,δ_c)	4	1	4	a	1	1	1
B (0,π,δ_c)	4	2	2	a	1	2	2
D (π,0,δ_c)	4	2	2	a	1	2	2
F (π,π,δ_c)	4	1	0	c	2	1	2
X (π,0,0)	8	2	4	a	1	2	2
Z (0,π,0)	8	2	4	a	1	2	2
Y (0,0,π)	8	2	4	a	1	2	2
S (π,0,π)	8	2	0	c	2	2	4
T (0,π,π)	8	2	4	a	1	2	2
U (π,π,0)	8	2	0	c	2	1	2
R (π,π,π)	8	2	0	c	2	2	4

t_s is degeneracy due to time reversal symmetry.

f_s is degeneracy due to space symmetry. Total degeneracy is $t_s \cdot f_s$.

$\chi^R(k,E)$ is a character of k group for identity operation.

Table-8 Symmetry property of the base functions for Σ at (0,0,0).

	R_1	R_2	R_7	R_8
Σ_1	1	1	1	1
Σ_2	1	-1	-1	1
Σ_3	1	1	-1	-1
Σ_4	1	-1	1	-1

Table-9 Symmetry of wave function of binary combination.

$\phi_\beta(-\delta)\cdot\phi_\alpha(+\delta)$	R_1	R_2	R_7	R_8	species in C_{2v}
$\Sigma_1^* \times \Sigma_2$	1	-1	1	-1	B_2
$\Sigma_1^* \times \Sigma_3$	1	1	-1	-1	A_2
$\Sigma_1^* \times \Sigma_4$	1	-1	-1	1	B_1
$\Sigma_2^* \times \Sigma_3$	1	-1	-1	1	B_1
$\Sigma_2^* \times \Sigma_4$	1	1	-1	-1	A_2
$\Sigma_3^* \times \Sigma_4$	1	-1	1	-1	B_2
$\Sigma_j^* \times \Sigma_j$	1	1	1	1	A_1

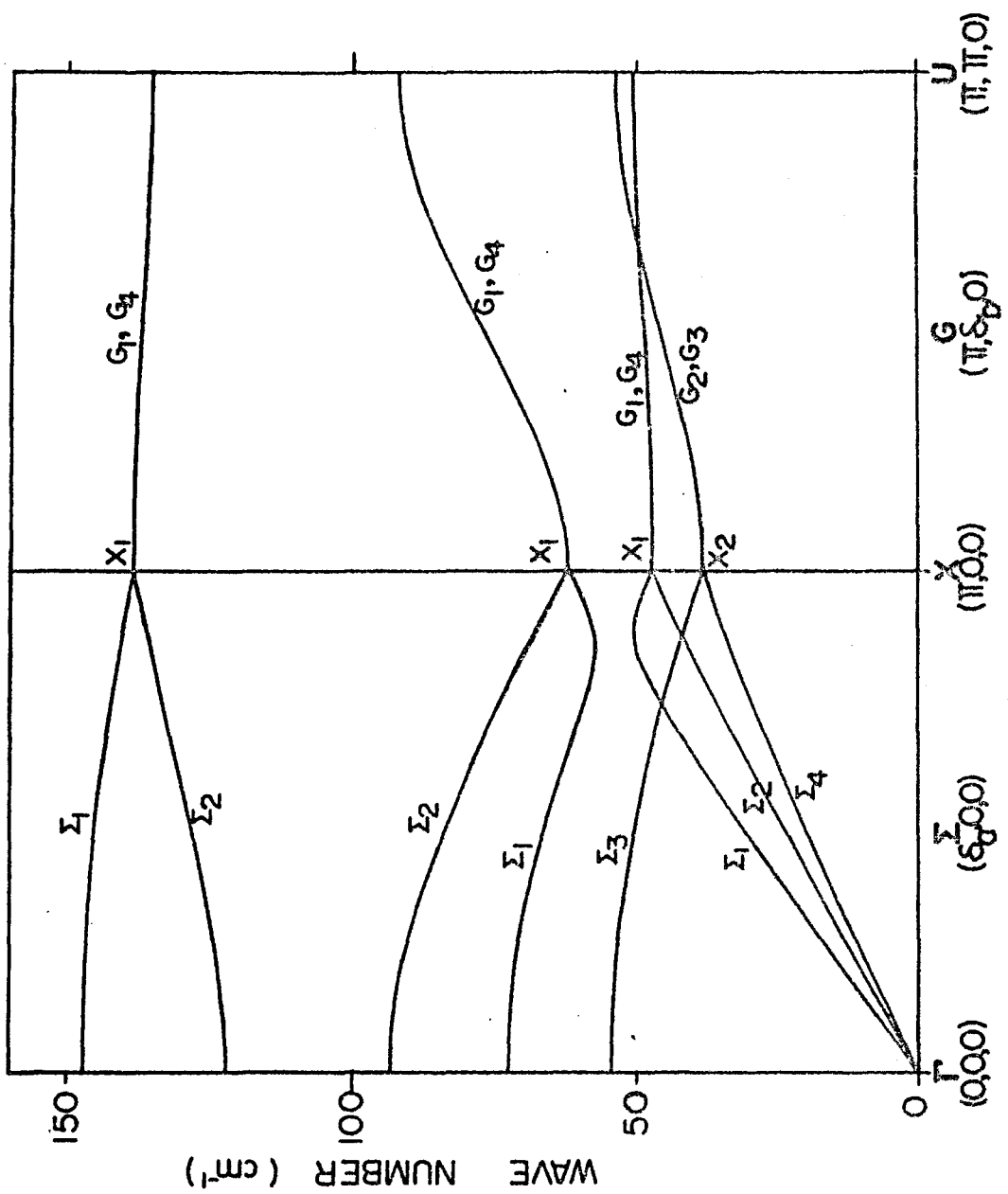

Fig. 1 Dispersion curves of frequency of crystal vibrations of normal polyethylene along $(\delta_a,0,0)$ and $(\pi,\delta_b,0)$.

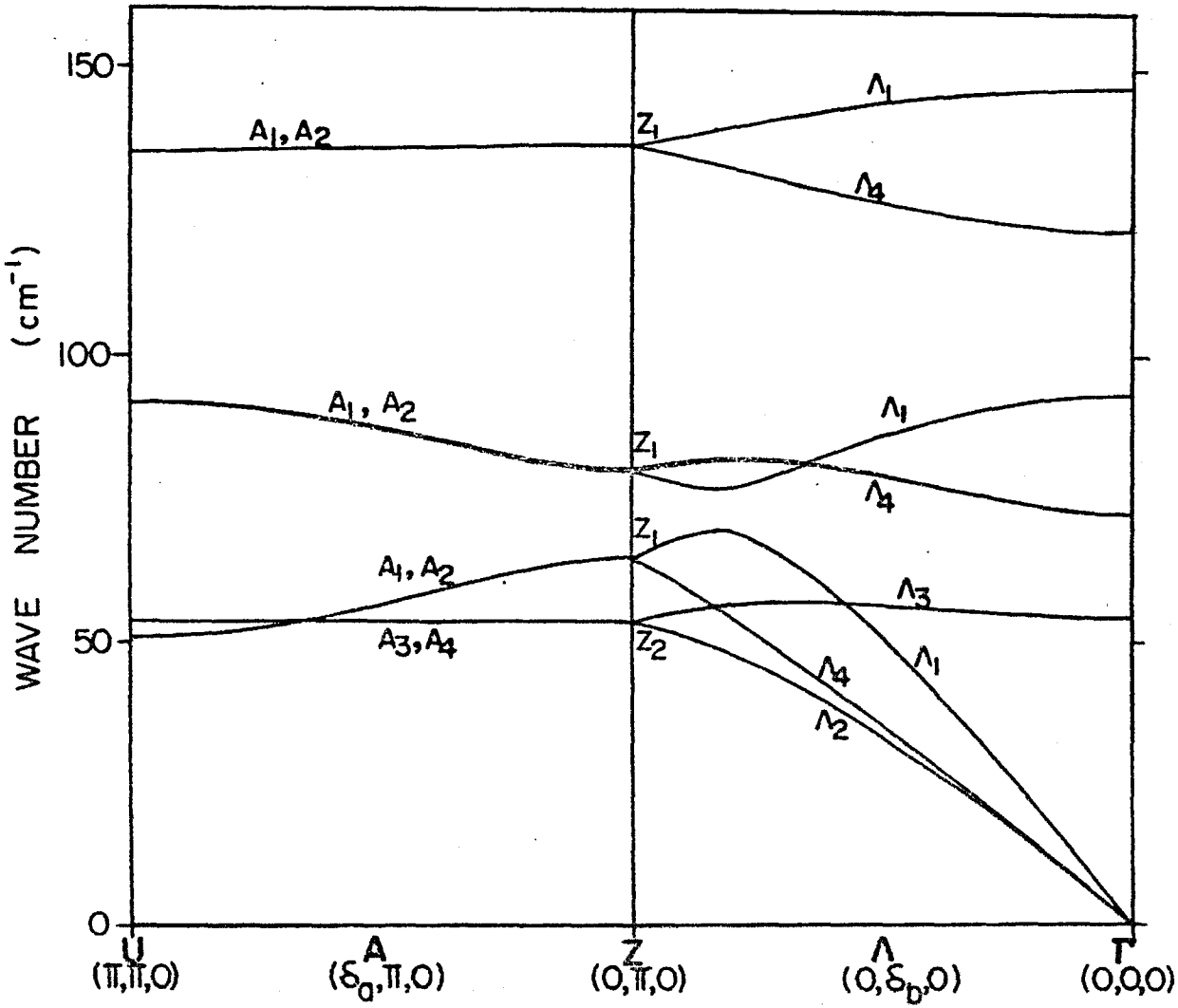

Fig. 2 Dispersion curves of frequency of crystal vibrations of normal polyethylene along $(\delta_a,\pi,0)$ and $(0,\delta_b,0)$.

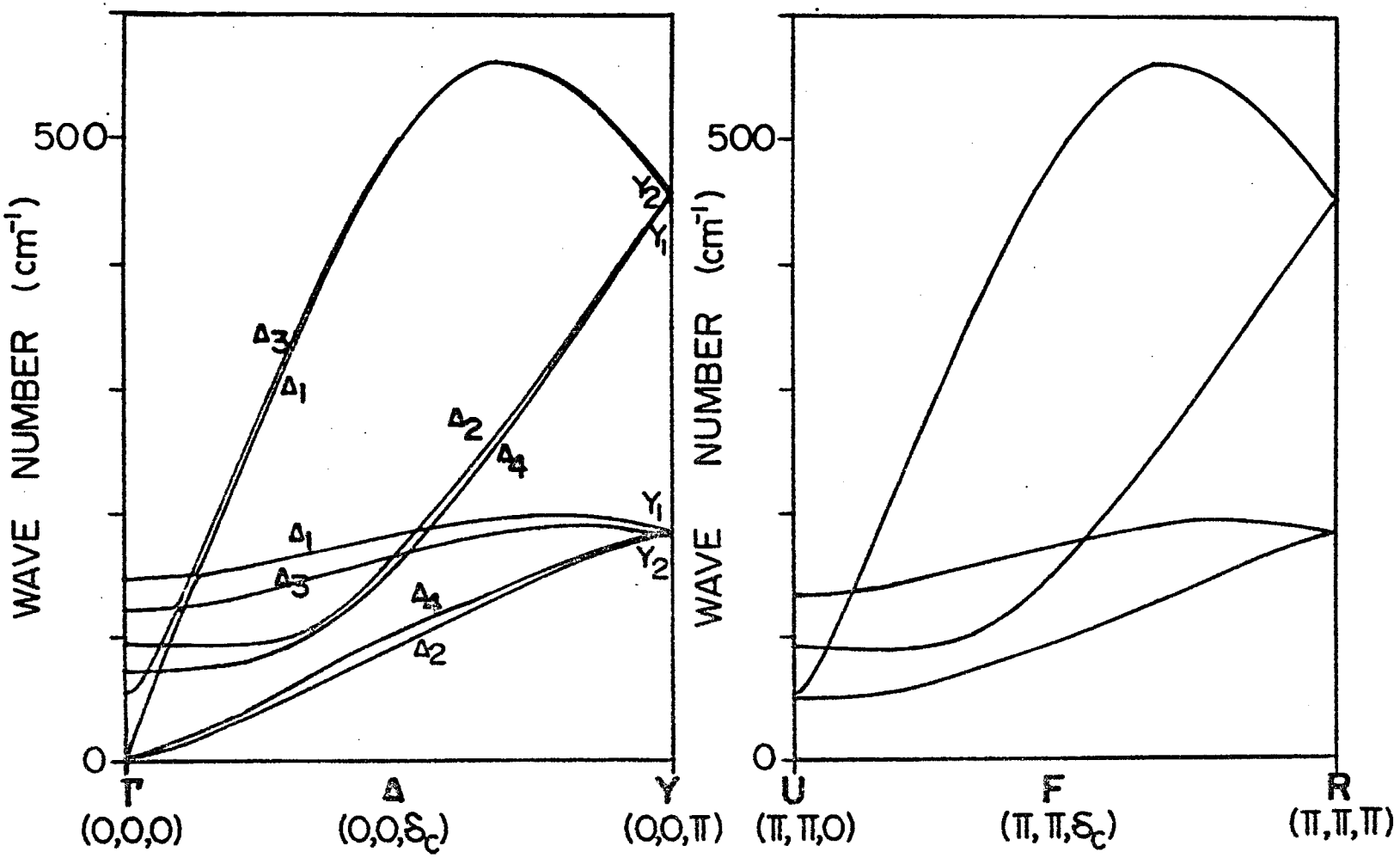

Fig. 3 Dispersion curves of frequency of crystal vibrations of normal polyethylene crystal along $(0,0,\delta_c)$ and (π,π,δ_c).

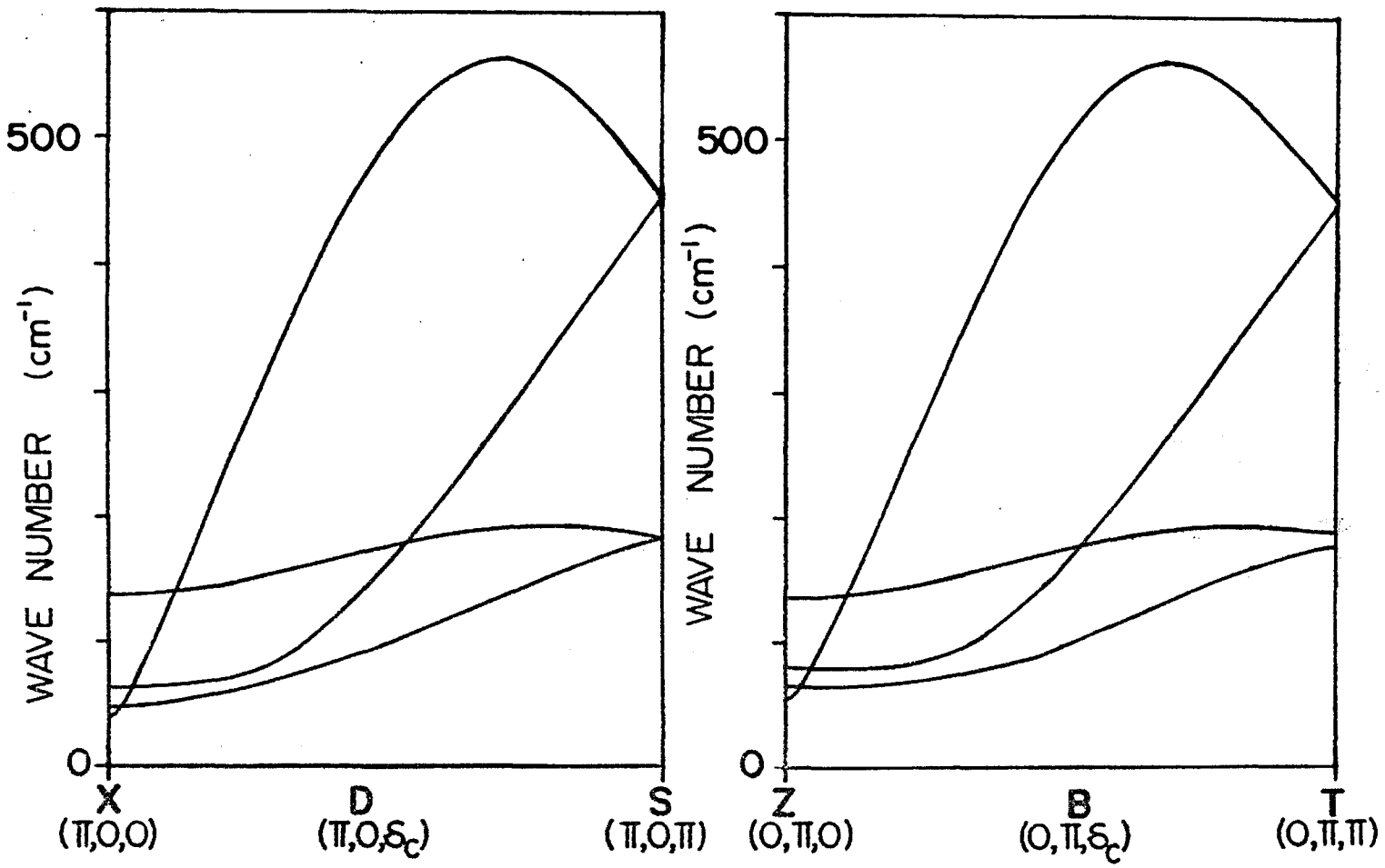

Fig. 4 Dispersion curves of frequency of crystal vibrations of normal polyethylene along $(\pi,0,\delta_c)$ and $(0,\pi,\delta_c)$.

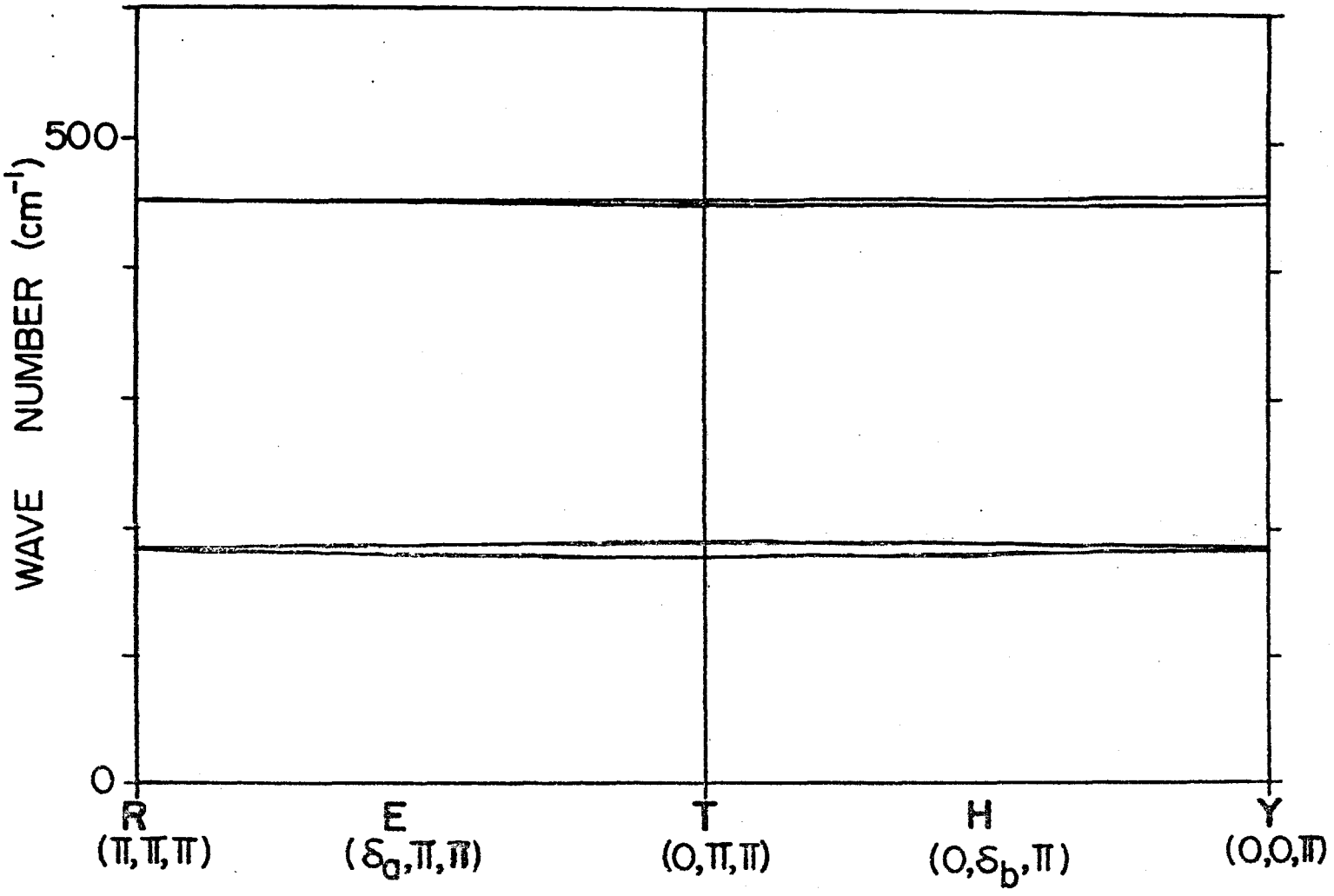

Fig. 5 Dispersion curves of frequency of crystal vibrations of normal polyethylene along (δ_a, π, π) and $(0, \delta_b, \pi)$.

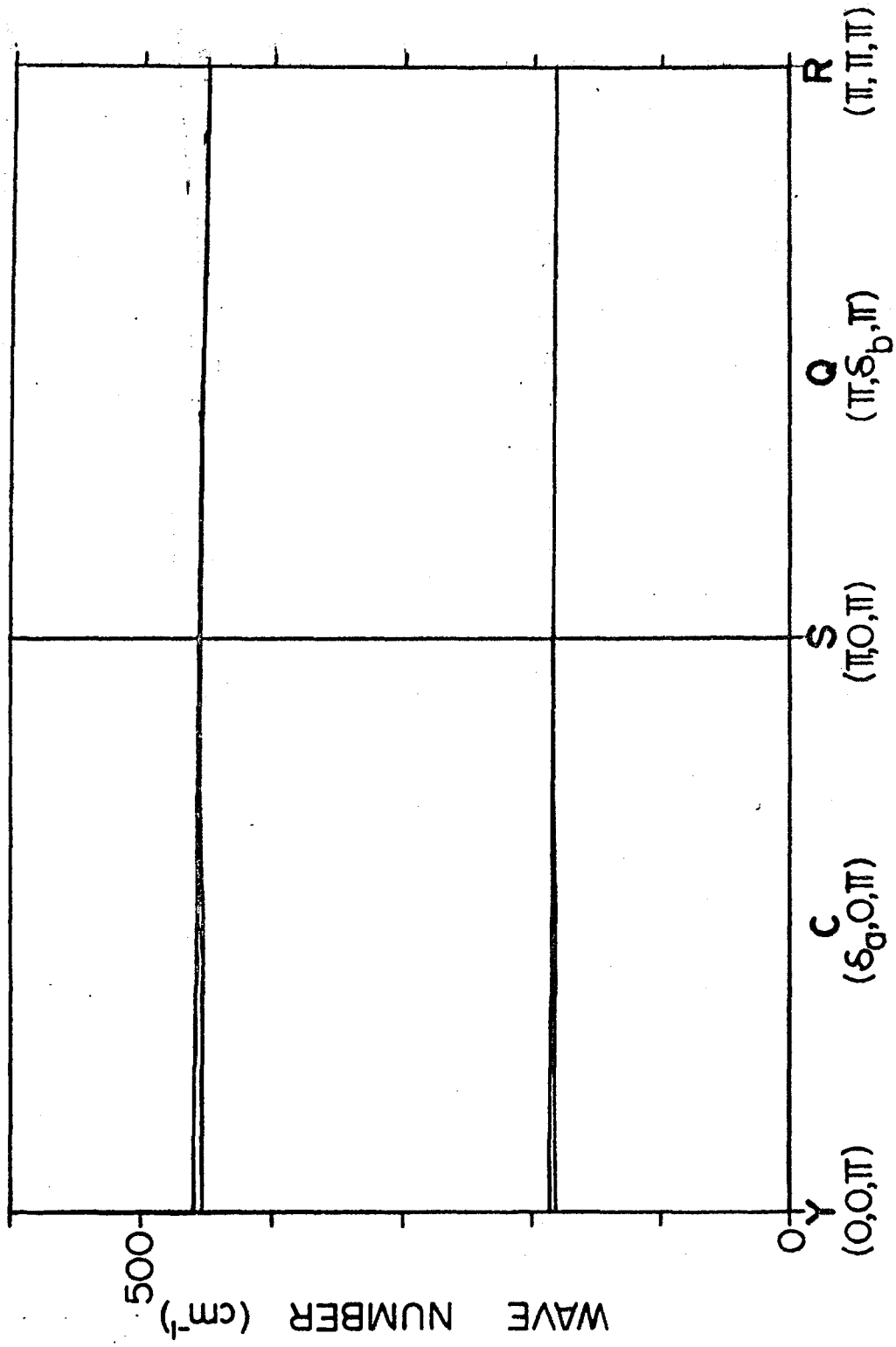

Fig. 6 Dispersion curves of frequency of crystal vibrations of normal polyethylene along $(\delta_a,0,\pi)$ and (π,δ_b,π).

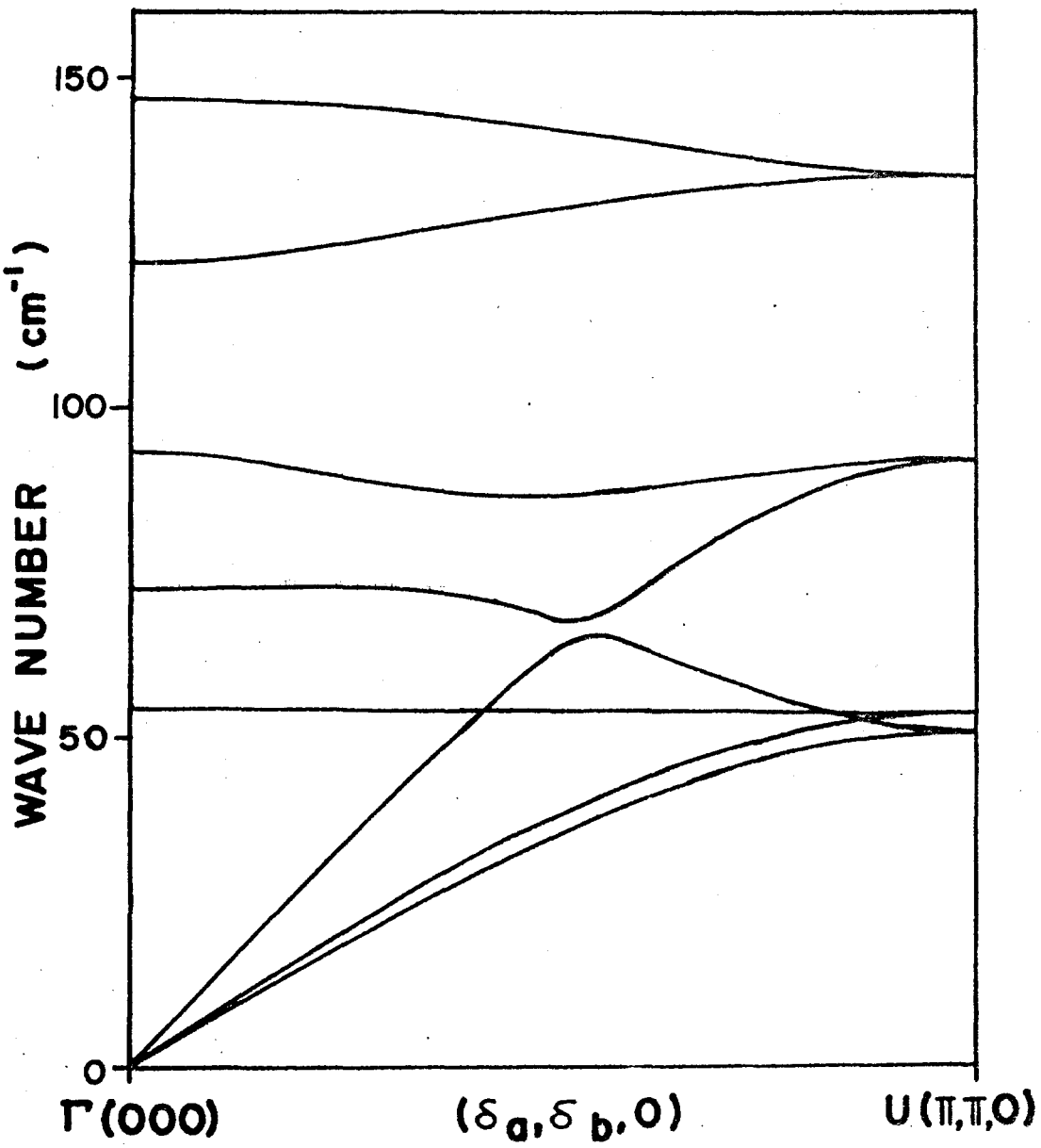

Fig. 7 Dispersion curves of frequency of crystal vibrations of normal polyethylene along $(\delta,\delta,0)$.

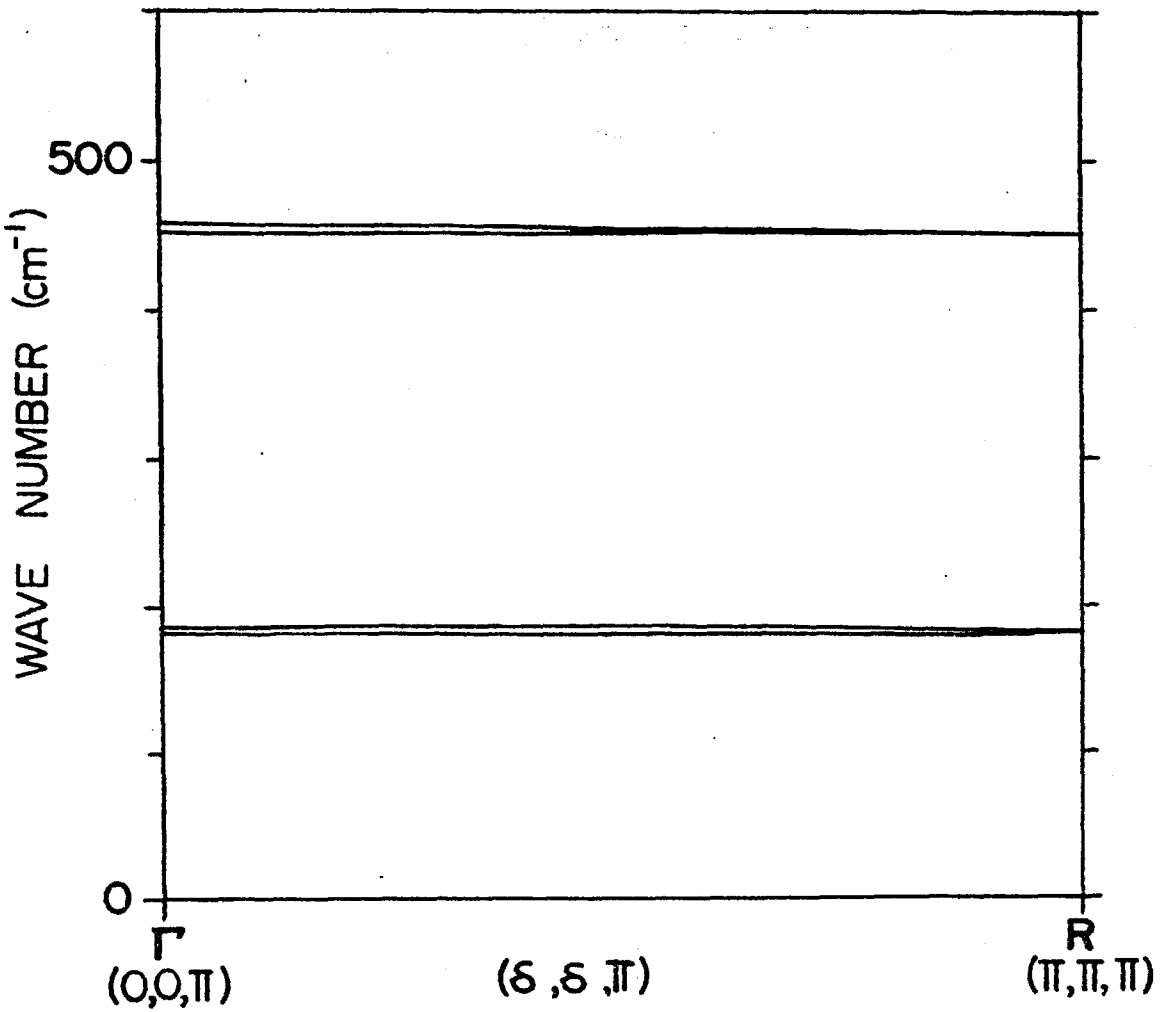

Fig. 8 Dispersion curves of frequency of crystal vibrations of normal polyethylene along (δ,δ,π).

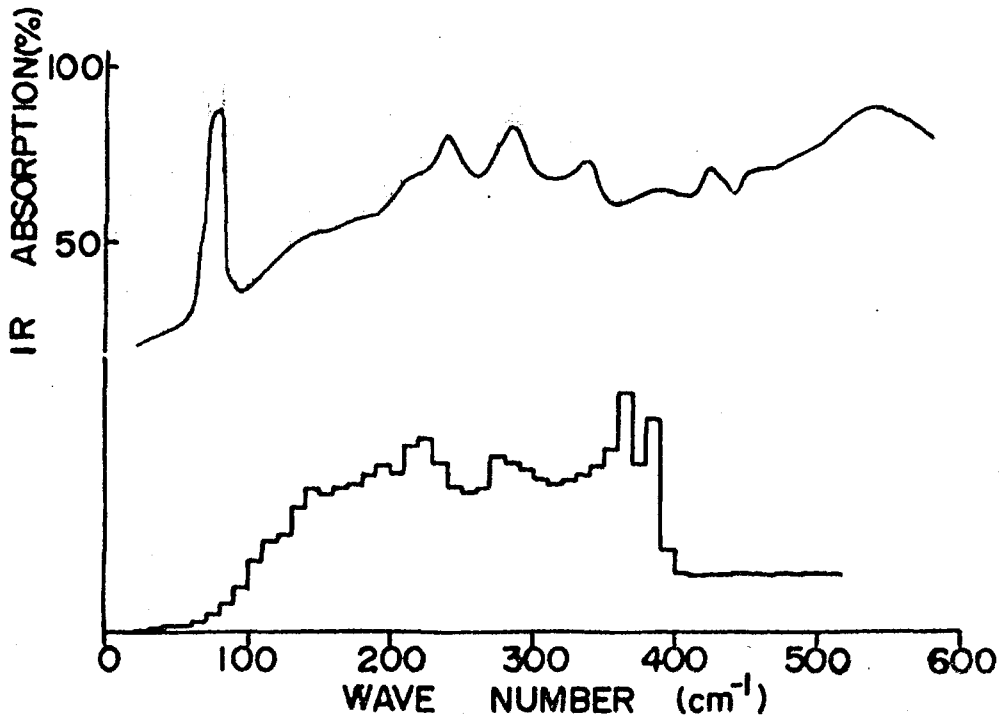

Fig. 9 Comparison of infrared spectrum (at 77°K) with the frequency distribution of binary combination tones.

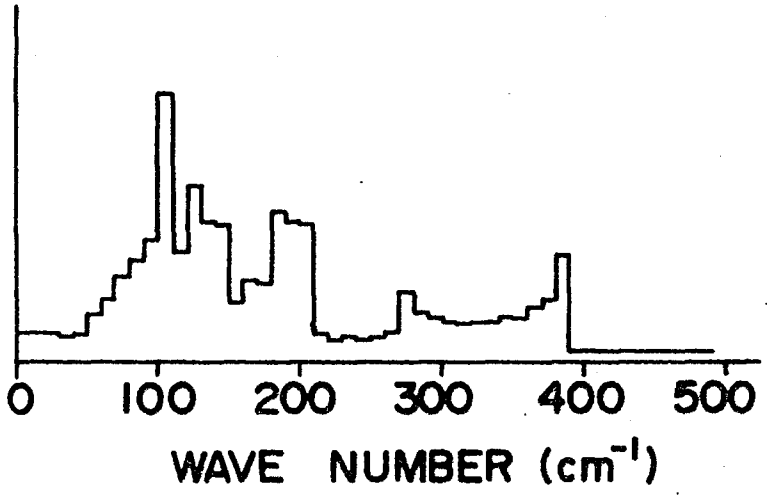

Fig. 10 Frequency distribution of infrared inactive binary combination tones.

Table-A1 Space group operations of polyethylene crystal (P_{nam})

		α_i	τ_i
R_1	E	$\begin{bmatrix} 1 & 0 & 0 \\ 0 & 1 & 0 \\ 0 & 0 & 1 \end{bmatrix}$	(0,0,0)
R_2	C_2^a	$\begin{bmatrix} 1 & 0 & 0 \\ 0 & -1 & 0 \\ 0 & 0 & -1 \end{bmatrix}$	$(\frac{1}{2},\frac{1}{2},\frac{1}{2})$
R_3	C_2^b	$\begin{bmatrix} -1 & 0 & 0 \\ 0 & 1 & 0 \\ 0 & 0 & -1 \end{bmatrix}$	$(\frac{1}{2},\frac{1}{2},0)$
R_4	C_2^c	$\begin{bmatrix} -1 & 0 & 0 \\ 0 & -1 & 0 \\ 0 & 0 & 1 \end{bmatrix}$	$(0,0,\frac{1}{2})$
R_5	i	$\begin{bmatrix} -1 & 0 & 0 \\ 0 & -1 & 0 \\ 0 & 0 & -1 \end{bmatrix}$	(0,0,0)
R_6	σ_g(bc)	$\begin{bmatrix} -1 & 0 & 0 \\ 0 & 1 & 0 \\ 0 & 0 & 1 \end{bmatrix}$	$(\frac{1}{2},\frac{1}{2},\frac{1}{2})$
R_7	σ_g(ac)	$\begin{bmatrix} 1 & 0 & 0 \\ 0 & -1 & 0 \\ 0 & 0 & 1 \end{bmatrix}$	$(\frac{1}{2},\frac{1}{2},0)$
R_8	σ_g(ab)	$\begin{bmatrix} 1 & 0 & 0 \\ 0 & 1 & 0 \\ 0 & 0 & -1 \end{bmatrix}$	$(0,0,\frac{1}{2})$

τ_i is nonprimitive translation vector which is represented as the coefficient vector for primitive translation vector (a_0,b_0,c_0).

Table-A2 Multiplication table of the space group operations for P_{nam}

	R_1	R_2	R_3	R_4	R_5	R_6	R_7	R_8
R_1	R_1	R_2	R_3	R_4	R_5	R_6	R_7	R_8
R_2	R_2	$e^{a}R_1$	$e^{b-c}R_4$	$e^{-a-b+c}R_3$	$e^{-a-b-c}R_6$	$e^{b+c}R_5$	$e^{a}R_8$	R_7
R_3	R_3	$e^{a}R_4$	$e^{b}R_1$	$e^{-a-b}R_2$	$e^{-a-b}R_7$	$e^{b}R_8$	$e^{a}R_5$	R_6
R_4	R_4	R_3	$e^{-c}R_2$	$e^{c}R_1$	$e^{-c}R_8$	$e^{c}R_7$	R_6	R_5
R_5	R_5	R_6	R_7	R_8	R_1	R_2	R_3	R_4
R_6	R_6	$e^{a}R_5$	$e^{b-c}R_8$	$e^{-a-b+c}R_7$	$e^{-a-b-c}R_2$	$e^{b+c}R_1$	$e^{a}R_4$	R_3
R_7	R_7	$e^{a}R_8$	$e^{b}R_5$	$e^{-a-b}R_6$	$e^{-a-b}R_3$	$e^{b}R_4$	$e^{a}R_1$	R_2
R_8	R_8	R_7	$e^{-c}R_6$	$e^{c}R_5$	$e^{-c}R_4$	$e^{c}R_3$	R_2	R_1

$e^{a}=\exp(i\delta_a)$, $e^{b}=\exp(i\delta_b)$, $e^{c}=\exp(i\delta_c)$

$e^{a+b}=\exp(i\delta_a+i\delta_b)$, $e^{a-b}=\exp(i\delta_a-i\delta_b)$, $e^{a+b-c}=\exp(i\delta_a+i\delta_b-i\delta_c)$

Table-A3 Irreducible representation of the k group (0,0,0)

	R_1	R_2	R_3	R_4	R_5	R_6	R_7	R_8
Γ_1 (A_g)	1	1	1	1	1	1	1	1
Γ_2 (A_u)	1	1	1	1	-1	-1	-1	-1
Γ_3 (B_{3g})	1	-1	-1	1	1	-1	-1	1
Γ_4 (B_{3u})	1	-1	-1	1	-1	1	1	-1
Γ_5 (B_{1g})	1	1	-1	-1	1	1	-1	-1
Γ_6 (B_{1u})	1	1	-1	-1	-1	-1	1	1
Γ_7 (B_{2g})	1	-1	1	-1	1	-1	1	-1
Γ_8 (B_{2u})	1	-1	1	-1	-1	1	-1	1

Table-A4 Matrix elements and characters of k group $(0<\delta_a<\pi)$

$(\delta_a,0,0)$	$(\delta_a,\pi,0)$	$(\delta_a,0,\pi)$	(δ_a,π,π)	R_1	R_2	R_7	R_8	
Σ_1	A_1	C_1	E_1	1	w_a	w_a	1	ϕ_1
Σ_2	A_2	C_2	E_2	1	$-w_a$	$-w_a$	1	ϕ_2
Σ_3	A_3	C_3	E_3	1	w_a	$-w_a$	-1	ϕ_3
Σ_4	A_4	C_4	E_4	1	$-w_a$	w_a	-1	ϕ_4

$$w_a = \exp(i\delta_a/2)$$

$$\phi_1 = [(R_1+R_8)+\exp(-i\delta_a/2)(R_2+R_7)]\cdot\exp(i\rho\delta)$$

$$\phi_2 = [(R_1+R_8)-\exp(-i\delta_a/2)(R_2+R_7)]\cdot\exp(i\rho\delta)$$

$$\phi_3 = [(R_1-R_8)+\exp(-i\delta_a/2)(R_2-R_7)]\cdot\exp(i\rho\delta)$$

$$\phi_4 = [(R_1-R_8)-\exp(-i\delta_a/2)(R_2-R_7)]\cdot\exp(i\rho\delta)$$

Table-A5 Matrix elements and characters of k group $(0<\delta_b<\pi)$

$(0,\delta_b,0)$	$(\pi,\delta_b,0)$	R_1	R_3	R_6	R_8	
λ_1	G_1	1	w_b	w_b	1	ϕ_1
λ_2	G_2	1	$-w_b$	w_b	-1	ϕ_2
λ_3	G_3	1	w_b	$-w_b$	-1	ϕ_3
λ_4	G_4	1	$-w_b$	$-w_b$	1	ϕ_4

$$w_b = \exp(i\delta_b/2)$$

Table-A5 continued

$$\phi_1 = [(R_1+R_8)+\exp(-i\delta_b/2)(R_3+R_6)]\cdot\exp(i\rho\delta)$$
$$\phi_2 = [(R_1-R_8)-\exp(-i\delta_b/2)(R_3-R_6)]\cdot\exp(i\rho\delta)$$
$$\phi_3 = [(R_1-R_8)+\exp(-i\delta_b/2)(R_3-R_6)]\cdot\exp(i\rho\delta)$$
$$\phi_4 = [(R_1+R_8)-\exp(-i\delta_b/2)(R_3+R_6)]\cdot\exp(i\rho\delta)$$

Table-A6 Matrix elements and characters of k group $(0<\delta_b<\pi)$

$(0,\delta_b,\pi)$	(π,δ_b,π)	R_1	R_3	R_6	R_8
$(H_1)_{11}$	$(Q_1)_{11}$	1	w_b	0	0
$(H_1)_{21}$	$(Q_1)_{21}$	0	0	$-w_b$	1
$(H_1)_{12}$	$(Q_1)_{12}$	0	0	w_b	1
$(H_1)_{22}$	$(Q_1)_{22}$	1	$-w_b$	0	0
$\chi(H_1)$	(Q_1)	2	0	0	0

$$\phi_1 = [(R_1+R_8)+\exp(-i\delta_b/2)(R_3+R_6)]\cdot\exp(i\rho\delta)$$
$$\phi_2 = [(R_1+R_8)-\exp(-i\delta_b/2)(R_3+R_6)]\cdot\exp(i\rho\delta)$$

Table-A7 Matrix elements and characters of k group $(0<\delta_c<\pi)$

$(0,0,\delta_c)$	R_1	R_4	R_6	R_7	
Δ_1	1	w_c	w_c	1	ϕ_1
Δ_2	1	$-w_c$	w_c	-1	ϕ_2
Δ_3	1	w_c	$-w_c$	-1	ϕ_3
Δ_4	1	$-w_c$	$-w_c$	1	ϕ_4

$$w_c = \exp(i\delta_c/2)$$
$$\phi_1 = [(R_1+R_7)+\exp(-i\delta_c/2)(R_4+R_6)]\cdot\exp(i\rho\delta)$$
$$\phi_2 = [(R_1-R_7)-\exp(-i\delta_c/2)(R_4-R_6)]\cdot\exp(i\rho\delta)$$
$$\phi_3 = [(R_1-R_7)+\exp(-i\delta_c/2)(R_4-R_6)]\cdot\exp(i\rho\delta)$$
$$\phi_4 = [(R_1+R_7)-\exp(-i\delta_c/2)(R_4+R_6)]\cdot\exp(i\rho\delta)$$

Table-A8 Matrix elements and characters of k group ($0<\delta_c<\pi$)

$(\pi,0,\delta_c)$	R_1	R_4	R_6	R_7
$(D_1)_{11}$	1	w_c	0	0
$(D_1)_{21}$	0	0	w_c	1
$(D_1)_{12}$	0	0	w_c	-1
$(D_1)_{22}$	1	$-w_c$	0	0
$\chi(D_1)$	2	0	0	0

$$\phi_1 = [(R_1+R_7)+\exp(-i\delta_c/2)(R_6+R_4)]\cdot\exp(i\rho\delta)$$

$$\phi_2 = [(R_1-R_7)+\exp(-i\delta_c/2)(R_6-R_4)]\cdot\exp(i\rho\delta)$$

Table-A9 Matrix elements and characters of k group ($0<\delta_c<\pi$)

$(0,\pi,\delta_c)$	R_1	R_4	R_6	R_7
$(B_1)_{11}$	1	w_c	0	0
$(B_1)_{21}$	0	0	$-w_c$	1
$(B_1)_{12}$	0	0	w_c	1
$(B_1)_{22}$	1	$-w_c$	0	0
$\chi(B_1)$	2	0	0	0

$$\phi_1 = [(R_1+R_7)+\exp(-i\delta_c/2)(R_4+R_6)]\cdot\exp(i\rho\delta)$$

$$\phi_2 = [(R_1+R_7)-\exp(-i\delta_c/2)(R_4+R_6)]\cdot\exp(i\rho\delta)$$

Table-A10 Matrix elements and characters of k group ($0<\delta_c<\pi$)

(π,π,δ_c)	R_1	R_4	R_6	R_7	
F_1	1	w_c	iw_c	1	ϕ_1
F_2	1	w_c	$-iw_c$	-1	ϕ_2
F_3	1	$-w_c$	$+iw_c$	-1	ϕ_3
F_4	1	$-w_c$	$-iw_c$	1	ϕ_3

$$\phi_1 = [(R_1-iR_7)+\exp(-i\delta_c/2)(R_4-iR_6)]\cdot\exp(i\rho\delta)$$

$$\phi_2 = [(R_1+iR_7)+\exp(-i\delta_c/2)(R_4+iR_6)]\cdot\exp(i\rho\delta)$$

$$\phi_3 = [(R_1+iR_7)-\exp(-i\delta_c/2)(R_4+iR_6)]\cdot\exp(i\rho\delta)$$

$$\phi_4 = [(R_1-iR_7)-\exp(-i\delta_c/2)(R_4-iR_6)]\cdot\exp(i\rho\delta)$$

Table-A11 Characters of k group $(0<\delta_a,\delta_b<\pi)$

$(\delta_a,\delta_b,0)$	R_1	R_8	base function
	1	1	$\phi = (R_1+R_8)\exp(i\rho\delta)$
	1	-1	$\phi = (R_1-R_8)\exp(i\rho\delta)$

Table-A12 Characters of k group $(0<\delta_a,\delta_c<\pi)$

$(\delta_a,0,\delta_c)$	R_1	R_7	base function
	1	w_a	$\phi = [R_1+\exp(-i\delta_a/2)R_7]\exp(i\rho\delta)$
	1	$-w_a$	$\phi = [R_1-\exp(-i\delta_a/2)R_7]\exp(i\rho\delta)$

$w_a = \exp(i\delta_a/2)$

Table-A13 Characters of k group $(0<\delta_b,\delta_c<\pi)$

$(0,\delta_b,\delta_c)$	R_1	R_6	base function
	1	w_{bc}	$\phi=[R_1+\exp(-i(\delta_b+\delta_c)/2)R_6]\exp(i\rho\delta)$
	1	$-w_{bc}$	$\phi=[R_1-\exp(-i(\delta_b+\delta_c)/2)R_6]\exp(i\rho\delta)$

$w_{bc} = \exp[i(\delta_b+\delta_c)/2]$

Table-A14 Matrix elements and characters of k group at point X.

$(\pi,0,0)$	R_1	R_2	R_3	R_4	R_5	R_6	R_7	R_8
$(X_1)_{11}$	1	0	1	0	0	1	0	1
$(X_1)_{21}$	0	1	0	1	1	0	1	0
$(X_1)_{12}$	0	-1	0	1	1	0	-1	0
$(X_1)_{22}$	1	0	-1	0	0	-1	0	1
$\chi(X_1)$	2	0	0	0	0	0	0	2
$(X_2)_{11}$	1	0	1	0	0	-1	0	-1
$(X_2)_{21}$	0	1	0	1	-1	0	-1	0
$(X_2)_{12}$	0	-1	0	1	-1	0	1	0
$(X_2)_{22}$	1	0	-1	0	0	1	0	-1
$\chi(X_2)$	2	0	0	0	0	0	0	-2

$\phi_1(X_1)=(R_1+R_3+R_6+R_8)\cdot\exp(i\rho\delta)$ $\quad$ $\phi_1(X_2)=(R_1+R_3-R_8-R_6)\cdot\exp(i\rho\delta)$

$\phi_2(X_1)=(R_2+R_4+R_5+R_7)\cdot\exp(i\rho\delta)$ $\quad$ $\phi_2(X_2)=(R_2+R_4-R_7-R_5)\cdot\exp(i\rho\delta)$

Table-A15 Matrix elements and characters of k group at point Z.

$(0,\pi,0)$	R_1	R_2	R_3	R_4	R_5	R_6	R_7	R_8
$(Z_1)_{11}$	1	1	0	0	0	0	1	1
$(Z_1)_{21}$	0	0	1	1	1	1	0	0
$(Z_1)_{12}$	0	0	-1	1	1	-1	0	0
$(Z_1)_{22}$	1	-1	0	0	0	0	-1	1
$\chi(Z_1)$	2	0	0	0	0	0	0	2
$(Z_2)_{11}$	1	1	0	0	0	0	-1	-1
$(Z_2)_{21}$	0	0	1	1	-1	-1	0	0
$(Z_2)_{12}$	0	0	-1	1	-1	1	0	0
$(Z_2)_{22}$	1	-1	0	0	0	0	1	-1
$\chi(Z_2)$	2	0	0	0	0	0	0	-2

$$\phi_1(Z_1)=(R_1+R_8+R_2+R_7)\exp(1\rho\delta)$$
$$\phi_2(Z_1)=(R_3+R_6+R_4+R_5)\exp(1\rho\delta)$$
$$\phi_1(Z_2)=(R_1-R_8+R_2-R_7)\exp(1\rho\delta)$$
$$\phi_2(Z_2)=(R_3-R_6+R_4-R_5)\exp(1\rho\delta)$$

Table-A16 Matrix elements and characters of k group at point Y.

$(0,0,\pi)$	R_1	R_2	R_3	R_4	R_5	R_6	R_7	R_8
$(Y_1)_{11}$	1	1	0	0	0	0	1	1
$(Y_1)_{21}$	0	0	1	1	1	1	0	0
$(Y_1)_{12}$	0	0	1	-1	1	-1	0	0
$(Y_1)_{22}$	1	-1	0	0	0	0	1	-1
$\chi(Y_1)$	2	0	0	0	0	0	2	0
$(Y_2)_{11}$	1	1	0	0	0	0	-1	-1
$(Y_2)_{21}$	0	0	1	1	-1	-1	0	0
$(Y_2)_{12}$	0	0	1	-1	-1	1	0	0
$(Y_2)_{22}$	1	-1	0	0	0	0	-1	1
$\chi(Y_2)$	2	0	0	0	0	0	-2	0

$$\phi_1(Y_1)=(R_1+R_2+R_7+R_8)\exp(1\rho\delta)$$
$$\phi_2(Y_1)=(R_3+R_4+R_5+R_6)\exp(1\rho\delta)$$
$$\phi_1(Y_2)=(R_1+R_2-R_7-R_8)\exp(1\rho\delta)$$
$$\phi_2(Y_2)=(R_3+R_4-R_5-R_6)\exp(1\rho\delta)$$

Table-A17 Matrix elements and characters of k group at point U.

$(\pi,\pi,0)$	R_1	R_2	R_3	R_4	R_5	R_6	R_7	R_8
U_1	1	1	1	1	1	1	1	1
U_2	1	-1	-1	1	1	-1	-1	1
U_3	1	1	1	1	-1	-1	-1	-1
U_4	1	-1	-1	1	-1	1	1	-1
U_5	1	1	-1	-1	1	1	-1	-1
U_6	1	-1	1	-1	1	-1	1	-1
U_7	1	1	-1	-1	-1	-1	1	1
U_8	1	-1	1	-1	-1	1	-1	1

$$\phi_1 = (R_1-1R_2-1R_3+R_4+R_5-1R_6-1R_7+R_8)\exp(1\rho\delta)$$
$$\phi_2 = (R_1+1R_2+1R_3+R_4+R_5+1R_6+1R_7+R_8)\exp(1\rho\delta)$$
$$\phi_3 = (R_1-1R_2-1R_3+R_4-R_5+1R_6+1R_7-R_8)\exp(1\rho\delta)$$
$$\phi_4 = (R_1+1R_2+1R_3+R_4-R_5-1R_6-1R_7-R_8)\exp(1\rho\delta)$$
$$\phi_5 = (R_1-1R_2+1R_3-R_4+R_5-1R_6+1R_7-R_8)\exp(1\rho\delta)$$
$$\phi_6 = (R_1+1R_2-1R_3-R_4+R_5+1R_6-1R_7-R_8)\exp(1\rho\delta)$$
$$\phi_7 = (R_1-1R_2+1R_3-R_4-R_5+1R_6-1R_7+R_8)\exp(1\rho\delta)$$
$$\phi_8 = (R_1+1R_2-1R_3-R_4-R_5-1R_6+1R_7+R_8)\exp(1\rho\delta)$$

Table-A18 Matrix elements and characters of k group at point T.

$(0,\pi,\pi)$	R_1	R_2	R_3	R_4	R_5	R_6	R_7	R_8
$(T_1)_{11}$	1	1	0	0	1	1	0	0
$(T_1)_{21}$	0	0	1	1	0	0	-1	-1
$(T_1)_{12}$	0	0	-1	-1	0	0	-1	-1
$(T_1)_{22}$	1	1	0	0	-1	-1	0	0
$\chi(T_1)$	2	2	0	0	0	0	0	0
$(T_2)_{11}$	1	-1	0	0	1	-1	0	0
$(T_2)_{21}$	0	0	-1	1	0	0	1	-1
$(T_2)_{12}$	0	0	1	-1	0	0	1	-1
$(T_2)_{22}$	1	-1	0	0	-1	1	0	0
$\chi(T_2)$	2	-2	0	0	0	0	0	0

$$\phi_1(T_1) = (R_1+R_2+R_5+R_6)\exp(1\rho\delta)$$
$$\phi_2(T_1) = (R_3+R_4-R_7-R_8)\exp(1\rho\delta)$$
$$\phi_1(T_2) = (R_1-R_2+R_5-R_6)\exp(1\rho\delta)$$
$$\phi_2(T_2) = (-R_3+R_4+R_7-R_8)\exp(1\rho\delta)$$

Table-A19 Matrix elements and characters of k group at point S.

$(\pi,0,\pi)$	R_1	R_2	R_3	R_4	R_5	R_6	R_7	R_8
$(S_1)_{11}$	1	1	0	0	0	0	1	1
$(S_1)_{21}$	0	0	1	1	1	1	0	0
$(S_1)_{12}$	0	0	-1	-1	1	1	0	0
$(S_1)_{22}$	1	1	0	0	0	0	-1	-1
$\chi(S_1)$	2	2i	0	0	0	0	0	0
$(S_2)_{11}$	1	-1	0	0	0	0	-1	1
$(S_2)_{21}$	0	0	-1	1	1	-1	0	0
$(S_2)_{12}$	0	0	1	-1	1	-1	0	0
$(S_2)_{22}$	1	-1	0	0	0	0	1	-1
$\chi(S_2)$	2	-2i	0	0	0	0	0	0

$$\phi_1(S_1) = [R_1+R_8-i(R_2+R_7)]\exp(i\rho\delta)$$
$$\phi_2(S_1) = [R_4+R_5-i(R_3+R_6)]\exp(i\rho\delta)$$
$$\phi_1(S_2) = [R_1+R_8+i(R_2+R_7)]\exp(i\rho\delta)$$
$$\phi_2(S_2) = [R_4+R_5+i(R_3+R_6)]\exp(i\rho\delta)$$

Table-A20 Matrix elements and characters of k group at point R.

(π,π,π)	R_1	R_2	R_3	R_4	R_5	R_6	R_7	R_8
$(R_1)_{11}$	1	-1	0	0	0	0	1	-1
$(R_1)_{21}$	0	0	1	-1	1	-1	0	0
$(R_1)_{12}$	0	0	1	1	1	1	0	0
$(R_1)_{22}$	1	1	0	0	0	0	1	1
$\chi(R_1)$	2	0	0	0	0	0	2i	0
$(R_2)_{11}$	1	1	0	0	0	0	-1	-1
$(R_2)_{21}$	0	0	-1	-1	1	1	0	0
$(R_2)_{12}$	0	0	-1	1	1	-1	0	0
$(R_2)_{22}$	1	-1	0	0	0	0	-1	1
$\chi(R_2)$	2	0	0	0	0	0	-2i	0

$$\phi_1(R_1) = (R_1+iR_2-iR_7-R_8)\exp(i\rho\delta)$$
$$\phi_2(R_1) = (R_5+iR_6-iR_3-R_4)\exp(i\rho\delta)$$
$$\phi_1(R_2) = (R_1-iR_2+iR_7-R_8)\exp(i\rho\delta)$$
$$\phi_2(R_2) = (R_5-iR_6+iR_3-R_4)\exp(i\rho\delta)$$

Table A21

The compatibility relations of the dispersion curves of the lattice vibrations

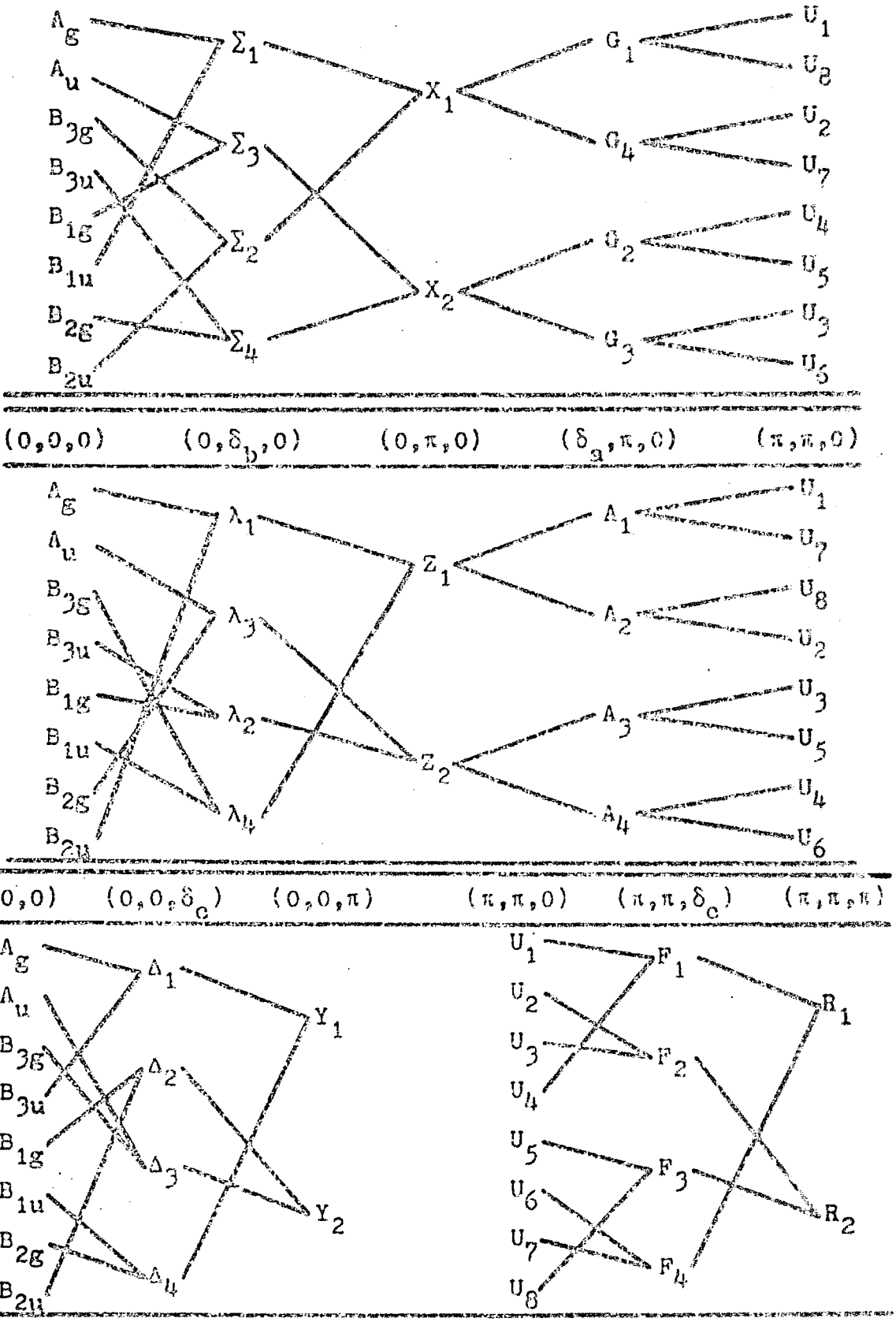

$(0,0,\pi)$	$(\delta_a,0,\pi)$	$(\pi,0,\pi)$	$(\pi,0,\delta_c)$	$(\pi,0,0)$

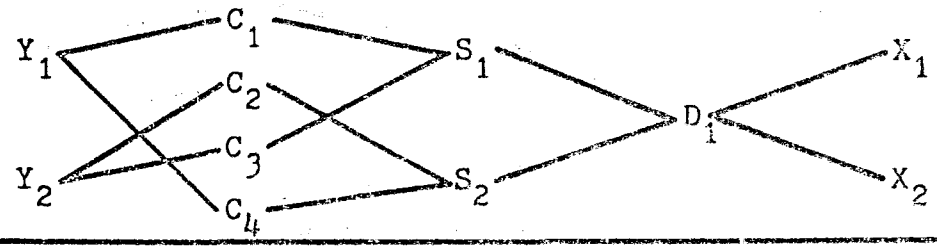

$(0,0,\pi)$	$(0,\delta_b,\pi)$	$(0,\pi,\pi)$	$(0,\pi,\delta_c)$	$(0,\pi,0)$

$(\pi,0,\pi)$	(π,δ_b,π)	(π,π,π)	(δ_a,π,π)	$(0,\pi,\pi)$

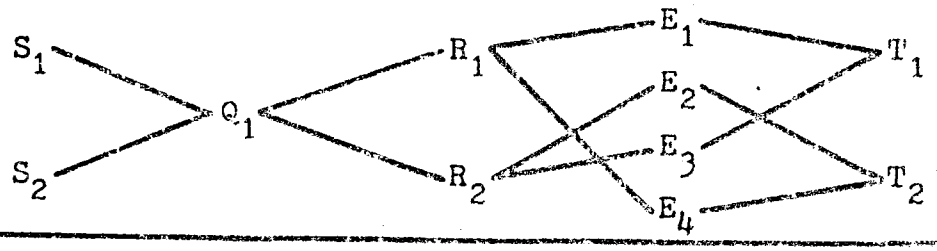

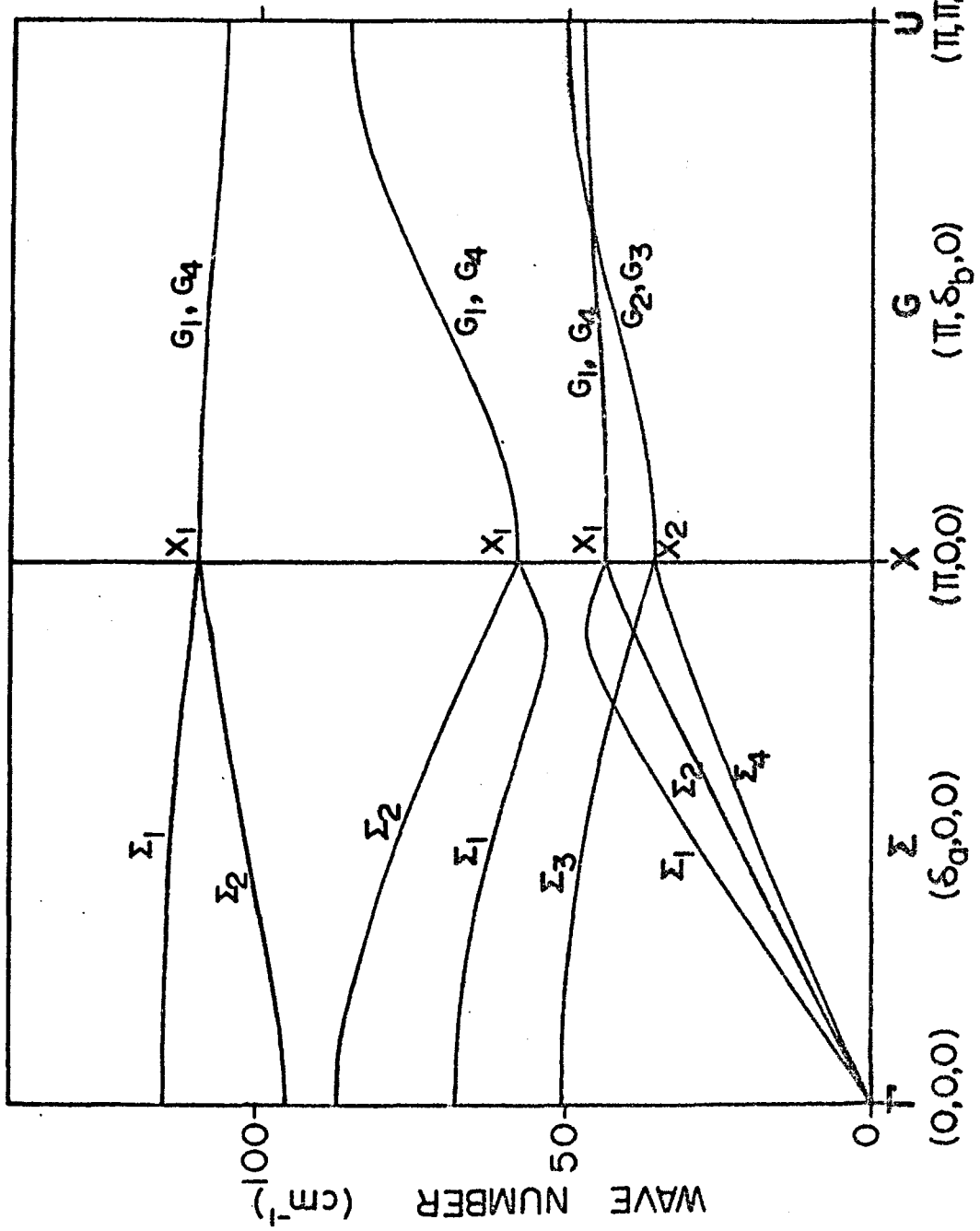

Fig. A1 Dispersion curves of frequency of crystal vibrations of deuterated polyethylene along $(\delta_a,0,0)$ and $(\pi,\delta_b,0)$.

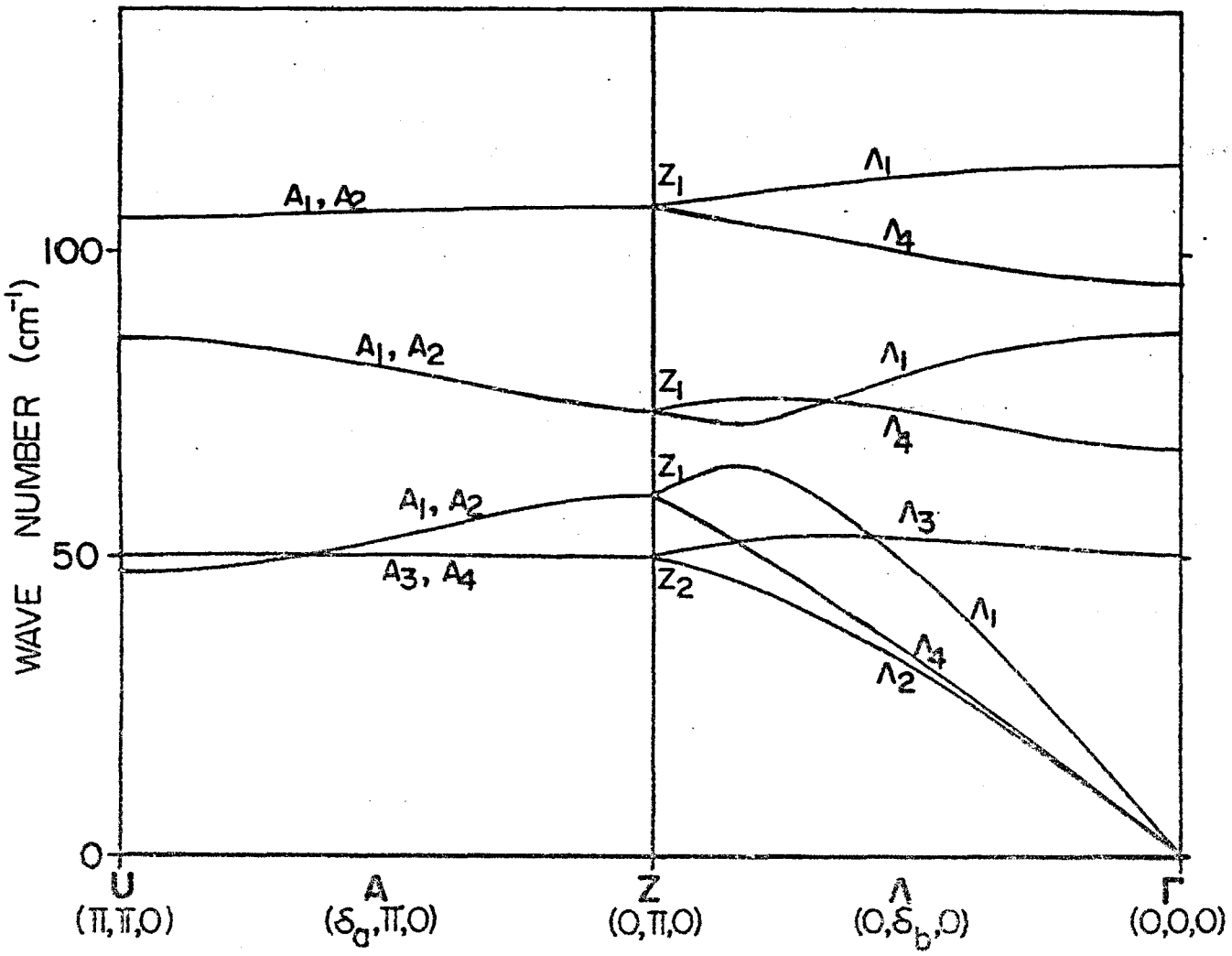

Fig. A2 Dispersion curves of frequency of crystal vibrations of deuterated polyethylene crystal along $(\delta_a, \pi, 0)$ and $(0, \delta_b, 0)$.

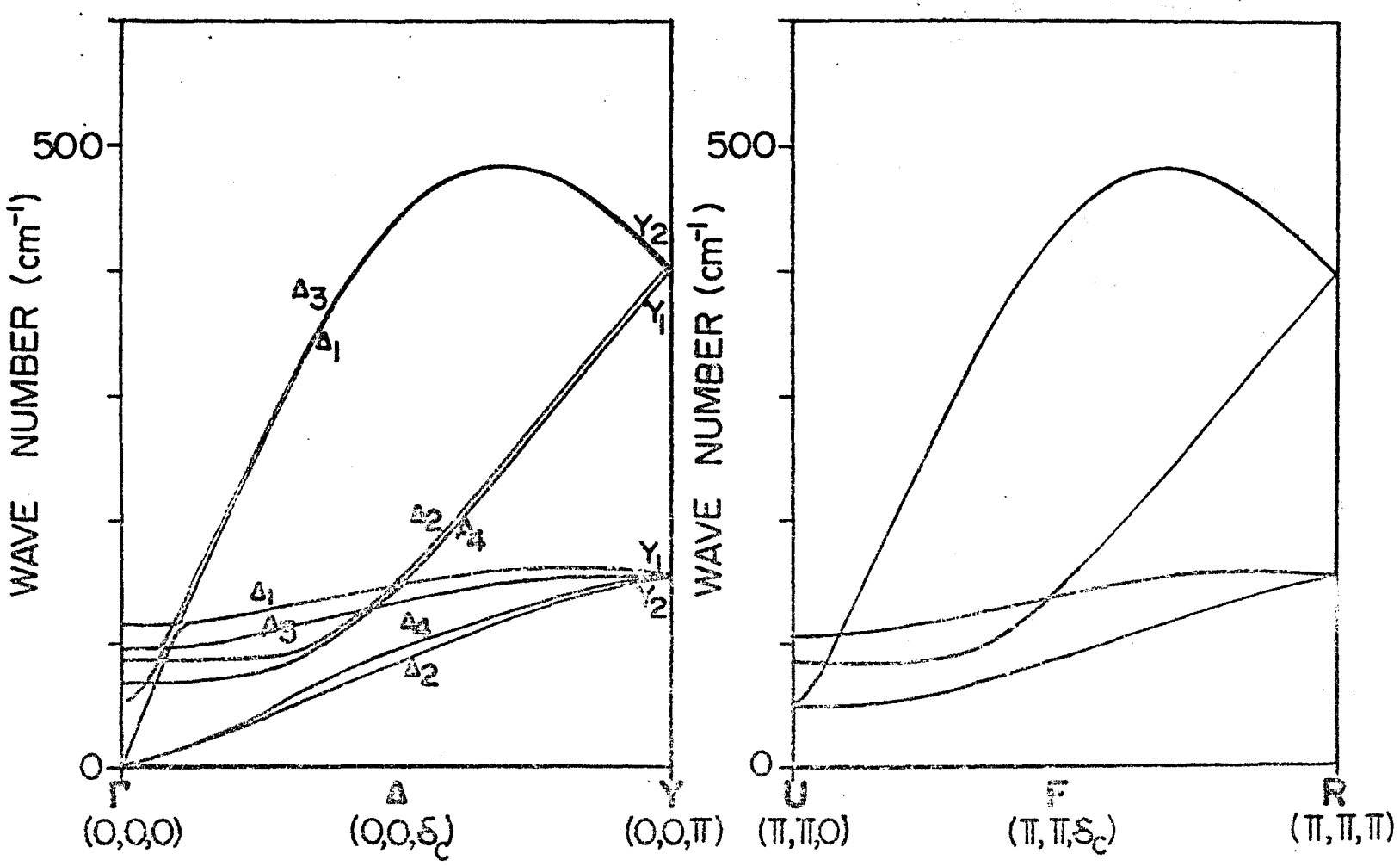

Fig. A3 Dispersion curves of frequency of crystal vibrations of deuterated polyethylene crystal along $(0,0,\delta_c)$ and (π,π,δ_c).

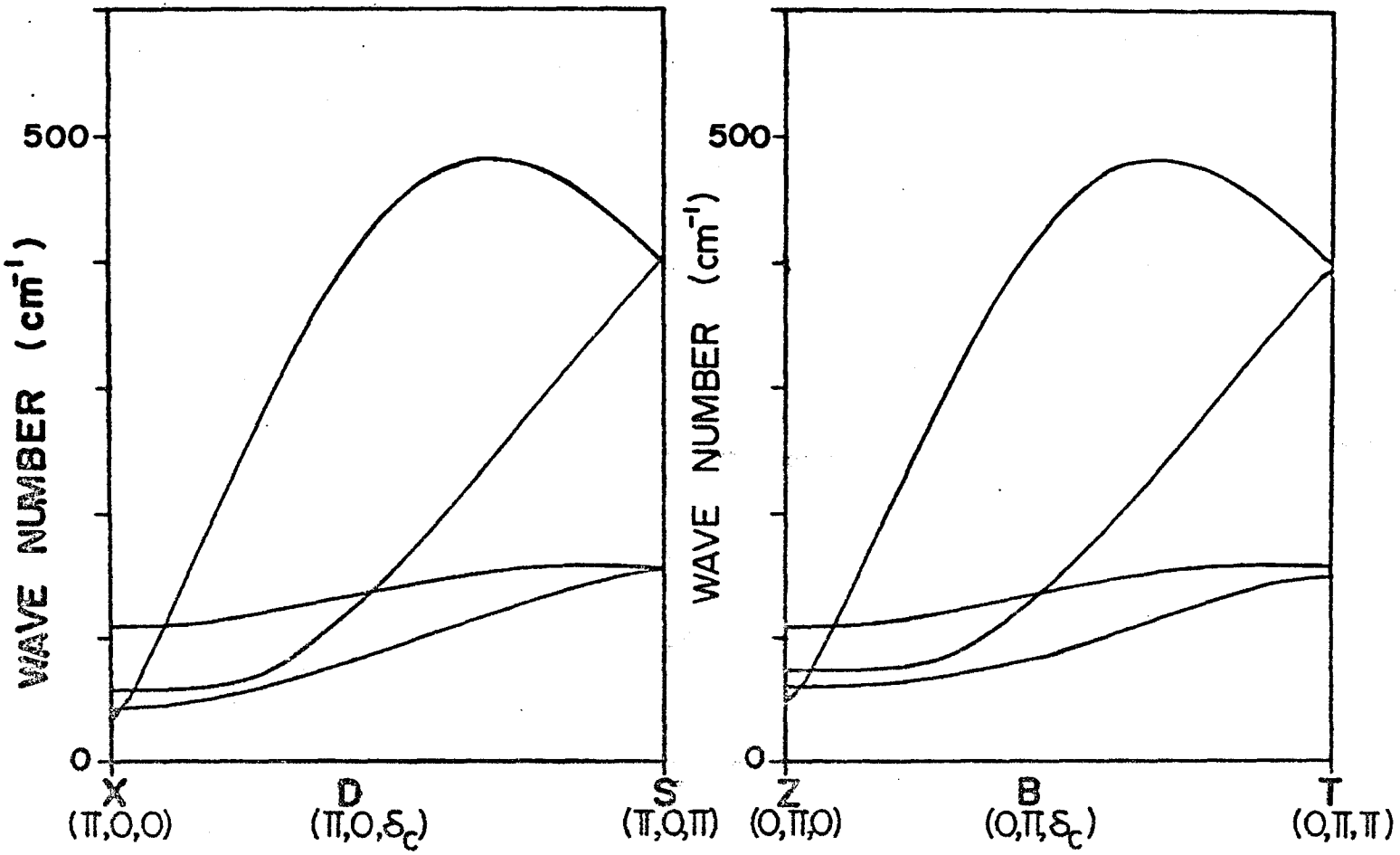

Fig. A4 Dispersion curves of frequency of crystal vibrations of deuterated polyethylene crystal along $(\pi,0,\delta_c)$ and $(0,\pi,\delta_c)$.

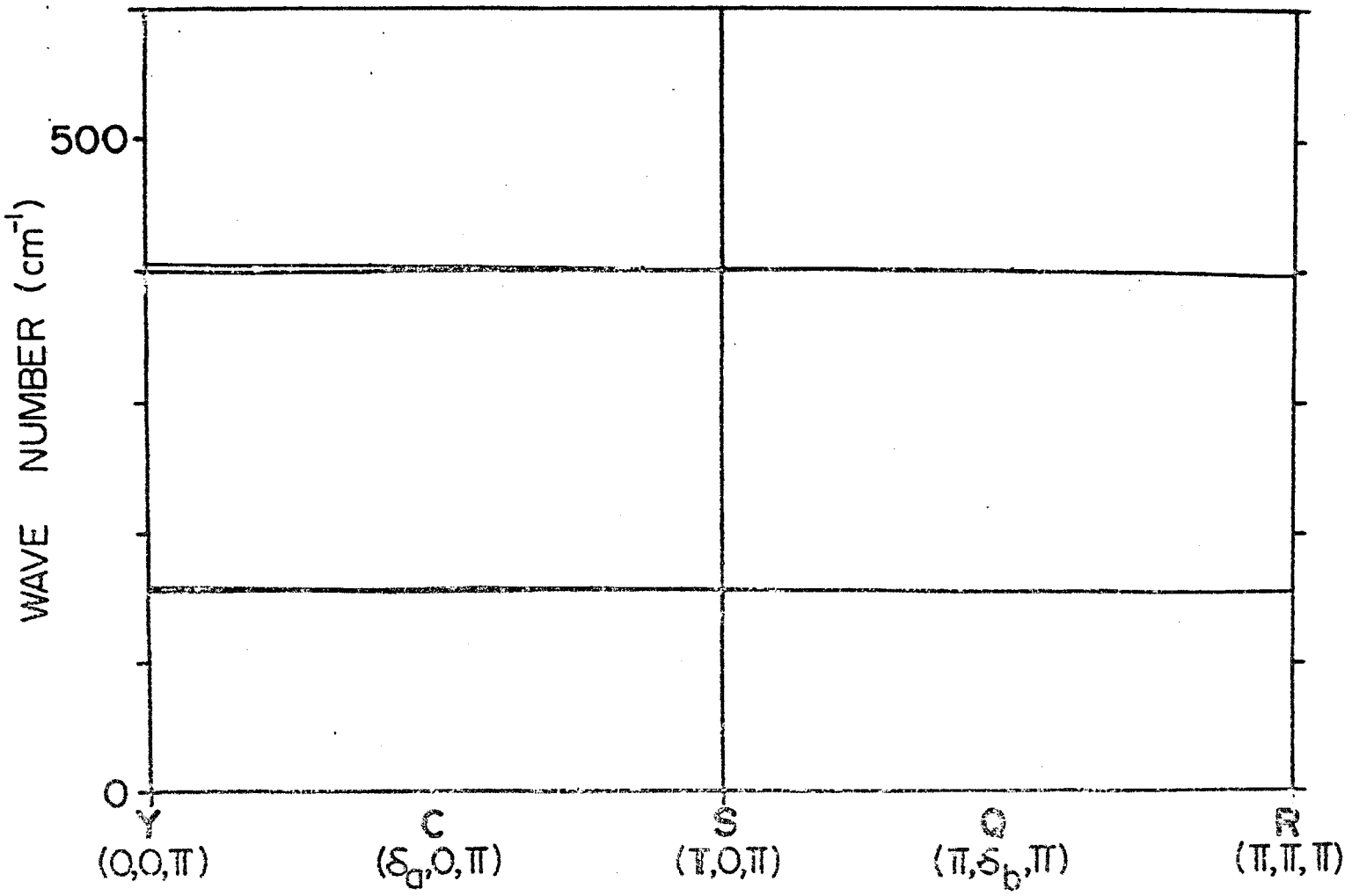

Fig. A5 Dispersion curves of frequency of crystal vibrations of deuterated polyethylene crystal along $(\delta_a, 0, \pi)$ and (π, δ_b, π).

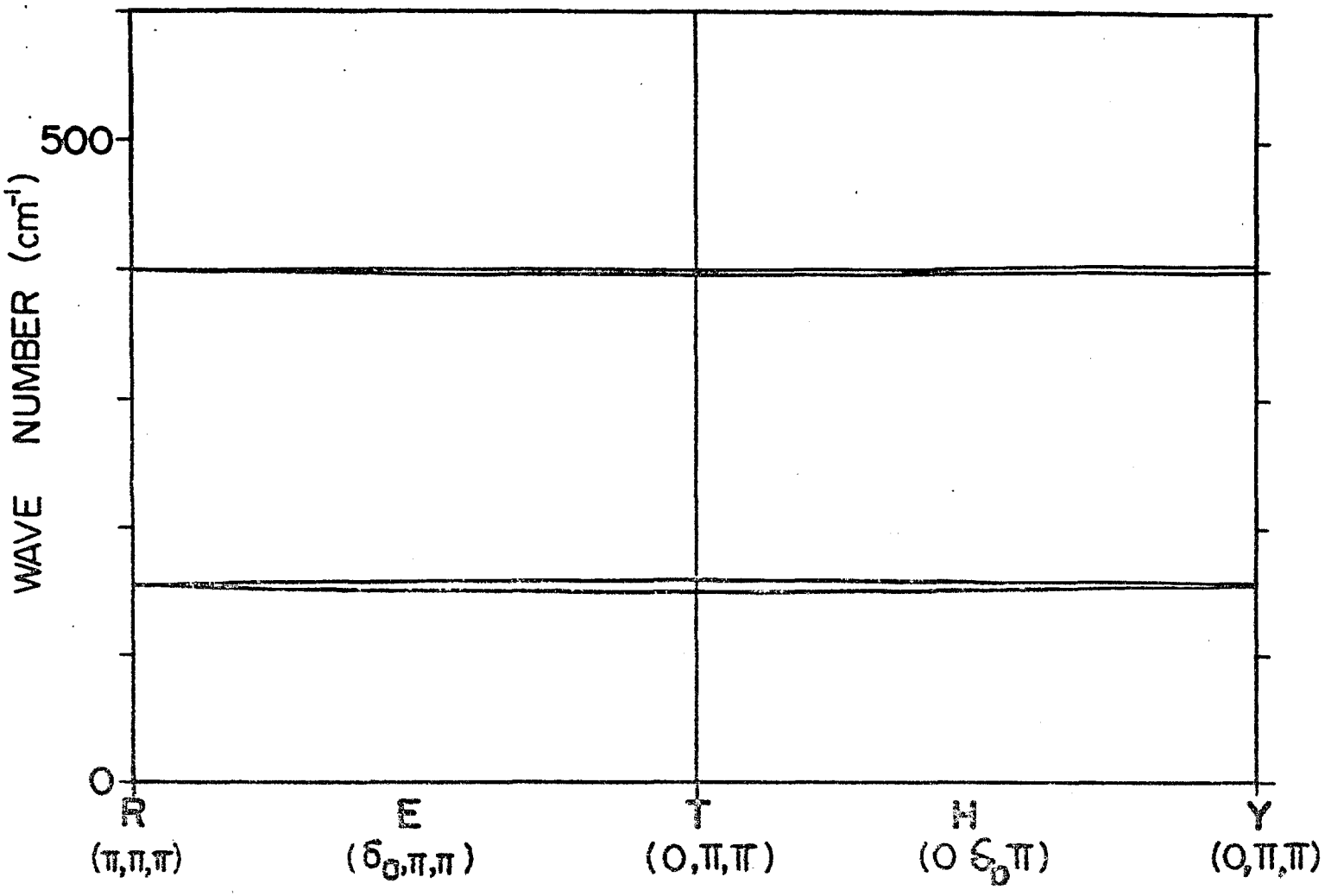

Fig. A6 Dispersion curves of frequency of crystal vibrations of deuterated polyethylene crystal along (δ_a,π,π) and $(0,\delta_b,\pi)$.

CHAPTER V

ELASTIC CONSTANTS OF POLYETHYLENE CRYSTAL

V-1 INTRODUCTION

Elasticity is a macroscopic feature of dynamical properties of crystal, which also originates in interatomic potential function. The observation of elastic constants provides good informations about the atomic force constants. Born and Huang have accomplished the basic formulation about elastic property of crystal.[1] The theory has been successfully applied to crystals of high symmetry such as diatomic ionic crystals.

In molecular crystals, elastic constants depends primarily upon intermolecular potential function. The experimental information about the intermolecular potential may be obtainable from the measurements of elasticity as well as optical spectrum, specific heat and neutron scattering cross section. On studying the force field of the crystal, it is advantageous to refer to all the experimental results. Shiro has improved the Born's formulation and incorporated the elastic constants into the least square analysis of force constants on treating normal coordinate problem of inorganic crystals.[2] The method is characterized with the application of the direct product representation to external deformation which would enable us to use the point group symmetry of crystal easily. Although the experimental values

of elastic constants are not obtained yet on polyethylene crystal, it is significant to calculate them from the present potential function, which reproduces other kinds of observed values in good fit.

Accordingly, in this chapter, the elastic constants are treated generally with the use of the Cartesian symmetry coordinates derived in (2.1) and then c_{ij} of polyethylene crystal is represented explicitly in terms of the interchain force constants. Also the relation of elastic constants with the frequency of acoustic phonons is derived. The elastic constants calculated from proper dispersion curves of crystal vibrations are in good agreement with those from the straightford calculation.

V-2 THEORY

When crystal lattice is subjected to arbitrary external force, the unit cells are assumed to take homogeneous deformation. Supposing $\mathbf{r}(l,k)$ and $\Delta\mathbf{r}(l,k)$ denote the equilibrium position and the displacement from it of the k-th atom in the l-th unit cell, respectively, then the external deformation $\Delta\mathbf{r}(l,k)$ is represented with tensor $\{u_{\alpha\beta}\}$ as[1)]

$$\Delta\mathbf{r}(l,k) = \begin{bmatrix}\Delta x(l,k)\\ \Delta y(l,k)\\ \Delta z(l,k)\end{bmatrix} = \begin{bmatrix}u_{xx} & u_{xy} & u_{xz}\\ u_{yx} & u_{yy} & u_{yz}\\ u_{zx} & u_{zy} & u_{zz}\end{bmatrix}\begin{bmatrix}x(l,k)\\ y(l,k)\\ z(l,k)\end{bmatrix} \tag{5.1}$$

which may be rewritten in the form of direct product[2)] as

$$\Delta\mathbf{r}(l,k) = \mathbf{W}(l,k)\cdot\mathbf{U} \tag{5.2}$$

where matrix $\mathbf{W}(l,k)$ and column vector $\mathbf{U}$ are defined as

$$W(l,k)=\begin{bmatrix} x(lk) & y(lk) & z(lk) & 0 & 0 & 0 & 0 & 0 & 0 \\ 0 & 0 & 0 & x(lk) & y(lk) & z(lk) & 0 & 0 & 0 \\ 0 & 0 & 0 & 0 & 0 & 0 & x(lk) & y(lk) & z(lk) \end{bmatrix} \tag{5.3}$$

$$\tilde{U} = (u_{xx}\ u_{xy}\ u_{xz}\ u_{yx}\ u_{yy}\ u_{yz}\ u_{zx}\ u_{zy}\ u_{zz}) \tag{5.4}$$

In the case of mono-atomic unit cell, this deformation is all which appears. However, if there are several atoms contained per unit cell, the external deformation is not the most stable deformation and it is assumed that, after the external deformation, the constituent atoms further change their relative position in the unit cell so as to minimize the energy increment due to the external deformation. Thus, $\rho(k)$, the atomic displacement associated with the internal deformation, is represented as a vector measured from the atomic position after the external deformation. Therefore, $\rho(k)$ depends only upon the type of atoms but does not depend upon the cell number. Then the ensemble of $\rho(k)$ $(k=1,2,\cdots,n)$ is common to all unit cells and becomes equivalent to the atomic displacement of crystal vibrations for $\delta=0$. Total Cartesian displacement coordinate vector of (l,k) atom is sum of displacement due to two types of deformations, that is,

$$X(l,k) = \rho(k) + \Delta r(l,k)$$

Since the external deformation may be considered as superposition of limiting modes of acoustic phonons to $\delta=0$, the displacement $X(l,k)$ also corresponds to the atomic displacement of $\delta=0$. Accordingly, the Cartesian displacement vector is transformed into internal displacement coordinate vector with the use of B matrix[3] corresponding to $\delta=0$.

$$R = \Sigma_{l,k} B(l,k)X(l,k) = \Sigma_{l,k} B(l,k)\rho(k) + D\,U \qquad (5.5)$$

where

$$D = \Sigma_{l,k} B(l,k)W(l,k) \qquad (5.6)$$

and R is internal displacement coordinate vector for $\delta=0$. Since the external deformation parameter includes the rotation of crystal as a whole, pure elastic deformation (σ) is separated from the rotation (ω) by

$$\begin{bmatrix}\sigma\\ \omega\end{bmatrix} = Z\,U \qquad (5.7)$$

where Z is an orthogonal matrix and the inverse transformation provides U in terms of σ and

$$U = Z^{-1}\begin{bmatrix}\sigma\\ \omega\end{bmatrix} \qquad (5.8)$$

The individual elements are represented as follows;

$$u_{xx} = \sigma_1 \qquad u_{xy} = (\sigma_6+\omega_z)/2 \qquad u_{xz} = (\sigma_5-\omega_y)/2$$
$$u_{yy} = \sigma_2 \qquad u_{yx} = (\sigma_6-\omega_z)/2 \qquad u_{yz} = (\sigma_4+\omega_x)/2$$
$$u_{zz} = \sigma_3 \qquad u_{zx} = (\sigma_5+\omega_y)/2 \qquad u_{zy} = (\sigma_4-\omega_x)/2$$

The second term of (5.5) denotes the internal displacement induced by the external deformations and is written as

$$D\,U = DZ^{-1}\begin{bmatrix}\sigma\\ \omega\end{bmatrix} = D_\sigma\sigma + D_\omega\omega \qquad (5.9)$$

Since there is no internal displacement due to the rotation of the crystal, D_ω becomes null matrix.

Supposing w is the energy increment per unit volume on the elastic deformation, then

$$w = (1/2v)(\widetilde{B\,\rho} + \widetilde{D_\sigma\,\sigma})\cdot F\cdot(B\,\rho + D_\sigma\,\sigma)$$
$$= (1/2v)(\tilde{\rho}\ \tilde{\sigma})\begin{bmatrix}\tilde{B}F_R B & \tilde{B}F_R D_\sigma\\ \tilde{D}_\sigma F_R B & \tilde{D}_\sigma F_R D_\sigma\end{bmatrix}\begin{bmatrix}\rho\\ \sigma\end{bmatrix} \qquad (5.10)$$

where F_R is a potential energy matrix for $\delta=0$ and v is the volume of the unit cell. Since both of the internal and external deformations satisfy the symmetry at $\delta=0$, they are classified in accordance with the point group of the space group. With the use of Cartesian symmetry coordinate vector defined by (2.1), as

$$S(\delta) = T(k,\delta)\rho(k)$$

then (5.10) is transformed into

$$w = (1/2v)(\widetilde{S}(0)\ \widetilde{\sigma})\begin{bmatrix} H_{\rho\rho} & H_{\rho\sigma} \\ H_{\sigma\rho} & H_{\sigma\sigma} \end{bmatrix}\begin{bmatrix} S(0) \\ \sigma \end{bmatrix} \qquad (5.11)$$

where

$$H_{\rho\rho} = T(k,0)\widetilde{B}(k)F_R B(k)\widetilde{T}(k,0)$$

which is equivalent to $F_S(0)$ of Eq(1.3) and

$$H_{\rho\sigma} = T(k,0)\widetilde{B}(k)F_R D_\sigma$$

Supposing M_k is the mass of the k-th atom, the matrix elements of $H_{\rho\rho}$ are easily obtained from the dynamical matrix $D_S(\delta)$ of (2.8) as

$$(H_{\rho\rho})_{kk'} = (M_k M_{k'})^{\frac{1}{2}} D_S(0)_{kk'} \qquad (5.12)$$

As described in Chapter I, $D_S(0)$ has already been completely factorized into symmetry species of D_{2h}. On the other hand, from the definition of σ_1 provided in Chapter III, the symmetry of σ_1 is isomorphous to the symmetry of the product of two translations of the crystal.

$$\Gamma(\sigma_1) = \Gamma(x)\times\Gamma(x) \qquad \Gamma(\sigma_4) = \Gamma(y)\times\Gamma(z)$$

$$\Gamma(\sigma_2) = \Gamma(y)\times\Gamma(y) \qquad \Gamma(\sigma_5) = \Gamma(z)\times\Gamma(x)$$

$$\Gamma(\sigma_3) = \Gamma(z)\times\Gamma(z) \qquad \Gamma(\sigma_6) = \Gamma(x)\times\Gamma(y)$$

$\Gamma(\sigma_1)$, $\Gamma(x)$, $\Gamma(y)$, and $\Gamma(z)$ are characters of group operations

for σ_1, x, y, and z, respectively. In D_{2h} system $\Gamma(x)$, $\Gamma(y)$ and $\Gamma(z)$ are all one dimensional and therefore $\Gamma(\sigma_1)$ is irreducible. In other words σ_i is symmetry coordinate as it is. In polyethylene crystal, σ_1, σ_2 and σ_3 belong to A_g species and σ_4, σ_5 and σ_6 belong to B_{1g}, B_{2g} and B_{3g}, respectively. $\mathbf{H}_{\rho\sigma}$ which results from the correlation of the internal and external deformation, has finite value only when $\mathbf{S}$ and $\boldsymbol{\sigma}$ belong to the same symmetry species. Accordingly (5.12) is represented as sum of small matrices which belong to each irreducible representation, as

$$w = (1/2v)\Sigma_\mu \, (\tilde{\mathbf{S}}^\mu(0) \; \tilde{\boldsymbol{\sigma}}^\mu) \begin{bmatrix} \mathbf{H}^\mu_{\rho\rho} & \mathbf{H}^\mu_{\rho\sigma} \\ \mathbf{H}^\mu_{\sigma\rho} & \mathbf{H}^\mu_{\sigma\sigma} \end{bmatrix} \begin{bmatrix} \mathbf{S}^\mu(0) \\ \boldsymbol{\sigma}^\mu \end{bmatrix} \qquad (5.13)$$

When a crystal has center of inversion, elastic deformation is always symmetric to inversion whereas the translation of the crystal as a whole is always antisymmetric to inversion. Therefore, in such crystals, $\mathbf{H}^\mu_{\rho\rho}$ of gerade species has unique inverse matrix.

On the other hand, the external force per unit volume, f_k, which caused the external deformation σ_k is now balanced with the restoring force $-(\partial w/\partial \sigma_k)$, and atoms have already been displaced so as to have no internal stress inside the unit cell, that is, $f_k = (\partial w/\partial \sigma_k)$, and $(\partial w/\partial S_j)=0$. If the external force per unit volume is represented as $\mathbf{f}$, the six component column vector, then the condition of equilibration is written as

$$\begin{bmatrix} \mathbf{0} \\ \mathbf{f} \end{bmatrix} = (1/v) \begin{bmatrix} \mathbf{H}_{\rho\rho} & \mathbf{H}_{\rho\sigma} \\ \mathbf{H}_{\sigma\rho} & \mathbf{H}_{\sigma\sigma} \end{bmatrix} \begin{bmatrix} \mathbf{S}(0) \\ \boldsymbol{\sigma} \end{bmatrix} \qquad (5.14)$$

In polyethylene crystal, there is center of inversion and with regard to the symmetry species concerned with elastic constants, the coefficient matrix of (5.14) has unique inverse matrix. The inverse transformation of (5.14) yields

$$\begin{bmatrix} \mathbf{S}(0) \\ \boldsymbol{\sigma} \end{bmatrix} = v \begin{bmatrix} \mathbf{H}_{\rho\rho} & \mathbf{H}_{\rho\sigma} \\ \mathbf{H}_{\sigma\rho} & \mathbf{H}_{\sigma\sigma} \end{bmatrix}^{-1} \begin{bmatrix} \mathbf{0} \\ \mathbf{f} \end{bmatrix} \tag{5.15}$$

The submatrix of (5.15) gives rise to $\boldsymbol{\sigma}$ in terms of f_k as

$$\sigma_j = \Sigma_k \, s_{jk} f_k \qquad (s_{jk}=s_{kj}) \tag{5.16}$$

where s_{jk} is elastic compliance constant. In orthorhombic system, all terms except for s_{11}, s_{22}, s_{33}, s_{44}, s_{55}, s_{66}, s_{12}, s_{23}, and s_{31} are zero. Young's moduli along α direction (α; x,y,z) is a ratio of the external force to the elastic deformation which is represented as

$$E_\alpha = (f_\alpha/\sigma_\alpha) = (1/s_{\alpha\alpha}) \tag{5.17}$$

The deformation, realized in the measurement of Young's moduli, is different from σ_1, σ_2 and σ_3 on the allowance of shortening in the direction perpendicular to the external tension. Poisson's ratio is a ratio of deformation, which is derived as

$$(\Delta a/a_0):(\Delta b/b_0):(\Delta c/c_0) = (s_{11}f_a+s_{12}f_b+s_{13}f_c): (s_{21}f_a+s_{22}f_b+s_{23}f_c):(s_{31}f_a+s_{32}f_b+s_{33}f_c) \tag{5.18}$$

where a_0, b_0 and c_0 are lattice constants and f_a, f_b and f_c are the a, b, and c axis component of the external tension, respectively.

The elastic stiffness constant matrix is given with the inverse transformation of Eq(5.16) as

$$\mathbf{f} = \mathbf{C}\,\boldsymbol{\sigma} \tag{5.19}$$

The elements, c_{ij}, are directly derived from Eq(5.14) as

$$c^{\mu}_{ij} = (H^{\mu}_{\sigma\sigma} - H^{\mu}_{\sigma\rho} H^{\mu\ -1}_{\rho\rho} H^{\mu}_{\rho\sigma})_{ij} \qquad (5.20)$$

V-3 RESULTS AND DISCUSSIONS

From the present potential, Young's moduli along the a, b and c axes are calculated as

$$E_a = 6.9, \quad E_b = 9.6, \quad E_c = 316 \qquad (\times 10^{10}\ \text{dyne/cm}^2).$$

When polyethylene molecule is assumed to be rigid, E_a and E_b may be given by Eq(1.26) and thus calculated values are E_a=7.0 and E_b=9.6 which agree with the values obtained from above. Thereby the Young's moduli perpendicular to the chain axis, in fact, depends upon the interchain potential.

Sakurada et al.[4] have observed the Young's moduli of polyethylene crystal with the X-ray diffraction method. The observed values at room temperature are E_a=3.1, E_b=3.8 and E_c=235. On the other hand, recently the measurement has been reexamined on more crystalline polyethylene and the observed value is revised to E_a=5.0,[5] which became closer to the calculated value. Because of weakness of diffraction spot, E_b could not be observed. Since the present potential function corresponds to that at low temperature, the calculated Young's moduli may be compared with the observed value of low temperature. It is reasonable that the present calculated values are slightly larger than the observed values of room temperature. Müller[6] has measured the linear compressibility of $C_{23}H_{48}$, from which Young's moduli are derived as E_a=10 and E_b=9.

The elastic stiffness constants are calculated from the present potential as

c_{11}=8.38 c_{22}=11.6 c_{33}=317 c_{44}=4.69 c_{55}=3.45
c_{66}=4.69 c_{12}=4.10 c_{13}=1.48 c_{23}=2.81 ($\times 10^{10}$dyne/cm^2)

The symmetry of c_{ij} and the intrachain potential terms associated with it are shown in Table 1. c_{33} is particularly large in polyethylene crystal. It results from the fact that the deformation corresponding to σ_3 is accompanied with deformation of molecule itself. Since the force constants of C-C stretching is so large that C-C-C valence angle undertakes the deformation. Then c_{33} depends primarily upon the force constant of skeletal bending potential. While c_{11} and c_{22} depend mainly upon the inter-molecular potential.

Elastic deformations are partly realized in the acoustic phonons travelling along special direction. The dynamical matrix for three acoustic branches was derived as (Chapter III)

$$\begin{array}{c} \\ T_a \\ T_b \\ T_c \end{array}\begin{bmatrix} \dfrac{c_{11}}{a_0^2}\delta_a^2+\dfrac{c_{66}}{b_0^2}\delta_b^2+\dfrac{c_{55}}{c_0^2}\delta_c^2 & & \text{symmetric} \\ \dfrac{(c_{12}+c_{66})\delta_a\delta_b}{a_0b_0} & \dfrac{c_{66}}{a_0^2}\delta_a^2+\dfrac{c_{22}}{b_0^2}\delta_b^2+\dfrac{c_{44}}{c_0^2}\delta_c^2 & \\ \dfrac{(c_{13}+c_{55})\delta_a\delta_c}{a_0c_0} & \dfrac{(c_{23}+c_{44})\delta_b\delta_c}{b_0c_0} & \dfrac{c_{55}}{a_0^2}\delta_a^2+\dfrac{c_{44}}{b_0^2}\delta_b^2+\dfrac{c_{33}}{c_0^2}\delta_c^2 \end{bmatrix} \quad (5.21)$$

where a_0, b_0 and c_0 are lattice constants and T_a, T_b and T_c mean that the atomic displacement is parallel to the a, b, and c axes, respectively. The eigenvalue of above dynamical matrix is $\rho\omega^2$ where ρ is density and ω is angular frequency.

As shown in Fig. 1, the atomic displacement in the mode of $T_a(\delta_a,0,0)$ is equivalent to σ_1 of the external deformation,

and the eigenvalue of $T_a(\delta_a,0,0)$ is given by $\rho\omega^2=(c_{11}\delta_a^2/a_0^2)$. $T_b(0,\delta_b,0)$ is the longitudinal vibration along the b axis and its eigenvalue is derived from (5.21) as $\rho\omega^2=(c_{22}\delta_b^2/b_0^2)$. The dispersion curves of $T_a(\delta_a,0,0)$ and $T_b(0,\delta_b,0)$ are Σ_1 and Λ_1 of acoustic branches in Fig. 1 and Fig.2 of Chapter III, respectively. In Fig. 2, some of transverse acoustic modes are drawn schematically. $T_a(0,\delta_b,0)$ indicates that phonon travells along the b axis and the atomic displacement is parallel to the a axis. The eigenvalue is derived as $\rho\omega^2=(c_{66}\delta_b^2/b_0^2)$ from (5.21). $T_b(\delta_a,0,0)$ is transverse mode in which phonon travells along the a axis and the atomic displacement is parallel to the b axis. The dispersion curve corresponds to Σ_2 of Fig. 1 of preceding chapter and the eigenvalue is given by $\rho\omega^2=(c_{66}\delta_a^2/a_0^2)$. Since both eigenvalues are commonly associated with the elastic constant, c_{66}, the similarity of the modes are expected. In Fig. 2, the atomic displacement in the shear deformation of σ_6 was also shown. $T_a(0,\delta_b,0)$ and $T_b(\delta_a,0,0)$ seem to compose the one side of the elastic deformation. Therefore, the dependence of the eigenvalues upon c_{66} is reasonable. However, homogeneous deformation is not a simple superposition of acoustic branches since $T_a(0,\delta_b,0)$ and $T_b(\delta_a,0,0)$ cannot be realized simultaneously. The mixing of T_a and T_b is possible only when phonon travells to the intermediate direction of the a and b axes. In the case of $\delta_c=0$ and $(\delta_a/a_0)=(\delta_b/b_0)=k_0$, the eigenvalues of T_a and T_b modes are

given by

$$\rho\omega^2 = \left\{(c_{11}+c_{22}+2c_{66}) + \left[(c_{11}-c_{22})^2+4(c_{12}+c_{66})^2\right]^{\frac{1}{2}}\right\}k_0^2/2$$

which shows that the eigenvalues depend upon c_{12}, c_{11} and c_{22} besides c_{66}. Therefore, the atomic displacement is not exactly identical with σ_6. Accordingly, it may be stated that the eigenvalues of transverse modes along the a, b, and c axes depend upon shear modulus such as c_{44}, c_{55} and c_{66}, whereas the elastic deformation cannot be exactly realized by acoustic vibrations.

On the other hand, for small value of phase difference, the frequency of acoustic vibrations is nearly proportional to phase difference. If arbitrary dispersion curves were observed in the experiment of inelastic coherent scattering of neutrons, the experimental values of the elastic constants would be obtained. Accordingly the coefficient of ν-$|\delta|$ line was derived for individual case and is summarized in Table 2. Since the theoretical dispersion curves are available the elastic constants were calculated from the inclination of those curves shown in the preceding chapter. Thus obtained values are as follows;

c_{11}=8.4	c_{22}= 11.2	c_{33}=317	c_{44}=4.7	c_{55}=3.5
c_{66}=4.7	c_{12}=3.2	c_{23}= ?	c_{13}=3.2	($\times 10^{10}$dyne/cm^2

The diagonal terms agree closely with those obtained directly from the potential function. Although c_{12}, c_{23} and c_{13} are to be calculated from the dispersion curves along $(\delta,\delta,0)$, $(0,\delta,\delta)$ and $(\delta,0,\delta)$, respectively, these off-diagonal terms actually cannot be determined precisely from dispersion curves.

Because these terms influence on the eigenvalues of acoustic phonons in second order together with shear modulus.

The partial derivative of elastic constants with respect to force constants are derived in general form,[7] which may be of great use especially for inorganic crystals. Regarding to the polyethylene crystal, the intrachain potential is fairly reliable and contributes little to the elastic constants except c_{33}. Accordingly the elastic constants were derived as function of the interchain force constants with the use of second order perturbation method described in chapter III, and are shown in Table 3. Thus calculated elastic constants are as follows;

c_{11}=8.44 c_{22}=11.1 c_{33}=314 c_{44}=4.73 c_{55}=3.53
c_{66}=4.80 c_{12}=3.88 c_{13}=2.04 c_{23}=2.82 ($\times 10^{10}$dyne/cm^2)

If the experimental values of the elastic constants were available, the force constants of interchain potential would become more definite.

The measurement of the velocity of sound wave also provides the experimental values of the elastic constants. The velocity of longitudinal acoustic phonon which travells along $(\delta_a,0,0)$ is equal to $(c_{11}/\rho)^{\frac{1}{2}}$ while the velocity of transverse acoustic phonon along the a axis are given by $(c_{66}/\rho)^{\frac{1}{2}}$ and $(c_{55}/\rho)^{\frac{1}{2}}$. Since the experiments about the sound velocity or coherent scattering of neutron requires fairly large single crystal, elastic constants have not been obtained yet on polyethylene crystal. However, it is very

desirable to obtain the exact experimental value of elastic constants for the study of inter-molecular potential.

SUMMARY

Elastic constants are derived in the proper form to molecular crystals with the Cartesian symmetry coordinates. The relation of frequency of acoustic phonons with elastic constants were derived and the elastic constants were calculated from the dispersion curves of the preceding chapter. The elastic constants were derived as function of the interchain force constants. The calculated values from these three methods are in good agreement with each other.

The Young's moduli along the a, b and c axes were also calculated, in reasonable agreement with the observed values.

REFERENCES

1) M.Born and K.Huang, " Dynamical Theory of Crystal Lattices" Clarendon Press, Oxford, (1954).

2) Y.Shiro, Symposium on Molecular Structure, 3C5, Sapporo (1967)

3) E.B.Wilson, J. Chem. Phys., 7, 1047 (1939); 9, 76 (1942).

4) I.Sakurada, T.Ito and K.Nakamae, J. Polymer Sci., C15, 75 (1966).

5) I.Sakurada, K.Kaji, K.Nakamae and E.Shikata, Symposium on Macromolecules, 22F09, Matsuyama (1968).

6) A.Müller, Proc. Roy. Soc., A154, 624 (1936); A178. 227 (1941)

7) Y.Shiro and T.Miyazawa, To be published.

Table-1 Symmetry of the elastic constants and the associated intrachain potential terms.

symmetry	c_{ij}	N_σ	N_ρ	R
A_g	c_{11}, c_{22}, c_{33} c_{12}, c_{23}, c_{13}	3	6	CH_2sym.str. CH_2scissor. C-Cstr. CH_2antisym.str. CH_2rock. C-C-C bend.
B_{1g}	c_{44}	1	3	CH_2wag. CH_2twist. C-Cstr.
B_{2g}	c_{55}	1	3	CH_2wag. CH_2twist. C-Cstr.
B_{3g}	c_{66}	1	6	CH_2sym.str. CH_2scissor. C-Cstr. CH_2antisym.str.* CH_2rock.* C-C-C bend.

N_σ is the dimension of $H^{\mu}_{\sigma\sigma}$.

N_ρ is the dimension of $H^{\mu}_{\rho\rho}$.

R is the internal coordinate. (sym.str.=symmetric stretching, antsym.str.=antisymmetric stretching, str.=stretching, scissor.=scissoring, rock.=rocking, twist.=twisting, wag.=wagging, and bend.=bending)

The coordinates marked with * do not contribute to D_σ.

Table-2 The inclination of ν-δ curve at the limit of $|\delta| \to 0$

direction	symmetry	mode	inclination
$(\delta_a, 0, 0)$	Σ_1	T_a (LA)	$(1/2\pi c)(c_{11}/\rho a_0^2)^{\frac{1}{2}}$
	Σ_2	T_b (TA)	$(1/2\pi c)(c_{66}/\rho a_0^2)^{\frac{1}{2}}$
	Σ_4	T_c (TA)	$(1/2\pi c)(c_{55}/\rho a_0^2)^{\frac{1}{2}}$
$(0, \delta_b, 0)$	Λ_1	T_b (LA)	$(1/2\pi c)(c_{22}/\rho b_0^2)^{\frac{1}{2}}$
	Λ_2	T_c (TA)	$(1/2\pi c)(c_{44}/\rho b_0^2)^{\frac{1}{2}}$
	Λ_4	T_a (TA)	$(1/2\pi c)(c_{66}/\rho b_0^2)^{\frac{1}{2}}$
$(0, 0, \delta_c)$	Δ_1	T_c (LA)	$(1/2\pi c)(c_{33}/\rho c_0^2)^{\frac{1}{2}}$
	Δ_2	T_a (TA)	$(1/2\pi c)(c_{55}/\rho c_0^2)^{\frac{1}{2}}$
	Δ_4	T_b (TA)	$(1/2\pi c)(c_{44}/\rho c_0^2)^{\frac{1}{2}}$

(LA) means longitudinal acoustic mode and (TA) means transverse acoustic mode.

Table-3 Explicit representation of the elastic constants with interchain force constants.

c_{11}	$\rho N_0 a_0^2 \cdot 10^{-13}(0.287P_1+2.090P_2+1.527P_3-155.6P_2^2-58.9P_3^2$ $-4.67P_1P_2+2.88P_1P_3+191.5P_2P_3)$
c_{22}	$\rho N_0 b_0^2 \cdot 10^{-13}(2.579P_1+0.688P_2+0.255P_3+5.212P_4-0.46P_1^2-74.4P_2^2$ $-14.3P_3^2-0.35P_4^2-11.7P_1P_2+5.12P_1P_3+0.80P_1P_4$ $+65.3P_2P_3+10.3P_2P_4-4.5P_3P_4)$
c_{33}	$\rho N_0 c_0^2 \cdot 10^{-13}(0.829P_1+1.024P_2+0.027P_3+0.681P_4+7.745)$
c_{44}	$\rho N_0 c_0^2 \cdot 10^{-13}(2.579P_1+2.908P_2+6.832P_4)$
c_{55}	$\rho N_0 a_0^2 \cdot 10^{-13}(0.698P_1+0.787P_2 \overline{+}0.008P_4)$
c_{66}	$\rho N_0 b_0^2 \cdot 10^{-13}(0.287P_1+2.090P_2+1.527P_3+0.067P_4-59.2P_1^2-7.23P_2^2$ $-23.8P_3^2+41.4P_1P_2+75.0P_1P_3+1.04P_1P_4-26.2P_2P_3$ $-0.66P_3P_4-0.36P_2P_4)$
$c_{12}+c_{66}$	$\rho N_0 a_0 b_0 \cdot 10^{-13}(1.722P_1+2.397P_2+1.249P_3)$
$c_{13}+c_{55}$	$\rho N_0 a_0 c_0 \cdot 10^{-13}(2.447P_1+3.673P_2+0.202P_3)$
$c_{23}+c_{44}$	$\rho N_0 b_0 c_0 \cdot 10^{-13}(2.804P_1+2.352P_2+0.082P_3+5.439P_4)$

N_0 is Avogadro's number.

c_{ij} is represented in (dyne/cm^2). If the force constants are given in (mdyne/Å), lattice constants in (Å) and ρ in (g/cm^3).

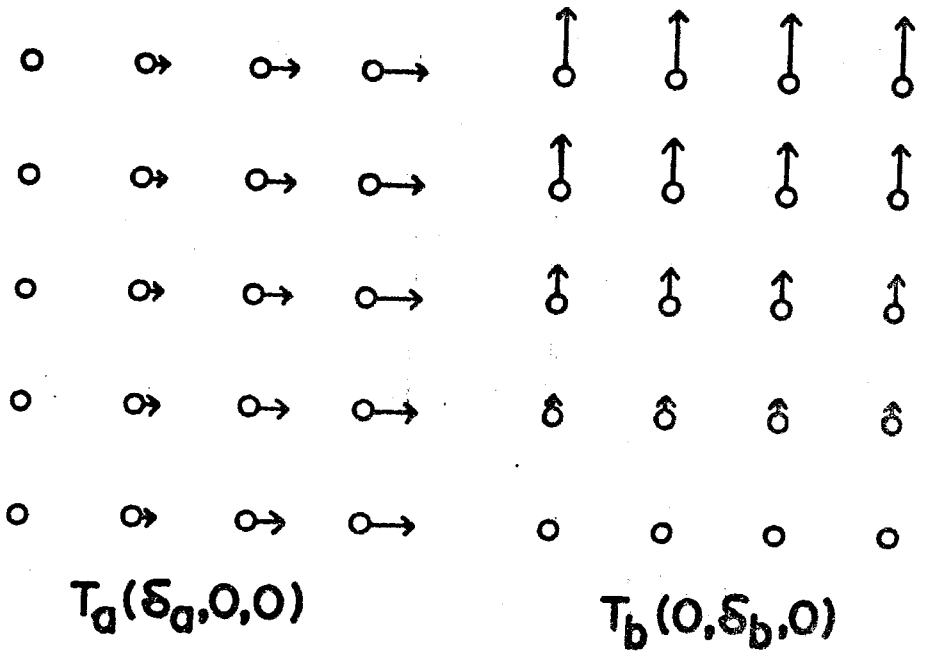

Fig. 1 The atomic displacement in two longitudinal acoustic vibrations. $T_a(\delta_a,0,0)$ and $T_b(0,\delta_b,0)$ correspond to Σ_1 and Λ_1 of dispersion curves, respectively.

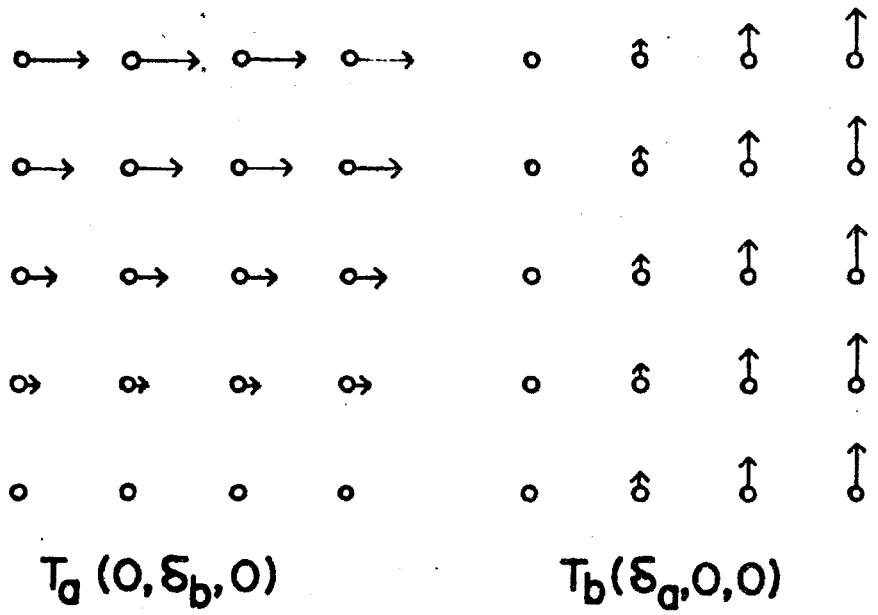

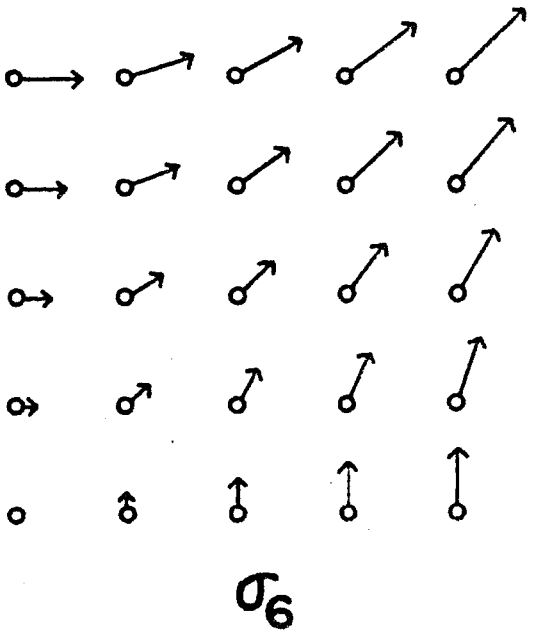

Fig. 2 The atomic displacement in two transverse acoustic vibrations and shear deformation σ_6. $T_a(0,\delta_b,0)$ and $T_b(\delta_a,0,0)$ correspond to Λ_4 and Σ_2 of crystal vibrations, respectively.

CHAPTER VI

A REFINED METHOD FOR TREATING ONE- AND MULTI-PHONON NEUTRON-SCATTERING CROSS SECTIONS

VI-1 INTRODUCTION

Recent development of neutron scattering has made it possible to measure the inelastic scattering cross section and to determine the dispersion curves of crystal vibrations experimentally.[1] Energy analysis of incoherently scattered neutrons from hydrogeneous compounds has also been current subject because of no selection rule for neutron specroscopy. The basic formulae about the scattering cross section of neutrons have already been derived[2-4] and up to date, the observed results have been commonly explained on the basis of the theory. However, the object of that theory are monoatomic crystal lattices such as metal crystal, and the observed results from molecular crystals have not been always analysed sufficiently. Although the use of time dependent correlation function[5] provides the straightforward representation of the scattering cross section, the concept of correlation function regarding to atomic displacement, does not necessarily lead us to concrete image of its physical meaning.

On the other hand, the scanning region of far infrared spectrometer has been extended to fairly long wavelength and also laser Raman technique has been developed considerably. Now the optical spectrum is of great use to investigate the

lattice vibrations. Also theoretical treatment of molecular vibrations has been advanced[6] and the assignment of vibrational frequency obtained from the infrared and Raman spectrum became reliable.[7] Generally the resolution is higher in infrared and Raman spectram than in neutron spectrum. However, the information from neutron spectroscopy is unique on the observation of the frequency distribution. Therefore, on the study of lattice vibrations, both experimental results of optical and neutron spectrum should be reasonably referred.

The scattering cross section of neutron by crystal vibrations may be derived on the basis of stationary state and the formulation would be easier for spectroscopists to get acquainted with neutron spectrum. Accordingly, in the present study, the incoherent scattering cross section of neutrons is derived in general form on the basis of transition probability. The result is same with that from the time dependent correlation function, while the present derivation would have analogy to that of optical spectrum and is relatively convenient for numerical computation with electronic computer, especially for multiphonon scattering cross section. The present result has been successfully applied to the analysis of the experimental results from polyethylene crystal, which would be described in next chapter.

VI-2 THE CONCEPT OF TRANSITION PROBABILITY

For arbitrary phase difference vector δ, normal vibrations are doubly degenerate and therefore, the atomic displacement associated with crystal vibrations are represented with degenerate pairs of two real normal coordinates as

$$u_\mu = (2/NM_\mu)^{\frac{1}{2}} \sum_{i,\delta} \left[L^a_{\mu i}(\delta) Q^a_i(\delta) + L^b_{\mu i}(\delta) Q^b_i(\delta) \right] \qquad (6.1)$$

where u_μ is the atomic displacement vector of μ-th atom[8], N is total number of unit cells in the crystal, M_μ is the mass of μ-th atom and $L_{\mu i}$ is the polarization vector of μ-th atom due to i-th branch of lattice vibrations. Summations runs over all branches on N/2 values[9] of δ in half of the first Brillouin zone. Because of the symmetry, the irreducible volume of the first Brillouin zone is reduced to 1/8 of the first Brillouin zone in the case of polyethylene crystal, that is

$$(0,0,0) \leq (\delta_a, \delta_b, \delta_c) \leq (\pi, \pi, \pi)$$

With the use of the matrix elements of symmetry transformation matrix, $U(\rho, \delta)$ of Eq(2.1), the polarization vector is written as

$$\begin{aligned} L^a_{\mu i}(\delta) &= A_{\mu i} \cos(\rho_\mu \delta) + B_{\mu i} \sin(\rho_\mu \delta) \\ L^b_{\mu i}(\delta) &= -A_{\mu i} \sin(\rho_\mu \delta) + B_{\mu i} \cos(\rho_\mu \delta) \end{aligned} \qquad (6.2)$$

where ρ_μ is the index vector of μ-th atom and $A_{\mu i}$ and $B_{\mu i}$ are vectors of order three which is subvector of eigenvector of the dynamical matrix. Numerical value of $A_{\mu i}$ and $B_{\mu i}$ are calculated with Eq(2.13) from the corresponding eigenvector of i-th branch.

In nonmagnetic crystals, the interaction of neutron with crystal lattice has been represented as sum of Fermi's pseudo potential.[10-11] For the scattering of low energy neutron from nuclei, Born's first approximation is practical. Then the differential cross section for incoherent scattering is represented as

$$(d\sigma/d\Omega)_{inc} = (|k_2|/|k_1|)(1/4\pi N) \sum_\mu s_\mu \left| M^\mu_{12} \right|^2_T \qquad (6.3)$$

$$M_{12}^{\mu} = \langle \psi_2^* | \exp[i(\mathbf{k}_1 - \mathbf{k}_2)\mathbf{u}_\mu] | \psi_1 \rangle \qquad (6.4)$$

where $\mathbf{k}_1$ and $\mathbf{k}_2$ are wave vectors of incident and scattered neutrons, respectively, and s_μ is the bound atom incoherent cross section[12] of μ-th atom and $|M_{12}^{\mu}|^2_T$ is temperature average of transition probability for the crystal vibrations to change from ψ_1 to ψ_2 together with the change of wave vector of neutron from $\mathbf{k}_1$ to $\mathbf{k}_2$, where ψ_1 and ψ_2 are the initial and final wave functions of the crystal vibrations, respectively. Under the harmonic approximation, the wave function of the crystal vibrations is written as product of wave function of each normal coordinate as

$$\psi = \phi_{v_1}(Q_1)\phi_{v_2}(Q_2)\cdots\cdots\phi_{v_i}(Q_i)\cdots\cdots \qquad (6.5)$$

where, for simplicity, the suffix i distinguishes both of phase differences and branch number.(then $i=1,2,3,\cdots,3nN/2$). This independency of normal coordinate lets the matrix element of Eq(6.4) be represented as product of the matrix element of each normal coordinate as

$$M_{12}^{\mu} = \prod_i \langle \phi_{v_i'}(Q_i) | \exp(iF_{\mu i}Q_i) | \phi_{v_i}(Q_i) \rangle \qquad (6.6)$$

where v_i and v_i' are initial and final quantum number of i-th normal coordinate and $F_{\mu i}$ is a scalar product of the atomic displacement vector of μ-th atom due to Q_i by the momentum transfer vector of neutron. Since each component of the degenerate pair of i-th normal coordinate is mutually linear independent , the wave function $\phi_{v_i}(Q_i)$ is againly expressed as the composite of two wave functions.

$$\phi(Q_i) = \phi(Q_i^a)\cdot\phi(Q_i^b)$$

$F_{\mu i}$ of Eq(6.6) is derived from Eqs(6.1), (6.2) and (6.4) as

$$F^a_{\mu i} = (2/M_\mu N)(k_1-k_2)\left[A_{\mu i}\cos(\rho_\mu \delta) + B_{\mu i}\sin(\rho_\mu \delta)\right]$$
$$F^b_{\mu i} = (2/M_\mu N)(k_1-k_2)\left[-A_{\mu i}\sin(\rho_\mu \delta) + B_{\mu i}\cos(\rho_\mu \delta)\right] \qquad (6.7)$$

Supposing $I_{v+\lambda,v}$ is the matrix element of exp(iFQ) with regard to two quantum states, v and v+λ, where Q is arbitrary nondegenerate normal coordinate, then $I_{v+\lambda,v}$ is derived in general form as[2)]

$$I_{v+\lambda,v} = \sum_{r=0}^{v} \left[(v+\lambda)!\, v!\right]^{\frac{1}{2}} \frac{(t^2/2)^{r+\lambda/2}\cdot\exp(t^2/4)}{(v-r)!\,(r+\lambda)!\,r!} \qquad (6.8)$$

where $t=i\gamma^{-\frac{1}{2}}F$, $\gamma = \omega/\hbar$ and ω is the angular frequency of Q. The proof of Eq(6.8) is given in Appendix II.

Then the thermal average of transition probability for the normal coordinate is given by

$$J_{v+\lambda,\lambda} = \sum_{v=0} w_v I^*_{v+\lambda,v}\cdot I_{v+\lambda,v} \qquad (6.9)$$

where w_v is the occupancy probability at initial state, $\phi_v(Q)$, which results from Bose-statistics.

$$w_v = (1-x)\cdot x^v \qquad (6.10)$$

where

$$x = \exp(-\hbar\omega/kT)$$

Then the transition probability of the crystal, $\left|M^\mu_{12}\right|^2_T$ is represented as product of $J_{v+\lambda,v}$ of the constituent normal coordinates.

VI-3 THE TRANSITION PROBABILITY FOR ELASTIC SCATTERING

In the elastic scattering, momentum of neutron changes without the change of energy. Crystal accepts the momentum transfer of $(k_1-k_2)\hbar$ whereas quantum number of crystal vibrations is not altered at all. The corresponding matrix

element is

$$I_{v,v} = \exp(t^2/4)\cdot\left[1 + vt^2/2 + v(v-1)t^4/16 + \cdots\right] \tag{6.11}$$

and the thermal average of the square of the $I_{v,v}$ is approximately represented as

$$J_{v,v} = \sum_{v}^{\infty} (1-x)x^v \cdot I^*_{v,v}\cdot I_{v,v} = \exp\left[t^2(1+x)/2(1-x)\right] \tag{6.12}$$

Since the vibration is degenerate, the transition probability for i-th pair of normal coordinate is written in the product of two terms corresponding to Q_i^a and Q_i^b, as

$$J_{v,v}(Q_i) = \exp\left[(t_a^2+t_b^2)(1+x_i)/2(1-x_i)\right] \tag{6.13}$$

where $t_a = i\gamma^{-\frac{1}{2}}F^a_{\mu i}$ and $t_b = i\gamma^{-\frac{1}{2}}F^b_{\mu i}$. From (6.7) and the definition of t, the exponent of Eq(6.13) is transformed into

$$t_a^2 + t_b^2 = (-2\hbar/M_\mu N\omega)\left[(K_0A_{\mu i})^2 + (K_0B_{\mu i})^2\right] \tag{6.14}$$

where $K_0 = k_1 - k_2$, is momentum transfer vector for elastic scattering. Then the transition probability of the crystal is

$$\left|M^\mu_{12}\right|^2_T = \exp\left[-2W_\mu(K_0)\right] \tag{6.15}$$

where $2W_\mu(K_o)$ is Debye-Waller factor of μ-th atom and represented as

$$2W_\mu(K_0) = \sum_i (\hbar/M_\mu N\omega_i)\left[(K_oA_{\mu i})^2+(K_0B_{\mu i})^2\right](1+x_i)/(1-x_i) \tag{6.16}$$

where summation runs over all branches for N/2 points in half of the first Brillouin zone. Thus derived Debye-Waller factor is used in terms of the temperature factor for X-ray diffraction.

Accordingly when momentum transfer vector is parallel to the atomic displacement, the transition probability for no energy transfer diminishes and the peak intensity of elastic

scattering cross section becomes low. In other words, under such circumstances energy is also apt to be transferred besides momentum.

VI-4 THE TRANSITION PROBABILITY FOR INELASTIC SCATTERING

A) SINGLE PHONON PROCESS

On the collision of neutron with crystal, neutron may lose (down-scattering) or gain (up-scattering) energy corresponding to the separation of vibrational energy levels, or to the contrary, the crystal gets or emitts the corresponding energy. These inelastic scatterings are conveniently classified in accordance with the transferred phonon number.

When a-th component of j-th normal coordinate is excited from v to v+1 (down-scattering), the energy, E_t and momentum, $K_t\hbar$ which neutron gives to crystal is

$$E_t = (|k_1|^2 - |k_2|^2)\hbar^2/2m = \hbar\omega_j \tag{6.17}$$

$$K_t = k_1 - k_2 \tag{6.18}$$

where m is mass of neutron, ω_j is the angular frequency of Q_j^a. The transition probability associated with this process is represented as

$$|M_{12}^{\mu}|_T^2 = J_{v+1,v}(Q_j^a) \prod_{1 \neq j_a} J_{v,v}(Q_1) \tag{6.19}$$

From Eqs(6.8) and (6.9), the transition probability about Q_j^a is derived as

$$J_{v+1,v} = \sum_{v}^{\infty} \tfrac{1}{2}(1-x)x^v \cdot (v+1) \cdot \exp(t_a^2/2) \times \left[t + vt^3/4 + v(v-1)t^5/48 + \cdots\right]^2 \tag{6.20a}$$

$$= J_{v,v} \cdot t_a^2/2(1-x) \tag{6.20b}$$

Substitution of $J_{v+1,v}(Q_j^a)$ from Eq(6.20b) into Eq(6.19) yields

$$\left|M_{12}^{\mu}\right|_T^2 = \left[t_a^2/2(1-x_j)\right]\prod_i J_{v,v}(Q_i) \qquad (6.21)$$

For the b-th component of j-th normal coordinate, the same amount of energy and momentum is transferred. Accordingly the transition probability of j-th degenerate pair of vibrations becomes sum of the constituent terms, which is derived as

$$\left|M_{12}^{\mu}\right|_T^2 = (\hbar/M_{\mu}N\omega_j)\left[(K_tA_{\mu j})^2+(K_tB_{\mu j})^2\right]\exp\left[-2W_{\mu}(K_t)\right]/(1-x_j) \qquad (6.22)$$

where $2W_{\mu}(K_t)$ is Debye-Waller factor for μ-th atom and represented as

$$2W_{\mu}(K_t) = \sum_i (\hbar/M_{\mu}N\omega_i)\left[(K_tA_{\mu i})^2+(K_tB_{\mu i})^2\right](1+x_i)/(1-x_i) \qquad (6.23)$$

In the case of up-scattering of the same energy transfer, the corresponding term $J_{v-1,v}$ is derived as

$$J_{v-1,v}(Q_j) = x_jJ_{v+1,v}(Q_j)$$

and the transition probability becomes

$$\left|M_{12}^{\mu}\right|_T^2 = (\hbar/M_{\mu}N\omega_j)\cdot\left[(K_tA_{\mu j})^2+(K_tB_{\mu j})^2\right]\cdot\exp\left[-2W_{\mu}(K_t)\right]\cdot x_j/(1-x_j) \qquad (6.24)$$

The factor x_j results from the lower population of phonons at higher state and therefore, at low temperature, up-scattering cross section becomes much smaller than the corresponding down-scattering cross section.

B) TWO PHONON PROCESS

Two phonon scattering includes all transitions in which vibrational quantum numbers are changed simultaneously by two units on single collision. The cross section is classified in accordance with the notation of spectroscopy, that is,

overtone, summation combination and difference combination. The transition probability for overtone band is derived as

$$J_{v+2,v} = \sum_{v=0}^{\infty} (1-x)x^v \cdot (v+1)(v+2) \cdot \exp(t^2/2) \times \left[t^2 + vt^4/6 + v(v-1)t^6/96 + \cdots\right]^2$$
$$= J_{v,v} t^4/8(1-x)^2 \qquad (6.25)$$

For the up-scattering process, the corresponding transition is $v \rightarrow v-2$ and the transition probability is derived as

$$J_{v-2,v} = x^2 J_{v+2,v} \qquad (6.26)$$

Because of low population proportional to x^2, overtone peak is rarely seen in the up-scattering cross section.

Combination-tone corresponds to the process in which vibrational quantum numbers of two different oscillators are changed simultaneously by one unit on single collision. For summation combination, both of j-th and k-th nondegenerate normal vibration change from v to v+1 and the corresponding transition probability is

$$\left|M_{12}^{\mu}\right|_T^2 = J_{v+1,v}(Q_j) J_{v+1,v}(Q_k) \prod_{i \neq j,k} J_{v,v}(Q_i) \qquad (6.27)$$

and for difference combination, it is

$$\left|M_{12}^{\mu}\right|_T^2 = J_{v-1,v}(Q_j) J_{v+1,v}(Q_k) \prod_{i \neq j,k} J_{v,v}(Q_i) \qquad (6.28)$$

where j-th vibration is assumed to change from v to v-1.

Because of degeneracy of each normal coordinate of crystal, overtone of j-th normal coordinate includes three types of transition

1) $v \rightarrow v+2$ for Q_j^a
2) $v \rightarrow v+2$ for Q_j^b
3) $v \rightarrow v+1$ for Q_j^a and $v \rightarrow v+1$ for Q_j^b

The energy transfers are common to these transitions and given by

$$E_t = (|k_1|^2 - |k_2|^2)\hbar^2/2m = 2\hbar\omega_j$$

The difference combination of Q_j^a and Q_j^b gives no energy transfer and it does not contribute to inelastic scattering at all. From Eqs(6.20) and (6.25),

$$J_{v+2,v}(Q_j^a)J_{v,v}(Q_j^b) + J_{v+1,v}(Q_j^a)J_{v+1,v}(Q_j^b) + J_{v,v}(Q_j^a)J_{v+2,v}(Q_j^b)$$

$$= J_{v,v}(Q_j^a)J_{v,v}(Q_j^b)\cdot(t_a^4+2t_a^2t_b^2+t_b^4)/8(1-x_j)^2 \qquad (6.29)$$

Accordingly the transition probability in the crystal is represented as

$$|M_{12}^{\mu}|_T^2 = \tfrac{1}{2}(\hbar/M_{\mu}N\omega_j)^2(1-x_j)^{-2}\left[(K_tA_{\mu j})^2+(K_tB_{\mu j})^2\right]^2\exp\left[-2W_{\mu}(K_t)\right] \qquad (6.30)$$

Regarding to the summation combination of j-th and k-th vibrations, there are four types of combinations; (Q_j^a,Q_k^a), (Q_j^a,Q_K^b), (Q_j^b,Q_k^a), and (Q_j^b,Q_k^b) which gives common energy transfer

$$E_t = (\omega_j + \omega_k)\hbar \qquad (6.31)$$

With Eqs(6.20) and (6.27), the transition probability of the crystal is derived as

$$|M_{12}^{\mu}|_T^2 = \frac{\hbar^2\left[(K_tA_{\mu j})^2+(K_tB_{\mu j})^2\right]\cdot\left[(K_tA_{\mu k})^2+(K_tB_{\mu k})^2\right]}{M_{\mu}^2N^2\,\omega_j\,\omega_k(1-x_j)(1-x_k)}\exp\left[-2W_{\mu}(K_t)\right] \qquad (6.32)$$

As for difference combination, in which Q_j changes from v to v+1, there are also four types of transitions. The transition probability is derived from Eqs(6.24) and (6.28)

$$|M_{12}^{\mu}|_T^2 = \frac{x_j\hbar^2\left[(K_tA_{\mu j})^2+(K_tB_{\mu j})^2\right]\cdot\left[(K_tA_{\mu k})^2+(K_tB_{\mu k})^2\right]}{M_{\mu}^2N^2\omega_j\,\omega_k(1-x_j)(1-x_k)}\exp\left[-2W_{\mu}(K_t)\right] \qquad (6.33)$$

and the corresponding energy transfer is given by

$$E_t = (|k_1|^2 - |k_2|^2)\hbar^2/2m = (\omega_k-\omega_j)\hbar \qquad (6.34)$$

In the same way, the transition probability for overtone of down-scattering is derived as

$$\left|M_{12}^{\mu}\right|_T^2=(x_j\hbar/M_\mu N\omega_j)^2(1-x_j)^{-2}\left[(K_tA_{\mu j})^2+(K_tB_{\mu j})^2\right]\exp\left[-2W_\mu(K_t)\right] \tag{6.35}$$

C) THREE PHONON PROCESS

On this scattering process, vibrational quantum number changes by three units simultaneously on single collision. When three different normal coordinates, Q_j, Q_k and Q_l participate in the scattering, the transition probability is derived in analogy with the combination tones of two-phonon scattering as

$$\left|M_{12}^{\mu}\right|_T^2 = (\hbar/M_\mu N)^3 \prod_{\kappa=j,k,l}\left[(K_tA_{\mu\kappa})^2+(K_tB_{\mu\kappa})^2\right]\exp\left[-2W_\mu(K_t)\right]/\omega_\kappa(1-x_\kappa) \tag{6.36}$$

and the corresponding energy transfer is

$$E_t = (\omega_j + \omega_k + \omega_l)\hbar \tag{6.37}$$

In the case of difference combination, in which p-th normal vibration changes from v_p to v_p-1, Eq(6.36) has to be multiplied by the population factor of x_p.

When two different normal coordinates take part in the scattering, the transition probability is represented as the product of the corresponding terms of overtone process by the term for single phonon process, that is,

$$\left|M_{12}^{\mu}\right|_T^2 = \frac{\hbar^3\left[(K_tA_{\mu j})^2+(K_tB_{\mu j})^2\right]^2\left[(K_tA_{\mu k})^2+(K_tB_{\mu k})^2\right]}{2M_\mu^3N^3(1-x_j)^2\omega_j^2(1-x_k)\,\omega_k}\exp\left[-2W_\mu(K_t)\right] \tag{6.38}$$

where Q_j is assumed to perform overtone process.

When one pair of degenerate normal vibrations are

concerned with three phonon scattering, the composite transition of eight sets of combinations are possibly classified into four types of the set; (Q_j^a,Q_j^a,Q_j^a), $3(Q_j^a,Q_j^a,Q_j^b)$, $3(Q_j^a,Q_j^b,Q_j^b)$, and (Q_j^b,Q_j^b,Q_j^b). From Eqs(6.8) and (6.9), $J_{v',v}$ is derived as

$$J_{v+3,v} = \sum_{v=0}^{\infty} (1-x)x^v\cdot(v+1)(v+2)(v+3)(t^2/2)^3\exp(t^2/2) \left[1/6 + vt^2/48 + v(v-1)t^4/960 + \cdots\cdots\right]^2$$
$$= J_{v,v}(t^2/2)^3/6(1-x)^3 \qquad (6.39)$$

Then the transition probability for three phonon process of one pair of degenerate normal vibrations is represented as

$$\left|M_{12}^{\mu}\right|_T^2 = (1/6)\left[\hbar/M_\mu N(1-x_j)\omega_j\right]^3\left[(K_tA_{\mu j})^2+(K_tB_{\mu j})^2\right]^3 \times\exp\left[-2W_\mu(K_t)\right] \qquad (6.40)$$

In the case of three phonon up-scattering, the population factor x_j^3 is multiplied with Eq(6.40).

VI-5 SETTLEMENT OF THE REPRESENTATION

So far the transition probability in one- two- and three-phonon scattering processes has been derived with regard to individual normal coordinate. In the crystal, there are so large number of normal vibrations that several transitions give rise to almost same amount of energy transfer. On the computation of the scattering cross section, it is more convenient to represent the transition probability regarding to the energy transfer. Accordingly, new function $H(K,\omega)$ is defined by

$$H_\mu(K_t,\omega_j)=\sum_{\Delta\omega_j}(\hbar/M_\mu N\omega_j)(1-x_j)^{-1}\left[(K_tA_{\mu j})^2+(K_tB_{\mu j})^2\right] \qquad (6.41)$$

where summation is performed for all the normal coordinates within the frequency division of $\Delta\omega_j$ which could be taken

arbitrarily in accordance with the experimental resolution or the number of points taken up in the first Brillouin zone.

Then the differential cross section of μ-th atom for one phonon transition is represented as

$$d^2\sigma/d\Omega dE = (1/4\pi N)(k_2/k_1)\sum_{\mu} s_\mu H_\mu(K_t,\omega_j)\exp[-2W_\mu(K_t)] \quad (6.42)$$

where $2W_\mu(K_t)$ is Debye-Waller factor, obtained from Eq(6.23), K_t is momentum transfer for the scattering angle θ which is given by

$$|K_t|^2 = |k_1|^2 + |k_2|^2 - 2|k_1|\cdot|k_2|\cos\theta \quad (6.43)$$

and the corresponding energy transfer is

$$E = (|k_1|^2 - |k_2|^2)\hbar^2/2m = \hbar\omega_j \quad (6.44)$$

For two phonon process of down-scattering, the differential cross section of overtone is united with that of summation combination as

$$d^2\sigma/d\Omega dE = (1/4\pi N)(k_2/k_1)\sum_{\mu}\tfrac{1}{2}s_\mu H_\mu(K_t,\omega_j)H_\mu(K_t,\omega_k)\exp[-2W_\mu(K_t)] \quad (6.45)$$

where the energy transfer is

$$E = (|k_1|^2 - |k_2|^2)\hbar^2/2m = (\omega_j+\omega_k)\hbar \quad (6.46)$$

The down scattering cross section for difference combination is represented as

$$d^2\sigma/d\Omega dE = (1/4\pi N)(k_2/k_1)\sum_{\mu} s_\mu (x_j/2)H_\mu(K_t\omega_j)H_\mu(K_t\omega_k)\exp[-2W_\mu(K_t)] \quad (6.47)$$

where ω_k is assumed to be larger than ω_j. The corresponding energy transfer is

$$E = (|k_1|^2 - |k_2|^2)\hbar^2/2m = (\omega_k-\omega_j)\hbar \quad (6.48)$$

On the up-scattering process, the population factor $x_j x_k$ is multiplied with Eq(6.45) as same with Eq(6.35).

The differential cross section for three phonon down-scattering process is a composite of the following three types of energy transfer.

For energy transfer of $E=(\omega_j+\omega_k+\omega_l)\hbar$ (6.49)

$$d^2\sigma/d\Omega dE = (1/4\pi N)(k_2/k_1)(1/3!)\sum_\mu s_\mu H_\mu(K_t\omega_j)H_\mu(K_t\omega_k) \times H_\mu(K_t\omega_l)\exp[-2W_\mu(K_t)] \quad (6.50)$$

For energy transfer of $E=(\omega_j+\omega_k-\omega_l)\hbar$ (6.51)

$$d^2\sigma/d\Omega dE = (1/4\pi N)(k_2/k_1)\sum_\mu s_\mu(x_l/3!)H_\mu(K_t\omega_j)H_\mu(K_t\omega_k) \times H_\mu(K_t\omega_l)\exp[-2W_\mu(K_t)] \quad (6.52)$$

For energy transfer of $E=(\omega_j-\omega_k-\omega_l)\hbar$ (6.53)

$$d^2\sigma/d\Omega dE = (1/4\pi N)(k_2/k_1)\sum_\mu s_\mu(x_k x_l/3!)H_\mu(K_t\omega_j)H_\mu(K_t\omega_k) \times H_\mu(K_t\omega_l)\exp[-2W_\mu(K_t)] \quad (6.54)$$

VI-6 DISCUSSIONS

In evaluating multi-phonon scattering cross section, Placzeck[13] has used the expansion about M_μ^{-1} because of its rapid convergence. Since the $H_\mu(K_t,\omega)$ includes factor M_μ^{-1}, the expansion is essentially same with the present treatment, however present expression provides the coefficient of M_μ^{-n} in explicit form.

With the use of time dependent correlation function[5]

$$G_s(r,t) = \left\langle \exp[i\mathbf{K}\mathbf{C}q(t)]\exp[i\mathbf{K}\mathbf{C}q(t)] \right\rangle_T$$

where $\mathbf{C}$ is polarization vector of normal vibration and $q(t)$ is time part of normal coordinate, the differential cross section for energy transfer of E is represented as[4]

$$d^2\sigma/d\Omega dE = \sum_\mu (s_\mu/4\pi N)(k_2/2\pi k_1)\exp[-Z(0)]\int_{-\infty}^{\infty}\exp[-iEt+Z(t)]dt \quad (6.55)$$

where

$$Z(t) = \Sigma_j (\mathbf{K}\mathbf{C}_\mu)^2\hbar(e^{-i\omega_j\hbar t} + x_j e^{i\omega_j\hbar t})/2M_\mu\omega_j(1-x_j) \quad (6.56)$$

Z(0) is Debye-Waller factor which is coincident with Eq(6.23). When $\exp[Z(t)]$ is expanded into power series of Z(t), the first term provides elastic scattering cross section while the second term yields one-phonon scattering cross section. The second power of Z(t) gives rise to the two-phonon scattering and third power of Z(t) contributes to three-phonon scattering cross section. Since Z(t) has time part in the exponential function, thus expanded Eq(6.55) includes Dirac's δ function about energy transfer. If non-vanishing terms of Eq (6.55) with regard to the δ function were picked up, they are exactly coincident with the present result. The equation (6.55) seems apparently simple, however the numerical evaluation is fairly complicated because of the δ function. Accordingly the representation introduced in the section VI-5 is realistic, at least, on the estimation of two- and three-phonon scattering cross section.

In X-ray crystallography as well as neutron diffraction study, Bloch's theorem is generally applied to estimate Eq(6.6), that is,

$$\langle \exp Q \rangle_T = \exp\left\{\tfrac{1}{2}\langle Q^2 \rangle_T\right\} \qquad (6.57)$$

where Q is an arbitrary non-degenerate normal coordinate and $\langle\ \rangle_T$ means the thermal average of the expectation value. Debye-Waller factor was classically introduced from Eq(6.57). Certainly, the thermal average of $I_{n,n}$ from Eq(6.8) is exactly transformed into

$$\sum_{v=0}^{\infty} \sum_{r=0}^{v} (1-x)x^v (t^2/2)^r \exp(t^2/4) v!/(v-r)!\, r!\, r! = \exp\left[t^2(1+x)/2(1-x)\right] \qquad (6.58)$$

and Eq(6.57) is derived. If the elastic scattering intensity were proportional to $I_{n,n}$, the application of Bloch's theorem might simplify the calculation. However, the transition probability is proportional to square of matrix element, and thermal average of $|I_{v,v}|^2$ has to be treated.

On the other hand, when the left side of Eq(6.12) was transformed into simple function such as right side, appropriate approximation was adopted. To examine the correctness of the approximation, the left side was numerically calculated with incorporation of v till 84 at 100°K. Arbitrary polarization vector of hydrogen atom in the acoustic branch of polyethylene crystal was picked up and fixed through the frequency range. The result is shown in Fig. 1 where solid line denotes the exact value of Eq(6.12) and open circles denote the right side of Eq(6.12). Small deviation is found below 15 cm^{-1}. As represented in Eq(6.23), 2W(K) is an integrated quantity of all vibrations and the number of vibrations below 15 cm^{-1} is much less compared with the total number of crystal vibrations. Accordingly the approximation incorporated at Eq (6.12) may be admitted. Since the experiment[16] on polyethylene crystal has been carried out with fixed final energy of 30 meV of neutron, the same type of calculation was carried out for the optical branches with varying temperature and initial energy and is summarized in Table 1. As temperature is raised, the approximation becomes worse especially for higher initial energy. However, for low initial energy, the right side of Eq(6.12) well reproduces the exact value.

On deriving the transition probability, a proper approximation was incorporated between Eqs(6.20a) and (6.20b). The calculated values from Eq(6.20a) are compared with those from Eq(6.20b) in Fig. 2, where solid line denotes Eq(6.20a) and open circles denote Eq(6.20b). On the exact calculation of Eq(6.20a), v was incorporated till 84, where the experimental conditions of k_2=30 meV, θ=90° and the polarization vector of hydrogen atom in the acoustic branch of polyethylene crystal were used. On account of the approximation, the inelastic scattering cross section is estimated to be relatively small below 18 cm^{-1}. It results from the fact that, for low frequency motion, F defined by Eq(6.7) becomes so large that higher terms in power series of Eq(6.20a) influence the results. On the other hand, the experimental resolution is not sufficient for separating the inelastic scattering of such small energy transfer as E=20 cm^{-1} from the elastic scattering. Generally this region is treated as the quasi-elastic scattering for which the incorporation of proper analytical functions[1] might be suitable. The same type of examination was carried out on optical branches. The result is shown in Table 2, which suggests that the approximation is sufficient for optical branches.

Accordingly, the present formulation is justified unless very small energy transfer becomes the subject of discussion.

SUMMARY

Incoherent scattering cross section of neutrons was treated on the basis of transition probability. Thus derived result is coincident with those derived previously from time dependent correlation function.

From the atomic displacement due to crystal vibrations of polyethylene, Debye- Waller factor was derived as function of momentum transfer. The approximation, included in the present derivation, was examined numerically and confirmed to be allowable.

To calculate the transition probability for arbitrary energy transfer, new function $H(K,\omega)$ was defined, with which one- two- and three-phonon scattering cross sections were represented in convenient form to computation.

REFERENCES

1) R.A.Egelstaff ed. "Thermal Neutron Scattering" Academic Press, New York (1965).

2) R.Weinstock, Phys. Rev., 65, 1 (1944).

3) L.S.Kothari and K.S.Singwi, Solid State Phys., 8, 109 (1959).

4) A.C.Zemach and R.J.Glauber, Phys. Rev., 101, 118 (1956)

5) L.Van Hove, Phys. Rev., 95, 249 (1954).

6) E.B.Wilson, J.C. Decius , and P.C.Cross, "Molecular Vibrations" McGraw-Hill, New York (1955).

7) T.Shimanouchi, Pure Appl. Chem. 7, 261 (1962).

8) In (2.13) the atomic displacement vector of atoms in ρ-th unit cell is represented as X_ρ. u_μ is a subvector of X_ρ. The elements of $\widetilde{U}(\rho,\delta)L_S(\delta)$ and $\widetilde{\bar{U}}(\rho,\delta)L_S(\delta)$ from Eq (2.13) correspond to $L^a_{\mu 1}(\delta)$ and $L^b_{\mu 1}(\delta)$ of Eq(6.1), resp. In this expression, Q^a and Q^b are treated as scalar and therefore, $L^a_{\mu 1}(\delta)$ and $L^b_{\mu 1}(\delta)$ are three component vector.

10) E.Fermi, Ricerca Sci., 7, 13 (1936).

11) G.Breit, Phys. Rev., 71, 215 (1947).

12) C.G.Shull and E.O.Wollan, Solid State Phys., 2, 138 (1956)

13) G.Placzek, Phys. Rev., 86, 377 (1952).

14) P.Debye, Ann. d. Physik, 43, 49 (1914).

15) I.Waller, Z. f. Physik, 17, 398 (1923); 51, 213 (1928)

16) W.Myers, G.C.Summerfield and J.S.King, J. Chem. Phys., 44, 184 (1966).

Table 1. Comparisons of the approximate values of Eq(6.12) with exact values.

k_1=30meV (λ=1.65Å)		T=100°K		T=298°K	
mode	ν(cm^{-1})	left	right	left	right
rot.	146.4	0.936	0.935	0.861	0.857
trans.(⊥)	91.4	0.973	0.973	0.912	0.910
trans.(//)	54.3	0.918	0.916	0.791	0.779

k_1=104meV (λ=0.88Å)		T=100°K		T=298°K	
mode	ν(cm^{-1})	left	right	left	right
rot.	146.4	0.863	0.861	0.727	0.708
trans.(⊥)	91.4	0.942	0.941	0.818	0.810
trans.(//)	54.3	0.829	0.822	0.617	0.572

Table 2. The examination of Eq(6.20b)

		T=100°K		T=298°K	
mode	ν(cm^{-1})	(6.20a)	(6.20b)	(6.20a)	(6.20b)
rot.	146.4	0.0556	0.0556	0.0886	0.0884
trans.(⊥)	91.4	0.0229	0.0229	0.0521	0.0520
trans.(//)	54.3	0.0549	0.0549	0.1106	0.1098

Final energy is set to be 30meV.

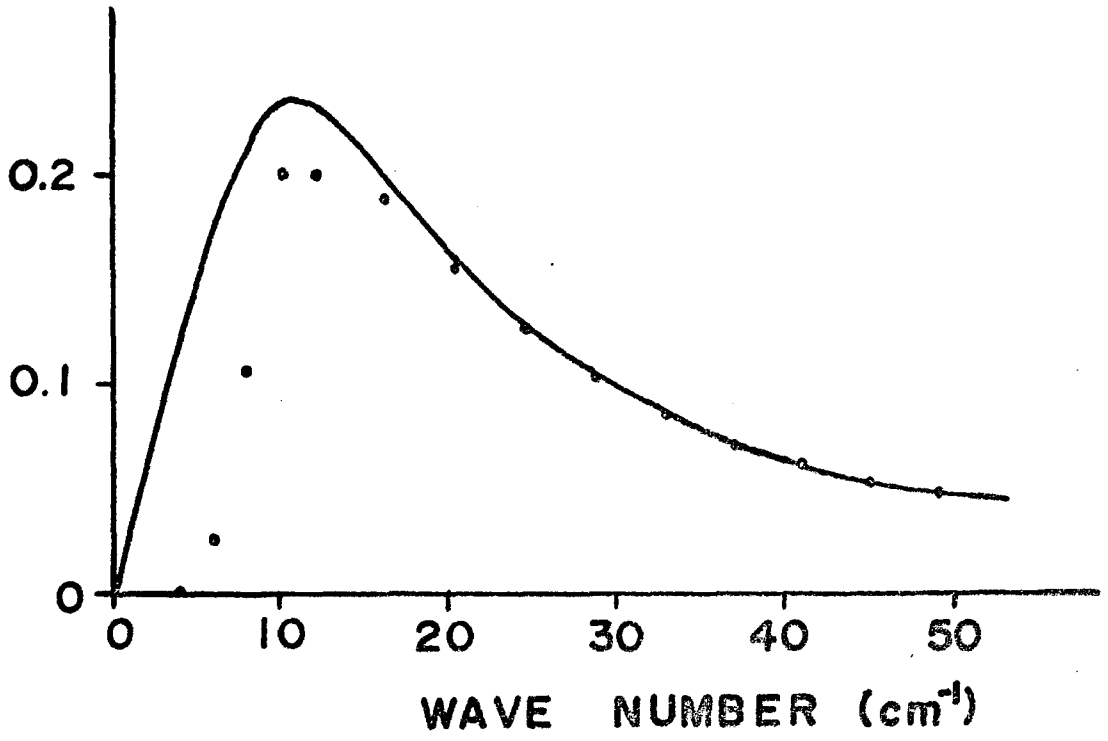

Fig. 1 Comparison of the approximate value of Eq(6.12) with exact value. Solid line represents the left side and open circles represent the right side of Eq(6.12).

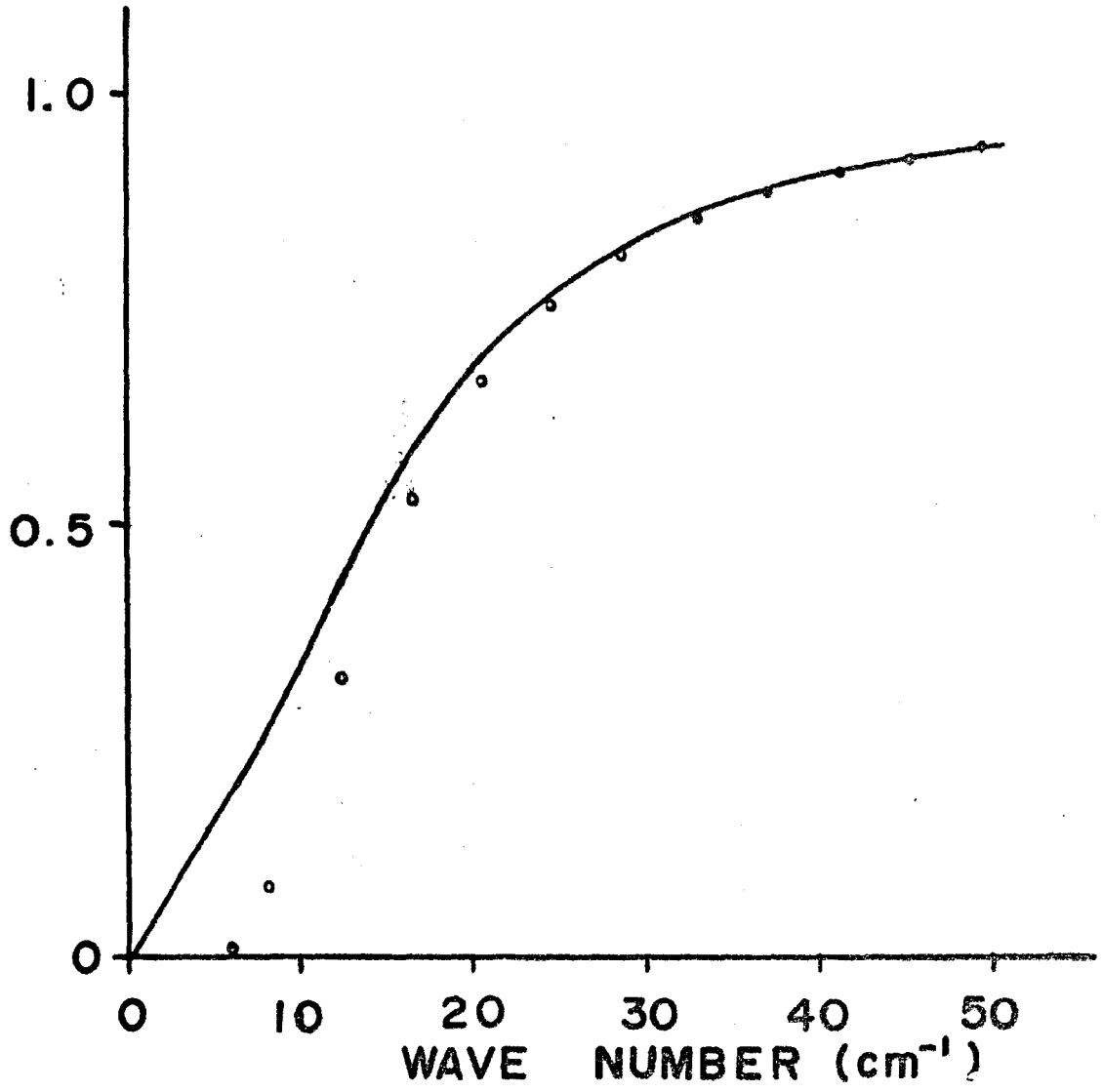

Fig. 2 Comparison of numerical results from Eq.(6.20b) with that of Eq(6.20a). Solid line represents Eq(6.20a) and open circles represent Eq(6.20b).

Appendix II

Proof for

$$\langle \phi_{v+\lambda} \exp(iFQ) \phi_v \rangle = \left[\frac{1}{(v+\lambda)!\, v!}\right]^{\frac{1}{2}} \sum_{r=0}^{v} \frac{(v+\lambda)!\, v!}{(v-r)!\, (\lambda+r)!\, r!} \left(\frac{t^2}{2}\right)^{r+\lambda/2} \exp\left(+\frac{t^2}{4}\right)$$

$\phi_v(Q)$; wave function of normal coordinate, Q, at quantum state, v.

$\gamma = (\omega/\hbar)$, ω; angular frequency of normal coordinate.

Since the wave function of normal coordinate is represented with Hermite polynomial of $z=\gamma^{\frac{1}{2}}Q$, [1] the integral is written as

$$I_{v+\lambda,v} = \int_{-\infty}^{\infty} \phi_{v+\lambda}(Q) \exp(iFQ) \phi_v(Q) dQ \qquad (A\text{-}1)$$

$$= \left(\frac{1}{\pi \cdot 2^{v+\lambda}(v+\lambda)!\, 2^v v!}\right)^{\frac{1}{2}} \int_{-\infty}^{\infty} \exp(-z^2) H_{v+\lambda}(z) H_v(z) \exp(i\gamma^{-\frac{1}{2}}Fz) dz$$

$$= \left(\frac{1}{\pi \cdot 2^{v+\lambda}(v+\lambda)!\, 2^v v!}\right)^{\frac{1}{2}} \int_{-\infty}^{\infty} \exp(-z^2+tz) H_{v+\lambda}(z) H_v(z) dz \qquad (A\text{-}2)$$

where $t=i\gamma^{-\frac{1}{2}}F$. With new variable, y, defined by (A-3),

$$y = z-(t/2) \qquad (A\text{-}3)$$

the exponential part of (A-2) is written as

$$\exp(-z^2+tz) = \exp(-y^2+t^2/4) \qquad (A\text{-}4)$$

and the integral of (A-2) becomes

$$\exp(+t^2/4) \int_{-\infty}^{\infty} \exp(-y^2) H_{v+\lambda}(y+t/2) H_v(y+t/2) dy \qquad (A\text{-}5)$$

With the use of the generating function of Hermite polynomial, [2] the Hermite polynomial of order v is a coefficient of v-th power of variable x.

$$\exp\left[-x^2+2x(y+t/2)\right] = \sum_{v=0} H_v(y+t/2) x^v/v! \qquad (A\text{-}6)$$

After development of left side of (A-6) into power series of x, putting the coefficient of v-th power of x to be equal to right side yields

$$H_v(y+t/2) = \sum_{r=0}^{\infty} H_{v-r}(y) t^r v!/(v-r)!\, r! \qquad (A\text{-}7)$$

Substituting of $H_v(y+t/2)$ and $H_{v+\lambda}(y+t/2)$ from (A-7) into (A-5) lead us to

$$\exp(+t^2/4)\sum_{s=0}^{v+\lambda}\sum_{r=0}^{v}\frac{(v+\lambda)!\,v!}{(v+\lambda-s)!\,s!\,(v-r)!\,r!}t^{s+r}\int_{-\infty}^{\infty}e^{-y^2}H_{v+\lambda-s}(y)H_{v-r}(y)dy \qquad (A-8)$$

Orthogonality of Hermite polynomials of (A-9),

$$\int_{-\infty}^{\infty}\exp(-y^2)H_n(y)H_m(y)dy = 2^n n!\,\pi^{\frac{1}{2}}\delta_{n,m} \qquad (A-9)$$

simplifies (A-8) into (A-10)

$$\sum_{r=0}^{v}\frac{(v+\lambda)!\,v!}{(v-r)!\,(r+\lambda)!\,r!}\exp(+t^2/4)t^{2r+\lambda}2^{v-r}\pi^{\frac{1}{2}} \qquad (A-10)$$

Substituting (A-10) for the integral part of (A-2) lead us to the final equation and the proof is completed.

$$I_{v+\lambda,v}=\left[\frac{1}{(v+\lambda)!\,v!}\right]^{\frac{1}{2}}\sum_{r=0}^{v}\frac{(v+\lambda)!\,v!}{(v-r)!\,(\lambda+r)!\,r!}\left(\frac{t^2}{2}\right)^{r+\lambda/2}\exp(t^2/4) \qquad (A-11)$$

1) E.B.Wilson, Jr, J.C.Decius and P.C.Cross, "Molecular vibrations" McGRAW-HILL, New York (1955).

2) H.Margenau and G.M.Murphy, "The mathematics of physics and chemistry" D. VAN NOSTRAND COMPANY (1943).

CHAPTER VII

NEUTRON SCATTERING BY CRYSTAL VIBRATIONS OF POLYETHYLENE

VII-1 INTRODUCTION

Since high density flux of thermal neutrons became available, great interest has been taken in the observation of frequency spectrum of polymer crystals.[1] Especially on polyethylene, many experimental results have been accumulated up to date, which is summarized firstly.

Danner et al.[2] have measured time of flight of neutrons and obtained the frequency spectrum of normal hydrocarbon crystals as well as polyethylene by the use of up-scattering of cold neutron. King et al.[3] have applied down-scattering technique of warm neutrons to the same sample of polyethylene with Danners'[2]. The frequency distribution, obtained from two different types of experiments, were like each other. Two prominent peaks near 550 cm^{-1} and 200 cm^{-1}, which had been expected from the normal coordinate treatment of polyethylene single chain[4], were assigned to the cut-off of the skeletal bending and internal rotation branch, respectively. Besides these two peaks, there were several weak peaks, which were assigned to lattice vibrations with reference to the calculated frequency distribution of polyethylene crystal.[5]

Summerfield[6] has pointed out that the peak intensity of the neutron spectrum depends upon the amplitude weighted frequency distribution and thereby, Myers[7] has measured the

anisotropy of scattering cross section on the stretch oriented polyethylene sample by the use of triple axis crystal spectrometer. When momentum transfer vector of neutron is parallel to the chain axis (parallel case), two peaks were recognized near 190cm^{-1} and 525 cm^{-1}. When the momentum transfer vector is perpendicular to the chain axis (perpendicular case), the additional peak was found near 150 cm^{-1} while the peak at 525 cm^{-1} was not found. The peak intensity of 190 cm^{-1} of parallel case was almost one half of that of perpendicular case. Trevino[8] has also measured the anisotropy of the scattering cross section independently by the use of time of flight spectrometer, and confirmed the result previously obtained by Myers. The observed anisotropy were qualitatively in good agreement with theoretical expectations[5]. However, the quantitative discussions were postponed to future study and two peaks at 240 and 340 cm^{-1} as well as the shoulder at 380 cm^{-1} were left unassigned because existence of these peaks was not deduced straightforwardly from the frequency distribution of the crystal vibrations.

On the other hand, the intrachain potential[4,9] and interchain potential[10-11] of the polyethylene crystal has been studied in detail and general method of treating the chain vibrations[12-13] and crystal vibrations[14] has been established. A practical method of calculating the incoherent scattering cross section of neutron from hydrogen atom by crystal vibrations has been developed in the preceding chapter. It is now practical to analyse the observed neutron spectrum on the basis of the theoretical treatment

of the crystal vibrations. And also thorough calculation about the polyethylene crystal not only provides the assignment of the observed neutron spectrum of polyethylene but also will serve the analysis of other experimental results with regard to estimation of the relative intensity of the multiphonon scattering and its anisotropy.

Accordingly, in the present study, the differential cross sections for one-, two-, and three-phonon scattering were computed with the method described in the preceding chapter. The calculation was carried out on two cases in which the momentum transfer vector is parallel and also perpendicular to the chain axis.

VII-2 RESULTS

A) DOWN-SCATTERING

On the measurement of anisotropy of scattering cross section, Myers[7] has applied down-scattering technique to the uniaxially oriented polyethylene kept at 100°K, where final neutron energy was fixed at 30 meV and scattering angle was set to be 90°. Since the scattering from hydrogen atom is predominant in polyethylene crystal, the differential cross sections of two types of hydrogen atoms (H_1 and H_2 in Fig. 1 of Chapter II) were calculated.

When momentum transfer vector is parallel to the chain axis (parallel to the z axis), z component of A_j and B_j contributes to the scattering. The function $H(K_t,\omega)$ defined by (6.41) for parallel case is represented as

$$H''(K_t,\omega)=\sum_{\Delta\omega_j}(\hbar/NM\omega_j)(1-x_j)^{-1}|K_t|^2(A_{jz}^2+B_{jz}^2) \quad (7.1)$$

$$2W''(K_t) = \sum_i (\hbar/MN\omega_i)\,|K_t|^2(A_{iz}^2 + B_{iz}^2)(1+x_i)/(1-x_i) \qquad (7.2)$$

where N is total number of unit cell in the crystal, M is mass of hydrogen atom, ω_j is the angular frequency of j-th normal coordinate and $x_j=\exp(-\hbar\omega_j/kT)$. On the calculation of one- and two-phonon scattering cross section, $\Delta\omega_j$ was taken to be 1 cm^{-1} while on the three-phonon scattering cross section, $\Delta\omega_j$ was taken to be 5 cm^{-1} to shorten the computation time. Summation about i runs over all branches on N/2 points in the unit cell of reciprocal lattice. D_{2h} symmetry of polyethylene crystal reduces the independent sets of phase differences to

$$(0,0,0) \leq (\delta_a,\delta_b,\delta_c) \leq (\pi,\pi,\pi).$$

Since the sample material is uniaxially oriented along the chain axis, random configuration of micro crystals around the chain axis has to be averaged. Supposing the direction of momentum transfer vector is along β from x axis, fixed in the micro crystal, then

$$(KA)^2 = |K|^2(A_x^2\cos^2\beta + A_y^2\sin^2\beta + 2A_xA_y\sin\beta\cos\beta)$$

and the average of random distribution of β leads us to

$$(KA)^2 = |K|^2(A_x^2+A_y^2)/2 \qquad (7.3)$$

where A_x and A_y are x and y component of polarization vector, respectively. Then, $H(K_t,\omega)$ corresponding to perpendicular case is represented as

$$H^{\perp}(K_t,\omega_j) = \sum_{\Delta\omega_j} \tfrac{1}{2}(\hbar/MN\omega_j)(1-x_j)^{-1}|K_t|^2(A_{jx}^2+A_{jy}^2+B_{jx}^2+B_{jy}^2) \qquad (7.4)$$

$$2W^{\perp}(K_t) = \sum_i (\hbar/2MN\omega_i)\,|K_t|^2(A_{ix}^2+A_{iy}^2+B_{ix}^2+B_{iy}^2)(1+x_i)/(1-x_i) \qquad (7.5)$$

A_i, B_i and ω_i were calculated for number of representative points of δ space, and also the interpolation of A_i, B_i and ω_i were performed with the use of equation (1.15) at the interval of 1° of δ_c. Since the scattering angle is fixed at 90°, the momentum transfer is given by

$$|K_t|^2 = 2k_2^2 + 2mc\nu/h \qquad (7.6)$$

where m is neutron mass, c is light velocity and ν is wave number corresponding to the energy transfer. In this experiment, final energy is fixed at 30meV.

The calculated Debye-Waller factor for above experimental condition is shown in Fig. 1, where $\exp[-2W(K_t)]$ is plotted against the energy transfer. The solid line represents parallel case while broken line denotes perpendicular case. The contribution from intrachain vibrations is also included. As energy transfer gets larger, $2W(K_t)$ becomes larger and therefore, the transition corresponding to higher energy transfer is suppressed in proportion to $\exp[-2W(K_t)]$. Experimentalists usually assume $\exp[-2W(K_t)]$ to be equal to unity on the analysis of neutron spectrum. However, this assumption is misleading the relative intensity. As $2W(K_t)$ is nearly proportional to temperature, scattering intensity becomes smaller as temperature is raised. It is, in fact, confirmed in the recent experiment.[15)]

Eq(6.15) states that the peak intensity of elastic scattering depends primarily upon Debye-Waller factor. Accordingly, $2W(K_t)$ and $\exp[-2W(K_t)]$ for the elastic scattering are shown in Table 1, where 'interchain' and 'intrachain' mean the contribution of the crystal vibrations below 700 cm^{-1} and

of chain vibrations above 700 cm^{-1}, respectively. The contribution from the intrachain vibrations cannot be neglected even at 100°K. The perpendicular component of $2W(K_t)$ due to interchain vibrations is especially large because the frequencies of the acoustic branches whose atomic displacements are perpendicular to the chain axis, are relatively low and the mean squared atomic displacement gets large compared with the acoustic branch along the chain axis. Therefore, the perpendicular component of total value of $2W(K_t)$ is larger than that of parallel component. In fact, the observed peak intensity of elastic scattering is reported to be weaker in perpendicular case than in parallel case[7].

The differential cross sections for one-, two- and three-phonon scattering processes were calculated with the use of Eqs(6.47)-(6.54). The calculated results are shown in Fig. 2. The one-phonon cross section for perpendicular case is so large below 200 cm^{-1} but so small above 200 cm^{-1} that the contribution of two-phonon scattering is recognizable above 200 cm^{-1}. To the contrary, the one-phonon cross section for parallel case is relatively small below 200 cm^{-1} but not so small above 200 cm^{-1}, that the contribution of two-phonon scattering is not remarkable. The three-phonon scattering cross section is recognized above 400 cm^{-1} only for perpendicular case whereas it makes no distinct peak. Accordingly, the three-phonon scattering might appear weakly as a back ground for perpendicular case.

The composite differential cross section is shown in Fig. 3, where histograms of values of $(d^2\sigma/d\Omega dE)$ per

frequency division of 10 cm^{-1} are drawn against the energy transfer and the scale unit of the ordinate is $(s/4\pi)(s;$ bound atom incoherent cross section of hydrogen atom). This figure may correspond to the intensity distribution directly observed from the neutron spectrum.

Since the experimental results are represented as phonon-density defined by

$$G(\omega) = (4\pi N/s\hbar)\omega(1-x)(k_1/k_2)|K_t|^{-2}(d^2\sigma/d\Omega dE) \qquad (7.7)$$

Originally, in the formal representation of $G(\omega)$, Debye-Waller factor was canceled from the cross section. However, on the transformation of the observed cross section to $G(\omega)$, Debye-Waller factor is usually assumed to be unity. Then the real quantity is equivalent to (7.7) and therefore $G(\omega)$ includes Debye-Waller factor. And also $(d^2\sigma/d\Omega dE)$ might include multi-phonon scattering. Accordingly, the resultant phonon density function may not always represent the amplitude weighted frequency distribution.

The calculated $G(\omega)$ is compared with the experimental one in Fig. 4, where solid lines represent parallel case while broken lines represent the perpendicular case. The calculated histograms of the lower figure of Fig. 4 may be compared with the experimental curves as given in Fig. 4 of ref. 7. However, the experimental curves for parallel and perpendicular cases have been tentatively adjusted[7] to provide equal peak heights at 195 cm^{-1}. The true experimental curves may be obtained from the published curves by multiplying the ordinate of the parallel curve by 56%.

These experimental curves, which are reproduced in the upper figure of Fig. 4, may be compared with our calculated results.

The perpendicular peak calculated at 195 cm^{-1} is twice as high as the corresponding parallel peak, and the peak near 560 cm^{-1} is almost completely parallel whereas the peak at 150 cm^{-1} is almost perpendicular, in good agreement with the experimental results. These peaks originates from one-phonon process of the internal rotation, skeletal bending and overall rotatory vibrations around the chain axis, respectively. The weak perpendicular peak calculated at 90 cm^{-1} is recognized as the fine structure of the experimental curve, which is due to optical branches of the translatory vibrations perpendicular to the chain axis.

Two weak perpendicular peaks calculated near 240 and 340 cm^{-1} are associated with the summation combination tones of the antiparallel translatory vibrations ($\sim$90 cm^{-1}) plus the overall rotatory vibrations ($\sim$150 cm^{-1}) and the internal rotation ($\sim$190 cm^{-1}) plus the overall rotatory vibrations around the chain axis ($\sim$150 cm^{-1}), respectively. The perpendicular cut-off calculated at 380 cm^{-1} corresponds to the overtone of the internal rotation branches. The relative intensity and anisotropy of these three peaks, associated with two-phonon scattering, agree closely with the experimental results.

The differential cross section due to the intrachain vibrations were also calculated. As shown in Fig. 5, two prominent parallel peaks are expected at 1080 cm^{-1} and

1320 cm^{-1} while one perpendicular peak is expected at 720cm^{-1}. Because of large $2W(K_t)$ for perpendicular case, the perpendicular cross section is strongly suppressed and therefore no peak seems to exist at 1470 cm^{-1}.

One-, two- and three-phonon scattering cross sections at 298°K were calculated as shown in Fig. 6. As temperature is raised, the scattering intensity through one-phonon process decreases whereas two- and three-phonon scattering increases, especially in their difference combinations. The resultant cross section seems to get larger for small energy transfer but smaller for large energy transfer as shown in Fig. 7. It may be expected that apparent peak width of the elastic scattering becomes broad on account of the increase of inelastic contribution of small energy transfer at higher temperature. Besides it, the peak of inelastic part becomes relatively obscure compared with that of low temperature(Fig.3). This tendency agrees with the recent experimental results[15] in which the measurement has been performed at 4.2°K, 77°K and 300°K with the use of the time of flight down-scattering technique. Previously, King et al.[3] have measured the differential cross section of unoriented polyethylene at 298°K with the same experimental condition with Myers'. The result is reproduced in the upper figure of Fig. 8 for comparison. The average of two calculated histograms of the lower figure of Fig. 8 may be compared with the experimental results.

B) UP-SCATTERING

Since the combination of beryllium crystal for monochromatizing filter plus time of flight analyser utilizes neutron beam most efficiently, many experiments on neutron spectrum have been performed by the use of the time of flight spectrum. Beryllium crystal kept at 77°K has fairly sharp cut-off at 5 meV, therefore the measurement has been carried out about the neutrons accelerated by the crystal vibrations. Trevino[8] has used time of flight method to measure the dichroism of neutron spectrum of polyethylene but the assignment explained there is not always appropriate. To make definite assignment of the observed spectrum, we have calculated the one-, two-, and three-phonon up-scattering cross sections, using the equivalent condition with the experiment, that is T=298°K, θ=90°(scattering angle), k_1=5.2 meV. The calculated Debye-Waller factor is shown in Fig. 8, where $\exp[-2W(K_t)]$ is plotted against the energy transfer. Because of small energy of the incident neutron, the elastic cross section is expected to be relatively large compared with Myers' experiment.

The calculated one-, two-, and three-phonon differential cross sections are shown in Fig. 10 (a), (b) and (c). The composite differential cross section is compared with the experimental results in Fig. 11. The calculated histogram is plotted against the frequency division of 10 cm^{-1} of energy transfer whereas the experimental results is published as time of flight spectrum, in which the division of energy

transfer is based on neutron velocity and is getting larger in proportion to $E_t^{\frac{1}{2}}$. Therefore, apparent intensity of time of flight spectrum seems stronger than the corresponding differential cross section for large energy transfer. The contribution of two-phonon scattering is expected for perpendicular case above 200 cm^{-1} and is, in fact, recognized in the time of flight spectrum.

Phonon density from up-scattering cross section is defined by

$$G(\omega) = (4\pi NM/s\hbar)\omega(1-x)x^{-1}|K_t|^{-2}(k_1/k_2)(d^2\sigma/d\Omega dE) \quad (7.8)$$

From the calculated differential cross section, the phonon density curve was derived and shown in Fig. 12. The average of two histograms may be compared with Fig. 4(b) of ref.2, in good agreement with the experimental results, where the peak height at 550 cm^{-1} is almost one half of the peak height at 200 cm^{-1} and the shoulder due to two-phonon scattering is observed near 250 cm^{-1}.

The composite of one-, two- and three-phonon up-scattering cross sections calculated at 100°K is shown in Fig. 13 and the corresponding phonon density curve is derived in Fig. 14. As temperature is lowered, $\exp[-2W(K_t)]$ becomes larger whereas the population of the phonons at excited level becomes smaller, and therefore the resultant cross section gets smaller. Since the measurement by Danner et al.[2] was carried out on polycrystalline sample, the average of two histograms in Fig. 14 may be compared with Fig. 3(b) of ref. 2. Two peaks calculated at 150 cm^{-1} (over-

all rotatory vibrations) and at 195 cm^{-1}(internal rotation) are, in fact, resolved in the experimental curve. The contribution of two-phonon scattering is expected to be centered at 300 cm^{-1} while pretty definite peak is recognized in the experimental results. The calculated peak intensity at 560 cm^{-1} is weaker than that of 190 cm^{-1} whereas the intensity ratio of observed peaks is the opposite.

On the other hand, Trevino et al[16] have attempted to obtain the frequency spectrum of intrachain vibrations of polyethylene and measured the anisotropy of the cross section for large energy transfer (k_1; 234 meV). They have found one peak at 760 cm^{-1} for perpendicular case while two peaks at 1080 cm^{-1} and 1320 cm^{-1} for parallel case. For comparison, the amplitude weighted frequency distribution was calculated and shown in Fig. 15, where solid line is associated with the parallel component of the mean squared atomic displacement, and broken line is for perpendicular components. The perpendicular peak calculated at 720 cm^{-1} is due to methylene rocking vibration, while two parallel peaks calculated at 1080 and 1320 cm^{-1} are associated with methylene twisting vibrations. These three peaks are in close agreement with the experimental results.[16] The perpendicular peak expected at 1470 cm^{-1} is due to methylene scissoring vibration which is not recognized in the experimental results.

VII-3 DISCUSSIONS

Experimental estimation of Debye-Waller factor includes some ambiguities because the observed cross section of the

elastic scattering is not apparently separated from that of the inelastic scattering. Summerfield et al.[17] have evaluated the elastic scattering cross section by subtracting the extrapolated inelastic cross section from the apparent elastic cross section and obtained $2W''=0.024\,|K|^2$ and $2W^{\perp}=0.027\,|K|^2$ at 77°K. Myers[15] has estimated $2W''=0.0153\,|K|^2$ and $2W^{\perp}=0.021\,|K|^2$ at 77°K with the same extrapolation method. From the present treatment, they are calculated as $2W''=0.021\,|K|^2$ and $2W^{\perp}=0.034\,|K|^2$ at 100°K which might be within the limit of the uncertainty of the experimental values. The ratio of $2W''/2W^{\perp}$ of the calculated value is 0.61 while the experimental value is 0.73 from Myers' and 0.89 from Summerfield's. Since the crystallinity of the sample used is 80~90% and besides the orientation of the chain axis by stretching is not complete, it is reasonable that the calculated anisotropy is a little larger than the observed values.

The weak peaks observed at 240 and 340 cm^{-1}, which were not expected from the frequency distribution of crystal vibrations of polyethylene, were considered as due to the disordered part such as 3-5 methylene groups of planar zigzag structure between two gauche linkages.[2] Recently Safford has given again the same explanation to these peaks.[1] To investigate it experimentally, Boutin et al.[18] have measured the inelastic cross section of the single crystal grown from solution. It became confident that these two peaks are associated with crystal part of polyethylene. Then, Trevino[8] has assigned the peak at 240 cm^{-1} to one of

two cut-off frequencies of the split branches of the internal rotation vibrations. On the other hand, from the dispersion curves shown in Chapter IV, the splitting may be expected certainly in the dispersion curves along $(0,0,\delta_c)$ whereas no splitting is found in the dispersion curves along (π,π,δ_c). The magnitude of the splitting varies continuously with δ_a and δ_b, therefore only one peak, in the frequency distribution, is expected as the cut-off of the internal rotation branches. The peak width may depend upon the magnitude of the splitting.

The relative intensity and anisotropy of the two peaks, calculated from the present study, are in good agreement with the experimental results. Therefore these peaks are reasonably assigned to the multi-phonon scattering.[19] Recently the identical assignment was proposed by Summerfield, who made the amplitude weighted frequency distribution taking simply 200 points on the dispersion curve along $(0,0,\delta_c)$[17]. Because of the limited number of vibrations incorporated, the relative intensity of the frequency distribution may include somewhat uncertainties. For instance, the anti-parallel translatory vibration along the chain axis does not make definite peak from the dispersion curve of $(0,0,\delta_c)$ while the peak is expected at 50 cm^{-1} from the dispersion curves along δ_a and δ_b. The perpendicular peak near 50 cm^{-1} in the scattering cross section (Fig. 3) results from the acoustic branches whose atomic displacements are perpendicular to the chain axis. These peaks are expected from the dispersion curves along $(\pi,\delta_b,0)$ and $(\delta_a,\pi,0)$. Two overall rotatory

vibrations around the chain axis splits into 147 and 122 cm^{-1} at (0,0,0) whereas they are degenerate on $(\pi,\delta_b,0)$ and $(\delta_a,\pi,0)$. Since the derivative of the vibrational frequency with regard to phase difference $(\partial\nu/\partial\delta)$ approaches to zero near zone boundaries, the dispersion curves along the edge of the first Brillouin zone is most significant to estimate the peak intensity of the frequency distribution.

Chang and Summerfield[20] have measured the multi-phonon scattering cross section with high energy incident neutrons (191 meV). The contribution of multi-phonon process to the inelastic scattering is fairly large at higher temperature, which may be probable, because $H(K_t,\omega)$ becomes larger in proportion to $|K_t|^2$ and higher terms of power series of $H(K_t,\omega)$ contribute to the cross section. In such a situation, the approximation incorporated in Eqs(6.12) and (6.20) becomes poor and then the present type of calculation would not be advantageous to analyze the the inelastic cross section.

Safford et al.[21] have measured the neutron spectrum with higher resolution and found peaks at 550, 200, 167, 147, 114, 67 and 39 cm^{-1}. In addition to them, ten weak peaks were found at 620, 445, 360, 330, 310, 285, 255, 230, 140 and 95 cm^{-1}, which were left unexplained. Unfortunately the number of points, taken in the first Brillouin zone in the present study, is not enough to decompose the broad peaks of the calculated phonon density curve into their component peaks. However, the existence of these weak peaks are not always confident, since Myers et al[15] could not find them even in the careful experiment with the use of time of flight

plus down-scattering technique at 4.2°K.

There is a discrepancy among the reported frequencies about the peak position of the neutron spectrum. Danner et al.[2] observed five peaks at 570, 340, 200, 130 and 60 cm^{-1} at 100°K. Although King et al.[3] used the identical sample, the reported frequencies are slightly different as 500, 340, 275, 200, 160, 95, 66 and 50 cm^{-1}. Myers et al.[7] have reported in their first paper the peaks at 550(//), 195(⊥, //) and 150(⊥) about stretch oriented polyethylene. Boutin et al.[18] has obtained six peaks, from the analysis of single crystal of polyethylene, at 500, 300, 200, 120, 80 and 40 cm^{-1} while Trevino[8] has found two peaks at 530(//) and 250(⊥) cm^{-1} about the oriented polyethylene. Myers[15] has performed the measurement at 300°K, 77°K and 4.2°K. The observed frequencies at 77°K are 524*, 201*, 186, 161, 133, 119*, 97*, 79 and 45* cm^{-1} for the parallel case and 387, 340, 197*, 165, 125*, 97*, 73, 52* and 32 cm^{-1} for the perpendicular case, where the mark * indicates the frequency of fairly definite peak. These frequencies are not always coincident with those reported by Safford[21]. Accordingly, the comparison between the calculated and observed spectram with regard to details is meaningless till the definite frequency of the neutron spectrum will be provided.

Myers[15] has discussed, from the experimental results from neutron spectrum, that the cut-off of the skeletal bending branch is not higher than 536 cm^{-1}. However, Schaufele[22] has, in fact, found Raman lines due to accordion vibration of $C_{94}H_{190}$ at 536 and 556 cm^{-1} in the laser excited

Raman spectrum. It suggests that the cut-off of the skeletal bending branch lies above 550 cm^{-1} and therefore supports the present calculated results.

Since the bound atom incoherent cross section of carbon atom (C^{12};0.01, C^{13};1.0 barn) is much smaller than that of hydrogen atom (80 barn), the scattering from carbon atom is not recognized except for the case in which the peak intensity of amplitude weighted frequency distribution of hydrogen is extremely weak whereas that of carbon is fairly strong. As the amplitude weighted frequency distirbution of carbon given in the following chapter, is similar to that of hydrogen atom, any peak due to carbon atom would not be expected in the neutron scattering of polyethylene.

Lynch[17] has obtained the frequency spectrum of deuterated polyethylene. Two prominent peaks are found at 165 cm^{-1} and 105 cm^{-1}. From the dispersion curves given in Appendix, the peak due to internal rotation branch is expected near 160 cm^{-1} from the curves along $(0,\delta_b,\pi)$ or $(\delta_a,0,\pi)$ and the peak due to the overall rotatory modes is expected near 105 cm^{-1} from the curves along $(\delta_a,\pi,0)$ and $(\pi,\delta_b,0)$, in good agreement with the observed results. The broad peak observed at 270 cm^{-1} might be combination-tone of the internal rotation (165 cm^{-1}) and the overall rotational modes (105 cm^{-1}). The cut-off of the skeletal bending mode is expected at 500 cm^{-1} while the experimental phonon density curve is available only below 440 cm^{-1}. The weak shoulder observed at 70 cm^{-1} might be associated with the translatory vibrations perpen-

dicular to the chain axis.

Recently, King et al.[23] has observed the dispersion curve itself along $(0,0,\delta_c)$ from the analysis of coherent scattering of neutron from deuterated polyethylene. The maximum frequency of bending branch lies relatively low compared with the calculated dispersion curves.

SUMMARY

Neutron scattering of polyethylene crystal was treated theoretically. Debye-Waller factor for elastic scattering was calculated as $2W^{//}=0.021\,|K|^2$ and $2W^{\perp}=0.034\,|K|^2$ at $100^{\circ}K$, which are in reasonable agreement with experimental values.

The differential cross sections for one-, two- and three-phonon down-scattering processes were calculated with the method developed in the preceding chapter. In the calculated phonon density, several prominant peaks at 560(//), 195($\perp$,//), 145($\perp$), 90($\perp$) and weak shoulder at 50($\perp$,//) cm^{-1} are expected, in good agreement with the experimental results. They are due to the skeletal bending, the internal rotation, the rotatory modes around the chain axis, antiparallel translatory vibrations perpendicular to the chain axis and that parallel to the chain axis, respectively.

Three broad peaks, observed at 240, 340, and 380 cm^{-1}, were shown to be associated with two-phonon scattering. Accordingly all the observed peaks were reasonably assigned.

The cross section for up-scattering process was also calculated and phonon density curves were derived at $100^{\circ}K$ and $298^{\circ}K$. The calculated results are in good agreement

with the observed results.

Peak position expected from the dispersion curves of deuterated polyethylene agreed with the recent experimental results.

REFERENCES

1) G.J.Safford and A.W.Naumann, Adv. Polymer Sci., 5, 1 (1967).

S.Trevino and H.Boutin, J. Macromol. Sci., A1, 723 (1967).

2) H.R.Danner, G.J.Safford, H.Boutin and M.Berger, J. Chem. Phys., 40, 1417 (1964).

3) J.S.King and J.L.Donovan, Bull. Am. Phys. Soc., II-9, 623 (1964).

W.R.Myers, J.L.Donovan and J.S.King, J. Chem. Phys., 42, 4299 (1965).

4) M.Tasumi, T.Shimanouchi, and T.Miyazawa, J. Mol. Spectry., 9, 261 (1962); 11, 422 (1963).

5) T.Kitagawa and T.Miyazawa, Rept. Progr. Polymer Phys. Japan, 8, 53 (1965).

6) G.C.Summerfield, J. Chem. Phys., 43, 1079 (1965).

7) W.Myers, G.C.Summerfield, and J.S.King, J. Chem. Phys.. 44, 184 (1966).

8) S.F.Trevino, J. Chem. Phys., 45, 757 (1966).

9) J.H.Schachtschneider and R.G.Snyder, Spectrochim. Acta., 19, 117 (1963).

10) M.Tasumi and T.Shimanouchi, J. Chem. Phys., 43, 1245 (1965).

11) T.Kitagawa and T.Miyazawa, Rept. Progr. Polymer Phys., Japan, 11, 219 (1968).

12) P.Higgs, Proc. Roy. Soc.,(London) A220, 472 (1953).

13) T.Miyazawa, J. Chem. Phys., 35, 693 (1961).

14) T.Miyazawa and T.Kitagawa, J. Polymer Sci., B2, 395 (1964).

15) W.R.Myers and P.D.Randolph, J. Chem. Phys., 49, 1043 (1968).

16) W.E.Moore, G.J.Kirouac and S.F.Trevino, private communication.

17) J.E.Lynch,Jr, G.C.Summerfield, L.A.Feldkamp, and J.S.King, J. Chem. Phys., 48, 912 (1968).

18) H.Boutin, H.Prask, S.F.Trevino and H.R.Danner, Inelastic Scattering of Neutrons, Solids, Liquids, Proc. Symp. Vienna, 1964 vol-2, 407 (1965).

19) T.Kitagawa and T.Miyazawa, J. Polymer Sci., B6, 83 (1968).

20) Y.I.Chang and G.C.Summerfield, private communication.

21) G.J.Safford, A.W.Naumann and F.T.Simon, J. Chem. Phys., 45, 3787 (1966).

22) R.F.Schaufele and T.Shimanouchi, J. Chem. Phys., 47, 3605 (1967).

23) L.A.Feldkamp, G.Venkataraman and J.S.King, private communication.

Table 1. Debye-Waller factor of hydrogen atom in polyethylene crystal.

		T=100°K		T=298°K	
		(//)	(⊥)	(//)	(⊥)
2W(K)	intrachain	0.370	0.318	0.373	0.325
2W(K)	interchain	0.243	0.683	0.543	1.726
2W(K)	total	0.612	1.001	0.916	2.051
exp[-2W(K)]		0.54	0.37	0.40	0.13

$K = k_1 - k_2$ and $k_1 = k_2 = 30meV$

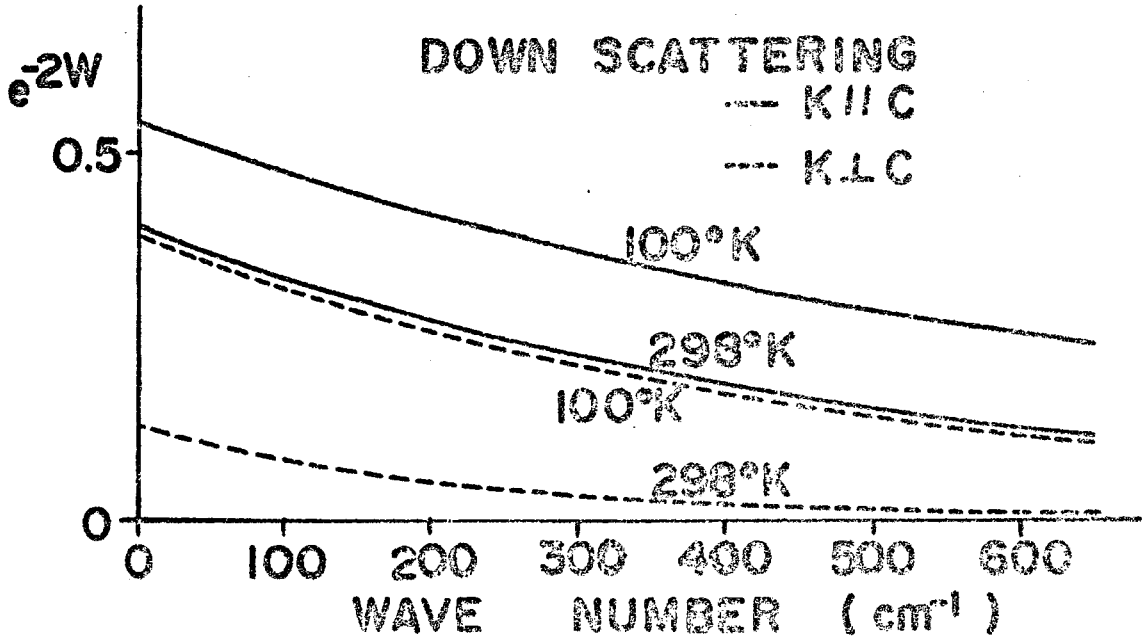

Fig. 1 The calculated Debye-Waller factor, $\exp[-2W(K_t)]$. The final energy is fixed at 30 meV and the scattering angle is set to be 90°.

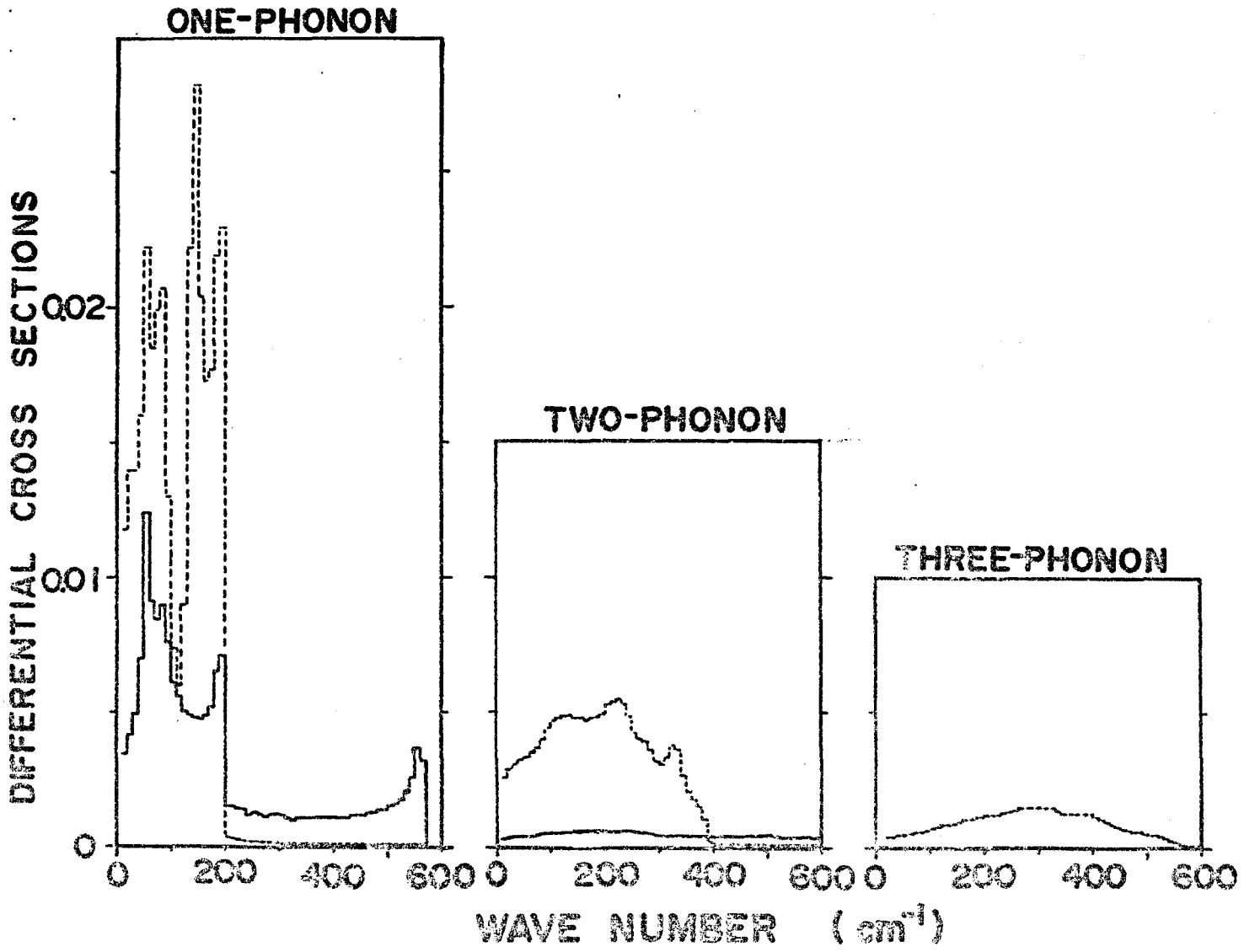

Fig. 2 The calculated differential cross sections for one-, two- and three-phonon scattering on Myers' experimental conditions[7]. $\theta = 90^{\circ}$, $k_2 = 30$ meV, $T = 100^{\circ}K$

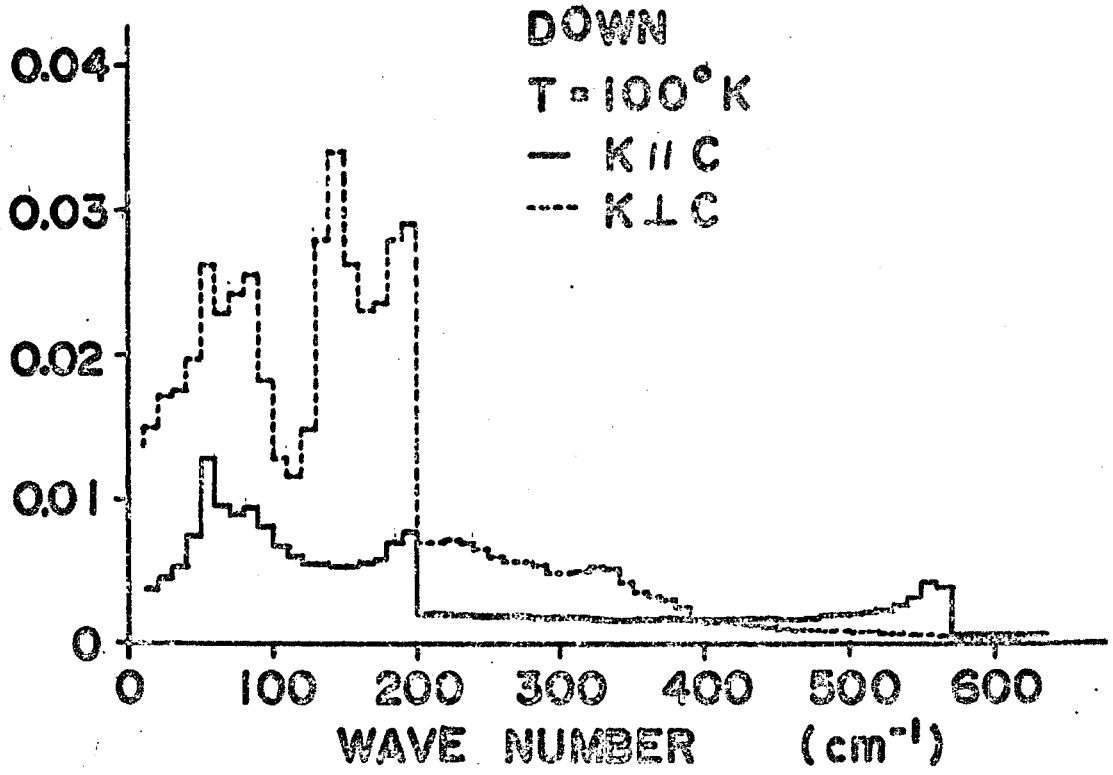

Fig. 3 The composite of the differential cross sections for one-, two-, and three-phonon scattering. The histograms of $d^2\sigma/d\Omega dE$ per frequency division of 10 cm^{-1} are drawn against the energy transfer. The scale unit of ordinate is $(s/4\pi)$.

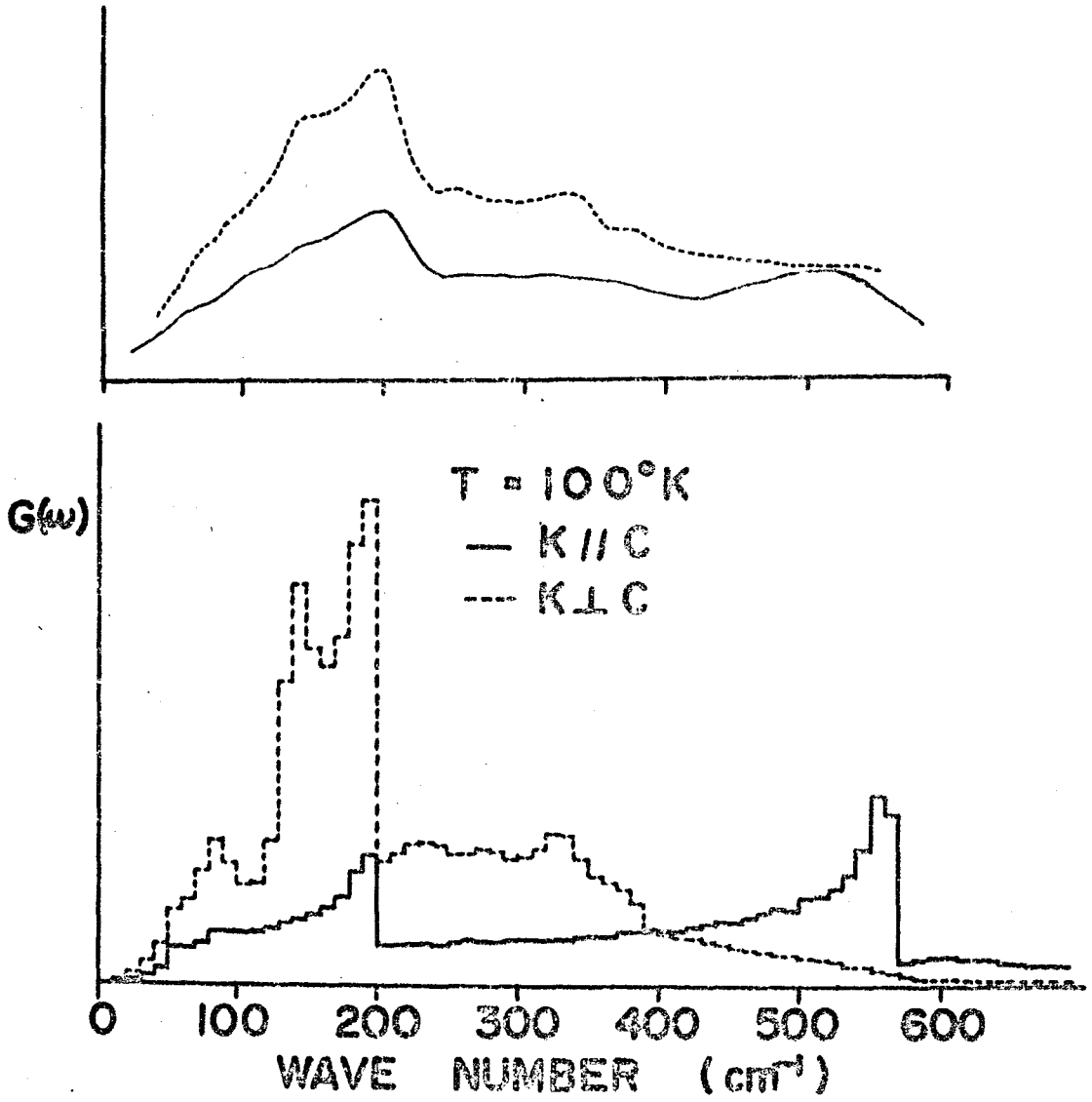

Fig. 4 Comparison between the observed and calculated phonon densities.

the upper figure; the observed result[7] (see text)

the lower figure; the calculated results.

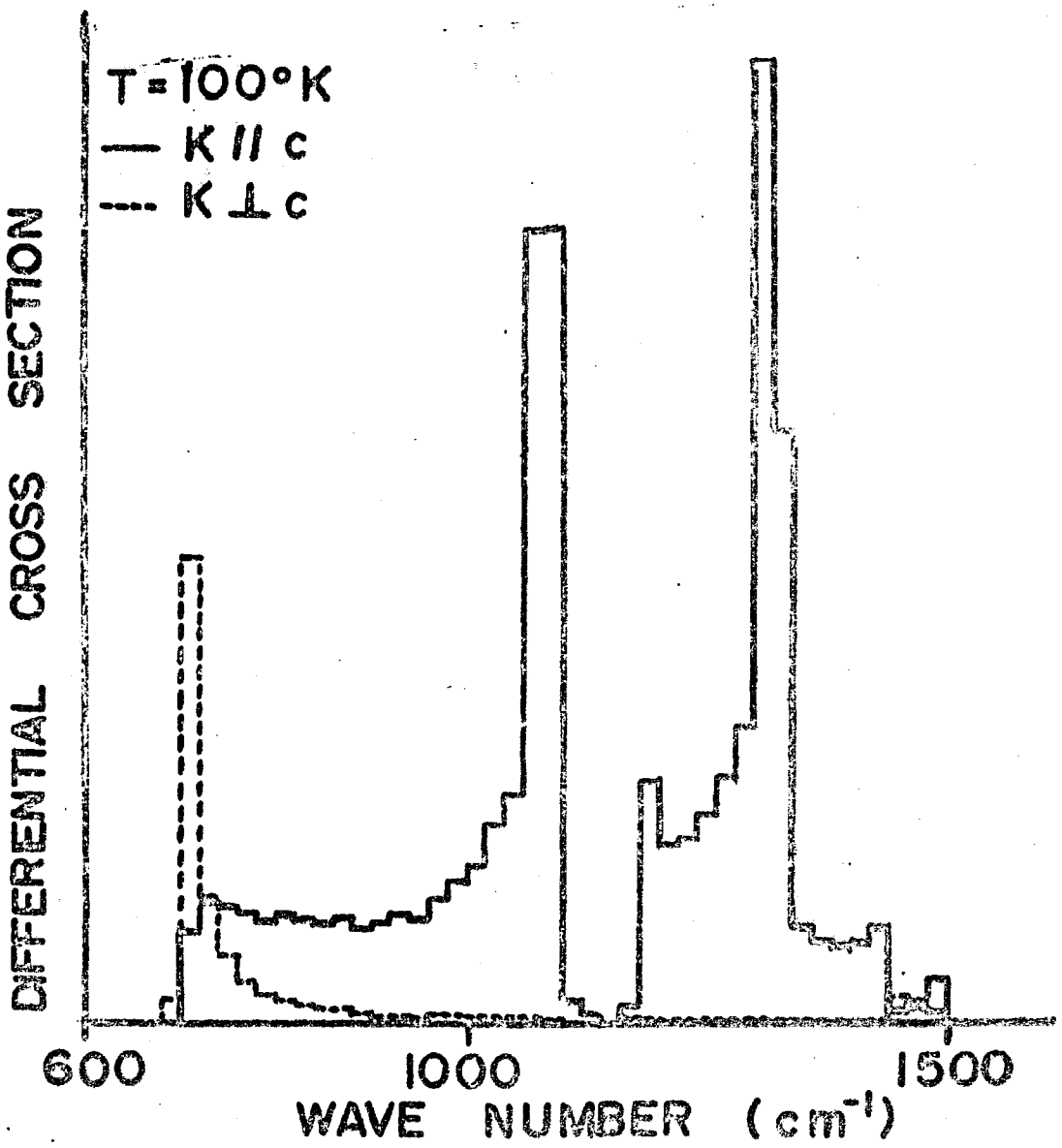

Fig. 5 The calculated differential cross section for intrachain vibrations. $(d^2\sigma/d\Omega dE)$ per frequency division of 20 cm^{-1} on Myers' experimental condition[7] are drawn against energy transfer.

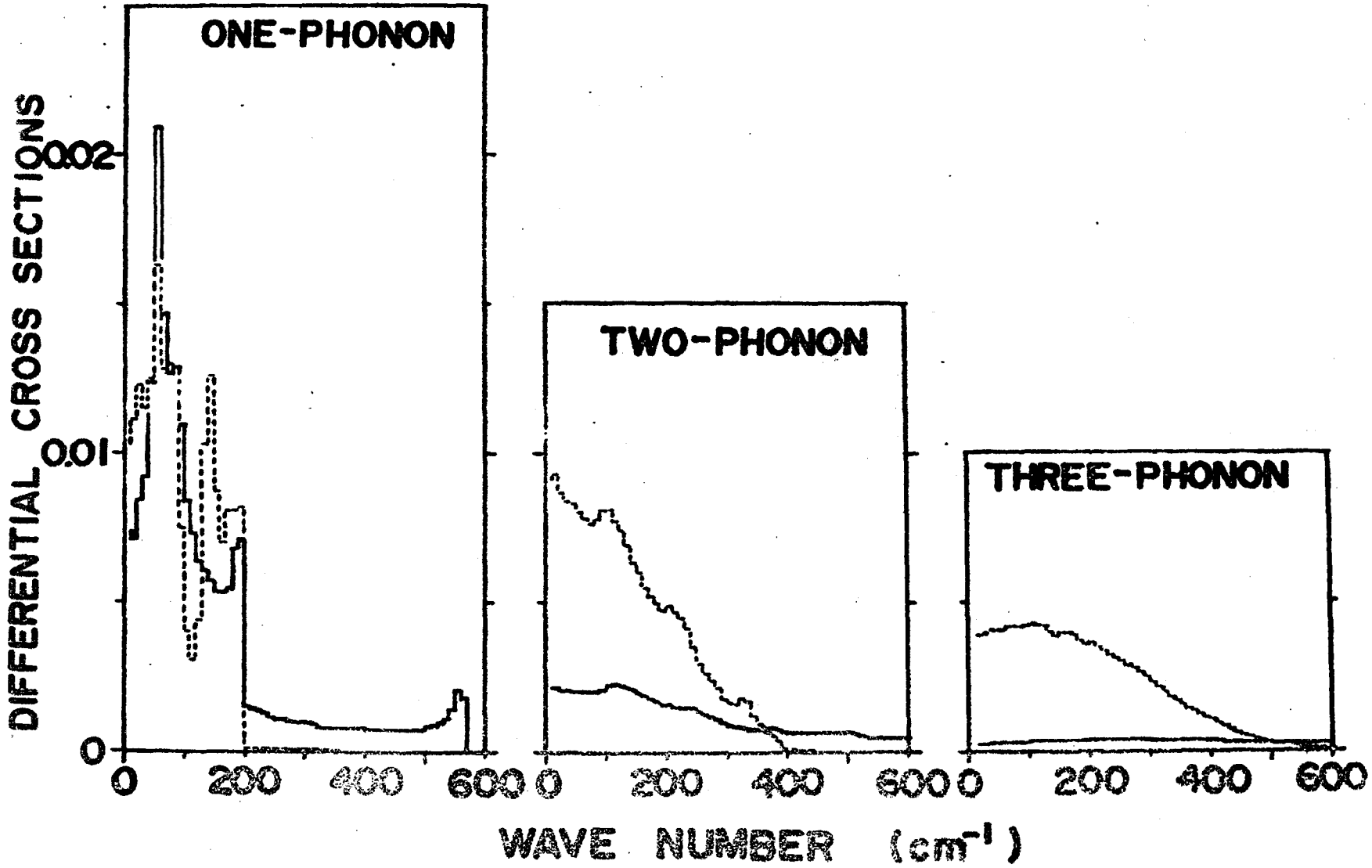

Fig. 6 The calculated differential cross sections for one-, two-, and three-phonon scattering on the experimental condition of k_2=30 meV, θ=90°, and T=298°K.

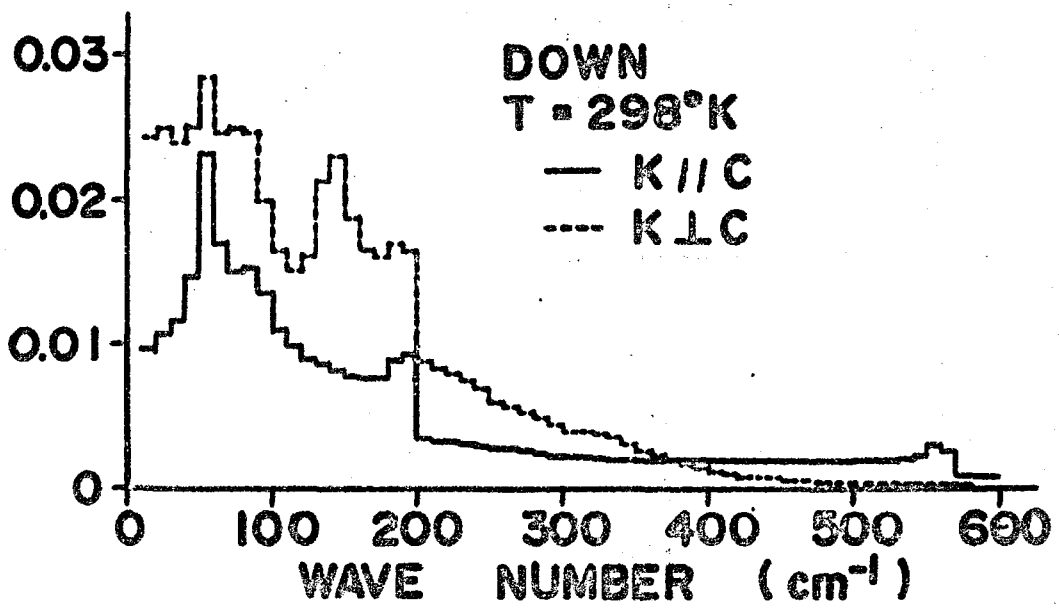

Fig. 7 The composite of the differential cross sections for one-, two-, and three-phonon scattering.
The histograms of $(d^2\sigma/d\Omega dE)$ per frequency division of 10 cm^{-1} are drawn against the energy transfer. The ordinate scale is $(s/4\pi)$.

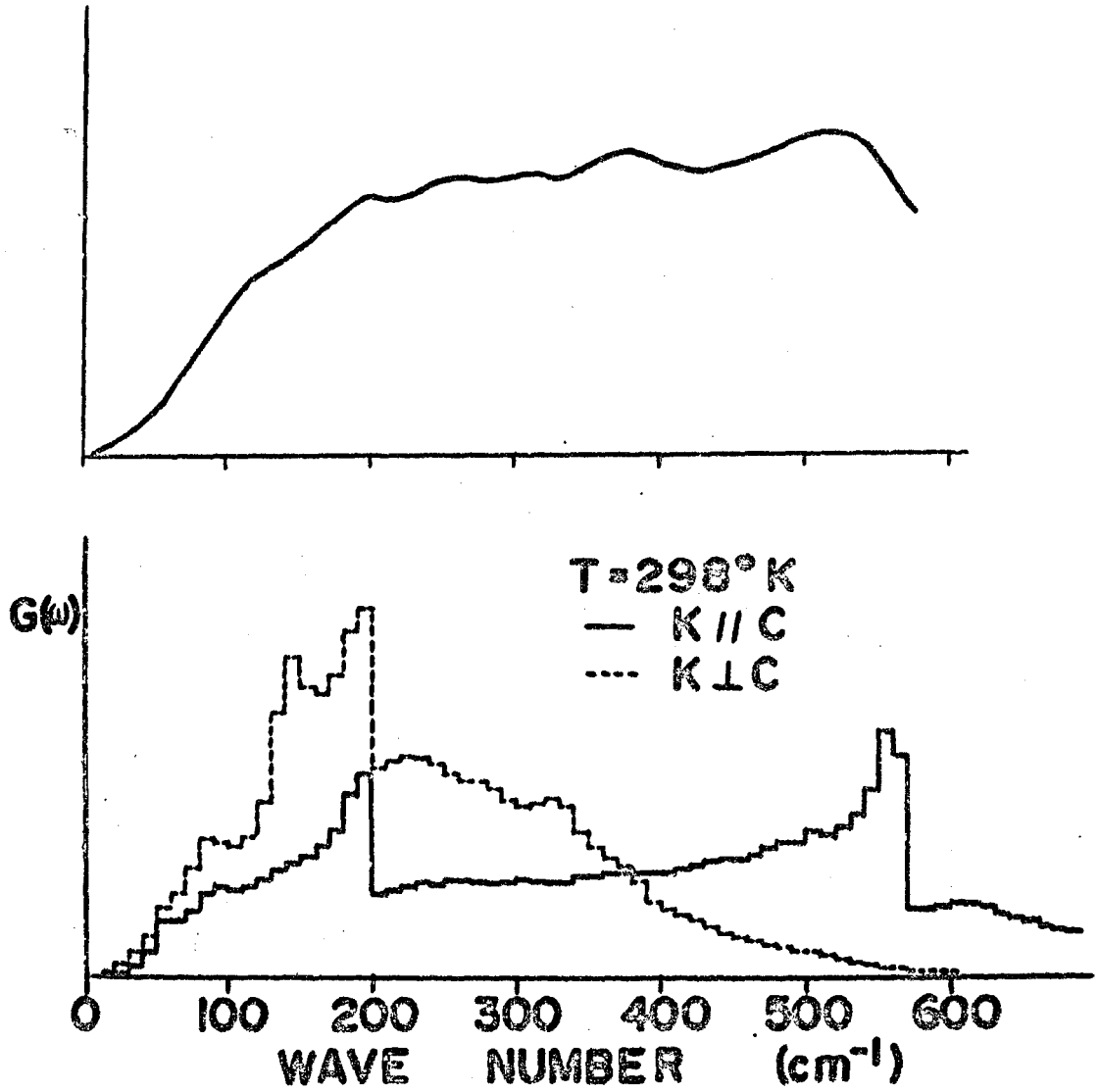

Fig. 8 Comparison between the calculated and observed phonon densities.

the upper figure; observed result on unoriented sample[3)]

the lower figure; calculated result

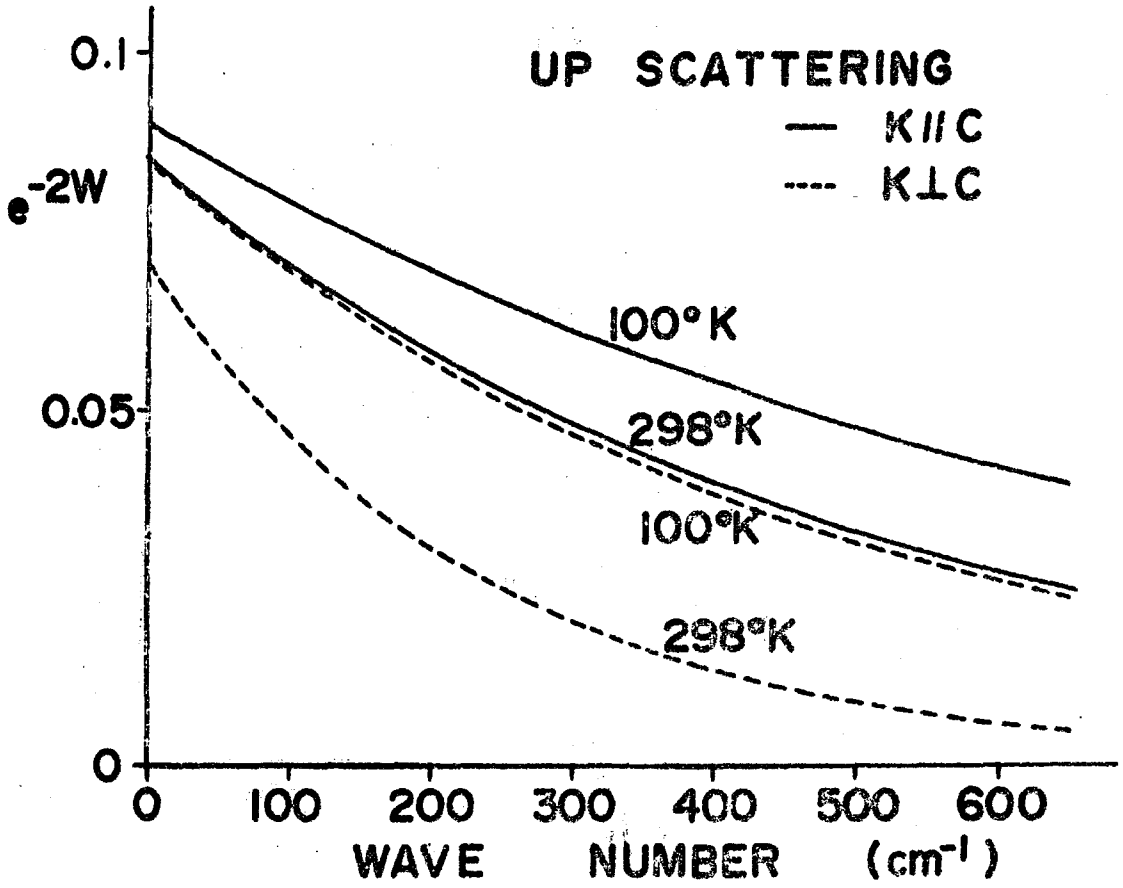

Fig. 9 The calculated Debye-Waller factor, exp[-2W(K)].

the incident neutron energy; 5.2 meV
the scattering angle; 90°

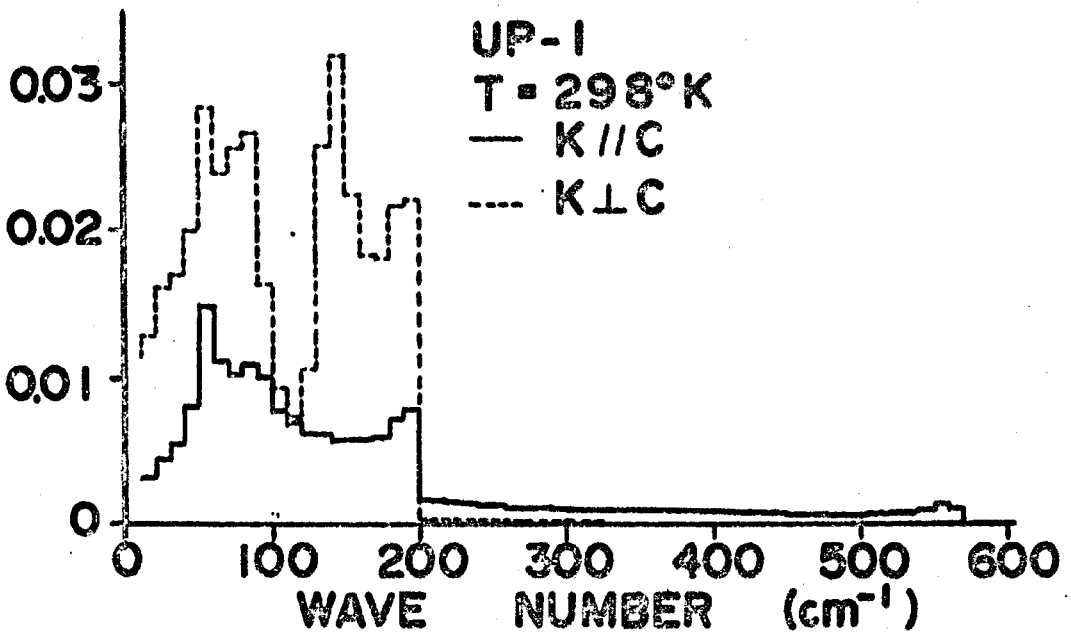

Fig. 10a The calculated differential cross section for one phonon scattering process.
The incident neutron energy is set to be 5.2 meV and the scattering angle is 90°.

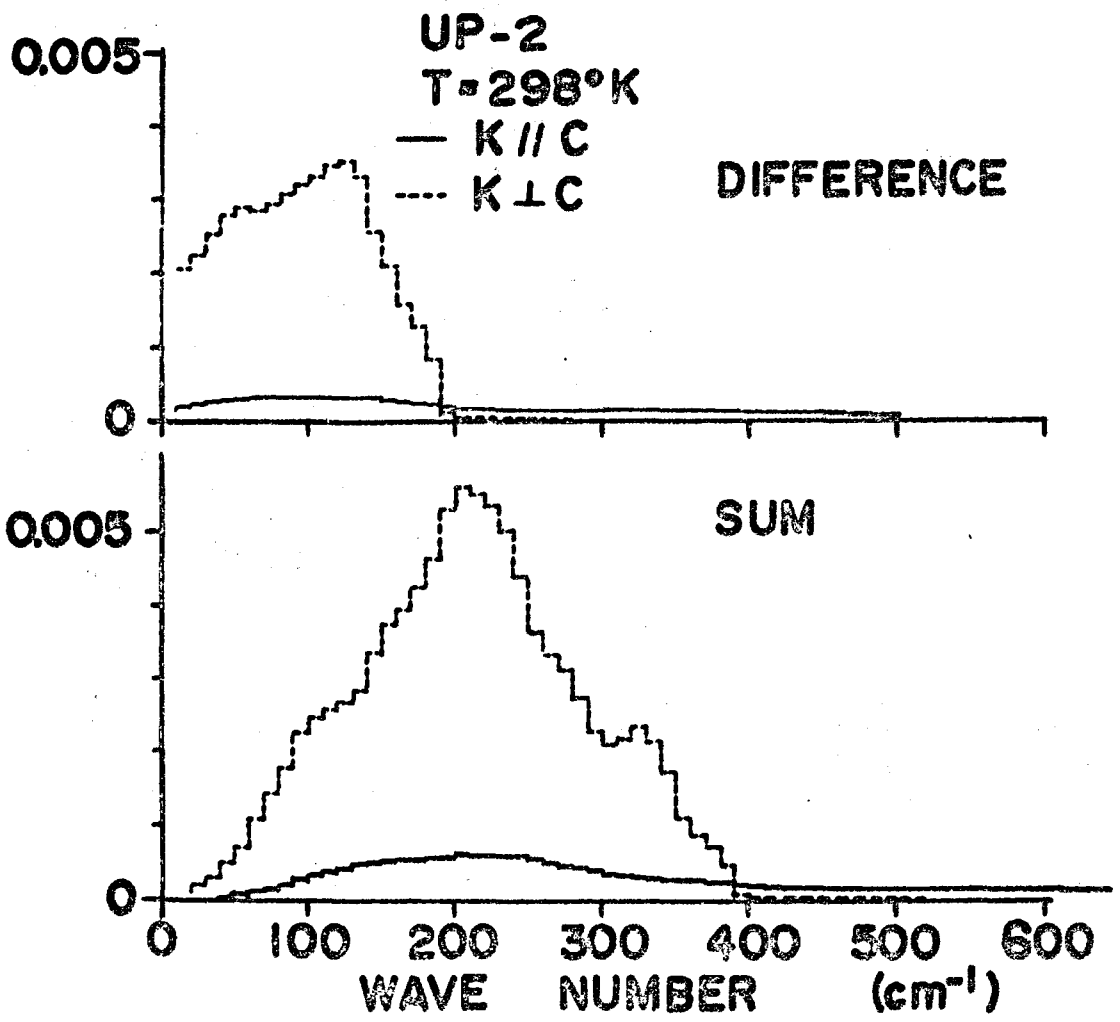

Fig. 10b The calculated differential cross section for two-phonon up-scattering process.

the upper figure; difference combination.

the lower figure; summation combination.

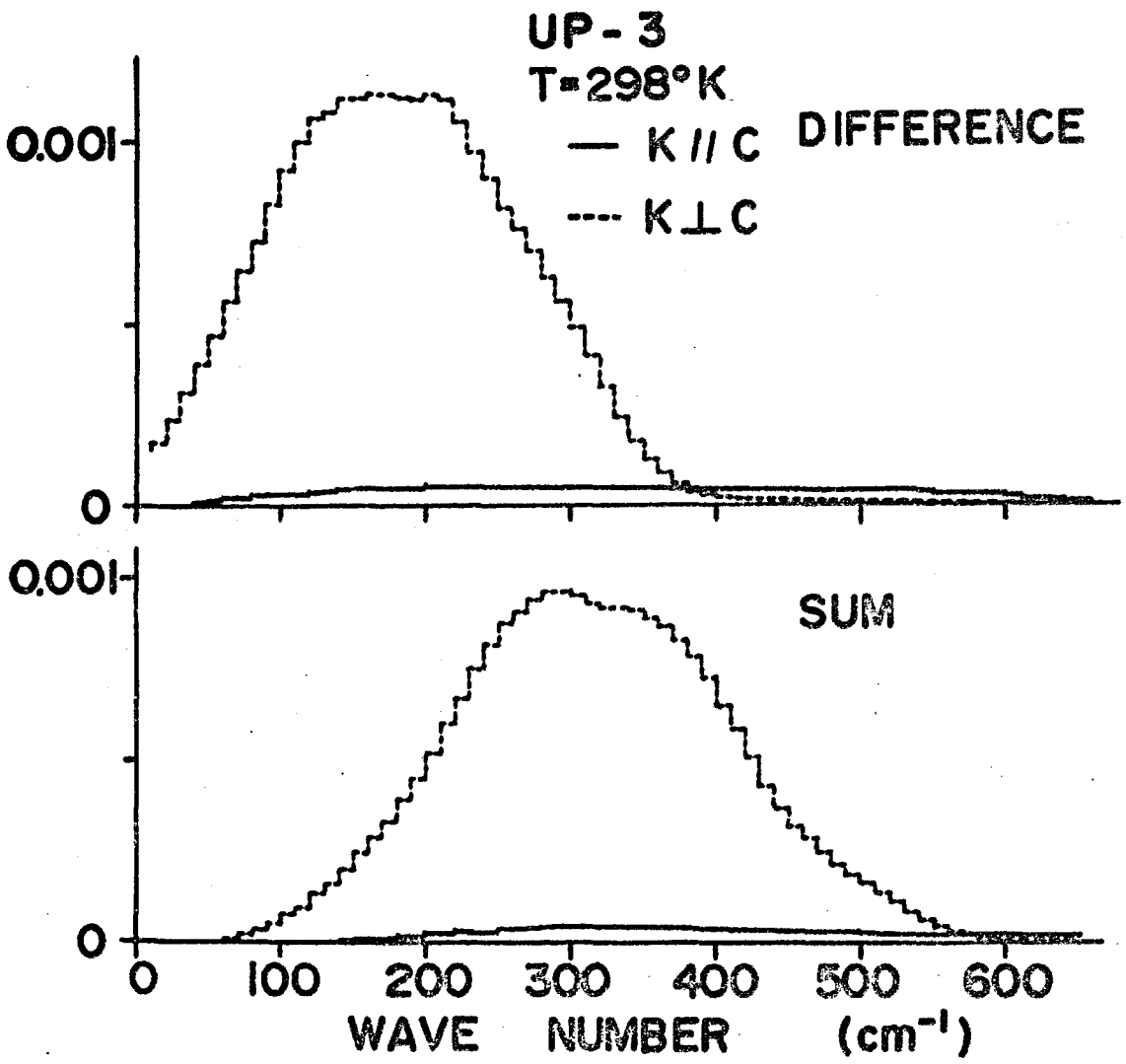

Fig. 10c The calculated differential cross section for three-phonon up-scattering process.

the lower figure; summation combination, (6.50).

the upper figure; difference combination, (6.52)+(6.54).

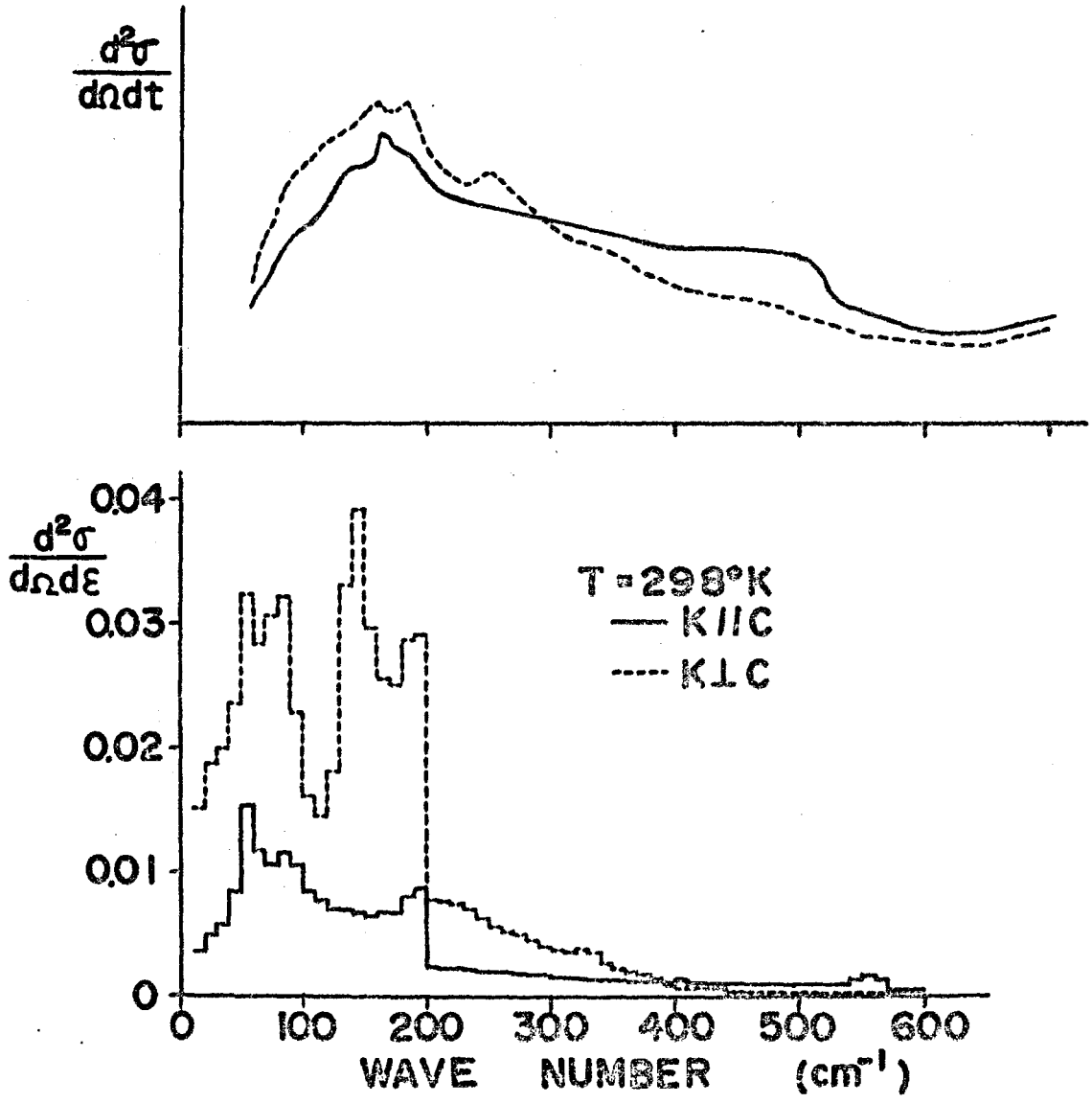

Fig. 11 Comparison between the calculated and observed cross sections.

the upper figure; observed time of flight spectrum.

the lower figure; calculated differential cross section.

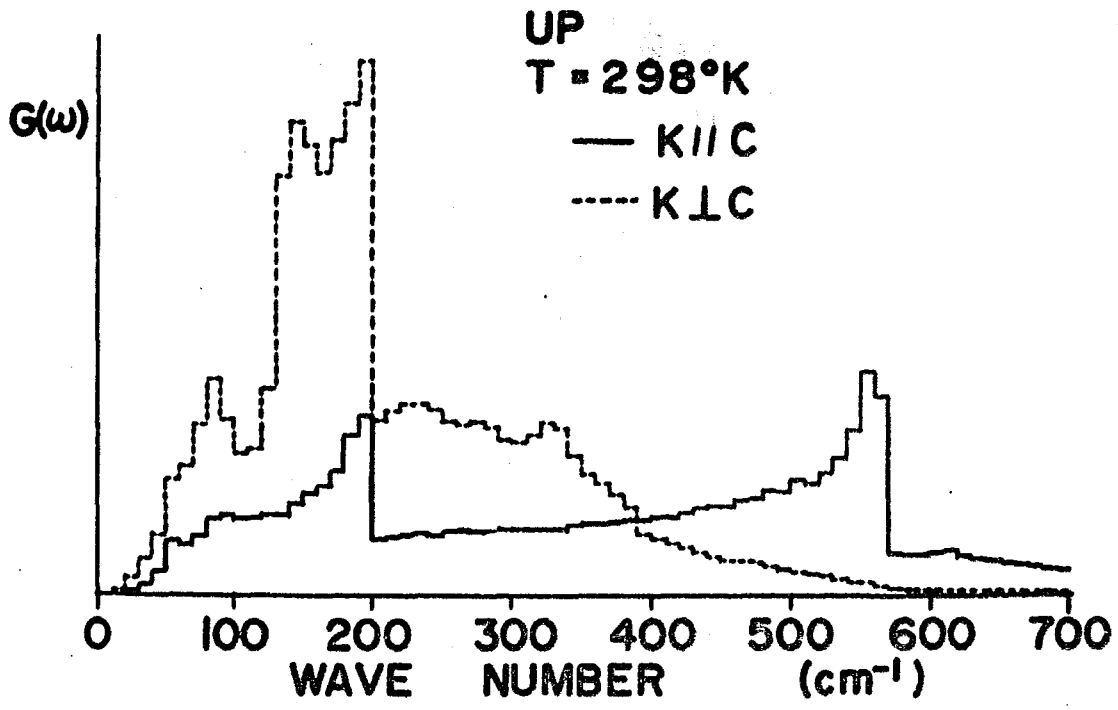

Fig. 12 The calculated phonon density from the up-scattering cross section.

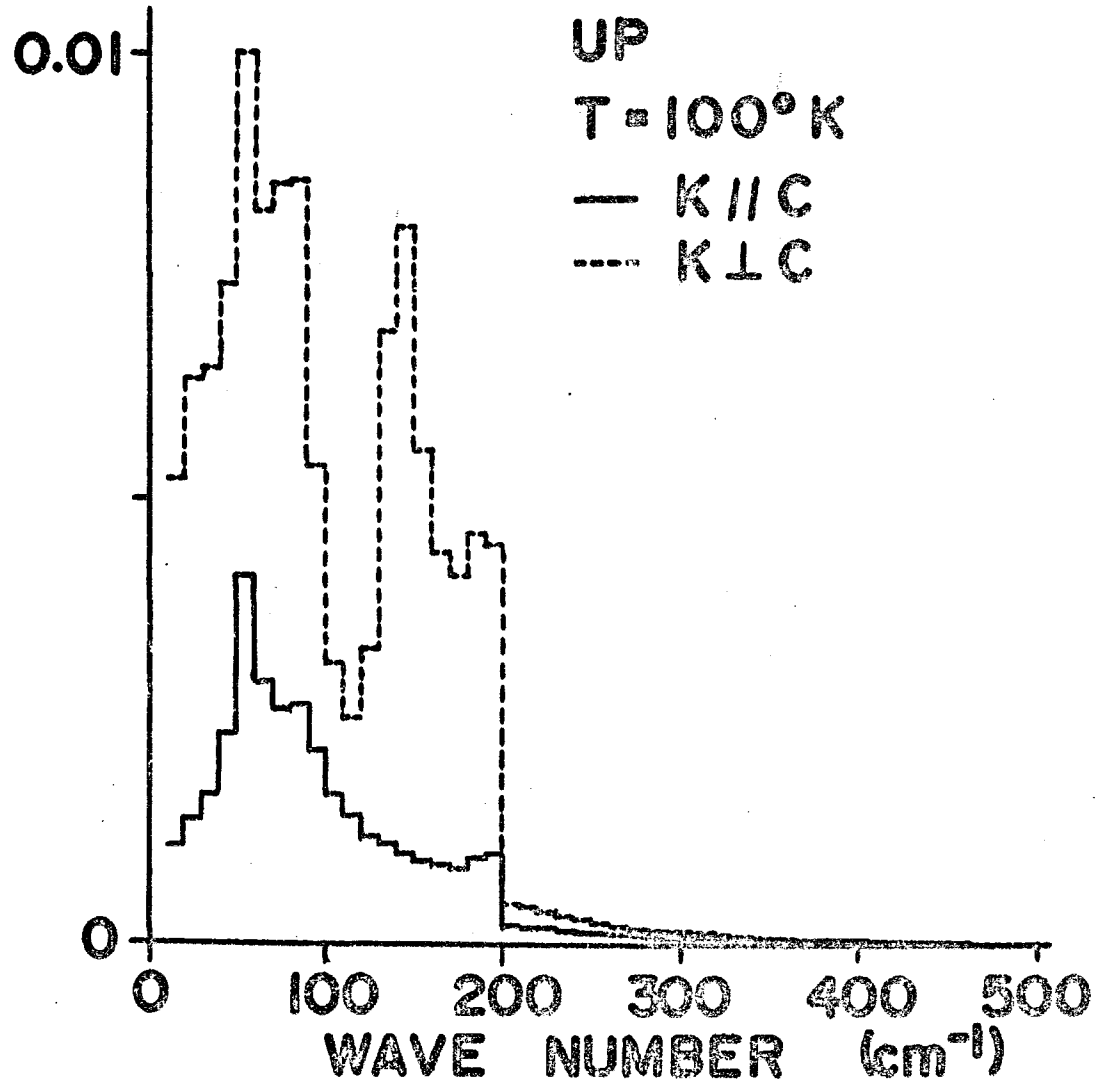

Fig. 13 The composite of the differential cross sections for one-, two-, and three-phonon up-scattering processes. The incident neutron energy is set to be 5.2 meV and the scattering angle is 90°.

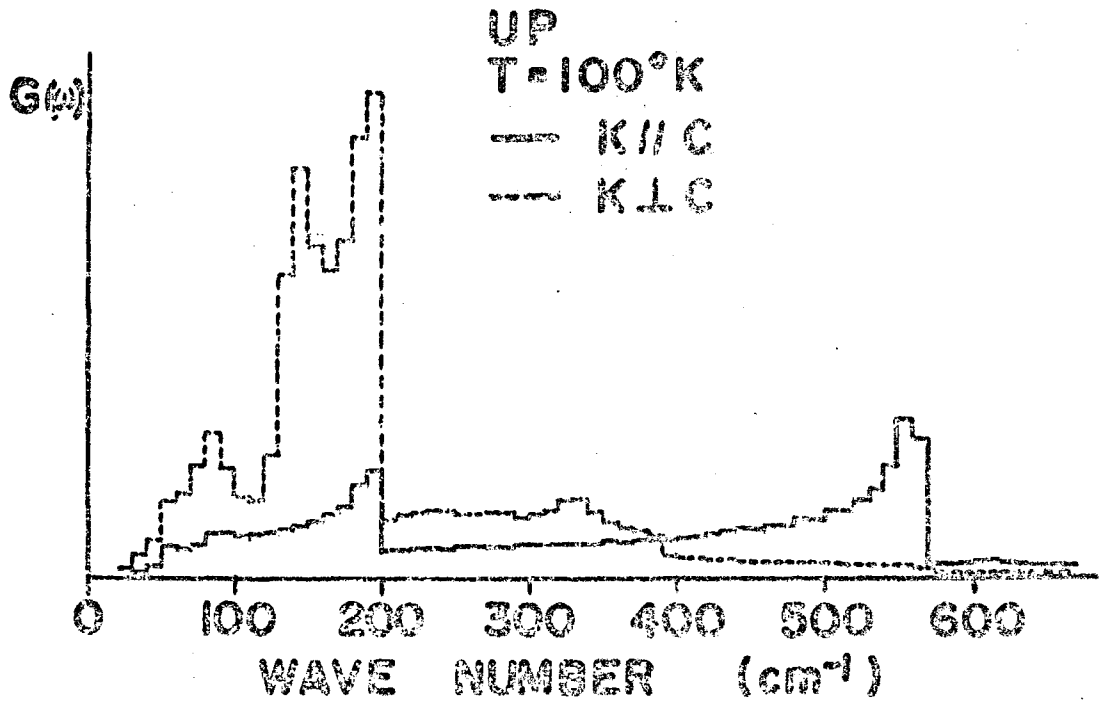

Fig. 14 The calculated phonon density from up-scattering cross section at 100°K.

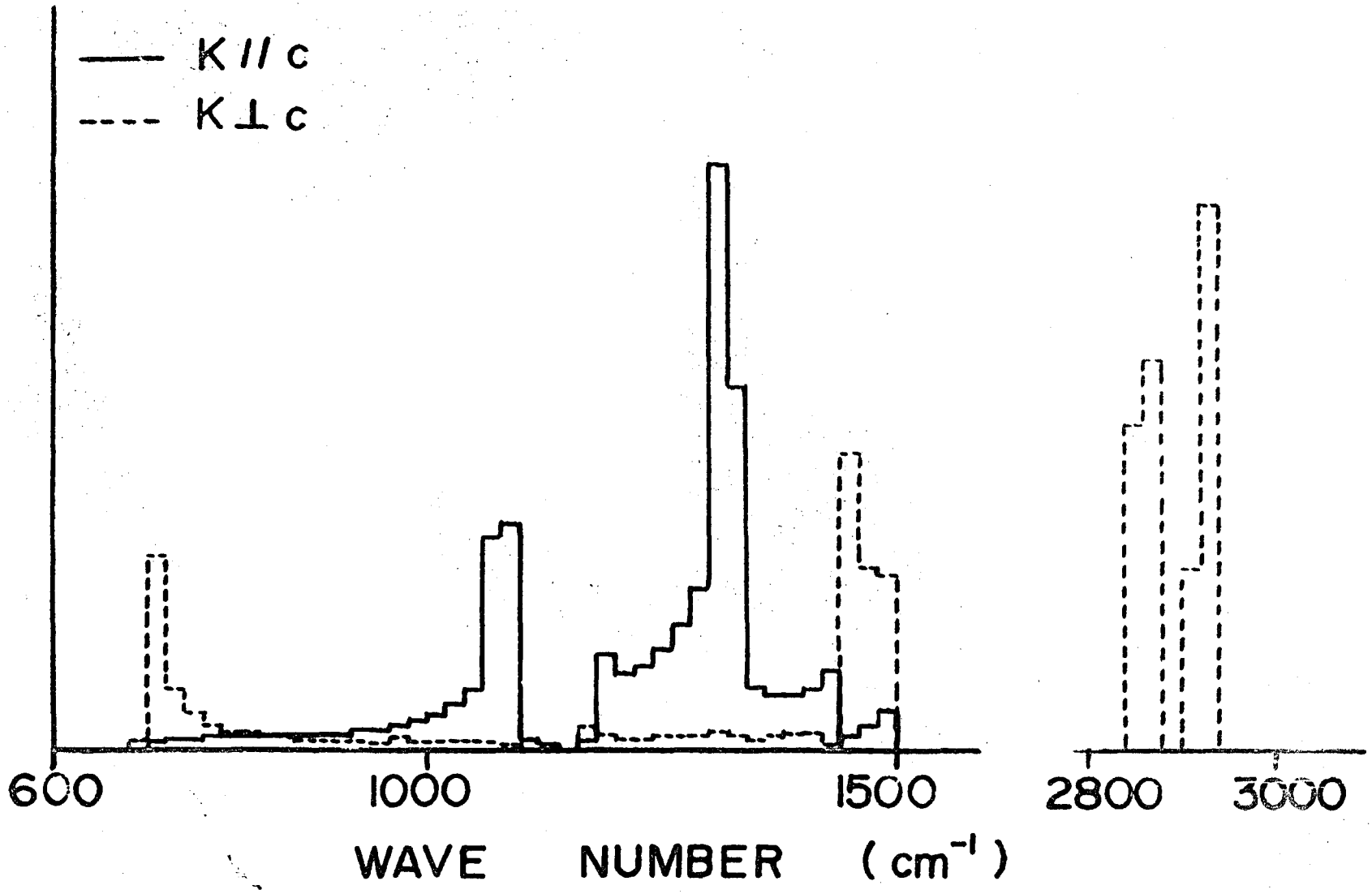

Fig. 15 The amplitude weighted frequency distribution of intrachain vibrations of polyethylene.

CHAPTER VIII

TEMPERATURE FACTOR FOR X-RAY DIFFRACTION OF POLYETHYLENE CRYSTAL

VIII-1 INTRODUCTION

X-ray diffraction utilizes the periodicity of the atomic position in crystals. If atoms rest at their equilibrium position, scattering intensity along Bragg angle would not depend upon the scattering angle. In real crystals, thermal vibrations disturb slightly the periodicity of the atomic position and decrease of the scattering intensity is recognized for large scattering angles. This phenomenon was studied theoretically by Debye[1] and Waller[2] and has been incorporated into X-ray diffraction analysis as a temperature factor. The absolute value of the observed temperature factor gives originally the thermal average of mean squared atomic displacement. However, the effects of various kinds of crystal defects or disorder upon X-ray diffraction have not been established and therefore, the experimental value of temperature factor includes all the effects of the disturbance of the periodicity.

Previously, we have treated the thermal vibrations of polyethylene crystal with the interchain as well as intrachain potential functions. The atomic displacements of hydrogen atoms were calculated on many points of the reciprocal unit cell and, from the thermal average of the mean squared atomic

displacement, differential cross section of neutron inelastic scattering was derived. The calculated anisotropy and relative intensity were in close agreement with the observed neutron spectrum. Debye-Waller factor of hydrogen atom for the elastic scattering of neutron was also calculated and it agreed closely with the experimental results on its absolute value and anisotropy.

On the other hand, X-ray is scattered by electron clouds around the nuclei while neutron is scattered by hydrogen nuclei. Then the scattering from carbon atom may be predominant in X-ray diffraction of polyethylene crystal. Accordingly, in the present study, theoretical value of temperature factor for X-ray diffraction was calculated from the thermal average of mean squared displacement of carbon atom and was compared with the experimental results.

VIII-2 THEORY

Since the extent of electron cloud of individual atom is as same order as the wave length of X-ray, scattered waves from different part of isolated atom might possibly interfere with each other. However, Bragg reflection is based on the interference of the scattered X-ray from other atoms, therefore apparent cross section of k-th atom for X-ray is simply represented as f_k. The intensity of scattered X-ray is written as[3)]

$$I = C\Sigma_{i',k'}\Sigma_{ik} f_k^* f_{k'} \exp\left[iK(\mathbf{r}_{i'}^{k'} - \mathbf{r}_i^k)\right] \qquad (8.1)$$

where C is constant factor which is not concerned with the atomic displacement, $\mathbf{r}_i^k$ is the position vector of k-th atom of i-th unit cell, and $K\hbar$ is momentum transfer vector defined by

$$\mathbf{K}\hbar = (\mathbf{k}_1 - \mathbf{k}_2)\hbar \tag{8.2}$$

where $\mathbf{k}_1$ and $\mathbf{k}_2$ are wave vectors of incident and scattered X-ray, respectively.

Since the energy of X-ray is extremely higher than the vibrational energy, the absolute value of $\mathbf{k}_1$ and $\mathbf{k}_2$ are almost equal unless atoms are electronically excited on the scattering. If the wave lengths of incident and scattered X-ray are commonly equal to λ, then the magnitude of momentum transfer vector is given by

$$|\mathbf{K}| = 4\pi\sin(\theta/2)/\lambda \tag{8.3}$$

where θ is scattering angle (twice of diffraction angle).

The position vector of the atom may be decomposed into

$$\mathbf{r}_i^k = \mathbf{R}_i + \mathbf{r}_k + \mathbf{u}_i^k \tag{8.4}$$

where $\mathbf{R}_i$ is the position vector of the i-th cell origin and $\mathbf{r}_k$ is the position vector of equilibrium position of the k-th atom from the cell origin. $\mathbf{u}_i^k$ is the atomic displacement vector of the k-th atom in the i-th unit cell due to thermal vibrations, which is derived from Eqs(6.1) and (6.2) as

$$\mathbf{u}_i^k = (2/M_k N)^{\frac{1}{2}} \sum_j \mathbf{A}_{kj}\left[Q_j^a\cos(\boldsymbol{\rho}_{ik}\delta) - Q_j^b\sin(\boldsymbol{\rho}_{ik}\delta)\right] + \mathbf{B}_{kj}\left[Q_j^a\sin(\boldsymbol{\rho}_{ik}\delta) + Q_j^b\cos(\boldsymbol{\rho}_{ik}\delta)\right] \tag{8.5}$$

where M_k is mass of k-th atom, N is total number of unit cell, $\boldsymbol{\rho}_{ik}$ is the index vector of k-th atom of i-th unit cell, and δ is phase difference vector. Q_j^a and Q_j^b are degenerate pair of j-th normal coordinate, the polarization vector of which is represented as $\mathbf{A}_{kj}$ and $\mathbf{B}_{kj}$. Since real number normal coordinates are used, summation runs over all branches on N/2 points of half of the first Brillouin zone.

Substitution of r_1^k from (8.4) into (8.1) provides

$$I = C\Sigma_{1',k'}\Sigma_{1k}F_0^{k*}F_0^{k'}\times\exp[iK(R_{1'}-R_1)]\cdot\exp[iK(u_{1'}^{k'}-u_1^k)] \quad (8.6)$$

where F_0^k is atomic structure factor defined by

$$F_0^k = f_k\exp(iKr_k)$$

The exponential function of (KR_1) becomes Laue function which is nonvanishing only on the reciprocal lattice point. The expectation value of the final factor gives rise to the temperature factor. For harmonic vibrations, the thermal average of exponential function of normal coordinate is exactly equal to the exponential function of thermal average of squared normal coordinate, that is,

$$\langle\exp(Q)\rangle_T = \exp\{\tfrac{1}{2}\langle Q^2\rangle_T\}$$

where Q is normal coordinate. This relation is derived from Bloch's theorem.[4] Since the atomic displacement is linear combination of normal coordinates, Debye-Waller factor was introduced originally from

$$\langle\exp(iKu_1^k)\rangle_T = \exp\{-\tfrac{1}{2}\langle(Ku_1^k)^2\rangle_T\} = \exp[-W_k(K)] \quad (8.7)$$

where $W_k(K)$ is Debye-Waller factor for k-th atom. However, the expectation value of the final factor of (8.6) is not exactly equal to the product of two functions of (8.7), because of the correlation among the atomic displacement.

Since the atomic displacement is relatively small compared with the wave length of X-ray, the final function of (8.6) is expanded into power series of (Ku_1^k) as

$$\langle\exp[iK(u_{1'}^{k'}-u_1^k)]\rangle_T = \langle[1 + iKu_{1'}^{k'} - \tfrac{1}{2}(Ku_{1'}^{k'})^2\cdots]\times[1 - iKu_1^k - \tfrac{1}{2}(Ku_1^k)^2\cdots]\rangle_T$$

$$=\left[1-\left\langle\tfrac{1}{2}(\mathrm{K}u_1^{k'})^2\right\rangle_T\cdots\right]\left[1-\left\langle\tfrac{1}{2}(\mathrm{K}u_1^{k})^2\right\rangle_T\cdots\right]$$
$$+\left\langle(\mathrm{K}u_1^{k'})(\mathrm{K}u_1^{k})\right\rangle_T \qquad (8.8)$$

where $\langle\ \rangle_T$ means the thermal average of the expectation value. If there is no correlation in the atomic displacement, the second factor of (8.8) vanishes. Debye-Waller factor may be regarded as the approximate value of the first factor of (8.8).

$$1-\left\langle\tfrac{1}{2}(\mathrm{K}u_1^{k})^2\right\rangle_T\cdots = \exp\left[-W_k(\mathrm{K})\right]$$

Then the scattering intensity is represented as

$$I = C\Sigma_{1',k'}\Sigma_{1k}F_0^{k*}F_0^{k'}\exp\left[-W_k(\mathrm{K})\right]\exp\left[-W_{k'}(\mathrm{K})\right]\exp\left[i\mathrm{K}(R_{1'}-R_1)\right]$$
$$+\Sigma_{1',k'}\Sigma_{1k}CF_0^{k*}F_0^{k'}\left\langle(\mathrm{K}u_1^{k})(\mathrm{K}u_{1'}^{k'})\right\rangle_T\exp\left[i\mathrm{K}(R_{1'}-R_1)\right] \qquad (8.9)$$

where the first term gives Bragg reflection and the second term yields thermal diffuse scattering which may be observed as the width of Bragg reflection peak. The decrease of Bragg reflection due to thermal vibrations is compensated by the increase of thermal diffuse scattering.

On the other hand, the representation of (8.1) is equivalent to Born's first approximation incorporated on the neutron scattering. Then the scattering intensity may be derived in the same way with Chapter VI. The first term of (8.9) comes from the matrix element for elastic scattering and the second term corresponds to single phonon inelastic scattering. Therefore, Debye-Waller factor is obtained in the same way with (6.16),

$$2W_k(\mathrm{K}) = \Sigma_1(\hbar/M_kN\omega_1)\left[(\mathrm{K}A_{k1})^2+(\mathrm{K}B_{k1})^2\right](1+x_1)/(1-x_1) \qquad (8.10)$$

where $x_i=\exp(-\hbar\omega_i/kT)$, ω_i is angular frequency of i-th normal vibration and summation runs over all branches on N/2 points in the reciprocal unit cell. Since in the X-ray diffraction analysis, temperature factor tensor $B_{\alpha\beta}$ is defined by

$$2W_k(K) = \sum_{\alpha\ \beta} 2B_{\alpha\beta}\left[\sin(\theta/2)/\lambda\right]_\alpha\left[\sin(\theta/2)/\lambda\right]_\beta \qquad (8.11)$$

then $B_{\alpha\beta}$ is represented as

$$B_{\alpha\beta}= \sum_i (8\pi^2\hbar/M_kN\omega_i)\left[(A_{ki})_\alpha(B_{ki})_\beta+(B_{ki})_\alpha(B_{ki})_\beta\right](1+x_i)/(1-x_i) \qquad (8.12)$$

On the numerical calculation, dynamical matrix was diagonalized about the representative sets of phase differences and then, with the use of the interpolation method described in (1.16), ω_i, A_{ki} and B_{ki} were obtained at the interval of 1° of δ_c for every set of (δ_a,δ_b).

VIII- 3 RESULTS AND DISCUSSIONS

Thus the mean squared atomic displacement of carbon atom was calculated for about 120,000 modes below 700cm^{-1} and collected in Fig. 1, where the histogram of amplitude weighted frequency distribution are shown against the frequency interval of 10 cm^{-1} and solid line represents the parallel component of the atomic displacement to the chain axis, while the broken line represents the average of two components perpendicular to the chain axis. Two prominent peaks appear at 90 cm^{-1} and 190 cm^{-1} in perpendicular case, which are due to antiparallel translatory vibrations perpendicular to the chain axis and the internal rotation, respectively. The atomic displacement of carbon atom and hydrogen are identical in the translatory vibrations whereas, in the rotatory modes around the chain axis, the atomic displacement

of carbon atom is smaller than that of hydrogen atom. Therefore, the perpendicular peak at 150 cm^{-1} which results from overall rotatory vibrations around the chain axis, is weak in the case of carbon atom compared with the corresponding peak of hydrogen atom. As for the parallel component, there is a peak at 560 cm^{-1}, which is associated with the skeletal bending modes. The contribution of the skeletal bending branch seems constant above 50 cm^{-1}. It may be expected from the dispersion curves along δ_c of Chapter IV, where optical branches of the skeletal bending modes start almost always from 50 cm^{-1}. It is noticeable that, in the case of hydrogen atom, the peak of parallel component of the internal rotation vibration is recognized at 190 cm^{-1} whereas there is no peak at 190 cm^{-1} in the case of carbon atom.

In Fig. 2, the amplitude weighted frequency distribution of carbon atom due to the intrachain vibrations are plotted against the frequency division of 20 cm^{-1}. The perpendicular peak above 2800 cm^{-1} is associated with C-H stretching vibrations. Near 1000 cm^{-1} region, the perpendicular peaks are weak and broad. Two weak peaks at 720 cm^{-1} and 1470 cm^{-1} are due to methylene rocking and scissoring vibrations, respectively. As for the parallel case, four prominent peaks are recognized. The strong peaks at 970 and 1080 cm^{-1} are associated with skeletal stretching vibration while the peaks at 1430 and 1490 cm^{-1} are mainly due to methylene wagging and scissoring vibrations. Vibrational displacement parallel to the chain axis (solid line in Fig. 1 and Fig. 2) reduces the intensity of Bragg reflection from the plane normal to the

chain axis, which is used for the determination of fiber period of polymer single chain.

Recent development of the growing technique of single crystal would make it possible to observe each element of the temperature factor tensor on polyethylene single crystal, although the exact experimental value is not available yet. Accordingly theoretical value of temperature factor tensor was calculated. The calculated results are shown in Table 1, where a, b and c mean the components of the scattering vector (unit vector along momentum transfer vector) along the a, b and c axes, respectively.

The value of temperature factor along the chain axis is relatively small compared with the values perpendicular to the chain axis, in good agreement with the experimental results.[5] On the analysis of X-ray diffraction from monoclinic single crystal of $C_{36}H_{74}$, Shearer and Vand[6] have obtained the isotropic temperature factor of $B=3$ Å^2, at room temperature. Bunn has assumed the perpendicular components of temperature factor as $B=5$ Å^2 on the structure analysis of polyethylene. Therefore it is reasonable that the calculated value of the temperature factor at room temperature is 3 Å^2 for perpendicular component and 1 Å^2 for parallel component.

Chiba et al.[7] have investigated the temperature dependency of the anisotropic temperature factor and found that the observed values lie on the straight line, drawn between two calculated values of 100°K and 298°K. Since, from the expansion of (8.10) into power series of $(\hbar\omega/kT)$, $B_{\alpha\beta}$ is

nearly proportional to T at higher temperatures, the experiment proved that the anisotropy of the coefficient of the calculated temperature factor against temperature well reproduces the observed results at low temperature.

On the other hand, the space group of the polyethylene crystal includes mirror perpendicular to the chain axis, therefore two cross terms of the temperature factor tensor, B_{ac} and B_{bc}, are always zero. Then, one of the pricipal axes of the temperature factor tensor is parallel to the chain axis and other two axes are in the ab plane. As mentioned in Chapter II, the setting angle of the skeletal plane to the a axis is set to be 45°, therefore the calculated value of B_{aa} is almost equal to B_{bb}. Numerical calculation about principal axes led us to the result that one of the pricipal axes is almost coincident with the normal of the skeletal plane and the other is in the skeletal plane. Two principal values perpendicular to the chain axis are given in Table 2, where out-of-plane component of the principal values is larger than the in-plane component. The result may be reasonable because, among low frequency crystal vibrations, rotatory vibrations around the chain axis contribute to out-of-plane component while only the translatory vibrations contribute to in-plane component. In fact, the projection on (0,0,1) plane of contours of electron density becomes more round as temperature is raised[8].

In Table 3, the temperature factor is represented as composite of the contribution of each modes. The contribution from acoustic branch is twice as large as the contribution from

the antiparallel translatory vibrations. Since the lattice modes vary with phase difference, the notation of the branch is not always exact.

With the use of Debye approximation, Debye-Waller factor for isotropic monoatomic crystal is represented as

$$2W_\kappa = (3|K|^2\hbar^2/M_\kappa k\theta_D)[1/4 + (T/\theta_D)\phi(\theta_D/T)] \qquad (8.13)$$

where M_κ is mass of κth atom, θ_D is Debye's characteristic temperature and

$$\phi(z) = (1/z)\int_0^z \beta d\beta/[\exp(\beta)-1] \qquad (8.14)$$

This approximation may be applied to more complex crystals if the frequency of optical branch of lattice vibrations is so high that the contribution from optical branch might be neglected such as in graphite. However, in polyethylene crystal, the contribution from optical lattice vibrations is not negligible even at 100°K. $B_{\alpha\beta}$ due to acoustic branches are almost proportional to T as shown in Table 3, whereas the temperature dependence of $B_{\alpha\beta}$ associated with optical lattice vibrations depends upon individual mode. The contribution from intrachain vibrations above 700 cm^{-1} may be disregarded in this temperature region. Accordingly, the approximation of (8.13) may be insufficient when several optical modes of lattice vibrations lie below the cut-off frequency of acoustic modes.

SUMMARY

The temperature factor for X-ray diffraction of polyethylene crystal was calculated from the thermal average of mean squared atomic displacement of carbon atom. The calculated values at room temperature is comparable with the experimental results.

The anisotropy and temperature dependence of the temperature factor was in good agreement with the observed results.

The amplitude weighted frequency distribution of carbon atom was calculated and discussed in comparison with that of hydrogen atom.

REFERENCES

1) P.Debye, Ann. d. Physik, 43, 49 (1914).

2) I.Waller, Z. f. Physik, 17, 398 (1923); 51, 213 (1928).

3) I.Nitta ed. "X-ray Diffraction Analysis", Maruzen, Tokyo (1961).

4) F.Bloch, Z. Physik, 74, 295 (1932).

5) C.W.Bunn, Trans. Faraday Soc., 35, 482 (1939).

6) H.M.Shearer and V.Vand, Acta Cryst., 9, 379 (1956).

7) Y.Aoki, A.Chiba and G.Kaneko, Annual Meeting on Polymer Science, 24B22, Tokyo (1968).

8) N.Kasai and M.Kakudo, Rept. Progr. Polymer Phys. Japan, 11, 145 (1968).

Table 1. Temperature factor tensor of polyethylene crystal.($Å^2$)

100^oK	a	b	c	298^oK	a	b	c
a	1.1_1	-0.2_0	0	a	3.3_1	-0.54	0
b	-0.2_0	1.10	0	b	-0.54	3.0_0	0
c	0	0	0.3_7	c	0	0	0.84

Table 2. Principal values of the temperature factor tensor.($Å^2$)

	100^oK	298^oK
in-plane component	0.8_5	2.6
out of plane component	1.36	3.7

Table 3. The contribution of each branch.

	mode		B_{aa}	B_{bb}	B_{cc}	B_{ab}
100^oK	rotatory		0.09	0.09	0	-0.08
	trans.($\perp$)	acoustic	0.72	0.65	0.01	-0.11
	trans.($\perp$)	optical	0.35	0.31	0.01	-0.01
	trans.(//)	acoustic	0	0	0.17	0
	trans.(//)	optical	0	0.01	0.11	0
	intrachain modes		0.04	0.04	0.06	0.01
298^oK	rotatory		0.19	0.19	0	-0.18
	trans.($\perp$)	acoustic	2.26	1.94	0.03	-0.31
	trans.($\perp$)	optical	0.80	0.81	0.03	-0.07
	trans.(//)	acoustic	0.01	0.02	0.51	0
	trans.(//)	optical	0.01	0.01	0.26	0
	intrachain modes		0.04	0.04	0.06	0.01

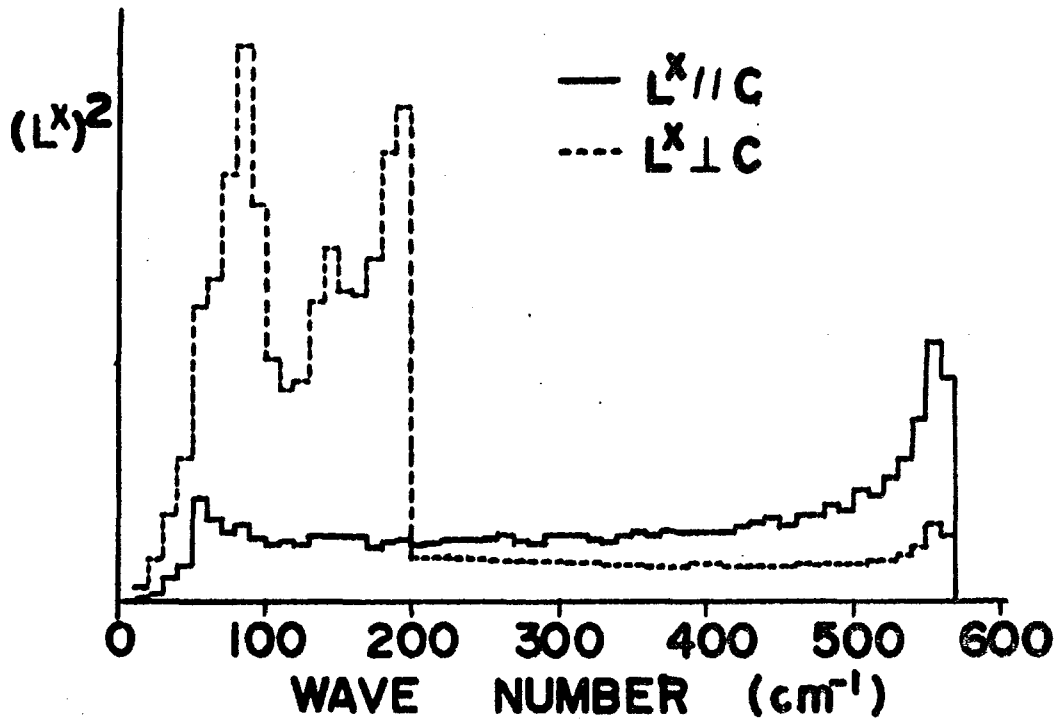

Fig. 1 The distribution of mean squared atomic displacement of carbon atom, for low frequency crystal vibrations.

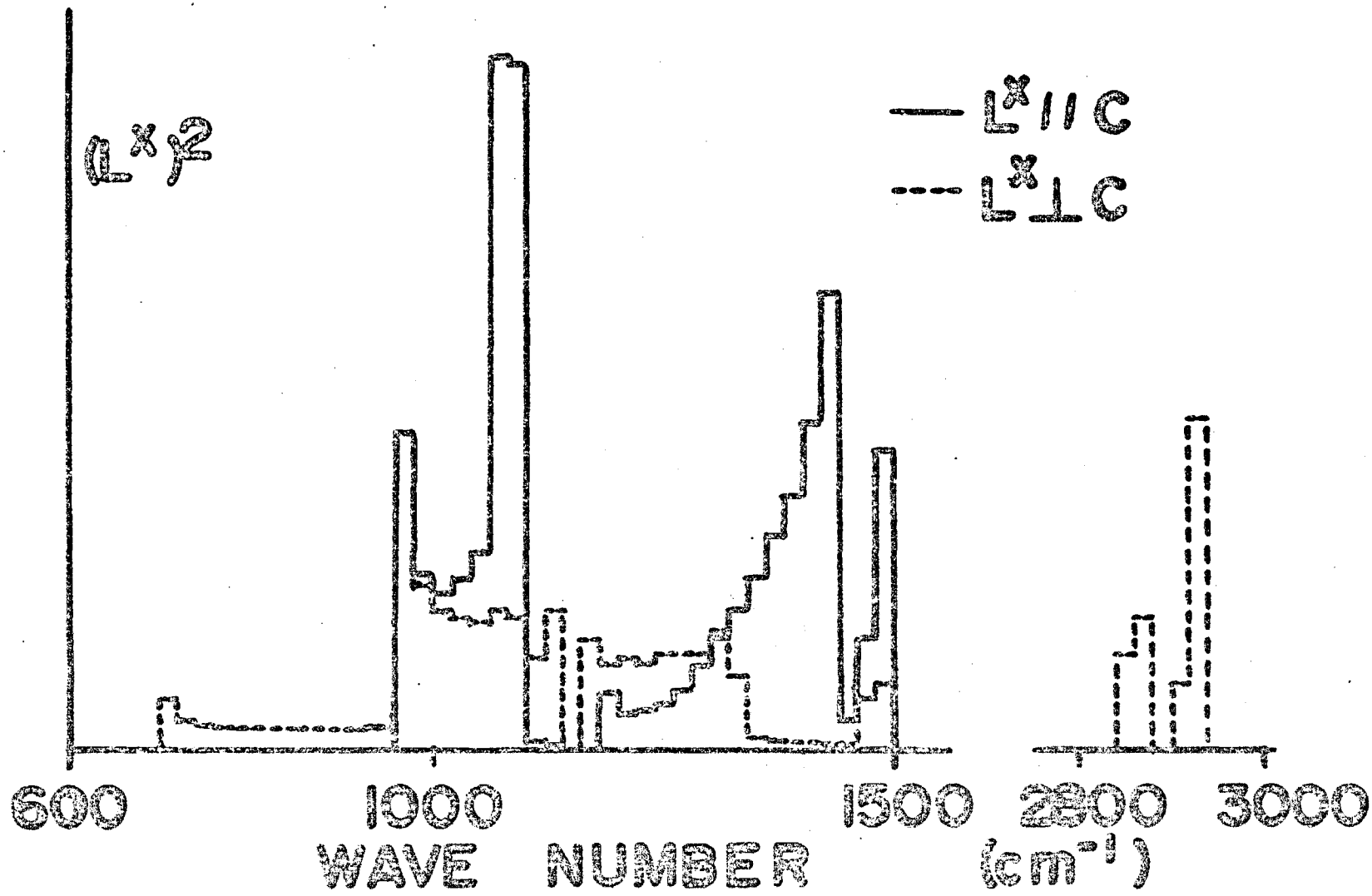

Fig. 2 The distribution of mean squared atomic displacement of carbon atom for the intrachain vibrations.

LIST OF TABLES

CHAPTER VII

CHAPTER VIII

LIST OF FIGURES

CHAPTER IV

APPENDIX I